

**The role of G-proteins in the sino-atrial node in
controlling heart rate**

**A thesis submitted to University College London, University of
London in part fulfilment of the requirement for the degree of**

Doctor of Philosophy

By

Sonia Sebastian

Department of Medicine

Clinical pharmacology

Rayne Institute

UCL

2015

I, Sonia Sebastian confirm that the work presented in this thesis is my own. Where information has been derived from other sources, I confirm that this has been indicated in the thesis.

A handwritten signature in blue ink that reads "Sonia".

Sonia Sebastian

Date: 5th March 2015

Abstract

Reciprocal physiological modulation of heart rate is controlled by the sympathetic and parasympathetic systems acting on the sino-atrial (SA) node. However there is little direct *in vivo* work examining the role of stimulatory and inhibitory G-protein signalling in the SA node. We have previously shown that the inhibitory G-proteins $G\alpha_{i2}$, is important in mediating vagal tone to the murine heart with global $G\alpha_{i2}$ knock-out mice developing tachycardia with loss of high frequency power and being resistant to the effects of the muscarinic agonist, carbachol (Zuberi et al. 2008). However, it is unclear whether the effect is mediated entirely via $G\alpha_{i2}$ signalling at the end-organ level or whether there is a central component. I sought to investigate this by studying mice with conditional knock outs (KO) of $G\alpha_{i2}$ and $G\alpha_o$ in cardiac tissue by using α MHC cre mice. Studies with α MHC cre mice using the cre lox-P approach were negative as there was no difference in heart rate variability (HRV) and electrocardiograph (ECG) parameters between controls and conditional KO of $G\alpha_{i2}$ and $G\alpha_o$, though by real-time polymerase chain reaction (RT-PCR) we could see reduction in the level of their expression. I assumed deletion of $G\alpha_{i2}$ and $G\alpha_o$ may not be complete in the SA nodal region where G-protein inwardly rectifying K^+ channels (GIRK) channels are active. I sought to investigate this further by studying mice with conditional deletion of $G\alpha_{i2}$ and $G\alpha_s$ in the conduction system of the murine heart using cre lox-P technology. I crossed mice in which cre recombinase expression was driven by a tamoxifen-inducible conduction system-specific construct with $G\alpha_s$ floxed and $G\alpha_{i2}$ floxed mice. I studied the heart rate responses of adult mice compared with littermate controls by using ECG radio-telemetry before and after administration of tamoxifen. The mice with conditional deletion of $G\alpha_s$ and $G\alpha_{i2}$ had a loss of diurnal variation and were bradycardic or tachycardic in the daytime respectively. In mice

with conditional deletion of $G\alpha_s$ there was a selective loss of low frequency power whilst with deletion of $G\alpha_{i2}$ there was a loss of high frequency power in power spectral analysis of heart rate variability. There was no evidence of pathological arrhythmia. Pharmacological modulation of heart rate by isoprenaline was impaired in the $G\alpha_s$ conditional knock-out mice but a muscarinic agonist was still able to slow the heart rate in $G\alpha_{i2}$ conditional knock-out mice. We conclude that $G\alpha_s$ and $G\alpha_{i2}$ mediated signalling in the sino-atrial node is important in the reciprocal regulation of heart rate through the autonomic nervous system.

Another way to look at the role of specific gene function is via gain of function mutation. Regulators of G-protein signalling (RGS) proteins are a recently discovered family of proteins that negatively regulate G-protein-coupled signalling pathways. Thus, I used RGS-insensitive (RGSi) mutant $G\alpha$ subunits, which contain a $G^{184}S$ point mutation in their switch I region that prevents binding of RGS proteins and the subsequent $G\alpha$ deactivation. RGS insensitive $G\alpha_{i2}$ and $G\alpha_o$ mice (RGSi $G\alpha_{i2}$ and RGSi $G\alpha_o$) were found to be tachycardic and lost diurnal variation in heart rate. The A_1 receptor agonist, 2-chloro-N⁶-cyclo-pentyladenosine (CCPA) and M_2 receptor agonist, carbachol showed an enhanced inhibitory response (bradycardic) to RGSi $G\alpha_o$ but this enhanced bradycardic response was observed only with carbachol for RGSi $G\alpha_{i2}$. HRV signature was found to be lost in RGSi $G\alpha_o$ but not with RGSi $G\alpha_{i2}$. Interestingly, studies with RGSi $G\alpha_{i2}$ and RGSi $G\alpha_o$ prove a role of the central nervous system in controlling the heart rate in these knock-ins.

$G\alpha_{i2}$ levels are up-regulated in heart failure. However, it was not clear whether its role is protective or maladaptive in the context of heart failure. Hence, I subjected the mice in which cre recombinase expression was driven by a tamoxifen-inducible conduction system-specific construct with $G\alpha_s$ floxed and $G\alpha_{i2}$ floxed mice to myocardial

infarction by left anterior descending (LAD) artery ligation. I found that cardiac-specific knock-out of $G\alpha_s$ attenuates left ventricular (LV) dilation and improves LV contractile function after myocardial infarction (MI). Conditional deletion of $G\alpha_s$ was found to be protective as this was reflected in increased fractional shortening (FS%), ejection fraction (EF%) and fractional area change (FAC%) on echocardiographic analysis after MI. LV remodelling was observed in cardiac-specific knock-out of $G\alpha_{i2}$ to a certain extent with chamber dilatation and decreased EF% and FS% and FAC%.

In summary absence of $G\alpha_s$ is found to preserve LV function may be by its bradycardic nature may protect the heart against the ischemic insult, although the precise mechanism that helps against the adverse LV remodelling need to be explored. On the other hand absence of $G\alpha_{i2}$ and moderate tachycardia in these mice didn't have any detrimental effects on LV remodelling.

Acknowledgements

First and foremost I would like to express my sincere thanks to Professor Andrew Tinker, who has given me the opportunity to pursue PhD with my job and also for partly funding my studies. It would not have been possible without your expert guidance, motivation, immense knowledge and support. With you and your team I have learnt a lot over the past years. I could not have imagined having a better advisor and guide for my PhD. Thanks Andy.

My sincere words of gratitude extend to members of Tinker laboratory, past and present (Zia Zuberi, John Gomes, Freya Geall, Steve Harmer, Keat Eng, Muriel Nobles, Sarah Schwarzer, Alison Thomas, Jem Lane, Richard Ang, Aaisha Opel, Justine Bhar Amato). Thank you for your support, help and advice over the years.

Special thanks to Qadeer Aziz for his valuable inputs and for reviewing my thesis.

I would also like to thank the University College London for partly funding my studies by providing me studentship and Wellcome Trust charity and British Heart Foundation for funding the project.

Above all, I would like to thank my dear loving husband Sebastian, my three beautiful and loving daughters Serena, Sanya and Sasha (who are my inspiration), my parents (Antony and Leelamma) and my in-laws (Devasia and Joyce) who have given me their unequivocal support throughout, as always, for which my mere expression of thanks likewise does not suffice.

Publications

Sebastian, S., Ang, R., Abramowitz, J., Weinstein, L.S., Chen, M., Ludwig, A., Birnbaumer, L., & Tinker, A. 2013. The *in vivo* regulation of heart rate in the murine sinoatrial node by stimulatory and inhibitory heterotrimeric G-proteins. *Am.J.Physiol Regul.Integr.Comp Physiol*, 305, (4) R435-R442 available from: PM:23697798

Zuberi, Z., Nobles, M., Sebastian, S., Dyson, A., Lim, S.Y., Breckenridge, R., Birnbaumer, L., & Tinker, A. 2010. Absence of the inhibitory G-protein Galpha_{i2} predisposes to ventricular cardiac arrhythmia. *Circ.Arrhythm.Electrophysiol.*, 3, (4) 391-400 available from: PM:20495013

Lane, J., Sebastian, S., Abramowitz, J., Birnbaumer, L., & Tinker, A. Effects of cardiac specific deletion of G α_{i2} on heart rate dynamics. In preparation.

Oral presentation

S. Sebastian, Z. Zuberi, L. Birnbaumer, A. Tinker. The effects of cardiac specific deletion of G α_{i2} and G α_o on heart rate dynamics *Physiology Conference Manchester* July 2010.

Poster

R. Ang, S. Sebastian, A. Ludwig, L. Birnbaumer and A. Tinker. Mice with conditional knockout of G α_{i2} in the cardiac pacemaker system exhibit tachycardia with loss of HF power on HRV analysis. *Frontiers in CardioVascular Biology* March 2012.

Commonly used abbreviations

AC	adenylyl cyclase
ACE	angiotensin converting enzyme
Ach	acetylcholine
ADP	adenosine diphosphate
ATP	adenosine triphosphate
AVN	atrio-ventricular node
A1	adenosine receptor 1
α MHC	alpha myosin heavy chain
β -AR	beta-adrenergic-receptor
β ARK	beta-adrenergic-receptor kinase
BHF	British Heart Foundation
bp	base pair
cAMP	cyclic adenosine 3'-5' monophosphate
CaM kinase II	Ca ²⁺ /Calmodulin-dependent protein kinase II
CCPA	2 chloro-N6-cyclo-pentyladenosine
cDNA	complementary DNA from messenger RNA
CHD	coronary heart diseases
CO	cardiac output
Cre	cre recombinase
CVD	cardio vascular diseases
DNA	deoxyribonucleic acid

<i>E. coli</i>	<i>Escherichia coli</i>
ECG	electrocardiogram
ERK	extracellular signal regulated kinases
ES	embryonic stem cells
FAC	fractional area change
FFT	fast fourier transform
flx/flx	floxed floxed allele
GAP	GTPase activating protein
GAPDH	glyceraldehyde 3-phosphate dehydrogenase
GDP	guanosine diphosphate
GEF	guanine nucleotide exchange factor
GIRK	G-protein inwardly rectifying K ⁺ channel
GPCR	G-protein coupled receptor
Gα _q /Gα11	G-protein subunit that activates PLC
Gα _s /GNAS	Stimulatory subunit of G-protein
Gα _{i/o}	Inhibitory/other G-protein subunit
Gα _t	G-protein subunit of transducin
Gβγ	G beta gamma subunit
GTP	guanosine triphosphate
G ¹⁸⁴ S	glycine to serine mutation at 184 th position
HCN	hyperpolarisation activated cyclic nucleotide
HCN4-KiT	tamoxifen inducible HCN4 knock-ins

Het	heterozygous
HF	high frequency
HF	heart failure
HR	heart rate
HRV	heart rate variability
I_{CaL}	L-type Ca^{2+} current
I_f/I_h	funny current/pacemaker current
I_{KACH}/K_{Ach}	K^+ channel current activated by Ach
I_{Ks}	delayed rectifying K^+ current slow activating
I_{Kr}	delayed rectifying K^+ current rapidly activating
IP	intraperitoneal
InsP3	inosito-1,4,5 triphosphate
IVSs	interventricular septum systolic
IVSd	interventricular septum diastolic
K^+	potassium ion
kb	kilo base
KDa	kilo dalton
KIns	knock-ins
KO/ (-/-)	knock-out
LAD	left anterior descending
LF	low frequency
LV	left ventricle

LVEDP	LV end-diastolic pressure
LVEF	left ventricle ejection fraction
LVIDd	left ventricle internal dimension diastolic
LVIDs	left ventricle internal dimension systolic
LVPWd	left ventricle posterior wall diastolic
LVPWs	left ventricle posterior wall systolic
MI	myocardial infarction
ms	millisecond
M ₂ R	muscarinic acetylcholine receptor 2
M-mode	Motion mode
Na ⁺	Sodium ion
NN	Normalised beat to beat interval
PBS	phosphate buffered saline
PCR	polymerase chain reaction
PI3-Kinase	phosphatidylinositol-4,5-bisphosphate 3-kinase
PKA	protein kinase A
PLC	phospholipase C
PSD	power spectral density
PTX	pertussis toxin
RAAS	renin angiotensin-aldosterone system
RGS	regulator of G-protein signalling
RGSiGα _{i2}	RGS-insensitive G-protein subunit _{i2}

RGSiG α_0	RGS-insensitive G-protein subunit α_0
RNA	ribonucleic acid
RTK	receptor tyrosine kinase
RV	right ventricle
SAN	sino-atrial node
SDNN	standard deviation of NN
SERCA2a	sarco/endoplasmic reticulum Ca ²⁺ ATPase
SHIFT	systolic heart failure with I _f inhibitor trial
SNS	Sympathetic nervous system
SV	stroke volume
SR	sarcoplasmic reticulum
Tam	tamoxifen
TP	total power
Tris	tris-(hydroxymethyl)-amino methane
Triton-X	octylphenol-polyethyleneglycoether
TTC	Triphenyl tetrazolium chloride
U	unit
VLF	very low frequency
WHO	World Health Organisation
WT/(+/+)	wild type
KO/(-/-)	knock out

Table of Contents

Title	1
Abstract	3
Acknowledgments	6
Publications and posters	7
Commonly used abbreviations	8
Table of Contents	13
List of Figures	19
List of Tables	23
Chapter 1 Introduction	24
Introduction	25
1.1 Heart Failure	26
1.1.1 Etiology	27
1.1.2 Pathophysiology	28
1.1.3 Compensatory mechanisms	29
1.1.4 Clinical outcome of HF and treatment	35
1.2 Epidemiological studies	36
1.2.1 Framingham study	36
1.2.2 Ivabradine SHIFT (systolic heart failure treatment with If inhibitor Ivabradine trial) in human heart failure treatment	37
1.3 Autonomic control of heart rate	40
1.4 Control of sino-atrial automaticity	44
1.5 G-proteins	46
1.5.1 History and discovery of G-proteins	47
1.5.2 G-protein signalling	49
1.5.3 G-protein coupled receptor (GPCR) super family	51
1.5.4 G-protein cycle	53

1.5.5 G-protein α subunit	54
1.5.6 The 4 $G\alpha$ subclasses.....	56
1.5.7 Activation of $\beta\gamma$ signalling.....	59
1.6 Regulators of G-protein signalling (RGS)	60
1.7 G-proteins and heart rate.....	64
1.7.1 Inhibitory G-protein $G\alpha_i$	65
1.7.2 $G\alpha_i$ expression and clinical relevance	66
1.7.3 Stimulatory G-protein $G\alpha_s$	68
1.7.4 GNAS gene and products encoded by Gnas	71
1.7.5 $G\alpha_s$ expression and clinical relevance.....	74
1.8 $G\alpha_{i/o}$ versus $G\alpha_s$ mediated signalling imbalance in cardiac pathology	75
1.9 Heart Rate Variability (HRV) as a measurement of autonomic tone	78
1.10 The mouse as a model system to study cardiac electrophysiology <i>in vivo</i>	79
1.11 Animal models in heart failure	84
1.12 Hypothesis.....	86
1.13 Aims.....	87
Chapter 2 Methods and Materials	88
2.1 Overview.....	89
2.1.1 Animal breeding and general conditions	89
2.1.2 Cardiac tissue-specific $G\alpha_{i2}$ and $G\alpha_o$ deletion using α MHC recombinase.....	90
2.1.3 Specific $G\alpha_{i2}$ deletion in the conduction system	92
2.1.4 Specific $G\alpha_s$ deletion in the conduction system	93
2.1.5 Transgenic RGS insensitive G_o (RGSi G_o) and G_{i2} (RGSi G_{i2}) mice.....	94
2.2 Mouse genotyping.....	94
2.2.1 DNA extraction of tail tips.....	95
2.2.2 DNA extraction from heart and SA node.....	95
2.2.3 $G\alpha_o$ lox p floxed allele, $G\alpha_{i2}$ lox p floxed allele and α MHC cre genotyping.....	96

2.2.4 RGSiG α_{i2} and RGSiG α_o genotyping	98
2.2.5 G α_s floxed and conduction system cre (HCN4) genotyping	100
2.3 Quantitative Real-time PCR on isolated ventricle and SA nodal tissue	103
2.4 Murine electrocardiogram (ECG) telemetry and heart rate analysis	106
2.5 Telemetry probe implantation	107
2.5.1 Heart rate variability assessment	109
2.5.2 Time-domain analysis	111
2.5.3 Frequency-domain analysis	113
2.6 Pharmacological studies	116
2.6.1 Intrinsic heart rate determination	116
2.6.2 Pharmacological provocations	117
2.7 Myocardial infarction (MI) and murine left ventricular remodelling	117
2.8 Murine in vivo model of myocardial infarction	120
2.8.1 Anaesthesia	121
2.8.2 Intubation	121
2.8.3 Chest Opening	122
2.9 Murine Echocardiography	124
2.9.1 Animal preparation	125
2.9.2 Measurements	126
2.10 Tissue processing and TTC staining	128
2.11 Statistical analysis	129
Chapter 3 Results I	130
3.1 <i>In vivo</i> cardiac modulation in RGS-insensitive G α_o knock-in mice (RGSiG α_o) and RGS-insensitive G α_{i2} knock-in mice (RGSiG α_{i2})	131
3.2 RGSiG α_o and RGSiG α_{i2} mice lost diurnal variation in heart rate	132
3.3 ECG analysis reveals shorter R-R intervals in RGSiG α_o and RGSiG α_{i2} mice compared to controls	134

3.4 HRV analysis reveals loss of HRV in RGSiG α_0 but no change in RGSiG α_{i2} mice compared to control	136
3.5 Enhanced bradycardic response to carbachol (M ₂ receptor agonist) with RGSiG α_0 and RGSiG α_{i2} mice	139
3.6 A1 receptor agonist (CCPA) showed increased inhibition with RGSiG α_0 mice but not with RGSiG α_{i2} mice	139
Discussion	141
3.7 RGSiG α_{i2} and RGSiG α_0 mice showed enhanced resting tachycardia and bradycardic responses with agonists	141
Chapter 4 Results II	144
4.1 Heart rate modulation in cardiac-specific deletion of G α_{i2} and G α_0 with α MHC cre	145
4.2 Cardiac specific-deletion of G α_{i2} and G α_0 with α MHC cre	147
4.3 Preservation of diurnal variation in heart rate in G α_{i2} flx/flx cre ⁺ and G α_0 flx/flx cre ⁺ mice	148
4.4 HRV in mice with cardiac-specific G α_{i2} and G α_0 deletion with α MHC cre is similar to control	149
Discussion	154
4.5 Mice with cardiac-specific deletion of G α_{i2} and G α_0 with α MHC cre exhibited no specific phenotype differences from their littermate controls	154
Chapter 5 Results III	157
5.1 Heart rate modulation in conduction system-specific deletion of G α_{i2} and G α_s with a conduction system cre (HCN4 cre ⁺)	158
5.2 Study plan for tamoxifen-induced cre deletion in the conduction system	159
5.3 Real-time PCR shows deletion of G α_{i2} and G α_s in SA nodal tissues	159
5.4 Diurnal variation in heart rate was lost in mice with conduction system-specific deletion of G α_{i2} and G α_s	161
5.5 HRV analysis reveals selective loss of the HF component in the conduction system-specific G α_{i2} knock-out mice	164
5.6 HRV analysis reveals selective loss of the LF component in the conduction system-specific G α_s knock-out mice	165

5.7 No change in ECG parameters measured by ambulatory telemetry in mice with conduction system-specific deletion of $G\alpha_{i2}$ and $G\alpha_s$	170
5.8 Intrinsic heart rate determination	172
5.9 Pharmacological modulation of heart rate	176
Discussion	178
5.10 Mice with conduction system-specific knock-out of $G\alpha_{i2}$ and $G\alpha_s$ with tamoxifen-induced cre showed patterns in HRV and ECG different from controls	178
Chapter 6 Results IV	182
6.1 Ventricular remodelling in $G\alpha_s$ flx/flx HCN4 cre ⁺ and $G\alpha_{i2}$ flx/flx HCN4 cre ⁺ mice after myocardial infarction	183
6.2 Survival rates in $G\alpha_{i2}$ flx/flx HCN4 cre ⁺ and $G\alpha_s$ flx/flx HCN4 cre ⁺ mice after MI ...	183
6.3 M-mode Echocardiography shows impaired LV function	184
6.4 $G\alpha_s$ flx/flx HCN4 cre ⁺ mice were found to be bradycardic and $G\alpha_{i2}$ flx/flx HCN4 cre ⁺ mice were found to be tachycardic under anaesthesia	185
6.5 Fractional shortening was not changed in $G\alpha_s$ flx/flx HCN4 cre ⁺ mice while it was reduced in $G\alpha_{i2}$ flx/flx HCN4 cre ⁺ mice post MI	187
6.6 There is no change in ejection fraction in $G\alpha_s$ flx/flx HCN4 cre ⁺ mice, while it is decreased in $G\alpha_{i2}$ flx/flx HCN4 cre ⁺ mice post MI	189
6.7 FAC% was found to be enhanced in $G\alpha_s$ flx/flx HCN4 cre ⁺ mice, while there was no change in $G\alpha_{i2}$ flx/flx HCN4 cre ⁺ mice	191
6.8 Structural analysis of left ventricular chamber shows changes in $G\alpha_s$ flx/flx HCN4 cre ⁺ mice but not in $G\alpha_{i2}$ flx/flx HCN4 cre ⁺ mice	193
6.9 Hypertrophy was observed in $G\alpha_{i2}$ flx/flx HCN4 cre ⁺ mice but not in $G\alpha_s$ flx/flx HCN4 cre ⁺ mice post MI	196
6.10 Triphenyltetrasodium chloride (TTC) staining reveals infarct size was found to be similar in all groups	197
Discussion	202
6.11 LV dysfunction and remodelling was not observed with $G\alpha_s$ HCN4 cre ⁺ mice after MI	202
6.12 LV remodelling was not remarkable in $G\alpha_{i2}$ HCN4 cre ⁺ mice after MI	203
6.13 Role of calcium in cardiac hypertrophy	205

Summary	209
Future directions	211
Bibliography	213

List of Figures

Figure 1.1 Neurohormonal and compensatory mechanisms in heart failure	33
Figure 1.2 Mean heart rate in ivabradine and placebo group over the study period	40
Figure 1.3 The opposing effect of sympathetic and parasympathetic system	43
Figure 1.4 Heterotrimeric G-protein signalling	51
Figure 1.5 The G-protein cycle	54
Figure 1.6 Activity of RGS proteins.	61
Figure 1.7 RGS-insensitive mutation or RGS knock-ins	62
Figure 1.8 Organisation and imprinting of GNAS locus.	73
Figure 1.9 Sympathetic and parasympathetic interactions.....	77
Figure 1.10 Comparison of human and murine cardiac action potentials	83
Figure 2.1 Cre lox-P mediated $G\alpha_{i2}$ and $G\alpha_o$ deletion	91
Figure 2.2 Generation of conduction system-specific $G\alpha_s$ mice.....	93
Figure 2.3 Gel of PCR of $G\alpha_{i2}$ floxed, $G\alpha_o$ floxed and cre allele	98
Figure 2.4 Gel of PCR of RGSi $G\alpha_{i2}$ and RGSi $G\alpha_o$ genotyping.....	100
Figure 2.5 Gel PCR of $G\alpha_{i2}$ flx/flx, $G\alpha_s$ flx/flx and cre allele	102
Figure 2.6 Real-time PCR using Taqman probe	105
Figure 2.7 Schematic diagram of murine telemetry and ambulatory ECG.....	107

Figure 2.8 Representative ECG telemetry and power spectral density transformation.....	111
Figure 2.9 Surgical set up for <i>in vivo</i> MI model	121
Figure 2.10 LAD occlusion in the mouse – positioning and ST elevation	123
Figure 2.11 Diagrams for basic mouse echocardiographic views	126
Figure 2.12 Wall dimension measurements on M-mode echocardiography	127
Figure 3.1 Loss of diurnal heart rate response in RGSiG α_0 and RGSiG α_{i2} mice	133
Figure 3.2 Representative ECG traces from RGSiG α_0 and RGSiG α_{i2} mice	135
Figure 3.3 HRV signatures in RGSiG α_0 and RGSiG α_{i2} mice	137
Figure 3.4 Representative PSD from RGSiG α_0 and RGSiG α_{i2} mice.....	138
Figure 3.5 Inhibition of heart rate by M ₂ R and A ₁ R on RGSiG α_0 and RGSiG α_{i2} mice	140
Figure 4.1 RT-PCR showing deletion of G α_{i2} and G α_0 in the cardiac tissue	148
Figure 4.2 Preservation of diurnal variation in the heart rate in G α_{i2} flx/flx cre ⁺ G α_0 flx/flx cre ⁺ and WT littermate controls	149
Figure 4.3 HRV in G α_{i2} flx/flx cre ⁺ and G α_0 flx/flx cre ⁺ mice presented in the time- domain recorded from conscious freely moving mice.....	151
Figure 4.4 HRV in G α_{i2} flx/flx cre ⁺ and G α_0 flx/flx cre ⁺ mice presented in the frequency-domain recorded from conscious freely moving mice	152
Figure 5.1 Study plan for tamoxifen-induced cre deletion in the conduction system	159
Figure 5.2 Real-time PCR showing cre-mediated deletion in SA node tissues of G α_{i2} and G α_s mice	160

Figure 5.3 Mean day and night heart rate in mice with selective $G\alpha_{i2}$ and $G\alpha_s$ deletion in the conduction system.....	163
Figure 5.4 HF and LF power in $G\alpha_{i2}$ flx/flx HCN4 cre ⁺ mice before and after tamoxifen	165
Figure 5.5 HF and LF power in $G\alpha_s$ flx/flx HCN4 cre ⁺ mice before and after tamoxifen	167
Figure 5.6 HRV from power spectral density (PSD) plots in $G\alpha_s$ flx/flx HCN4 cre ⁺ and $G\alpha_{i2}$ flx/flx HCN4 cre ⁺ mice	168
Fig 5.7 Representative ECG traces from $G\alpha_s$ flx/flx HCN4 cre ⁺ and $G\alpha_{i2}$ flx/flx HCN4 cre ⁺ mice	172
Figure 5.8 Autonomic blockade in $G\alpha_{i2}$ flx/flx HCN4 cre ⁺ and $G\alpha_s$ flx/flx HCN4 cre ⁺ mice.....	174
Figure 5.9 Response of heart rate to pharmacological agents.....	177
Figure 6.1 Study plan for the myocardial infarction protocol.....	184
Figure 6.2 Representative M-mode image of a control mouse before and after MI.....	185
Figure 6.3 Heart rate in $G\alpha_{i2}$ flx/flx HCN4 cre ⁺ and $G\alpha_s$ flx/flx HCN4 cre ⁺ mice before and after tam and before and after MI	186
Figure 6.4 FS% in $G\alpha_s$ flx/flx HCN4 cre ⁺ and $G\alpha_{i2}$ flx/flx HCN4 cre ⁺ mice before and after tam and before and after MI	188
Figure 6.5 EF% in $G\alpha_s$ flx/flx HCN4 cre ⁺ and $G\alpha_{i2}$ flx/flx HCN4 cre ⁺ mice before and after tam and before and after MI	190

Figure 6.6 Measurement of FAC % by tracing the endocardial border and FAC% in $G\alpha_s$ flx/flx HCN4 cre ⁺ and $G\alpha_{i2}$ flx/flx HCN4 cre ⁺ mice before and after MI	192
Figure 6.7 LVPWd and LVIDd measurements in $G\alpha_s$ flx/flx HCN4 cre ⁺ and $G\alpha_{i2}$ flx/flx HCN4 cre ⁺ mice before and after MI.....	195
Figure 6.8 Heart weight : body weight and LV mass in $G\alpha_s$ flx/flx HCN4 cre ⁺ and $G\alpha_{i2}$ flx/flx HCN4 cre ⁺ mice before and after MI.....	197
Figure 6.9 TTC staining and % infarct size after MI.....	199
Figure 6.10 Role of Ca ²⁺ in the hypertrophy signalling pathway	207

List of tables

Table 1.1 Current management of HF patients	36
Table 1.2 Imprinting pattern of GNAS locus.....	70
Table 2.1 Commonly used heart failure models	117
Table 3.1 ECG and HRV parameters in conscious ambulatory telemetered RGSiG α_0 and RGSiG α_{i2} mice	136
Table 4.1 Comparison of effect of Global KOs of G α_{i2} and G α_0 on heart rate dynamics ..	146
Table 4.2 HRV and ECG parameters measured in the time and frequency-domains during conscious ambulatory telemetry G α_{i2} flx/flx cre ⁺ , G α_0 flx/flx cre ⁺ and their WT littermate controls	153
Table 5.1 Summarised HRV parameters for mice with conditional G α_{i2} deletion and G α_s deletion compared with littermate controls in time and frequency-domains	169
Table 5.2 Mean ECG parameters in conscious ambulatory mice with conditional G α_{i2} deletion and G α_s deletion compared with littermate controls	171
Table 5.3 HRV parameters after atropine and propranolol (autonomic blockade) in G α_{i2} flx/flx HCN4 cre ⁺ and G α_s flx/flx HCN4 cre ⁺ mice.	175

Chapter 1

INTRODUCTION

Introduction

Cardiovascular disease (CVD) includes all the diseases of the heart and circulation including coronary heart disease (CHD) which includes angina and myocardial infarction, heart failure, congenital heart disease, stroke and peripheral vascular disease - caused by narrowing of the arteries to the peripheries. CVD continues to be the most common threat to life and health in spite of a major decrease in mortality rates. The life time risk of developing CHD after 40 is 49% in men and 32% in women (Lloyd-Jones et al. 1999). In 2010 CVD was the UK's biggest killer. Almost 180,000 people died from CVD, around 80,000 of these deaths being from CHD and around 49,000 from stroke. In the same year CVD caused 46,000 premature deaths in UK; 68% of these were men. Collectively, heart and circulatory diseases cause more than **a quarter of all deaths** in the UK (BHF statistics 2012). It is predicted that by 2020, CVD will annually claim 25 million deaths worldwide, and will surpass infectious disease as the world's number one cause of death and disability (Braunwald et al. 2001). Myocardial infarction (MI) is the most common presentation of CVD. A heart attack (myocardial infarction) is usually caused by a blood clot (thrombosis), which precipitates as a result of rupture of plaques or deposits (atheroma) in the inner lining of arteries, which in turn initiates blood clot formation and stops the blood flowing to a part of the heart muscle. This puts the heart muscle at high risk of dying unless the blockage is quickly removed. Myocardial infarction (MI) leads to necrotic heart muscle and hence leads to impaired cardiac function. If left untreated, this can lead to further complications such as heart failure (which is discussed in depth in this thesis), abnormal heart rhythm or a further MI. The good news is that mortality from CVD is falling and the credit for this can be attributed to the use of innovative, preventive and therapeutic measures developed as a result of cardiovascular research.

There is an increase in use of laboratory animals for cardiovascular research and a vast number of animal models have been developed to model human diseases and investigate their physiological and pathological processes. Animal models of heart failure play an important role here by helping us to analyse physiological effects of cardiac dysfunction and also to understand the genetic mechanism underlying heart failure which will further help to improve therapies for the future. It has become clear that the analysis of rodent and in particular gene-targeted murine models of cardiac disease gives important insights into the pathogenesis of abnormal heart function and rhythm in man. This gives us an experimental platform to further investigate and explore more developmental pharmacological agents that might be of benefit to patients. In this thesis I will discuss the role of the well-known signalling proteins - G-proteins ($G\alpha_s$ - stimulatory G-protein and $G\alpha_i$ - inhibitory G-protein), in controlling the heart rate and their role in heart failure using murine models.

1.1 Heart Failure

Heart failure (HF) is the end stage of many cardiac diseases. It is a growing public health concern for which, despite effective therapy, outcome remains poor with a 5-year mortality at 50% (Braunwald, Zipes, & Libby 2001). Clinically, HF is a chronic and severely debilitating syndrome that generally ends up in a vicious cycle of progressive functional decline and it is characterized by the insufficient pumping of blood to meet the needs of the body (Cannavo et al. 2013). It is estimated that over 100,000 annual admissions to hospital medical wards in the UK have heart failure and this accounts for 5% of total admissions. In the UK the overall prevalence of heart failure is 3-20 per 1000 population, although this exceeds 100 per 1000 in those aged 65, years and over. Although the annual incidence of heart failure is 1-5 per 1000, the

relative incidence doubles for each decade of life after age 45. With an increasingly ageing population and improved survival of patients with impaired cardiac function due to newer therapeutic advances in the management of acute MI, the overall percentage is likely to increase in the future (Davis et al. 2000). Two million new cases of HF are diagnosed worldwide, leading to a prevalence of over 22 million people across the globe (WHO, Cardiovascular Diseases, Fact sheet no.317). The 30 year follow up Framingham epidemiological heart study (a longitudinal study on HF) which started in 1948, shows that prevalence of HF increased dramatically with increasing age, with doubling of prevalence with each decade and it is more common in males until the age of 65, after which the prevalence is equal among both the sexes and the survival rate in women is much better than in males (Ho et al. 1993). But later studies show that at any given age prevalence of CVD is more among men (12-15%) than in women (Roger et al. 2011). Data from Framingham study also indicates that hypertension, coronary heart diseases, diabetes mellitus and ventricular hypertrophy are associated with increased risk of heart failure. Unfortunately, as many features of heart failure are not organ specific, in the past it was difficult to diagnose clinically and there may be few clinical features in the early stages of the disease. Due to advancement in technologies, early recognition of heart failure is now possible and it is important also, as modern drug treatment has the potential to reduce hospital admission rates, slow the rate of disease progression, improve symptoms and quality of life and improve survival (Davis, Hobbs, & Lip 2000).

1.1.1 Etiology

Sir Thomas Lewis (1933) said it very well, “The very essence of cardiovascular practice is the early detection of heart failure” (Lewis 1933). Heart failure emanates

from injury to the myocardium from a variety of causes including ischemic heart disease, hypertension and diabetes. Less common etiologies include cardiomyopathies, valvular disease, myocarditis, infections, systemic toxins, and cardio toxic drugs. Pre-existing hypertension is quite common in HF patients and this risk factor alone doubles the risk of developing HF compared to normotensive patients. As the heart fails, patients develop symptoms which include dyspnea from pulmonary congestion, and peripheral oedema and ascites from impaired venous return. Symptoms such as nausea, lack of appetite, and fatigue are also prevalent. Heart failure involves changes in the contractility, electrical conduction and energy metabolism of the heart, making it difficult to cope with circulatory demands (Stanley et al. 2005). This in turn leads to neurohormonal compensatory mechanisms that occur as the failing heart attempts to maintain adequate function. Although initially beneficial in the early stages of heart failure, compensatory mechanisms eventually lead to a vicious cycle of worsening heart failure. Henceforth, the physiological and gene expression changes observed in heart failure are not constantly 'adaptive' or 'maladaptive' and because of this reason it is not easily responsive to pharmacological modulations and thus has introduced therapeutic confusion over the years (Breckenridge 2010).

1.1.2 Pathophysiology

Cardiac output (CO) is defined as the amount of blood pumped by the heart over a given time period and is the product of heart rate (HR) and stroke volume (SV). SV is the blood ejected by the ventricle per beat and is affected by various factors like synergistic ventricular contraction, wall integrity and valvular competence. The primary abnormality in non-valvular heart failure is impairment in left ventricular

function, leading to a fall in cardiac output. This left ventricular (LV) dysfunction can be either systolic (impaired contraction and ejection) or diastolic (impaired relaxation and filling) and 70% of the patients with HF have systolic dysfunction. LV systolic dysfunction is defined as a LVEF (Left Ventricle Ejection Fraction) less than 40% and the leading cause of LV systolic dysfunction is due to the loss of functional myocardium due to ischemic disease and infarction, uncontrolled hypertension leading to excessive pressure overload and also from impaired contractility from cardiotoxic drugs. One of the consequences of LV dysfunction is decreased CO and this causes an increase in the amount of blood in the ventricle and therefore an increase in both end-systolic and end-diastolic volumes. This further leads to an increase in LV end-diastolic pressure (LVEDP) which causes increase in left atrial pressures which further lead to an increase in the pressure of the capillaries in the lungs. The fluid from the pulmonary capillaries is forced out due to this elevated pressure in the lungs and leads to pulmonary congestion and is the major clinical symptom of dyspnea. On the other hand the most common cause of right ventricular (RV) failure is LV failure. As the RV fails, there is a similar reduction in CO, increase in the amount of blood in the ventricle, which further leads to increased right atrial pressure and increased pressure in the venacaval system which diminishes venous drainage from the body. This leads to increased pressure in organs like the liver, the gastrointestinal tract and the lower extremities which further leads to the clinical signs and symptoms of abdominal pain, hepatomegaly, and peripheral oedema (Kemp and Conte 2012).

1.1.3 Compensatory mechanisms

The fall in cardiac output sparks the stimulation of several neurohormonal compensatory mechanisms which play a crucial role in the early stages of HF, directed

at improving the mechanical neighbourhood of the heart (Fig 1.1). For example, activation of the sympathetic system, with an increase in heart rate, increased myocardial contractility and peripheral vasoconstriction (increased catecholamines-norepinephrine and epinephrine) tries to maintain cardiac output. Chronic sympathetic activation however has detrimental effects, causing a further deterioration in cardiac function. Sympathetic activity in the heart, further leads to an increase in sympathetic outflow to the skeletal muscle and the kidneys. Continued sympathetic stimulation activates the renin-angiotensin-aldosterone system (RAAS) and other neurohormones, leading to increased vascular tone, increased plasma noradrenaline concentrations, progressive retention of salt and water and finally edema. Excessive sympathetic activity is also associated with cardiac myocyte apoptosis, hypertrophy and myocardial necrosis (Jackson, Gibbs, Davies, & Lip 2000). The sympathetic nervous system exerts its effects through the adrenoreceptors: β_1 , β_2 , and α_2 . In HF patients, along with the α_2 receptors, both β_1 and β_2 receptors are activated which eventually leads to myocardial toxicity, marked by decreased EF, arrhythmias and tachycardia due to overstimulation by the sympathetic nervous system (SNS) (Kemp & Conte 2012). Activation of the β_1 and α_1 receptors in the peripheral vasculature, leads to activation of RAAS which causes vasoconstriction, sodium retention and thirst (Chaggar et al. 2009). In the long run, by a down regulation in β receptors, the ability of the myocardium to respond to chronic high concentrations of catecholamines is crippled, although this may be associated with baroreceptor dysfunction and a further increase in sympathetic activity. Abnormalities of baroreceptor function are well reported in chronic heart failure, along with reduced parasympathetic tone, leading to abnormal autonomic modulation of the sinus node. In chronic heart failure patients, a reduction in heart rate variability (HRV) has consistently been observed potentially

due to excess SNS activity and concurrent reduced vagal modulation of the sinus node. Reduced HRV is a prognostic marker in patients with chronic heart failure (Jackson, Gibbs, Davies, & Lip 2000).

Stimulation of RAAS also results in vasoconstriction (increased angiotensin II), an increase in blood volume with the retention of salt and water (increased aldosterone). Renin is secreted by the kidneys in response to this sympathetic activation and also due to diminished renal blood flow from a decrease in mean arterial pressure (MAP). Renin then acts on angiotensinogen in the liver to make angiotensin I. Angiotensin-converting enzyme (ACE) converts circulating angiotensin I in the lungs to angiotensin II which directly increases vasoconstriction and promotes the release of aldosterone. Activation of this particular neurohormonal system facilitates release of norepinephrine, promotes sodium reabsorption, stimulates vasopressin release, and increases contractility in the end. Vasopressin a peptide hormone and a vasoconstrictor, is synthesized in the hypothalamus and secreted by the posterior pituitary gland. Its release is facilitated by angiotensin II formation and is also controlled via a negative feedback loop. In HF patients the central baroreceptors detect the fall in MAP, which decreases their inhibitory impulses to the hypothalamus, thereby lifting the negative regulation and leading to an increase in vasopressin release. Increased vasopressin causes vasoconstriction as well as increased water retention, both of which enhance the decrease in MAP in HF (Kemp & Conte 2012; Rea and Dunlap 2008).

Natriuretic peptides exert a wide range of effects on different organs like the heart, kidneys and central nervous system. Atria release atrial natriuretic peptide in response to an increase in cardiac chamber volume, leading to natriuresis (excretion of sodium

via urine) and vasodilatation. In humans, brain natriuretic peptide is also released from the heart, predominantly from the ventricles, and its actions are similar to those of atrial natriuretic peptide. Another variant, C-type natriuretic peptide has less effect on natriuresis and vasodilatation and is limited to the vascular endothelium and central nervous system. The atrial and brain natriuretic peptides act as physiological antagonists to the effects of angiotensin II on vascular tone, aldosterone secretion and renal-tubule sodium reabsorption and their levels increase in response to volume expansion and pressure overload of the heart. There has been interest in modulating natriuretic peptide pathways in patients with heart failure in the diagnostic and therapeutic potential of these peptides (Jackson, Gibbs, Davies, & Lip 2000).

Another potent vasoconstrictor is endothelin which is secreted by vascular endothelial cells and it has definite vasoconstrictor effects on the renal vasculature, promoting the retention of sodium. The concentration of endothelin-1 in plasma is increased in proportion to the symptomatic and haemodynamic severity of heart failure and has prognostic significance. Due to the vasoconstrictor properties of endothelin, there is an interest in developing endothelin receptor antagonists as cardio-protective agents which inhibit endothelin-mediated vascular and myocardial remodelling (Jackson, Gibbs, Davies, & Lip 2000).

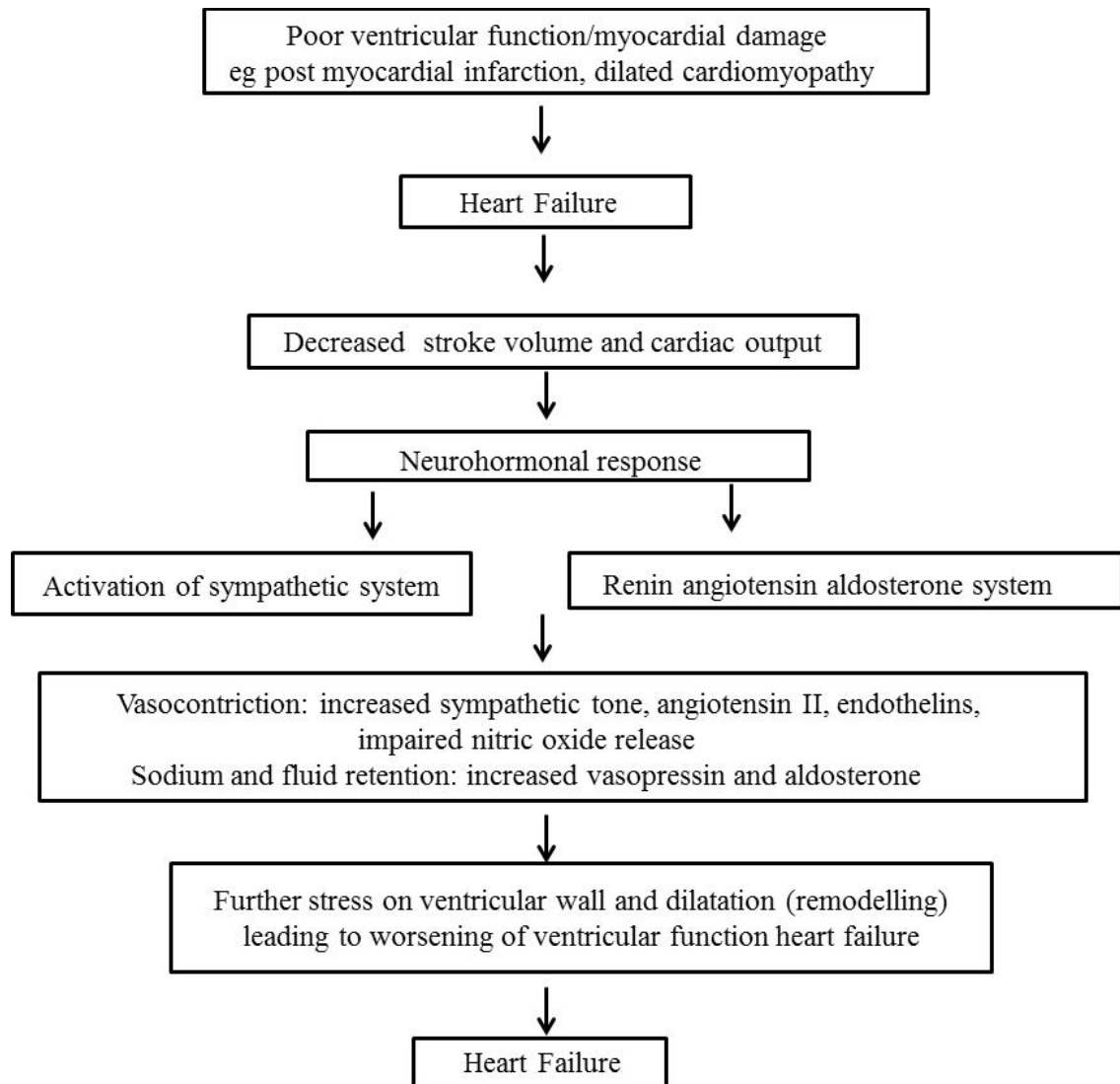


Figure 1.1 Neurohormonal and compensatory mechanisms in heart failure. Adapted from (Jackson et al. 2000).

During early-stages of HF, these neurohormonal systems play an important role, nevertheless long-term results of activation of these systems result in ventricular remodelling which further accelerates myocardial dysfunction. Furthermore, there may be progressive cardiac dilatation or alterations in cardiac structure (remodelling) or both. The sustained haemodynamic stresses on the heart lead to alterations in the size, shape, structure and function of the ventricle in a process known as remodelling (Curry et al. 2000). There are changes in ventricular mass, composition and volume as

remodelling happens and the overall geometry of the ventricles changes as it becomes less elliptical and more spherical. These remodelling-induced geometric changes initially are compensatory as a failing heart enlarges to increase ventricular volume which leads to greater SV and higher CO despite a reduced EF. Ventricular contractility is also increased by myocardial wall thickness and an overall increase in ventricular mass. The remodelling process in HF is progressive and eventually becomes deleterious. The enlargement of the ventricles further leads to hypertrophy of the myocardium, this leads to increased ventricular wall tension and later fibrosis. All this impairs the contractility of the cardiac muscles and eventually leads to an increase in myocardial apoptosis. In addition, the pumping action of the heart is impaired as there is significant contractile dyssynchrony in the dilated and remodelled ventricle.

The neurohormonal systems that are activated in HF are constantly switched on in an attempt to compensate for the failing heart's inability to maintain normal cardiovascular homeostasis. The haemodynamic abnormalities present in HF are aggravated by the sustained presence of the circulating neurohormones which, in a vicious cycle, encourage further remodelling and neurohormone release and further haemodynamic deterioration. Continued progression of HF eventually leads to a severe reduction in blood flow to all vital organs. In this terminal phase, to redirect blood flow to these critical organ systems the body maximizes all of its vasoconstrictive mechanisms, which only add to the haemodynamic burden of the failing heart; thus, ventricular function continuously worsens, and terminal HF sets in (Kemp & Conte 2012).

1.1.4 Clinical outcome of HF and treatment

Diagnosis of heart failure is made by observing clinical symptoms and signs consistent with heart failure, which are reduced LVEF (left ventricular function), dyspnea, elevated jugular venous pressure, ankle oedema, hepatomegaly, enlarged heart silhouette and presence of pulmonary congestion or pleural effusion on chest x-ray and also by the presence of arrhythmias or conduction disturbances by electrocardiogram (ECG). Initially during HF, SNS hyperactivity serves to compensate for the reduced cardiac output, but long-term exposure to high levels of circulating catecholamines causes maladaptive changes to the heart through dysregulation of their β -adrenergic receptor (β -AR) targets and also causes myocyte death that leads to maladaptive remodelling of the stressed and failing heart (Woo and Xiao 2012). Pharmacological intervention with β -AR antagonists, inhibitors of angiotensin II and aldosterone and diuretics are currently standard treatments for HF (Table 1.1). Diuretics relieve fluid retention and improve exercise tolerance. ACE inhibitors block the conversion of angiotensin I to angiotensin II and reduce activation of RAAS. β -blockers help to slow down the heart rate and allow efficient contraction (Kemp & Conte 2012). Introduction of these pharmacological interventions have substantially increased survival and decreased morbidity in HF. However, β -blockers and other neurohormonal blocking strategies are still not ideal therapies as not all patients respond favourably to these agents. Also anti arrhythmic drugs can increase the risk of new arrhythmias while suppressing others (Coplen et al. 1990; Echt et al. 1991). Electronic devices resynchronize the normal ventricular activation cycle and terminate life-threatening arrhythmias. However, there are limitations to this technology featuring complications such as pulmonary collapse, haemorrhage, bacterial infection and lead/ generator failure (Cho and Marban 2010). So currently

HF therapy is nonspecific or rather palliative and thus, new therapeutic strategies are urgently needed. In this regard, a deeper understanding of the underlying biology and molecular mechanisms contributing to the development and progression of the disease will open up prospects for new alternatives for future therapeutic advances.

Table 1.1 Current management of HF patients (Kemp & Conte 2012)

Stage A At high risk	Stage B Asymptomatic structural heart disease	Stage C Symptomatic structural heart disease	Stage D Refractory HF
Therapy	Therapy	Therapy	Therapy
Treat hypertension	Everything under stage A	Everything under stage A	Everything under stage A,B and C
Treat lipid disorders	ACE inhibitors β blockers	ACE inhibitors β blockers	Mechanical assist devices Heart transplantation
Regular exercise		Diuretics	Continuous IV infusions
Discourage alcohol		Digitalis	Hospice care
ACE inhibitors		Dietary salt restriction	

1.2 Epidemiological studies

1.2.1 Framingham study

The Framingham study is one of the first epidemiological studies which examined incidence, prevalence and prognosis of congestive heart failure where patients and their offspring were followed for four decades. The study enrolled 5,209 residents of Framingham, Massachusetts aged between 28 and 62 in 1948 who were evaluated at 2 year intervals for medical history, physical examination, investigations like an ECG, incidence of angina, myocardial infarction, blood pressure monitoring and other

laboratory tests. In 1971 offspring of these participants and their spouses aged 6 to 70 years were studied in the Framingham offspring study with a follow-up after 8 and 12 years. The mean age for incidence of heart failure (presence of either diastolic or systolic dysfunction) was 70 ± 10.8 years. The incidence of heart failure dramatically increased with age and was one third lower in women than in men after adjustment for age. The prevalence of congestive heart failure also increased with age. It was found that hypertension, diabetes and left ventricular hypertrophy were the main risk factors contributing to heart failure while serum cholesterol and smoking had less effect. Even though improved therapies became available to treat ischemic heart disease and hypertension, the age-adjusted incidence of heart failure has decreased only by 11-17% per decade during this 40 year period of the study and is associated with a shorter life-span than many other diseases. Use of vasodilators and ACE inhibitors can prolong survival but come with their own disadvantages. So improved therapies and strategies are in demand for the treatment of heart failure by taking into consideration the heterogeneous nature of this syndrome (Ho, Pinsky, Kannel, & Levy 1993).

1.2.2 Ivabradine SHIFT (systolic heart failure treatment with I_f inhibitor Ivabradine trial) in human heart failure treatment

Clinical trials, along with epidemiological studies clearly establish a strong link between heart rate and associated risk in patients with a wide range of cardiac diseases. At present, β -blockers are widely in use to treat heart failure and acute myocardial infarction and due to their heart rate lowering effect; their usage has reduced morbidity and mortality in the past few decades. Raised resting heart rate is a major risk factor for fatality for all cardiovascular diseases. In patients with coronary

artery disease and left-ventricular dysfunction, a heart rate of 70 beats per minute (bpm) or higher is associated with a 34% increased risk of cardiovascular death and a 53% increase in admission to hospital for heart failure compared with heart rate lower than 70 bpm (Fox et al. 2008). Despite treatment with β -blockers, heart rate remains increased in most patients which necessitate new therapeutic strategies. Ivabradine is a selective inhibitor of the I_f ion channel found in cardiac pacemaker cells of the sinoatrial node (DiFrancesco 2006). This drug reduces heart rate at rest while maintaining myocardial contractility and atrioventricular conduction even in patients with impaired systolic function and it was used in this trial to tease out the effect of heart rate lowering (Fox, Ford, Steg, Tendera, Robertson, & Ferrari 2008). The SHIFT trial was reported in 2010 with the aim of evaluating the addition of ivabradine to standard therapy on the symptoms, quality of life and mortality in participants with chronic heart failure. SHIFT was a multinational, randomised, double blind, placebo controlled clinical trial in patients with moderate to severe heart failure with a heart of rate 70 bpm and above and on treatment with β -blockers and RAAS antagonists. With an ivabradine dose of 7.5 mg twice daily along with other treatment drugs, heart rate was maintained between 50-60 bpm in most of the patients and primary end point was a combination of cardiovascular death or hospital admission for worsening heart failure. The main findings were that 29% of the placebo group had a cardiovascular death or hospital admission for worsening heart failure (primary end point) compared to 24% in the ivabradine group. Hospital admissions (other end point) were found to be only 16% in the ivabradine group compared to 21% in the placebo group. Deaths (mortality end point) from heart failure were 3% in the ivabradine group compared to 5% in the placebo group. Treatment with ivabradine was associated with an average reduction in heart rate of 15 bpm from a baseline value of 80bpm which was

maintained largely throughout the course of the study (Fig. 1.2). Symptomatic and asymptomatic bradycardia was more commonly observed in the ivabradine group than in the placebo group. These findings support the idea that heart rate plays a significant role in the pathophysiology of heart failure and the modulation of heart rate can hinder the progression of the disease. The effect of ivabradine was achieved together with β -blockers, so assumptions about the effect of ivabradine per se in the absence of β -blockers cannot be drawn. But SHIFT was the first trial to explicitly study the effect of isolated heart rate reduction in a population with heart failure. So these results suggest the role of ivabradine in reducing the heart rate and improving clinical outcomes in heart failure (Swedberg, Komajda, Bohm, Borer, Ford, Dubost-Brama, Lerebours, & Tavazzi 2010).

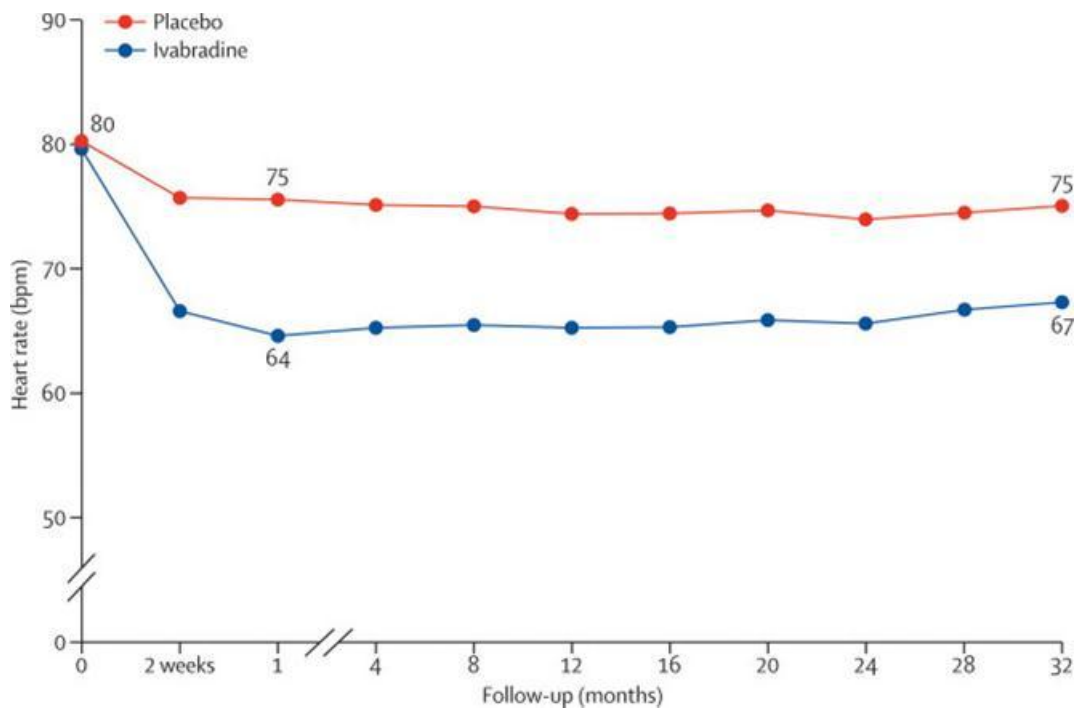


Figure 1.2 Mean heart rate in ivabradine and placebo group over the study period. There was a significant reduction in heart rate in the ivabradine group compared to the placebo group (Swedberg et al. 2010).

1.3 Autonomic control of heart rate

Cardiac automaticity or heart rate is controlled by both the sympathetic and the parasympathetic nervous system and they are opposing in nature. More specifically release of acetylcholine (Ach) from vagal nerve efferents slows down the heart rate while stimulation by β adrenergic signals has the opposite effect. There are two potential electrophysiological mechanisms in cardiac pacemaking tissues i.e. sino-atrial node (SAN) and atrio-ventricular node (AVN). Stimulation of the sympathetic nervous system in response to exercise or stress results in a rapid increase in heart rate, which is mediated by activation of the stimulatory G-proteins (G_{α_s}) coupled to β -AR. Subsequently, adenylyl cyclase is activated, which leads to an increase in cAMP level and activation of protein kinase A (PKA). A wide spectrum of ion channels (pacemaker current (I_f), delayed rectifier current (I_{Ks}), L-type Ca^{2+} current (I_{CaL})) can

be regulated by phosphorylation or by direct binding of cyclic nucleotides, leading to increased pacemaker currents (I_f or I_h) (DiFrancesco 2006;Robishaw and Foster 1989). On the other hand, vagal stimulation by Ach suppresses activation of adenylyl cyclase through muscarinic receptors (M_2R) which are coupled to inhibitory G-proteins ($G_{\alpha_i/o}$), there by counteracting the effect of the sympathetic activation. Meanwhile, $G\beta\gamma$ subunits released from $G_{\alpha_i/o}$ can directly activate G protein-coupled inward rectifying K^+ channels (GIRK) (Fig. 1.3). This GIRK channel activation results in membrane hyperpolarisation and heart rate slowing (Wickman et al. 1998;Yamada et al. 1998). The generation of GIRK4 knockout mice (Wickman, Nemec, Gendler, & Clapham 1998) clearly demonstrated that this second-messenger-independent pathway contributes to ~50% of the bradycardic response mediated by M_2R without affecting basal heart rate. Even though the GIRK channel is characteristically activated by Ach binding to muscarinic (M_2) receptors they are also stimulated via adenosine, sphingosine-1-phosphate and endothelin-A receptors in the heart (Bosche et al. 2003;Ochi et al. 2006;Ono et al. 1994;Ono et al. 2001).

Adenosine a catabolite of ATP reduces myocardial injury by binding to four specific adenosine receptors or purinergic receptors: A_1 , A_{2a} , A_{2b} , and A_3 . A_1 and A_3 receptors are coupled through G_{α_i} protein to adenylyl cyclase (AC) inhibition, while A_{2a} and A_{2b} receptors are coupled to AC activation through G_{α_s} protein. However, adenosine metabolism and its receptor mediated signalling in patients with chronic heart failure remain unclear (Asakura et al. 2007). Ischemic preconditioning involves a series of intracellular events that are initiated with the activation of the A_1 receptor, and end at the K^+ sensitive ATP channels of the mitochondria. The phosphorylation and opening of these channels would cause the protective effect (Donato et al. 2003). Another

study (Kirchhof et al. 2003) used transgenic mice over expressing A₁R and found that these mice had an increased tolerance to ischemia. A₁R overexpression slows heart rate in isolated hearts suggesting that A₁R contribute to the physiological regulation of heart rate and AV nodal function in mice *in vivo* and that an enhanced expression or function of A₁R may represent a potential patho-mechanism by which A₁R could contribute to sinus node and AV nodal dysfunction in patients.

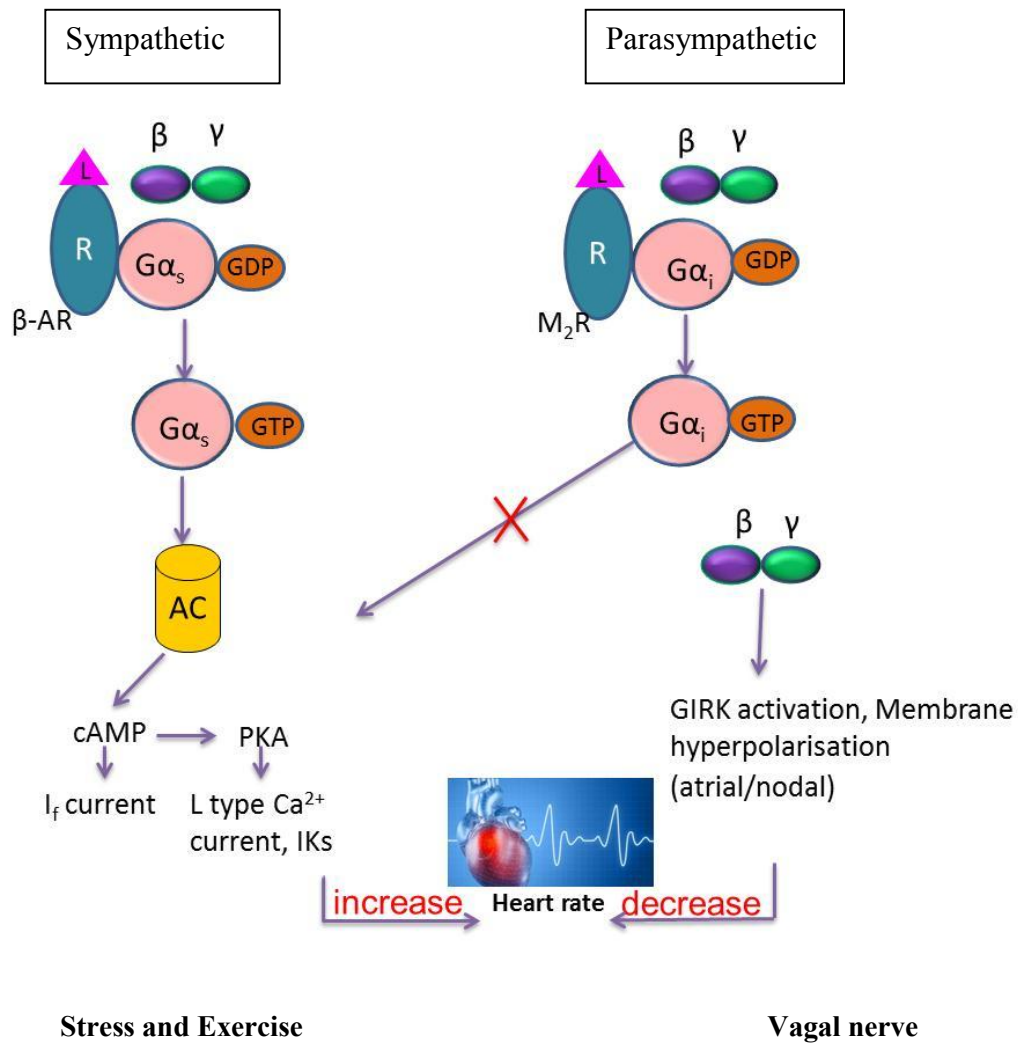


Figure 1.3 The opposing effect of sympathetic and parasympathetic system. Stimulation of the sympathetic nervous system in response to exercise or stress results in a rapid increase in heart rate, which is mediated by activation of the $G\alpha_s$ -coupled β -AR. Subsequently, AC is activated, which leads to an increase in cAMP level and activation of PKA leading to an increase in heart rate. On the other hand, vagal stimulation suppresses activation of AC through M_2R , which are coupled to $G\alpha_{i/o}$, thereby counteracting the effect of sympathetic activation. Meanwhile, $G\beta\gamma$ subunits released from $G\alpha_{i/o}$ can directly activate G protein-coupled inward rectifying K channels (GIRK), causing a decrease in heart rate. R=receptor, L=ligand.

1.4 Control of sino-atrial automaticity

The pacemaker cells in the sino-atrial node have an intrinsic electrical excitability which leads to firing spontaneous regular action potentials even in the absence of nervous innervation. Initiation of each heart beat by SA nodal cells automaticity initiates atrial depolarisation\contraction, conduction through the AV node and His purkinje system and subsequent excitation of the ventricles and ventricular contraction. It is known that spontaneous diastolic depolarization of SAN cells regularly initiates action potentials to generate the rhythm of the heart but the exact mechanism is unclear. It is understood that ion channels and intracellular Ca^{2+} signalling are necessary for pacemaker automaticity. Recent evidence indicates that the voltage clock/M clock (cyclic activation and deactivation of membrane ion channels) and Ca^{2+} clock (rhythmic spontaneous sarcoplasmic reticulum Ca^{2+} release) jointly regulate SAN automaticity (Joung et al. 2009). It was thought that voltage clock mediated by voltage-sensitive membrane currents like hyperpolarization-activated cyclic nucleotide (HCN)\ I_f currents regulated by cAMP controls the spontaneous diastolic depolarisations. I_f is a non-selective cation current activated by hyperpolarization and unlike voltage-sensitive currents, it is modulated by autonomic nervous system. The HCN or I_f channel then depolarises the membrane to a level at which Ca^{2+} channels open to initiate the action potential (DiFrancesco 1985). Mutation in these channels and treatment with drugs which block I_f (ivabradine) are associated with reduced baseline heart rate, which further confirms their role in controlling cardiac automaticity (Noble 1960;Zhang and Vassalle 2001). Apart from the I_f current, Ca^{2+} release from sarcoplasmic reticulum (SR) in response to Ca^{2+} inside the cell though the membrane Ca^{2+} channels, has also been suggested for sinus rhythm generation. It is important to understand that SR Ca^{2+} is controlled in part by

the membrane voltage, so the Ca^{2+} clock and membrane ionic clock are interdependent. Spontaneous rhythmic Ca^{2+} release from the SR in SAN cells is manifested as Ca^{2+} sparks or Ca^{2+} clock. The elevated intracellular Ca^{2+} causes diastolic depolarization via Na-Ca exchange current (I_{NCX}) activation (Bogdanov et al. 2001; Maltsev and Lakatta 2008; Vinogradova et al. 2002). Studies on isolated SAN myocytes showed that late diastolic intracellular Ca^{2+} elevation relative to action potential upstroke is the key determinant of pacemaking by Ca^{2+} clock (Huser et al. 2000). Various voltage-dependent ionic currents have been established in cardiac pacemaker cells which might contribute to diastolic depolarisation and this includes $I_{\text{Ca L}}$, T-type Ca current ($I_{\text{Ca T}}$) and delayed rectifier currents like (fast $I_{\text{K r}}$) and (slow $I_{\text{K s}}$). $I_{\text{Ca L}}$ also enhances late diastolic intracellular Ca^{2+} levels and so the stimulation of sinus rate by both voltage clock and Ca^{2+} clock. SR inhibitors and I_{f} blockers curtail the sinus rate under normal conditions and also attenuate the isoprenaline-induced increase in sinus rate. Consequently, association and harmony between the voltage clock and Ca^{2+} clock is evident (Dobrzynski et al. 2007).

During exercise SNS activation results in increased levels of catecholamines that activate β -AR-mediated G_{α_s} activation which in turn leads to an increased level of cAMP that further activates cAMP-dependent PKA. PKA phosphorylates key Ca^{2+} handling proteins like $I_{\text{Ca L}}$, ryanodine receptor (RyR2) and phospholamban (PLB) (Wehrens et al. 2006). The net result is increased Ca^{2+} influx through voltage-gated $I_{\text{Ca L}}$, increased sarcoplasmic reticulum (SR) Ca^{2+} release via RyR2 and enhanced SR Ca^{2+} uptake by the SR Ca^{2+} pump (SERCA2a) pump. SERCA2a pump is activated by the phosphorylation of PLB which removes its inhibition. These increased Ca^{2+} transients significantly enhance contractility of the heart (Ginsburg and Bers 2004).

1.5 G-proteins

Cells in organisms are in constant communication with each other. Signal transduction, represents a cellular communication mechanism crucial to all living organisms. All transmembrane signalling has two basic elements: a receptor which is able to recognize an external stimulus and an effector which can generate intracellular stimulus (Wettschureck and Offermanns 2005). G-proteins are a family of transmembrane cellular signalling systems that provide the basis for signalling pathways to serve particular functions in different cell types. G-proteins are called so because they bind the guanine nucleotides GDP and GTP and they are heterotrimers (i.e. made of three different subunits α , β and γ) and are associated with transmembrane receptors of hormones called G-protein coupled receptors (GPCRs). The interaction between a specific membrane receptor and an individual G-protein determines the pattern of downstream signal effector activity, and thus its specific physiological effect. Binding of the heterotrimer to the agonist occupied receptor catalyses the exchange of GTP for GDP on the $G\alpha$ subunit, and subsequent dissociation of $G\alpha$ and $G\beta\gamma$. These individual functional units are then free to modulate the activity of downstream signalling effectors, typically AC. Two main classes of $G\alpha$ subunits discussed in this thesis are $G\alpha_s$ - the stimulatory G-protein and $G\alpha_i$ - the inhibitory G-protein. In the context of cardiac function and pathology, these two classes of G-proteins are most important in transducing signals through the β AR and M_2R systems, respectively.

1.5.1 History and discovery of G-proteins

Heterotrimeric G-proteins function to transduce signals from a wide range of GPCRs to effector systems including enzymes and ion channels that release or alter the rate of production or degradation of intracellular secondary messengers. But the mere existence of G-proteins was suggested only by 1970s. The Nobel Prize in Physiology or Medicine for 1994 was awarded jointly to Alfred G. Gilman and Martin Rodbell for their discovery of "G-proteins and the role of these proteins in signal transduction in cells". Much of our present knowledge comes from the studies of bacterial toxins and mutant cell lines. Studies on the action of cholera exotoxin showed that the addition of toxin to cells produced sustained generation and elevation of cAMP levels via the action of mono ADP ribosyl transferase (Gill and Meren 1978). Another mutagenesis study on mouse lymphoma cell lines S49, showed treatment of membranes of wild-type S49 cells with activated cholera toxin and [³²P] NAD⁺ resulted in incorporation of radioactivity into a 45 kDa polypeptide, and this did not occur when membranes of S49^{cyc-} cells (mutant) were used. Membranes of S49^{cyc-} cells thus lacked a key component of the cAMP generation cascade and hence provided a background for studies designed to purify the cholera toxin substrate (Coffino et al. 1975). Using rabbit liver as a source, it was identified that this 45 kDa polypeptide corresponds to the cholera toxin substrate and transducing protein (Northup et al. 1980). By using a range of chromatographic steps, the 45 kDa polypeptide co-purified with a 35 kDa and a 8–10 kDa polypeptide. The 45 kDa protein was thus defined as the α subunit of the stimulatory G-protein and the corresponding 35 and 8–10 kDa polypeptides as the β and γ subunits that make up the functional G-protein heterotrimer. For this, and a host of other key studies on the function and structure of heterotrimeric G-proteins Alfred

G. Gilman was awarded the Nobel Prize for Physiology or Medicine in 1994 along with Martin Rodbell (Gilman 1995;Rodbell 1995).

From ligand binding studies it was well accepted that certain receptor ligands were able to reduce, rather than increase, cAMP levels and serious efforts were undertaken to identify an equivalent adenylyl cyclase inhibitory G-protein (G_i). This study was further enlightened with information from an apparently unrelated research area and the consolidation of relevant information in a review from Martin Rodbell (Rodbell 1980). Studies on the action of an exotoxin produced by *Bordetella pertussis*, the causative agent of whooping cough, showed the exotoxin as a mono-ADP-ribosyl transferase which is able to modify covalently a 41 kDa polypeptide present in the membranes of essentially all cells (Katada and Ui 1982). Additionally, in a physiological context, this exotoxin (now known as 'pertussis toxin'-PTX) disabled α_2 -adrenoceptor regulation of insulin secretion from islet cells, implying that the molecular target for PTX might be G_i . Later purification of the PTX substrate in fractions enriched in high-affinity GTPase activity resulted in the identification of the 41 kDa polypeptide as the α -subunit of G_i , along with 35 and 8–10 kDa polypeptides that appeared identical to the β - and γ -subunits of G_s (Bokoch et al. 1984).

Research on cholera toxin-catalysed [32 P] ADP-ribosylation had indicated the prevalence of two forms of $G\alpha_s$ with varying amounts of the two forms between tissues. Cloning of cDNAs encoding $G\alpha_s$ now revealed that these variants were derived from a single gene via alternative splicing of exon 3 (Bray et al. 1986). On the other hand, cloning of cDNAs encoding the various PTX-sensitive G_i -protein α -subunits indicated each of $G\alpha_{i1}$, $G\alpha_{i2}$ and $G\alpha_{i3}$ to be the products of different genes. ' $G\alpha_0$ ' was also the product of a separate gene that can be differentially spliced to

generate at least two polypeptides, $G\alpha_{oA}$ and $G\alpha_{oB}$. Both $G\alpha_{i1}$ and the forms of $G\alpha_o$ have more restricted distribution patterns that can generally be described as 'neuroendocrine' but the $G\alpha_{i2}$ and $G\alpha_{i3}$ gene products are widely expressed. Studies on specialized sensory systems, including olfactory, visual and lingual tissues uncovered other G-protein α subunits, $G_{olfactory}$ (G_{olf}), cone transducin (G_{t2}) and $G_{gustducin}$, (G_{gust}) respectively, with highly restricted distribution patterns that were highly related to, but different from G_s or the previously identified G_i family members (Milligan and Kostenis 2006).

1.5.2 G-protein signalling

Three mechanisms of membrane-dependent signalling are commonly employed. These typically operate over distinct time courses. However they all share the common features of an extracellular ligand, a membrane-linked receptor and an effector mechanism.

- Ligand-gated ion channel receptor systems such as the nicotinic acetylcholine receptor have extremely rapid kinetic properties. Neuronally released ACh binds to a receptor site on the channel/receptor complex causing conformational change to facilitate rapid channel opening and membrane depolarisation.
- In contrast, receptor tyrosine kinases (RTK's) such as the Erb-2 receptor for example, operate over much slower time courses. RTK pathways are typically involved in modulating cell growth, apoptosis and differentiation processes.
- However the most widely employed membrane-dependent receptor system, involves heterotrimeric G-proteins which interact with a large superfamily of GPCRs to facilitate guanine nucleotide exchange protein signalling. The

GPCRs represent a very large superfamily of receptors that are capable of responding to an enormous number and variety of extracellular stimuli (light, odorant, neurotransmitters, hormones and proteases). They are coupled to the heterotrimeric G-proteins that function as the transducers to relay information to different signalling pathways. This complex design of G-proteins allows assembling and scattering at the interfaces of receptor and G-proteins as well as of G-protein and effector. Also each component in the transmembrane signalling cascade can be further controlled by various means - proteins, soluble mediators - or at transcriptional level. This highly complex and versatile system of G-protein mediated transmembrane signalling provides a variety of transmembrane signalling pathways that are adapted to each particular cell types. Fig. 1.4 (Wettschureck & Offermanns 2005).

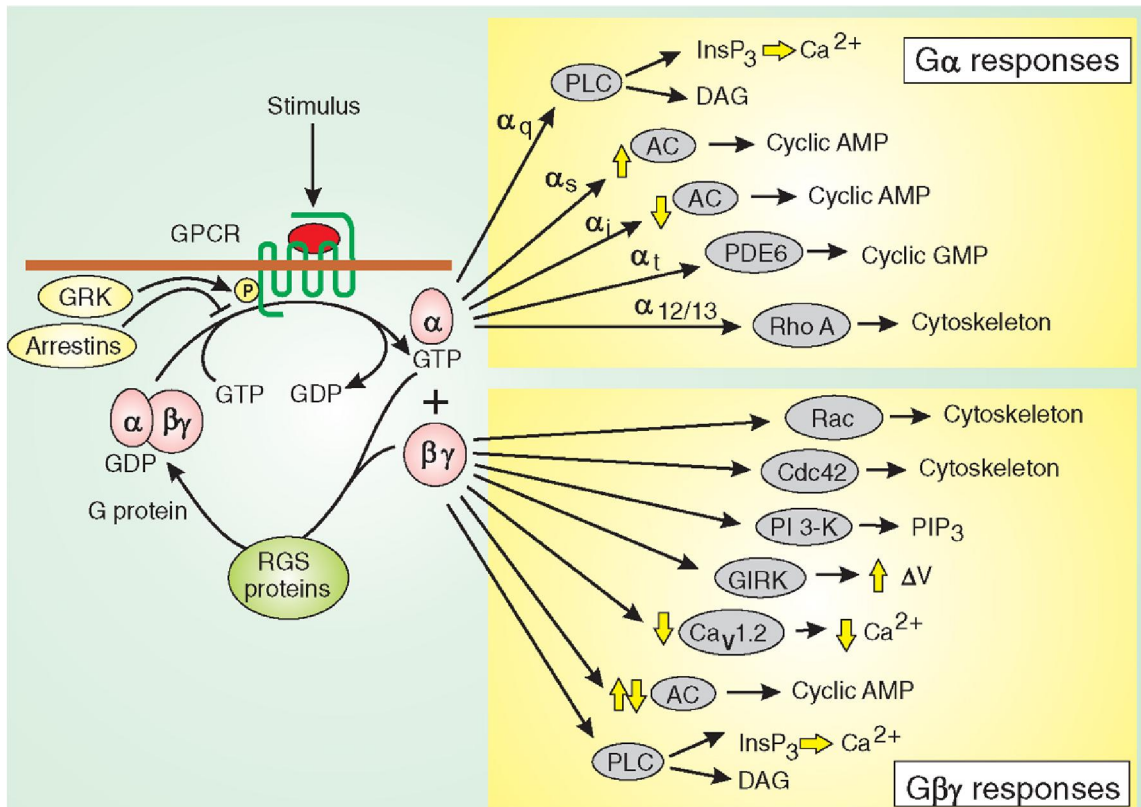


Figure 1.4 Heterotrimeric G-protein signalling External stimuli that bind to GPCRs act as guanine nucleotide exchange factors (GEFs) for the heterotrimeric G proteins. When the GDP on the $G\alpha$ subunit is replaced with GTP, the complex dissociates into $G\alpha$ /GTP and $G\beta\gamma$ subunits that are then capable of activating or inhibiting a wide range of signalling systems. Most of the actions are stimulatory, but some are inhibitory, as illustrated by the yellow arrows. The regulators of G protein signalling (RGS) proteins function as GTPase-activating proteins (GAPs) to facilitate the GTPase activity of the $G\alpha$ subunit, which is the OFF reaction that terminates signalling. G protein receptor kinase (GRK) phosphorylates active receptors and provides binding sites for arrestin that result in receptor desensitization by preventing the heterotrimeric G proteins from binding the receptor. Adapted from Cell Signaling Biology (Berridge 2006).

1.5.3 G-protein coupled receptor (GPCR) superfamily

As their name implies, GPCRs interact with G-proteins in the plasma membrane. When an external signalling molecule binds to a GPCR, it causes a conformational change in the GPCR. The common architecture of these GPCR receptors (comprised of an extracellular N- terminus, 7 membrane spanning domains- TM I-TM VII- connected by 3 intracellular and 3 extracellular loops, and an intracellular C- terminal

tail) allows the receptor protein to transduce signals across the cell membrane (Kobilka 2007). Additionally, GPCRs feature an extracellular largely variable N-terminus important for ligand specificity and an intracellular C-terminus. Within the structure there is an obligate requirement to be able to interact with heterotrimeric G-proteins in a dynamic fashion to facilitate G-protein cycling (Oldham and Hamm 2008). Large variations in the length and sequence of extracellular loops contribute to the profound differences in ligand binding between the GPCRs. Also the variability within the intracellular terminus and the three intracellular loops of GPCRs govern the specificity of activating certain G-protein subfamilies and therefore their ability to target a distinct subset of effectors. Binding of an activating ligand (or agonist) to the extracellular face of GPCR induces a conformational change in the GPCR that triggers an interaction on its cytoplasmic face with heterotrimeric G-proteins (Oldham & Hamm 2008).

GPCRs are one of the largest families of proteins encoded within the human genome. More than 1000 GPCRs are encoded in mammalian genomes. GPCRs have been the focus of intense clinical research and commercial interest. They are key modulators of disease pathogenesis and some 30-40% of all therapeutic agents used in clinical practice target GPCR's (Overington et al. 2006). Within the cardiovascular system, adrenergic and muscarinic receptors are two prototypical GPCRs, whose signal transduction cascades modulate critical cardiovascular functions such as heart rate and contractile response via autonomic efferents (Wettschureck & Offermanns 2005). Different classes of GPCR exist and despite the lack of sequence homology between classes, all GPCRs share a common structure and mechanism of signal transduction. In view of the known existence of alternatively spliced variants of GPCRs, it is likely that the true number of GPCR is higher than estimated. The human genome encodes

several hundreds of G-coupled receptors, about 350 of which detect hormones, growth factors, and other endogenous ligands. Approximately 150 of the GPCRs found in the human genome have unknown functions (Fredriksson et al. 2003).

1.5.4 G-protein cycle

As mentioned earlier heterotrimeric G-proteins are composed of α , β and γ -subunits which dynamically interact with GPCRs within the plasma membrane as part of the G-protein cycle. Under basal conditions, in the inactivated state, the heterotrimer exists as a GDP-bound α -subunit associated tightly with a $\beta\gamma$ -dimer. GPCR activation by ligand binding to the extracellular face causes conformational change such that the intracellular face can act as a guanine nucleotide exchange factor (GEF). Receptor activation then facilitates “nucleotide exchange” of GDP for free cytoplasmic GTP which is present at high concentration. GTP binding transforms the G-protein into an “activated” configuration causing dissociation of GPCR, GTP-bound $G\alpha$ and $\beta\gamma$. This event provides 2 separate signals for interaction with various effectors such as K^+ -channels, Ca^{2+} channels and secondary messenger systems such as AC (Wickman and Clapham 1995). For example activation of the inhibitory G-protein, $G\alpha_{i2}$ as a result of Ach binding to M_2 muscarinic receptor results in the $\beta\gamma$ - dimer directly activating the GIRK channel to cause membrane hyperpolarisation, slowing down pacemaker depolarisation and sinus rate (Robinson and Siegelbaum 2003). More over the activation of the inhibitory $G\alpha$ subunit will inhibit AC and thus modulate I_h/I_f also slowing the pacemaker depolarisation and sinus rate. The system is switched off/deactivated by GTP-ase activity intrinsic to $G\alpha$. GTP is hydrolysed back to GDP allowing re-association of GDP-bound $G\alpha$ with free $\beta\gamma$ to begin another cycle. Activation of the stimulatory G-protein by β -AR will have the opposite effects.

GTPase activity of the α subunit *in vitro* has been found to be slower than *in vivo* suggesting that termination of G-protein activity is not due to the α subunit alone. This has led to the identification of GTPase accelerating proteins (GAP), which include regulators of G-protein signalling (RGS) (Dohlman and Thorner 1997; Tinker 2006).

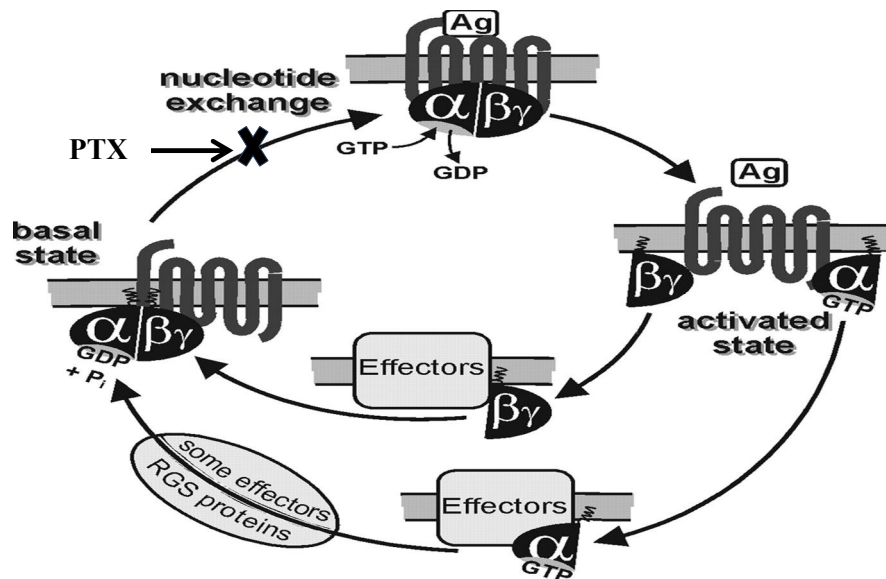


Figure 1.5 The G-protein cycle The $G\alpha$ subunit bound to GDP, which is the inactive state interacts with $G\beta$ subunit through the N terminal domain and GTP binding domain. Agonist binding to the GPCR/G-protein complex facilitates GDP/GTP nucleotide exchange on the $G\alpha$ subunit. This activated state allows for $G\alpha$ subunit and $G\beta\gamma$ to interact freely with effectors. The $G\alpha$ subunit had intrinsic capacity to hydrolyse GTP to GDP allowing reassembly with $G\beta\gamma$ to return to the resting state. $G\alpha$ subunit responses are terminated by GTP hydrolysis. RGS proteins facilitate GAP and help terminate response. $G\beta\gamma$ responses are also terminated by recombining with GDP-bound $G\alpha$ to form the heterotrimeric G-protein complex. PTX modifies the G-protein α subunit and prevents interactions of the $G\alpha$ GDP $\beta\gamma$ -heterotrimer with GPCR. Figure adapted from (Wettschureck & Offermanns 2005).

1.5.5 G-protein α subunit

$G\beta$ and $G\gamma$ form a functional dimer which never dissociates under physiological conditions. In comparison GTP bound- $G\alpha$ can freely dissociate from $G\beta\gamma$ upon receptor-mediated activation. A major focus of this work is the potential selective

function of inhibitory G-proteins ($G_{i/o}$). The $G\alpha$ -subunit has a conserved structure consisting of a ras like-GTPase domain (15kDa) and an α -helical domain (25kDa). A guanine nucleotide binding cleft is sandwiched between the two domains. The GTPase domain is conserved amongst all GPCRs so far identified. Additional to GTP-hydrolysis, it provides binding sites for $G\beta\gamma$, GPCRs and effector proteins. Within the domain there are 3 flexible loops, named switches I, II and III. These “switches” undergo dramatic conformational change between GDP-bound and GTP-bound states shown from crystallography studies. The crystal structures of $G\alpha_{t/i}\beta_1\gamma_1$ and $G\alpha_1\beta_1\gamma_2$ suggest that GDP-bound α -subunit and $\beta\gamma$ interaction occurs primarily in a hydrophobic pocket between switch 1 and switch 2 of $G\alpha$. GTP binding attenuates the polarity of this binding domain substantially resulting in reduced binding affinity of $G\alpha$ with $G\beta\gamma$ allowing separation (Oldham & Hamm 2008).

All $G\alpha$ subunits are GTP hydrolases. The intrinsic hydrolysis rates by different G-protein isoforms vary differently. Turnover numbers for G_s are low ($\sim 0.3\text{min}^{-1}$) while $G_{i/o}$ α subunits have greater hydrolysis rates of ($\sim 1.3\text{min}^{-1}$) (Gilman 1987). GTP hydrolysis is rate-limited by the dissociation rate of the product, GDP. Different $G\alpha$ isoforms also have different rates of GDP release. For example receptor stimulated GDP/GTP exchange is faster for $G_{i/o}$ G-proteins while G_t , G_s , $G_{q/11}$ have slower exchange rates and $G_{12/13}$ are very slow exchangers (Kleuss et al. 1994; McCudden et al. 2005).

1.5.6 The 4 G α -subclasses

- **G α_s** is expressed ubiquitously and stimulates all isoforms of AC. It is encoded by the complex imprinted GNAS gene locus that can give rise to several gene products (discussed later in section 1.7.4). G α_s couples GPCRs exclusively to AC activation and thereby increases cAMP concentration. This in turn activates cAMP-dependent PKA which phosphorylates target proteins. In the heart these include effectors such as cardiac Ca²⁺ channels, phospholamban and troponin which mediate the acute physiological effects of sympathetic activation (Kim et al. 1999;Rockman et al. 1997;Rockman et al. 2002). Chronic G α_s activation (Iwase et al. 1997) however, is associated with pathological myocyte hypertrophy, cardiac apoptosis and abnormal Ca²⁺ handling involving CaM Kinase II (Ca²⁺/calmodulin-dependent protein kinase II) in particular (Grueter et al. 2007;Zhang et al. 2005). One of the chapters in this study is focused on this stimulatory subunit of G α_s .

- **G $\alpha_{q/11}$** couple to various β isoforms of phospholipase C (PLC) initiating signalling via Diacylglycerol (DAG) and Inositol Phosphate (IP₃) pathways. Activation of PLC results in breakdown of a membrane phosphatidylinositol 4,5-bisphosphate (PIP₂) into 2 signals: cytoplasmic IP₃ that releases Ca²⁺ from intracellular stores, and membrane-bound DAG that is a potent activator of certain isozymes of PKC. G $\alpha_{q/11}$ subfamily also modulates the activity of certain families of non-receptor tyrosine kinases. The constitutively active cardiac restricted G α_q overexpression in transgenic mice is associated with cardiac hypertrophy (D'Angelo et al. 1997) whilst G α_q blockade (Esposito et al. 2001) prevents cardiac hypertrophy responses.

- **G $\alpha_{12/13}$** is expressed ubiquitously and often activated by receptors that couple to G $\alpha_{q/11}$. Identifying their function has been hampered by the lack of specific inhibitors

and their ability to activate other G-proteins. They have however been associated with effectors such as phospholipase A₂, Na⁺/H⁺ exchangers and activation of the RhoA pathway which modulates cytoskeletal activity such as platelet activation.

- **Gα_{i/o}** Inhibitory G-proteins were initially discovered on the basis of their ability to “inhibit” AC activity and so lower cAMP concentration (Rudolph et al. 1996; Wong et al. 1991). They are now known to additionally modulate several key “effectors” including Ca²⁺ channels, (Zhang et al. 2001), (Nagata et al. 2000) the PI₃ Kinase pathway, MAP-Kinase and GIRK channels (Reuveny et al. 1994; Wickman & Clapham 1995) via the activation of Gβγ subunit of G-protein. GIRK channels are expressed in brain and atrial tissue and within the heart they are involved with vagal modulation and slowing of the heart rate (Wickman, Nemeč, Gendler, & Clapham 1998) (discussed later). Different isoforms of Gα_{i/o} exist namely Gα_{i1}, Gα_{i2}, Gα_{i3} and Gα_o (with splice variants Gα_{oA} and Gα_{oB}) all known to regulate cAMP dependent heart rate modulation. All isoforms are widely expressed with Gα_{i2} being the prominent cardiac isoform (Gohla et al. 2007) and Gα_o abundantly expressed in neuronal cells (Wettschureck & Offermanns 2005). The structural similarity between Gα isoforms suggests they might have partially overlapping functions.

The study of Gα_{i/o} has been particularly advanced with the use of PTX toxin isolated from the bacterial species *Bordetella pertussis*. PTX toxin, encodes a region termed a promoter A subunit and a B subunit (pentameric protein assembly important for cell binding). The A subunit selectively and irreversibly ADP-ribosylates a C-terminal cysteine residue in Gα_{i/o} subunits (Pizza et al. 1988; Vivaudou et al. 1997). This covalent modification prevents selective Gα_{i/o} interaction with GPCRs and results in functional uncoupling of the receptor mediated signal transduction cascade. Use of

PTX toxin has been a critical tool in our understanding of the selective function of inhibitory $G\alpha$ -subunits. Interestingly, site-directed mutagenesis of this C-terminal cysteine residue to leucine/isoleucine renders the $G\alpha_{i/o}$ -subunit PTX resistant yet still functional. In this way it becomes possible to delineate the individual coupling of GPCRs to $G\alpha_{i/o}$ isoforms (Leaney and Tinker 2000). Tissue expression patterns suggest relatively widespread $G_{i/o}$ distribution but specific tissue expression profiles exist. For example, G_0 is expressed at high levels in neurons (Jiang et al. 1998) whilst in cardiac tissue, $G\alpha_{i2}$ appears to be the predominant inhibitory G-protein isoform (DeGeorge and Koch 2008; Gohla, Klement, Piekorz, Pexa, vom, Spicher, Dreval, Haussinger, Birnbaumer, & Nurnberg 2007). Absolute quantification of inhibitory G-protein expression has been problematic on account of generating truly isoform-specific $G\alpha_i$ antibodies for Western blot on account of structural homology. Within $G\alpha_{1,2,3}$ and $G\alpha_0$ isoforms there appears to be 87-94% primary sequence homology (Birnbaumer 2004). Some have taken this to mean that different $G\alpha_i$ isoforms are capable of at least partially overlapping function, especially when expressed artificially in *in vitro* systems (Yatani et al. 1988). However there are now numerous examples of receptor mediated $G\alpha_{i/o}$ selectivity documented within the literature. There appears to be inter-species conservation of individual $G_{i/o}$ isoform structure, for example, human and rat $G\alpha_{i2}$ show 98% sequence homology which suggests an evolutionary conservation of structure and biological function (Birnbaumer 2004).

Inhibitory G-proteins ($G\alpha_{i/o}$) are considered the predominant species followed by G_s , then $G_{q/11}$ and finally $G_{12/13}$ shows limited expression relatively. Each subclass consists of various members with functional and structural similarities. Some GPCRs couple specifically with one G-protein subclass, the muscarinic M_2 receptor couples

faithfully to $G\alpha_{i/o}$ signalling pathways (Sadja et al. 2003; Sowell et al. 1997) whilst other GPCRs such as the β_2 adrenergic receptor are capable of coupling via multiple G-proteins including $G\alpha_s$ and $G\alpha_{i/o}$ (Foerster et al. 2003; Xiao et al. 2003). Interestingly, GPCR phosphorylation can act as a molecular switch to channel inactivation preferentially down a particular G-protein pathway (Oldham & Hamm 2008).

1.5.7 Activation of $G\beta\gamma$ signalling

Apart from its role in supporting GPCR-dependent $G\alpha$ interactions, $G\beta\gamma$ acts to directly regulate downstream signalling in its own way. The first candidate found to be activated by $G\beta\gamma$ was the acetylcholine-regulated inwardly-rectifying K^+ channel in atrial myocytes (Logothetis et al. 1987). It was observed in isolated inside-out patches from atrial myocytes that the acetylcholine driven channel activation was independent of soluble second messengers, suggesting that the subunits of the $G\alpha_i$ protein could directly activate the channel. This tempted various groups to directly activate the channel in excised atrial membrane patches with $G\beta\gamma$ and $G\alpha$ subunits (Logothetis, Kurachi, Galper, Neer, & Clapham 1987) (Codina et al. 1987). After much controversy it was concluded that $G\beta\gamma$ subunits are the primary mediators of channel activation through direct binding to the channel (Clapham and Neer 1997; Wickman et al. 1994). It was quite controversial in the beginning to recognize $G\beta\gamma$ as the primary mediator of channel activation because $G\beta\gamma$ mediating direct downstream functions had not been previously demonstrated, and also because precedent with AC demonstrated that $G\alpha_s$ was responsible for direct stimulation of AC activity. Further evidence to support its role as a signal mediator in its own right came from genetic analysis of the pheromone signalling pathway in yeast, indicating that $G\beta\gamma$ is the key

activator of downstream signalling from the G-protein coupled pheromone receptor (Whiteway et al. 1989). In the case of MAPK/ERK (Mitogen-activated protein kinases/ Extracellular signal-regulated kinases) pathway, expression of G $\beta\gamma$ in cells leads to ERK activation, but the exact mechanism and the direct binding target for this activation has not been fully understood. However, it is now well established that the G $\beta\gamma$ subunits play major roles in mediating downstream signalling from GPCRs and may be as prevalent as those mediated by G α subunits.

1.6 Regulators of G-protein signalling (RGS)

RGS proteins are critical to signal modulation through G-proteins. They were first discovered in yeast and *C. Elegans* (Dohlman & Thorner 1997). Besides being a major effector mechanism for negative chronotropic regulation upon vagal stimulation, GIRK currents are highly regulated by endogenous RGS proteins (Doupnik et al. 1997). RGS function primarily as GAPs through their conserved RGS domains (Geurts et al. 2003; Hollinger and Hepler 2002). RGS proteins enhance the intrinsic GTPase activity of G-proteins and accelerate the turn-off step of the G-protein cycle, thereby serving as negative modulators (Fig. 1.6). More than 10 mammalian RGS proteins have been found in myocardium (Doupnik et al. 2001; Kardestuncer et al. 1998; Wieland and Mittmann 2003) with minimal distinction in their expression pattern between atria and ventricles (Wieland & Mittmann 2003). In addition, the specificity of different RGS proteins toward G- protein isoforms is rather loose. The majority of these RGS proteins can act as a GAPs for most members of the G $\alpha_{i/o}$ and G α_q families (Hollinger & Hepler 2002).

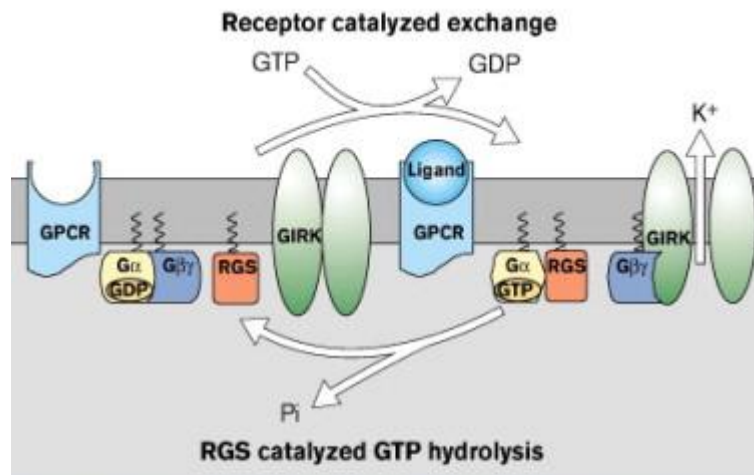


Figure 1.6 Activity of RGS proteins: GPCRs bind to ligand and catalyze nucleotide exchange; free Gβγ then binds and activates GIRK channels. RGS bound to Gα hydrolyse GTP back to GDP returning Gα to its inactive form where it is associated with Gβγ.

Even though there is scant knowledge about the role of endogenous cardiac RGS proteins, they are dynamically regulated in a variety of pathophysiological conditions, like cardiac hypertrophy (Rogers et al. 1999) and heart failure (Owen et al. 2001). Recently RGS proteins have become a potential new therapeutic target for cardiovascular diseases (Riddle et al. 2005). Because of their functional redundancy properties, it has been difficult to ascertain the full physiological role of endogenous RGS proteins *in vivo*. Thus, I used RGS-insensitive (RGSi) mutant Gα subunits, which contain a G¹⁸⁴S point mutation in their switch I region that prevents binding of RGS proteins and the subsequent Gα deactivation (Lan et al. 1998) Fig. 1.7. Importantly these Gα mutations do not affect the intrinsic GTPase activity, Gβγ subunit binding, receptor stimulation or the ability to signal to downstream effectors (Fu et al. 2004). At the same time expression of these RGSi Gα subunits significantly enhances Gα_{i/o}-mediated signalling.

muscarinic receptors (Tinker 2006). It has been observed that RGS's translocate to the membrane on expression with particular GPCRs e.g. β_2 -AR with RGS-2 and the M₂R with RGS-4 (Roy et al. 2003). The latter observation has been strengthened by the recent demonstration that sinus node myocytes isolated from RGS-4 deficient mice have enhanced M₂ receptor mediated K_{ACh} currents (Cifelli et al. 2008). RGS discovery has had important consequences for our understanding of GIRK channel kinetics. When GIRK channels are expressed in *Xenopus* oocytes, they deactivate more slowly than native atrial currents upon termination of receptor stimulus. Co-expression of RGS-4 or RGS-8 could recapitulate native GIRK deactivation profiles (Doupnik, Davidson, Lester, & Kofuji 1997).

Six main subclasses of RGS exist: R4, R7, R12, RA, RL and RZ (Ross and Wilkie 2000). These are based on sequence similarities within the RGS domain and named according to the prototypical member of each group. Each subclass also displays sequence homology in the regions flanking the RGS domain. The R4 family consists of RGS 1 to 5, 8,13,16,18 and 21 and members have small N- and C- termini as well as a conserved domain. The R7 family which consists of RGS 6, 7, 9 and 11 are more complex than the R4 family and have several additional domains which mediate protein-protein interactions and stability (Anderson et al. 2009). Each member of the RGS protein family contains a highly conserved domain of 120-130 amino acids known as the RGS box (De et al. 1995;Siderovski et al. 1996). The vast majority of RGSs are GAPs for inhibitory G-proteins but some have activity to $G\alpha_{q/11}$ family as well. For example RGS4 inhibits inhibitory G-protein $G\alpha_{i/o}$ and $G\alpha_{q/11}$ signalling through this GAP activity (Mittmann et al. 2002;Snabaitis et al. 2005;Tamirisa et al. 1999). RGS-2 has greater selectivity for $G\alpha_{q/11}$, whereas the R7 family have GAP activity solely for $G\alpha_{i/o}$. RGS-4 and RGS-16 accelerate hydrolysis on both $G\alpha_q$ and

$G\alpha_{i/o}$ subunits while RGS-8 and 10 are selective for $G\alpha_{i/o}$ subfamily (Ross & Wilkie 2000).

1.7 G-proteins and Heart rate

The $G\alpha$ subunit of the G-protein is the major element of signalling selectivity which is largely carried out by a) stimulatory subunit of $G\alpha$ ($G\alpha_s$) by activation of AC, b) inhibitory subunit of $G\alpha$ ($G\alpha_{i/o}$) by inhibition of AC, and c) $G\alpha_q$ by activation of phospholipase C (Feuerstein and Rozanski 2000). The importance of research on cardiac G-proteins is relevant due to 3 main reasons. First and foremost, GPCRs exist in the heart and major signalling pathways associated with cardiac remodelling are handled by them as manifested by the action of angiotensin-II, endothelin-1 and the sympathetic neurohormonal systems. Secondly, heart failure is characterized by significant alteration in the expression and function of $G\alpha$ proteins, e.g. increase in $G\alpha_i$ (Braunwald, Zipes, & Libby 2001). Lastly, in heart failure patients there are proven benefits of specific antagonists of GPCRs like that of angiotensin II, AT1 receptors and β -AR blockers to induce beneficial reversal of cardiac remodelling (Braunwald 1997). G-proteins are regulators of cardiac calcium, potassium and pacemaker currents so it paves the way to speculate that G-protein modifications or alterations can contribute to arrhythmias and sudden cardiac death. I will be concentrating on 2 major classes of $G\alpha$ subunit which are the primary elements of receptor effector coupling: $G\alpha_s$ (stimulatory subunit) and $G\alpha_i$ (inhibitory subunit) which conducts signals through β -AR and M_2R respectively and has opposing physiological effects.

1.7.1 Inhibitory G-proteins $G\alpha_i$

Actions of the parasympathetic system on the heart rate are negatively inotropic (force of contraction), chronotropic (heart rate) and lusitropic (rate of relaxation). Acetylcholine released from the vagus nerve acts via muscarinic receptors and PTX-sensitive α subunit of inhibitory G-proteins to bring forth this action and inhibitory G-proteins can also be activated by β_2 -AR (Robishaw and Hansen 1994; Xiao et al. 1995). In addition, $G\beta\gamma$ subunit released from $G\alpha_{i/o}$ directly activates GIRK channels leading to membrane hyperpolarisation and all these mechanism contribute to modulating the heart rate (Ang et al. 2012). In the heart different types of PTX-sensitive α subunits are expressed: α_{i1} , α_{i2} , α_{i3} and α_o with significant possibility of redundancy (Birnbaumer 2007). In our lab we addressed the question of which inhibitory G-protein isoform *in vivo* governs heart rate modulation and dynamics using mice with global genetic deletion of $G\alpha_{i2}$, $G\alpha_{i1}$ and $G\alpha_{i3}$ combined and $G\alpha_o$ (Zuberi et al., 2008). This was done by implanting telemetry probes in these global transgenic knockout mice and measuring heart rate dynamics and ECG parameters in conscious awake mice in the time and frequency-domain. We found that $G\alpha_{i2}$ deficient mice were generally tachycardic with preservation of diurnal variation, and had attenuated bradycardic response to the muscarinic agonist carbachol. These abnormalities on heart rate modulation were compatible with a role of that protein in the SA node and so I focussed my studies on the deletion of $G\alpha_{i2}$ in the SA node. There is one conflicting study suggesting inhibitory subunit $G\alpha_o$ and not $G\alpha_{i2}$ is necessary in muscarinic-mediated parasympathetic activity which may be due to methodological issues as the mice were studied very early after probe implantation (Duan et al. 2007). In keeping with our observations, (where we found an attenuated bradycardic response to the muscarinic agonist carbachol) mice with a G^{184S} knock-in point mutation in the

switch I region of $G\alpha_{i2}$, preventing the binding of RGS proteins and deactivation of $G\alpha_{i2}$, had marked enhancement of muscarinic agonist mediated bradycardia (Fu et al. 2007).

Differential coupling of G-protein subtypes to adenosine A_1 and muscarinic M_2R mediated heart rate slowing was also demonstrated in *vitro* using RGS-insensitive $G\alpha_o$ and $G\alpha_{i2}$ ES-derived cardiomyocytes (Fu et al. 2006). The RGS-insensitive $G\alpha_o$ homozygous knock-in cells demonstrated enhanced adenosine A_1 and muscarinic M_2 receptor mediated bradycardic responses. In contrast, RGS-insensitive $G\alpha_{i2}$ homozygous knock-in cells showed enhanced responses to M_2 but not A_1 receptors. Blocking GIRK channels largely abolished the mutation-induced enhancement of the M_2 receptor-mediated response but had a minimal effect on A_1 responses. Taken together, the evidence suggests that M_2 -mediated GIRK channel activation is coupled preferentially to the $G\alpha_{i2}$ subunit whereas coupling to voltage-gated L-type calcium channel appears to be less specific with both $G\alpha_o$ and $G\alpha_{i2}$ implicated (Ang, Opel, & Tinker 2012). It is clear then, that there are a number of isoforms of inhibitory G-proteins and RGSs expressed in the heart and other tissues, which have potentially overlapping functions. Using PTX-insensitive point mutants of $G_{i/o}$ in vitro cellular systems (HEK cell lines), it was shown that G-protein coupled receptors couple well with a number of isoforms and there is variable preferences of a receptor for an inhibitory G-protein isoform and there are only minor differences in the ability of these variants to activate the channel (Leaney & Tinker 2000).

1.7.2 $G\alpha_i$ expression and clinical relevance

The evidence for up-regulation of $G\alpha_i$ occurring in heart failure comes from a study by Neumann and colleagues in 1988 where they found an association between

catecholamine desensitization and heart failure (Neumann et al. 1988). In that study, where they compared failing hearts (idiopathic dilated cardiomyopathy) with non-failing hearts, they found that $G\alpha_i$ protein content was increased with an impaired responsiveness to isoprenaline. In the same study, in another patient with inflammatory heart disease, the contractile response to isoprenaline was not reduced and likewise content of G_i -proteins was not changed. Another study by Hershberger and colleagues compared myocardial tissue from failing and non-failing hearts for cAMP response to $G\alpha_i$ coupled A_1 receptors and non- $G\alpha_i$ mediated activation of AC by forskolin, fluoride and manganese and found similar activities of AC in both failing and non-failing hearts. There were no differences in adenosine receptor-mediated AC inhibition. However, $G\alpha_i$ was found to be increased by 30% in failing hearts and basal cyclase activity was decreased by 70% (Hershberger et al. 1991). In animal models of heart failure there was an increase in the amount of $G\alpha_i$ protein assessed by immunoblotting, and an increase in $G\alpha_i$ function assessed by Ach induced inhibition of AC (Kawamoto et al. 1994). Increased levels of $G\alpha_i$ and decreased AC activity cannot be looked upon as a primary event in cardiac hypertrophy as they are demonstrated in various forms of experimental and genetic hypertension models where there is hypertrophy without heart failure (Bohm et al. 1995). Feldman and co-workers examined RNA levels by northern blot analysis and found that in failing human hearts there is an increase in both $G\alpha_i$ and $G\alpha_s$ but later by real time PCR found no differences in $G\alpha_i$ and $G\alpha_s$ (Feldman et al. 1989; Feldman et al. 1991). Later studies in human and experimental heart failure further reported an increase in $G\alpha_i$ mRNA levels (Eschenhagen et al. 1992). In cultured cardiac myocytes using $G\alpha_{i2}$ gene promoter reporter constructs it was demonstrated that increase in cAMP levels upregulate $G\alpha_{i2}$ promoter activity by CREB binding which could provide a credible

mechanism for transcriptional up-regulation of $G\alpha_{i2}$ in heart diseases (Eschenhagen et al. 1996a).

Ventricular myocytes taken from patients with cardiac failure demonstrate poor contractile reserve to β -adrenergic stimulation accompanied by β_1 -AR down-regulation (resulting in a higher β_2/β_1 ratio) and increased expression of PTX-sensitive $G\alpha_i$ (with no changes in $G\alpha_s$ expression) (Xiao, Zhang, Chakir, Avdonin, Zhu, Bond, Balke, Lakatta, & Cheng 2003;Zheng et al. 2005). These events correlate with attenuation of AC activity and isoprenaline-stimulated cAMP production. However pharmacological data suggests that cardiomyocytes can in principle develop maximal contractile force by cAMP independent means e.g. Ca^{2+} loading (Brown and Harding 1992). Therefore abnormal cAMP-generation by the receptor G-protein AC system appears to be of central importance for the reduced inotropic state seen in clinical heart failure. Also these studies suggest that increased levels of noradrenaline reported in heart failure lead to raised levels of the inhibitory G-protein, and that this contributes to the observed β -AR desensitization in patients with moderate or end-stage heart failure.

1.7.3 Stimulatory G-protein $G\alpha_s$

Heterotrimeric $G\alpha_s$ subunit is ubiquitously expressed and binding of β -AR to stimulatory G-proteins leads to its dissociation into $G\alpha_s$ -GTP bound and $G_{\beta\gamma}$ complex similar to that of inhibitory G-protein. The $G\alpha_s$ -GTP complex, which dissociates from the $G_{\beta\gamma}$ complex, then binds to and activates AC. This activation leads to generation of cAMP and increased levels of cAMP can directly modulate HCN channels (I_h/I_f) leading to an increase in heart rate (DiFrancesco and Tortora 1991). This also leads to

increased activity of PKA, resulting in modulation of downstream effectors such as intracellular Ca^{2+} handling pathways for example phospholamban and the ryanodine receptor leading to increased contractility of cardiac muscles (Weinstein et al. 2001). $\text{G}\alpha_s$ is deactivated by intrinsic GTPase activity of G-protein itself which hydrolyses bound GTP to GDP. RGS proteins appear to play much less of a role in modulating GAP activity (Zheng et al. 2001). Apart from regulation of cardiac contraction, stimulation of AC is also important for many physiological processes including growth and development, learning and memory and endocrine functions, including those of the thyroid, pituitary, and parathyroid glands. In addition to activation of AC, $\text{G}\alpha_s$ has been implicated in a number of processes for which the effector protein is unknown, such as adipogenesis and regulation of vesicular trafficking (Berlot and Bourne 1992).

GNAS is a complex gene with imprinting that encodes multiple gene products through the use of alternative promoters and first exons. In addition to $\text{G}\alpha_s$, the gene also encodes for a neuroendocrine specific $\text{G}\alpha_s$ isoform (XL α_s) which is expressed from paternal allele and chromogranin like protein NESP55 which is expressed from maternal allele (Weinstein et al. 2007). $\text{G}\alpha_s$ itself is imprinted (though not in cardiac tissues) in tissue specific manner, in both mice and humans being expressed primarily from maternal allele (but paternally silenced) in several tissues including pituitary, thyroid, renal proximal tubules and gonads, but biallelically expressed in most tissues (Table 1.2). Mice which are homozygous knockouts of *Gnas* die early in embryonic development (Yu et al. 1998). Heterozygous inactivation of $\text{G}\alpha_s$ mutations results in Albright Hereditary Osteodystrophy (AHO) and it presents a skeletal phenotype characterized by subcutaneous ossifications, short stature and brachydactyly

(shortening and widening of long bones in the hands and feet). Heterozygous mutation of $G\alpha_s$ on the maternal (but not the paternal) allele also leads to early lethality, severe obesity and multihormone resistance (parathyroid stimulating hormone -PTH, thyroid stimulating hormone TSH and gonadotropins) while the paternal mutation leads to only mild obesity and insulin resistance along with AHO. This is due to the fact that $G\alpha_s$ is mainly expressed from maternal allele in the target tissues of these hormones (thyroid, ovaries, renal proximal tubules) and mutations in the maternal allele lead to $G\alpha_s$ deficiency and hormone resistance on the other hand mutation on the dormant paternal allele have no effect on $G\alpha_s$ expression. These parent-of-origin differences are the result of tissue-specific $G\alpha_s$ imprinting (Weinstein 2001). $XL\alpha_s$ (which has a long amino terminal extension) deficiency leads to a perinatal suckling defect and a lean phenotype with increased insulin sensitivity. The opposite metabolic effects of $G\alpha_s$ and $XL\alpha_s$ deficiency are associated with decreased and increased sympathetic nervous system activity, respectively. NESP55 deficiency has no metabolic consequences (Weinstein, Xie, Zhang, & Chen 2007).

Table 1.2 Imprinting pattern of GNAS locus

GNAS Locus	Imprinting Pattern
$G\alpha_s$	Tissue specific, expressed mainly from maternal allele in various hormone target tissues, biallelically expressed in most tissues
$GXL\alpha_s$	Paternally
NESP55	Maternally
Exon 1A	Paternally

1.7.4 GNAS gene and products encoded by Gnas

Genomic imprinting is a epigenetic phenomenon which results in partial or complete suppression of gene expression from one parental allele (Reik and Walter 2001). The imprinting is either by allele specific DNA methylation or histone modification which distinguish the 2 parental alleles which are wiped out in primordial germ cells and re-established in either male or female gametes, and maintained in somatic tissues throughout development. DNA methylation is the most well-established imprint mark, as all imprinted genes have one or more regions in which the maternal and paternal allele are differentially methylated. The mouse and human $G\alpha_s$ gene (*gnas* and GNAS respectively) generates multiple gene products through the use of 4 alternative promoters and first exons that splice onto a common exon (Fig. 1.8). The major product $G\alpha_s$, is generated from the most downstream alternative exon $G\alpha_s$ exon 1, which generates transcripts encoding $G\alpha_s$ and it spans 13 exons (12 exons in mice) and generates 2 long and 2 short forms of $G_s\alpha$ protein by alternative splicing of exon 3 and both are biologically active and similar in function (Bray, Carter, Simons, Guo, Puckett, Kamholz, Spiegel, & Nirenberg 1986;Kozasa et al. 1988) (Jones et al. 1990). $G\alpha_s$ is imprinted in a tissue-specific manner in both mice and humans, being expressed primarily from the maternal allele in several tissues, including pituitary, thyroid, renal proximal tubules and gonads but biallelically expressed in most tissues (Davies and Hughes 1993;Hayward et al. 2001;Weinstein 2001).

Another alternative promoter which is most upstream of GNAS locus (~ 45 kb upstream of $G\alpha_s$ exon 1), generates transcript that encode the neuroendocrine-specific protein of 55 kDa (NESP55) which is structurally and functionally unrelated to $G\alpha_s$ (Hayward et al. 1998;Peters et al. 1999) (Fig. 1.8). The entire NESP55 coding

sequence is within its specific first upstream exon and $G\alpha_s$ exons 2–13 form majority of 3' untranslated region of NESP55-specific transcripts. NESP55 is only transcribed from the maternal allele and its promoter region is methylated only on the paternal allele (Li et al. 2000). In adults, it is primarily expressed in neuroendocrine tissues, like adrenal medulla, pituitary, hypothalamus and brain stem regions and a proteolytic product of NESP55 has been shown to be an endogenous antagonist to serotonin receptors (Ischia et al. 1997) and deficiency of NESP55 in humans does not produce any pronounced phenotype so its role is presently unknown (Liu et al. 2000).

Lying ~30 kb upstream of $G\alpha_s$ exon 1 is the third alternative promoter which generates transcripts encoding neuroendocrine specific $G\alpha_s$ isoform, XL α_s (Kehlenbach et al. 1994). GXL α_s has a long amino-terminal extension encoded by its specific first exon (422, 367, and 551 amino acids in mice, rats, and humans, respectively) while the rest of the protein is identical to $G\alpha_s$, being encoded by $G\alpha_s$ exons 2–13. In GXL α_s 47 amino acids of $G\alpha_s$ are replaced by a large amino terminal domain with manifold repeat regions which are encoded by its specific 1st exon. GXL α_s is oppositely imprinted to NESP55, being methylated on the maternal allele and transcriptionally active only on the paternal allele (Hayward, Moran, Strain, & Bonthron 1998; Li, Vu, Zeng, Nguyen, Hayward, Bonthron, Hu, & Hoffman 2000; Peters, Wroe, Wells, Miller, Bodle, Beechey, Williamson, & Kelsey 1999). GXL α_s mutations have little effect in humans though its biological functions are not fully established.

Located ~ 2.5 kb upstream of $G\alpha_s$ exon 1 is a fifth alternative promoter referred to as exon 1A and is methylated on the maternal allele and generates paternal-specific

transcripts that are presumably untranslated (Ishikawa et al. 1990). The exon 1A region appears to be a primary imprinting control centre as its maternal-specific methylation is established during gametogenesis and maintained throughout development in mice (Liu, Litman, Rosenberg, Yu, Biesecker, & Weinstein 2000). Pseudohypoparathyroidism type 1b (PHP1b) is a form of parathyroid hormone resistance resulting from an imprinting defect leading to tissue specific G_{α_s} deficiency.

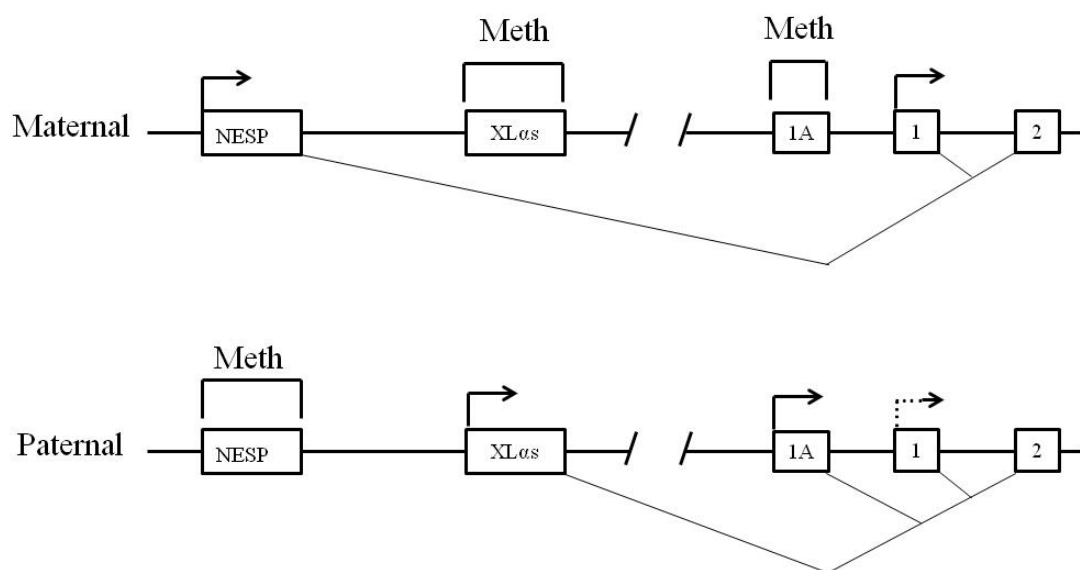


Figure 1.8 Organisation and imprinting of GNAS locus. Maternal and paternal alleles of GNAS are shown here with alternative first exons for NESP55 (NESP), XL α_s , untranslated (exon 1A) and G_{α_s} (exon 1) and their mRNAs splicing to a common exon (exon 2). The exons further extend till exon 13 in the sense direction (not shown). Methylated promoters (Meth) are shown above, and splicing patterns of each gene are shown below each panel. Transcriptionally active promoters are indicated by horizontal arrows in the direction of transcription. Transcription from the paternal G_{α_s} (exon 1) promoter is suppressed in some tissues, which is indicated with a dashed arrow. Figure modified from (Weinstein et al. 2004).

Tissue-specific G_{α_s} knockout models have identified important roles for G_{α_s} signaling pathways in skeletal development, renal function and glucose and lipid metabolism but not in relation to cardiac function. Here in this present study I have explored the

role of $G\alpha_s$ in relation to cardiac function using tissue specific knockouts *in vivo* studies.

1.7.5 $G\alpha_s$ expression and clinical relevance

Increased expression of inhibitory G-proteins has been widely accepted as a contributing factor for β -AR desensitization in heart failure models but the exact act of altered $G\alpha_s$ is not clear. $G\alpha_s$ activity and $G\alpha_s$ mRNA is decreased by approximately 30% both in the failing and non-failing pressure overload hearts of animal models. Followed by this decrement in these models there was a decrease in AC, both basal and stimulated (Chen et al. 1991). Low levels of $G\alpha_s$ have been observed in rat post infarction heart failure models (Sethi et al. 1998) and pacing induced heart failure in swine models (Roth et al. 1993). Although in human and experimental heart failure models there was no report of decreased $G\alpha_s$, though most of these studies did find increased $G\alpha_i$ and decreased AC activity in the heart tissues (Bohm et al. 1993; Brodde et al. 1998; Eschenhagen, Mende, Nose, Schmitz, Scholz, Haverich, Hirt, Doring, Kalmar, & Hoppner 1992). And there are even reports supporting that $G\alpha_s$ content is upregulated in heart failure (Feldman, Cates, Bristow, & Van 1989; Sethi et al. 1994). As a result the current literature is not ample enough to conclude that regulation of $G\alpha_s$ contributes to the pathophysiology of human heart failure. Studies using transgenic mice overexpressing $G\alpha_s$ under the control of myosin heavy chain promoter (which achieves cardiomyocyte-specific post natal gene expression), showed that there was an increase in $G\alpha_s$ activity along with an increase in the amount of β -AR coupled to $G\alpha_s$ (Gaudin et al. 1995). In a separate study, Iwase and colleagues found that overexpression of $G\alpha_s$ leads to enhanced isoprenaline stimulation but with basal

ventricular systolic function (FS) measured by echocardiography (Iwase et al. 1996). These mice also exhibited increased collagen content with fibrosis and cardiomyocyte hypertrophy with age. These findings in mice are consistent with increased cardiomyocyte death by apoptosis and replacement fibrosis in $G\alpha_s$ overexpressing hearts (Geng et al. 1999).

1.8 $G\alpha_{i/o}$ versus $G\alpha_s$ mediated signalling imbalance in cardiac pathology

In addition to modulation of cardiac automaticity, inhibitory G-proteins appear to regulate a number of distinct biological processes at the level of the ventricular cardiomyocyte. Signalling through $G\alpha_{i/o}$ by β_2 -AR affects cardiac contractility (Brown & Harding 1992), cardiac apoptosis (DeGeorge & Koch 2008) and has a direct role in modulating several cardiac ion channels (Nagata, Ye, Jain, Milstone, Liao, & Mortensen 2000). During exercise an appropriate increase in sympathetic tone (and parasympathetic withdrawal) occurs to increased inotropic and chronotropic function with reference to metabolic requirements. This is beneficial in acute physiological circumstances; however abnormal sympatho-vagal balance (sympathetic predominance) occurring in heart failure appears maladaptive. At a cellular level, sympathetic G_s activation of AC is inhibited by G_i signalling to control a multitude of cellular processes. Transgenic models of $G\alpha_s$ and $G\alpha_i$ have got different informative stories to reveal with regards to heart failure. *In vivo* expression of GiCT, a specific Gi inhibitor peptide, that inhibits Gi signals and not G_s or G_q in transgenic mice effectively causes a “functional knockout” of cardiac $G\alpha_{i2}$ signalling and these mice when subjected to ischemia/reperfusion injury demonstrated a significant increase in infarct size, increased myocardial apoptosis and the resultant decreased contractile performance indicating that up-regulation of $G\alpha_{i2}$ is an adaptive protective response

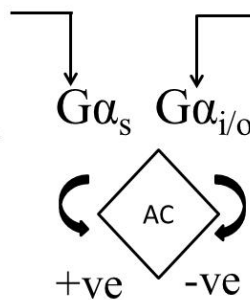
(Degeorge, Jr. et al. 2008). Thus G_i component on balance provides cardio protection against cardiac hypertrophy/apoptosis/progressive cardiac failure. Fig 1.9 shows different effects of sympathetic and parasympathetic control.

Activation of cardiac β_1 -adrenergic receptors via stimulatory G-proteins is the main mechanism that increases heart rate and contractility. Therefore several pharmacological and gene transfer strategies employed for the prevention of heart failure aim at improving the function of the cardiac β -AR system. Several studies have been undertaken to address this issue but still the answer is not complete. In acute MI, increase in cardiac specific AC type IV expression is associated with reduced mortality (Takahashi et al. 2006). The authors of this study found that cardiac directed expression of AC type IV mice had less LV dilation and increased ejection fractions. On the other hand in another study cardiac specific overexpression of β_1 -AR lead to a transitory improvement of cardiac function (at a young age), but developed marked myocyte hypertrophy followed by progressive heart failure with functional and histological deficits typical for humans with heart failure (Engelhardt et al. 1999). Another study with cardiac specific overexpression of $G\alpha_s$ showed enhanced β_1 -adrenergic receptor signalling with elevated heart rate due to enhanced sympathetic activity and ultimately led to cardiomyopathy (Uechi et al. 1998). Studies in transgenic mice over expressing β_2 -AR display increased contractility (Milano et al. 1994a; Rockman et al. 1996) and they appear to have normal life expectancy. It is tempting to hypothesize that β_2 -AR, besides its known cardiac stimulatory effects, exerts some sort of protection against hypertrophy and heart failure, possibly by parallel chronic $G\alpha_i$ signalling compared to β_1 -AR activated by stimulatory G-protein $G\alpha_s$. Testing this idea could shed some light on the question whether the well-known

up-regulation of $G\alpha_i$ found in human heart failure (Neumann, Schmitz, Scholz, von, Doring, & Kalmar 1988) is maladaptive or beneficial (Eschenhagen et al. 1996b; Grimm et al. 1998).

Sympathetic effects

Activation of $G\alpha_s$
 I_f channel activation via cAMP
 HR acceleration
 β adrenergic receptor desensitisation
 Cardiac apoptosis
 Reduced HRV
 Activation of renin-angiotensin system



Parasympathetic effects

Activation of $G\alpha_{i2}$
 Activation of GIRK channels by $\beta\gamma$
 Inhibition of cAMP via ($G\alpha_{i2}$)
 Reduced HR
 Improved baroreceptor sensitivity
 Improved HRV
 Direct antiarrhythmic effects

Figure 1.9 Sympathetic and parasympathetic interactions. Sympathetic and parasympathetic signals (e.g. from baroreceptors and chemoreceptors) are integrated by specific brainstem centres. Efferent impulses are then transmitted to the heart to modulate heart rate and contractility via the sympathetic chain and parasympathetic vagus nerve. Central to cardiac failure is the balance between $G\alpha_s$ and $G\alpha_{i/o}$ signalling as modulators of AC activity. Chronic elevation in cAMP concentration may for example trigger abnormal Ca^{2+} handling, cAMP triggered arrhythmia and apoptosis.

In recent years a clearer understanding of the biological impact of individual proteins within the heart has been determined at a molecular level by combining transgenic technology with physiological analysis of cardiovascular phenotype. This combined approach has been informative in several situations (Berul et al. 1997; Gehrman and Berul 2000; James et al. 1998) and may be applied to the study of G-protein signalling in the context of physiological measurement of autonomic tone which can be measured using heart rate variability (HRV) analysis which I have employed in my studies.

1.9 Heart Rate Variability (HRV) as measurement of autonomic tone

As its name suggests HRV refers to patterns of heart rate change (beat to beat interval variation) during physiological recording (Pumpřla et al. 2002;Stauss 2003). Cardiac automaticity originating from the sinus node is the heart's primary pacemaker and is modulated by several factors including sympathetic (causing tachycardia via $G\alpha_s$ signalling) and parasympathetic (causing bradycardia via $G\alpha_{i/o}$ signalling) afferents that add variability to the basic heart rate (R-R interval) signal at different characteristic frequencies over time. Analysis of these patterns of variation constitutes HRV analysis.

Patterns of heart rate variation can be divided into particular frequency ranges. Whilst parasympathetic responses slow heart rate, their signal transduction mechanisms are rapid with fast turnover allowing for fast (high frequency) beat to beat changes in heart rate. In contrast, sympathetic responses operate over a “relatively” slower timescale contributing to slow (low frequency) beat to beat changes in heart rate. From looking at a sufficiently long trace of sinus rhythm it is possible to discern specific patterns in heart rate variation.

HRV frequency ranges in humans include (Pumpřla, Howorka, Groves, Chester, & Nolan 2002):

- Ultra low frequency (ULF; > 5 hr. cycle length) that underlies circadian rhythm.
- Very low frequency (VLF; > 25s cycle length) modulated by temperature regulation mechanisms.
- Low frequency (LF; >6s cycle length) represents combined sympathetic and parasympathetic nerve activity.

- High frequency (HF; 2.5 – 6s cycle length) exclusively parasympathetic modulation.

HRV has been correlated with clinical outcome and represents a reproducible non-invasive measurement as a quantitative measure of cardiac autonomic modulation. A high variability in heart rate is generally considered as a sign of good cardiovascular adaptability, implying a healthy individual with well-functioning autonomic control mechanisms. In contrast, attenuation of HRV, particularly HF power is associated with adverse cardiovascular outcome in myocardial infarction (Bigger et al. 1993), heart failure (Adamson et al. 2004), mitral valve disease (Stein et al. 1992) and hypertension (Frenneaux 2004). Using prospectively recorded HRV data, prognostic insight can be determined, which could be used as an adjunct to guide treatment decisions e.g. consideration of implantable cardioverter-defibrillator (ICD) implantation therapy in patients at risk of sudden cardiac death (Pruvot et al. 2000).

1.10 The mouse as a model system to study cardiac electrophysiology *in vivo*

The mouse has turned out to be a potentially invaluable tool in cardiovascular research due to progress in molecular genetics. There are several reasons for this (Doevendans et al. 1998).

- It is relatively easy to perform gene targeting and transgenic experiments in mice.
- It is fairly reproducible to manipulate mouse embryonic stem cells with a very good success rate.
- There is an ever expanding knowledge of the mouse genome available.

- Gestation period of mice is short and it is relatively low cost for breeding and housing compared to other mammalian models.

More recently, technological advances such as the mapping of the murine genome have enabled investigators to modify genes quickly and with great accuracy to study various aspects of cardiovascular biology. The availability of genetically engineered transgenic mice has allowed for detailed investigation of the *in vivo*, *ex vivo*, and *in vitro* electrophysiological consequences of human mutations associated with arrhythmias (Remme 2013). However certain cardiac electrophysiological properties are inherently different between mouse and man reviewed by (Kaese and Verheule 2012). Transgenic mouse models may nevertheless successfully mimic human arrhythmia syndromes although observations regarding arrhythmia mechanisms may only be extrapolated to the human situation with caution. For example, mice with genetic alterations in the *Scn5a* gene encoding the cardiac sodium channel have provided insight into the role of this channel in both progressive cardiac conduction disease and Brugada syndrome, as detailed by (Huang et al. 2012). However the currents responsible for repolarization are different in the mouse (see below).

Technical developments have reduced the size of the equipment for physiological measurements to the mouse level. It is possible to obtain functional data from mouse circulation both *ex vivo* and *in vivo* (Grupp et al. 1993). Micro-surgery has developed to the level where most manipulations previously performed in larger animals can now be applied to mice. Although there are some major differences in the morphology of the heart between genera, the differences within mammalian species are only subtle (reviewed later). In terms of ventricular structure, the mouse heart is similar to the human heart, with the arrangement of valves providing the best discriminator between

the morphological right and left ventricle. In contrast to the human heart, there is little distinction between the apical trabeculations of the left and right ventricle in mice. The most important differences in cardiac structure of man and mouse are confined to the atrial and venous parts. In the mouse heart, unlike the human heart, the left superior caval vein persists and drains into the right atrium. The pulmonary vein has a solitary opening in the left atrium (Doevendans et al. 1998).

Coronary artery anatomy in the mouse is comparable to that of other mammals, with early branching of a large septal coronary artery (also seen in hamsters and rabbits) from the left coronary system. Controversy exists on the origin and importance of the circumflex branch in the mouse. The existence of a minor or rudimentary circumflex coronary artery was suggested by (Michael et al. 1995) in male FVB mice. Doevendans and group observed in 6 Swiss adult mice, the coronary system through a casting technique, and found a single left coronary artery, which branches into a large septal artery and left anterior descending artery, supplying the left ventricular free wall. In addition the right coronary artery branches proximal into a right ventricular and circumflex vessel supplying the left ventricular posterior wall.

The heart weight of an adult mouse shows considerable strain differences, and varies between 150 mg in FVB mice to 180 mg in Swiss mice (Gottshall et al. 1997). This implies a heart to body weight ratio of approximately 5.0–6.0 mg/g. The mouse body weight is approximately 0.05% of the average adult human. The heart weight is proportionally reduced in size, although 20% smaller than predicted from the regression equation developed by Stahl (Hein et al. 1997;Reiss et al. 1996). A significant increase in heart to body weight ratio to 7 mg/g was found in transgenic

mice overexpressing a constitutively active α_{1B} -adrenergic receptor in the heart (Milano et al. 1994b).

The murine conduction system is similar to larger mammalian systems in a number of ways. A sinoatrial (SA), atrioventricular (AV) and a His-Purkinje conduction network exist. A number of cardiac ion channels in humans and mice are generally conserved (Nerbonne et al. 2001) and so the transmural conduction velocities. Action potential heterogeneity, a critical substrate for arrhythmia mechanisms, is displayed by both mouse and human and it is similar. (Killeen et al. 2008). Various forms of heart block (Hagendorff et al. 1999), long QT with spontaneous ventricular torsades de pointes (Nuyens et al. 2001) and sudden cardiac death secondary to ventricular fibrillation (Danik et al. 2008) have been reported in murine models. Additionally, atrial (Kovoor et al. 2001) and ventricular arrhythmia (Berul et al. 1996;Korte et al. 2002;Park et al. 2008) can be recorded in mice using programmed electrical stimulation, however they are typically non-sustained compared to man. Whilst similarity exists there are notable differences also. Cardiac size is much smaller - the ventricular area is 100mm^2 and the atrial surface area is less than 35mm^2 . Traditionally the induction of fibrillation in a heart of this size was impossible on the basis of critical mass hypothesis (by Garry in 1914) as he suggested more than $100\text{-}200\text{mm}^2$ is required to induce fibrillation. But this hypothesis has been disputed (Vaidya et al. 1999;Wakimoto et al. 2001). The mouse heart rate is ~ 10 times faster than man and this is reflected in intrinsic differences between murine and human cardiac action potentials measured from individual cardiac myocytes (See Fig. 1.10). Repolarising K^+ currents are different in mouse and man. The fast and slow components of the I_{to} , transient outward current is critical in mouse and inactivation of these results in the Long QT syndrome in mouse (Salama and London 2007). By comparison these currents are much less important in

man and instead replaced by I_{K_s} (encoded by *KCNQ1* and *KCNE1*) and I_{K_r} (encoded by *HERG1*) which play a major contribution to ventricular repolarisation in man (and larger mammals). Despite these important differences, manipulation of several cardiac ion channels within the murine heart has provided insight into cardiac electrophysiology and highlighted the importance of ion channel dysfunction in a number of defined cardiac disease states (Kannankeril et al. 2006; Killeen, Thomas, Sabir, Grace, & Huang 2008; Salama & London 2007; Splawski et al. 2004).

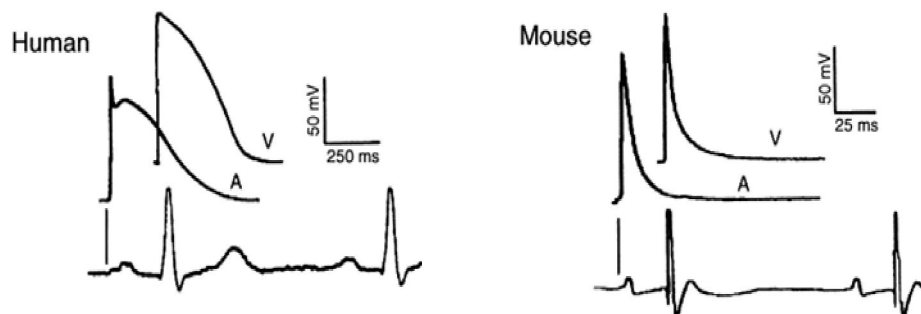


Figure 1.10 Comparison of human and murine cardiac action potentials. Transmembrane action potentials recorded from human atria (A) and ventricle (V) (left) compared with murine cardiomyocytes (right). Waveform kinetics is ~10 fold faster in mice and repolarisation signature is markedly different reflecting the relative species importance of different K_v channels in repolarisation. At the bottom of each trace surface ECG traces are also shown. In humans an isoelectric interval can be seen between QRS and T-wave. In the mouse the T wave merges with the terminal component of the QRS.

Genetic manipulation of the mouse genome can be done in 2 different ways. One is through transgenesis where naked DNA containing the gene sequence of interest is inserted into a fertilised embryo, and is expressed if the transgene is dominant. Promoters such as myosin heavy chain has been developed to drive cardiomyocyte specific expression of the transgene at particular development times, although this might integrate randomly and in varying copy numbers. Pharmacological agents such as tamoxifen can allow control of transgene induction through activation or

inactivation of transcriptional proteins. A second method is gene targeting which depends on homologous recombination where the modified DNA sequence is inserted and replaces the normal sequences. This is usually done in stem cells which are then injected into blastocysts (16 cell staged embryo). This method produces both knock-out and knock-in mutations depending on the site of integration. Conditional gene deletion is a method of tissue/ temporal specific targeting which utilises cre recombinase to recognise a lox-P site which is 13 base pair inverted repeats separated by an 8 base pair asymmetrical spacer region (Yutzey and Robbins 2007).

1.11 Animal models of heart failure

Animal models of heart failure have been used extensively in the past decades to characterize the pathophysiological and genetic mechanisms of this remodelling and failure for therapies to circumvent this adverse effect. A vast number of animal models have developed to mimic cardiovascular diseases and investigate their physiological and pathological processes. The aim of animal modelling of heart failure is to simplify an extremely complex syndrome into manageable research questions. Animal models of heart failure have contributed greatly to our understanding and analysis of the physiological effects of cardiac dysfunction, which are of great importance in the overall heart failure phenotype, as opposed to isolated organs or cells. Because of relatively complete annotation and simple manipulation of the mouse genome, it is possible to have significant mechanistic insights into human disease. Mouse models are indispensable tools in many areas of medical research and the mouse is, most often, the animal system of choice in disease modelling. Also the tremendous progress in molecular genetics and biology has opened up new horizons for the management of heart diseases.

The main aim of mice models of heart failure is to understand the complex syndrome of heart failure and this needs a viable model whereby persistent change in myocardial structure and function can be studied and the progression of heart failure and LV dysfunction can be quantified. A mouse model of coronary ligation to induce MI was first described 3 decades ago (Zolotareva and Kogan 1978). After that models of permanent coronary ligation were developed by several groups which is reviewed very well by Patten and Hall (Patten and Hall-Porter 2009). The most commonly used mouse models for heart failure is by surgical intervention by banding an aorta or clipping a coronary artery or by angiotensin infusion (Lohmeier 2012; Michael, Entman, Hartley, Youker, Zhu, Hall, Hawkins, Berens, & Ballantyne 1995; Rockman et al. 1991). These models closely mimic human conditions of myocardial infarction (coronary ligation) and heart failure owing to hypertension (angiotensin infusion) or aortic valve stenosis (aortic banding). A genetic model of dilated cardiomyopathy was developed by Arber and colleagues in which homozygous deletion of muscle lim protein (an actin based cytoskeletal protein that regulates myogenic differentiation) causes LV hypertrophy, dilation, systolic dysfunction and heart failure. Another genetic model of heart failure is mice with cardiomyocyte specific overexpression of TNF- α (a circulating cytokine that contributes to heart failure) that leads to LV hypertrophy, dilatation, systolic dysfunction and heart failure (Kubota et al. 1997). Apart from these administration of single toxin or drug like ethanol (Berk et al. 1975) and doxorubicin (Delgado, III et al. 2004) are also used to induce heart failure phenotype in mice. Different commonly used heart failure models are discussed in Materials and Methods (Table 2.1 Commonly used heart failure models).

My study focusses primarily on the *in vivo* role of inhibitory G-protein $G\alpha_{i2}$ and stimulatory G-protein $G\alpha_s$ predominantly in the SA node on heart rate, heart rate

variability and their responses to different pharmacological challenges. These mice are selective genetic models of bradycardia and tachycardia and I assess how they both respond to heart failure after myocardial infarction induced by coronary artery ligation. The role of RGSiG α_{i2} knock-ins and RGSiG α_0 knock-ins are also investigated.

1.12 Hypothesis

Neurotransmitters released from sympathetic and parasympathetic nerve terminals exert their effects via G-protein-coupled receptors in the sino-atrial node (SAN).

1. In the SA node, the inhibitory G-protein G α_{i2} slows down heart rate via muscarinic mediated vagal stimulation while the stimulatory G-proteins, G α_s , increases the heart rate by β adrenergic mediated signalling.
2. Deletion of RGS has opposite effects on heart rate compared to deletion of G α_{i2} .
3. Deletion of G α_s in the SA node leads to bradycardia and is protective in a heart failure.

1.13 Aims

- To conditionally delete $G\alpha_{i2}$ and/or $G\alpha_s$ in the SA node in mice. In the process I studied mice with cardiac specific deletion of $G\alpha_o$ and $G\alpha_{i2}$.
- To examine *in vivo* heart rate (HR) regulation by radio telemetry and pharmacological challenge in conditional deletion of $G\alpha_{i2}$, $G\alpha_o$ and $G\alpha_s$ mice and in mice with knock-in of RGS-insensitive G-proteins.
- To develop an MI model in mice and study LV contractile function in $G\alpha_{i2}$ or $G\alpha_s$ mice using serial echocardiography.

Chapter 2

MATERIALS AND METHODS

Materials and Methods

2.1 Overview

1. Animal breeding strategies and genotyping using a PCR based approach.
2. Describe the set-up of ECG telemetry hardware and its application to the study of heart rate dynamics in a physiological setting in mice with tissue specific G-protein transgenic deletion and RGS-insensitive knock-ins of $G\alpha_{i2}$ and $G\alpha_o$.
3. RNA isolation and real time PCR of heart samples of knockout mice.
4. Describe the methodological approach for performing a mouse MI model similar to MI in human.
5. Describe echocardiographic settings and its usage in analysing ventricular function in mice.

2.1.1 Animal breeding and general conditions

Mice were maintained at UCL and QMUL animal core facilities under the U.K. Home Office guidelines relating to animal welfare. All mice were kept in a pathogen-free temperature controlled environment (21-23°C) with 12hr day/12hr night light cycles. Animals were allowed access to standard rodent chow and water *add-libitum*. Mice of both sexes were studied between 12-14 weeks of age under standardised conditions. Use of animals in all the studies was in accordance with the United Kingdom Animal (Scientific Procedures) Act of 1986. Mice showing signs of poor health and barbarisation were excluded from use.

2.1.2 Cardiac tissue-specific $G\alpha_0$ and $G\alpha_{i2}$ deletion using α MHC cre recombinase

$G\alpha_0$ (-/-) mice demonstrate early postnatal death due to seizure activity and abnormal neurodevelopment which impairs the ability of $G\alpha_0$ (-/-) mice to feed appropriately. Given this neurological phenotype, published survival into adulthood is of the order of $\approx 6\%$ (Valenzuela et al. 1997). In $G\alpha_{i2}$ (-/-) mice growth retardation was observed, few litters were produced and occasional unexpected death was seen. In order to improve survival rates, mice with tissue specific (cardiac only) $G\alpha_0$ and $G\alpha_{i2}$ deletion were generated using a cre lox-P approach (see Fig. 2.1). Cre-recombinase is a gene product of the bacteriophage P1 and can identify specific 34bp DNA sequences (lox-P sites). Cre facilitates the deletion of DNA fragments flanked by two lox-P sites and splices together the cut ends. Cardiac specific cre expression has been published using an α -myosin heavy chain (α MHC) promoter (Agah et al. 1997). Professor Micheal Schneider kindly donated an α MHC cre line on a C57/black background for our experiments. $G\alpha_0$ and $G\alpha_{i2}$ floxed mice ($G\alpha_0$ flx/flx) ($G\alpha_{i2}$ flx/flx) on a Sv129 background were generated and donated by Professor Lutz Birnbaumer.

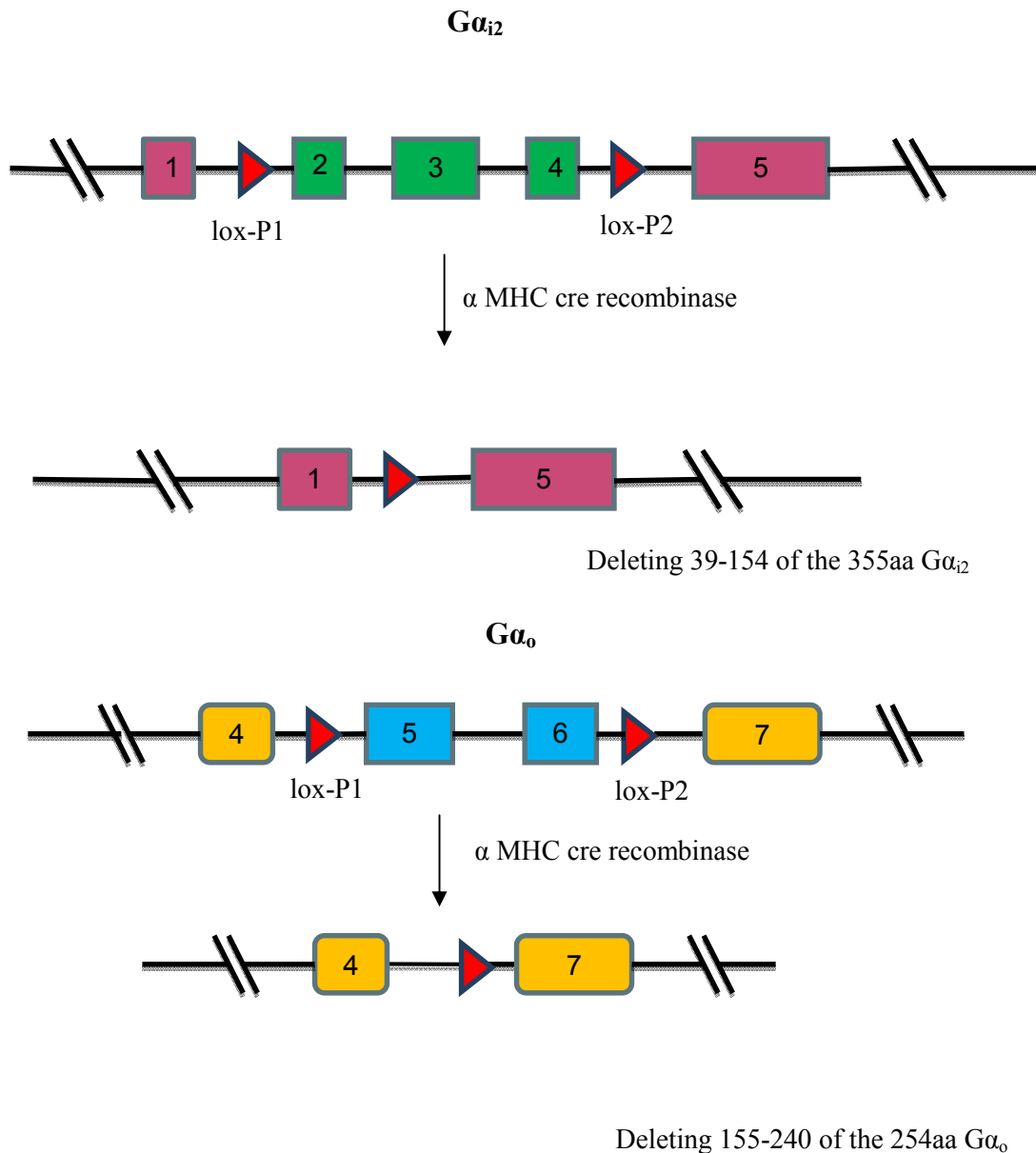


Figure 2.1 Cre lox-P mediated $G\alpha_{i2}$ and $G\alpha_o$ deletion. Lox-P sites in the floxed allele of $G\alpha_{i2}$ were placed into the intron upstream of exon 2 (lox-P1) and in the intron downstream of exon 4 (lox-P2). After cre-mediated excision this will leave an allele coding for an inactive $G\alpha_{i2}$ that lacks sequences encoded in exons 2 through 4, i.e. amino acids 39-154 of the 355aa $G\alpha_{i2}$. In the $G\alpha_o$ floxed allele, the loxP sites are in the upstream of exon 5 (loxP-1) and in the downstream of exon 6 (loxP-2). After cre-mediated excision this will leave an allele that codes for $G\alpha_o$ that lacks sequences encoded in exons 5 and 6, i.e. lacking amino acids 155-240 of the 254aa $G\alpha_o$. In both disruptions, portions of the GTPase domain are lost and the proteins are predicted to misfold and to be degraded.

By intercrossing of α MHC cre mice with floxed $G\alpha_o$ ($G\alpha_o$ flx/flx) and floxed $G\alpha_{i2}$ ($G\alpha_{i2}$ flx/flx), heterozygote ($G\alpha_o$ flx/wt) and ($G\alpha_{i2}$ flx/wt) mixed background mice

containing the α MHC cre transgene were produced. Mice containing both the transgenes ($G\alpha_0$ flx/wt- α MHC cre and $G\alpha_{i2}$ flx/wt- α MHC) were further crossed to obtain $G\alpha_0$ flx/flx/ α MHC cre⁺ and $G\alpha_{i2}$ flx/flx/ α -MHC cre⁺ mice and all other genetic combinations were used as controls.

2.1.3 Specific $G\alpha_{i2}$ deletion in the cardiac conduction system

I used a knock-in of tamoxifen inducible cre into the hyperpolarization activated cyclic nucleotide-gated cation channel 4 (HCN4) locus resulting in HCN4-KiT mice which effectively delete floxed genes in the pacemaker cells after treatment with tamoxifen (Hoesl et al. 2008). They were kindly provided by Professor Andreas Ludwig. Briefly the 5' homology arm (2.3 kb immediately upstream of the HCN4 start codon) and the 3' homology arm (4.7 kb encoding parts of exon 1 and intron 1) were sub-cloned from a P1 phage. The CreER^{T2} sequence followed by a SV40 polyadenylation signal and a neomycin selection cassette was placed in-frame into the HCN4 start codon. The targeting vector was electroporated into embryonic stem cells and G418/ganciclovir resistant clones were screened by Southern blot. A positive clone was injected into C57BL/6blastocysts to generate chimeric mice which transmitted the modified locus to the germ line (Hoesl, Stieber, Herrmann, Feil, Tybl, Hofmann, Feil, & Ludwig 2008).

By inter-crossing of HCN4-KiT cre with floxed $G\alpha_{i2}$ ($G\alpha_{i2}$ flx/flx), heterozygote ($G\alpha_{i2}$ flx/wt) mixed background mice containing the HCN4-KiT cre transgene were produced. These were then further crossed with mice containing both the transgenes to obtain $G\alpha_{i2}$ flx/flx HCN4-KiT cre mice and the other genetic combinations of wt cre⁻ and wt cre⁺ were used as controls.

2.1.4 $G\alpha_s$ deletion in the cardiac conduction system

To complement the studies of $G\alpha_{i2}$ deletion using the conduction system cre recombinase, mice with cardiac-specific deletion of $G\alpha_s$ in the conduction system using the same conduction system cre (HCN4-KiT cre) were also studied. A description of the targeting strategy to produce $G\alpha_s$ flx/flx lines has been described (Chen et al. 2005). They were kindly provided by Professor Lee Weinstein. After breeding with HCN4-KiT cre mice in our lab we generated $G\alpha_s$ flx/flx cre⁺ mice and littermate “controls”, which consisted of WT cre⁺ WT cre⁻ (Fig. 2.2). We observed no prominent differences among the latter groups and thus pooled them into single littermate control populations.

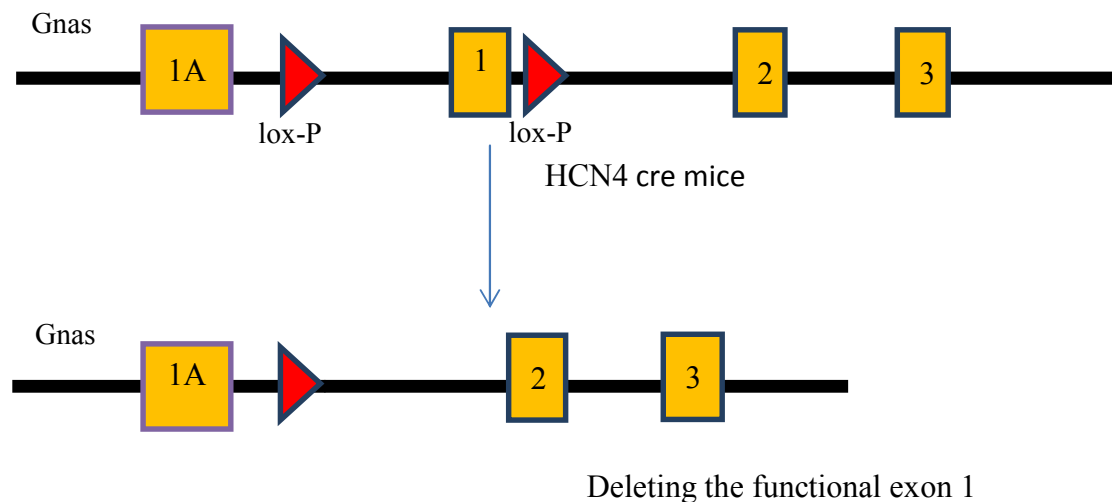


Figure 2.2 Generation of conduction system-specific $G\alpha_s$ mice. Floxed $G\alpha_s$ mice were crossed with HCN4 cre mice. After successive rounds of breeding, we generated $G\alpha_s$ flx/flx cre⁺ mice and littermate “controls”, which consisted of wild-type, cre⁺ and wild-type, cre⁻.

In order to achieve selective deletion of $G\alpha_{i2}$ and $G\alpha_s$ in the conduction system tissues double transgenic mice with $G\alpha_{i2}$ flx/flx HCN4 cre⁺ and $G\alpha_s$ flx/flx HCN4 cre⁺ were injected with tamoxifen (Sigma T5648-1G). Tamoxifen was freshly dissolved in

sunflower oil (10mg in 900 μ l of sunflower oil and 100 μ l ethanol) and 1 mg tamoxifen/25g body weight was injected IP (intraperitoneal) on 5 consecutive days and mice were studied 7-10 days after the last dose. Mice of both sexes were used in this study.

2.1.5 Transgenic RGS-insensitive G_o (RGSiG_o) and G_{i2} (RGSiG_{i2}) mice.

It has been difficult to ascertain the full function of endogenous RGS proteins *in vivo* because of their functional redundancy (Fu, Huang, Zhong, Mortensen, D'Alecy, & Neubig 2006). Thus to investigate the role of endogenous RGS proteins in heart rate regulation, we used G α_{i2} RGSi and G α_o RGSi knock-in mice where the expression of the mutant protein is under the control of its own promoter. They were kindly donated to us by Professor Richard Neubig. These knock-ins have G α subunits containing a G¹⁸⁴S point mutation in their switch I region that prevents binding of RGS protein and subsequent G α deactivation (Lan, Sarvazyan, Taussig, Mackenzie, DiBello, Dohlman, & Neubig 1998). Generation of G α_{i2} RGSi and G α_o RGSi knock-in mice are described here (Fu, Zhong, Nanamori, Mortensen, Huang, Lan, & Neubig 2004; Huang et al. 2006). Knock-ins maintain normal distribution and levels of G α_{i2} and G α_o expression compared to transgenic models.

2.2 Mouse genotyping

Mice were tail clipped (~2mm) at 3-4 weeks of age. Genomic DNA was isolated from tail clips. Polymerase chain reaction (PCR) based genotyping was then performed on isolated DNA to confirm the genotype of individual mice.

2.2.1 DNA extraction of tail tips

Mice were ear-marked for identity purposes and then tail tips were snipped with scissors and placed in ependorf tubes. Tail lysis buffer stock was made as follows.

3.35ml 2M Tris-HCl pH 8.8,

1.66ml 1M (NH₄)₂SO₄,

1.34ml 0.5M MgCl₂ ,

0.5ml Triton X-100,

92.2ml H₂O.

To 1.0 ml of this stock 10 μ l of β -mercaptoethanol (Sigma M 3148) was added and 150 μ l of this tail lysis buffer was then added to tail samples and the samples were heated to 100°C for 10 minutes in a heating block to denature mouse proteins. Samples were then cooled and 5 μ l of proteinase K (20mg/ml) was added at 55°C for 12 hours to cause non-specific protein digestion. Samples were then reheated to 100°C for a further 10 minutes and then spun down at 13000rpm for 3minutes in a tabletop centrifuge to sediment tail debris. 1.0 μ l of sample (mouse genomic DNA) was used per genotyping PCR.

2.2.2 DNA extraction from heart and SA node

Ventricular heart tissues were obtained from $G\alpha_{i2}$ flx/flx α -MHC cre mice, $G\alpha_o$ flx/flx α -MHC cre mice and SA nodal tissue was obtained from the cardiac conduction system-specific $G\alpha_{i2}$ and $G\alpha_s$ knock-out mice and processed as discussed above (for the tail) for genomic DNA extraction. 1.0 μ l of genomic DNA from ventricular heart tissue was subjected to PCR to confirm cre mediated deletion of $G\alpha_{i2}$ and $G\alpha_o$ in the

heart and not in other tissues for $G\alpha_{i2}$ flx/flx α MHC cre mice and $G\alpha_o$ flx/flx α MHC cre mice. In addition 1.0 μ l of genomic DNA from SA nodal tissue was subjected to PCR to confirm cre-mediated deletion of $G\alpha_{i2}$ and $G\alpha_s$ in the SA node of $G\alpha_{i2}$ flx/flx HCN4Ki-T mice and $G\alpha_s$ flx/flx HCN4Ki-T mice at the genomic level.

2.2.3 $G\alpha_o$ lox-P floxed allele, $G\alpha_{i2}$ lox-P floxed allele and α MHC cre genotyping

$G\alpha_o$ lox-P (floxed allele) genotyping was performed using the following primers from Invitrogen 25nmole desalted: GnaoF1B 5'- AAG AAT AGA ACC TAG GAC TGG AGG - 3' and GnaoR 5'-GCA GAC AAG TGA ACA AGT GAA ACC C-3'. A hotstart PCR strategy (using Qiagen hot start master mix- 203443) was used to detect the presence of a 1868bp band corresponding to WT, a 2142bp band corresponding to the $G\alpha_o$ lox-P (floxed) allele and a 442bp band after cre recombinase activation (Fig. 2.3).

$G\alpha_{i2}$ lox-P (floxed allele) genotyping was performed using the following primers from Invitrogen 25nmole desalted: $G\alpha_{i2}$ LoxF5'- GGA GCC TGG ACT TTG CTT CTG ACC-3' and $G\alpha_{i2}$ LoxR5'- GGC TAT GAT CCC AAA ACT CCC CG- 3' $G\alpha_{i2}$ LoxF2 5'- GTG GTA AGC CTG TGT GTT TGT GAG AG-3'. A hotstart PCR strategy using Qiagen hot start master mix (Qiagen 203443) was used to detect the presence of a 400bp band corresponding to WT, a 500bp band corresponding to the $G\alpha_{i2}$ lox-P (floxed) allele using: G_{i2} LoxF and $G\alpha_{i2}$ LoxR and a 400bp band after cre recombinase activation, using $G\alpha_{i2}$ LoxF2 and G_{i2} LoxR (Fig. 2.3). PCR conditions are summarised below.

Gα_o lox-P allele PCR

Qiagen hot startaq	10.0 µl
GnaoF1B (10µM)	2.5 µl
GnaoR (10µM)	2.5 µl
Deionised water	9.0 µl
Genomic DNA	1.0 µl

Gα_{i2} lox-P allele PCR


Qiagen hot startaq	10.0 µl
Gα _{i2} LoxF5 (10µM)	2.5 µl
Gα _{i2} LoxR5 (10µM)	2.5 µl
Deionised water	9.0 µl
Genomic DNA	1.0 µl

Gα_o lox-P allele PCR programme

Heated lid 110°C for 15min

94°C for 15 min

94°C for 1 min
62°C for 1 min
72°C for 2 min



35 cycles

72°C for 10 min


Samples stored at 8°C until gel run

Gα_{i2} lox-P allele PCR programme

Heated lid 110°C for 15min

94°C for 15 min

94°C for 30 sec
60°C for 30 sec
72°C for 1 min



35 cycles

72°C for 10 min

Samples stored at 4°C until gel run

Identification of α-MHC cre expression was determined using the following primer sets: cre F 5'-ATGAC AGACA GATCC CTCCT ATCTC C-3' and cre R 5'-CTCAT CACTC GTTGC ATCAT CGAC-3'. The presence of the cre transgene was determined by the presence of a cre band (300bp).

αMHC cre PCR


NEB 10x buffer	10.0 µl
25mM dNTP	1.0 µl
100µM cre F	1.0 µl
100µM cre R	1.0 µl
NEB taq polymerase	1.0 µl
Deionised water	84.0 µl
Use 35 µl of above mix and genomic DNA	1.0 µl

αMHC cre PCR programme

Heated lid 110°C for 15min

94°C for 5 min

94°C for 1 min
60°C for 1 min
72°C for 1 min



35 cycles

72°C for 10 min

Samples stored at 8°C until gel run

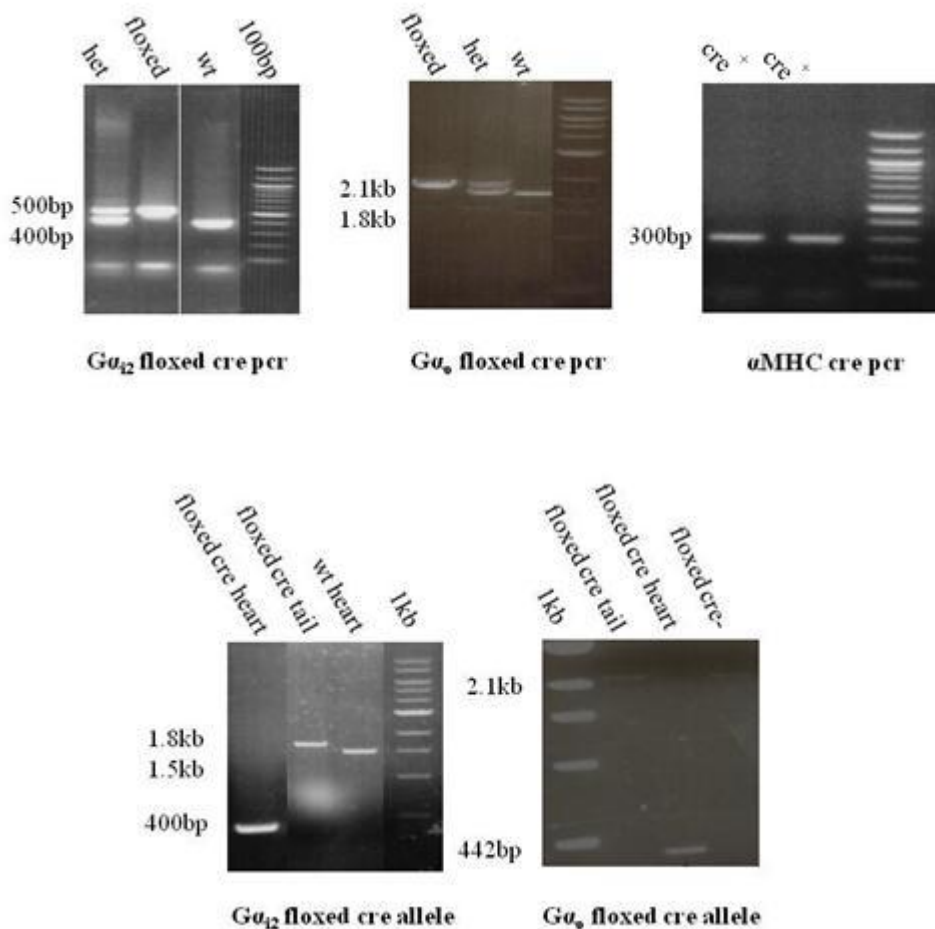


Figure 2.3 Gel of PCR of $G\alpha_{i2}$ floxed, $G\alpha_o$ floxed and cre allele. Upper panel shows floxed allele and cre allele where floxed allele shows a higher bp band due to the presence of lox-P sites for $G\alpha_{i2}$ (500bp) and $G\alpha_o$ (2.1kb). Cre allele is confirmed as a 300bp band. Lower panel shows floxed cre allele, where after cre mediated deletion shows 400bp band in the heart of $G\alpha_{i2}$ floxed cre allele and 442bp in the heart of $G\alpha_o$ floxed cre allele.

2.2.4 RGSi $G\alpha_{i2}$ and RGSi $G\alpha_o$ genotyping

RGSi $G\alpha_o$ and RGSi $G\alpha_{i2}$ genotyping were performed using the following primers:

$G\alpha_{i2}$ FlankLoxF 5'- CAC ACT TCA CCT TCA AGG AC-3'



$G\alpha_{i2}$ FlankLoxR 5'- CTG ATG CCT AGG TGA CAG AC-3'

$G\alpha_o$ FlankLoxF 5'- CGC AGG CTC TGA GGG CCT AAG-3'

$G\alpha_o$ FlankLoxR 5'- TGC CTC ACC TCT CCG TCT CC -3'.

Conventional PCR strategy was used to detect the presence of heterozygote yielding two bands one at 400bp and another at 200bp and wild type at 200bp alone for both RGSiG α_0 and RGSiG α_{i2} (Fig. 2.4).

PCR reaction mix and conditions are as follows.

RGSiGα_{i2} PCR		RGSiGα_0 PCR	
NEB 10x buffer	2.5 μ l	NEB 10x buffer	2.5 μ l
2.5mM dNTP	2.5 μ l	2.5mM dNTP	2.5 μ l
G α_{i2} FlankLox F (10 μ M)	2.5 μ l	50mM MgCl ₂	1.0 μ l
G α_{i2} FlankLox R (10 μ M)	2.5 μ l	G α_0 FlankLox F (10 μ M)	2.5 μ l
NEB taq polymerase	0.2 μ l	G α_0 FlankLox R (10 μ M)	2.5 μ l
Deionised water	13.8 μ l	NEB taq polymerase	0.2 μ l
Genomic DNA	1.0 μ l	Deionised water	12.8 μ l
		Genomic DNA	1.0 μ l
RGSiGα_{i2} PCR programme		RGSiGα_0 PCR programme	
Heated lid 110°C for 15min		Heated lid 110°C for 15min	
95°C for 4 min		95°C for 4 min	
95°C for 30 sec 62°C for 30 sec 72°C for 30 sec  34 cycles		95°C for 30 sec 64°C for 30 sec 72°C for 30 sec  32 cycles	
72°C for 7 min		72°C for 7 min	
Samples stored at 8°C until gel run		Samples stored at 8°C until gel run	

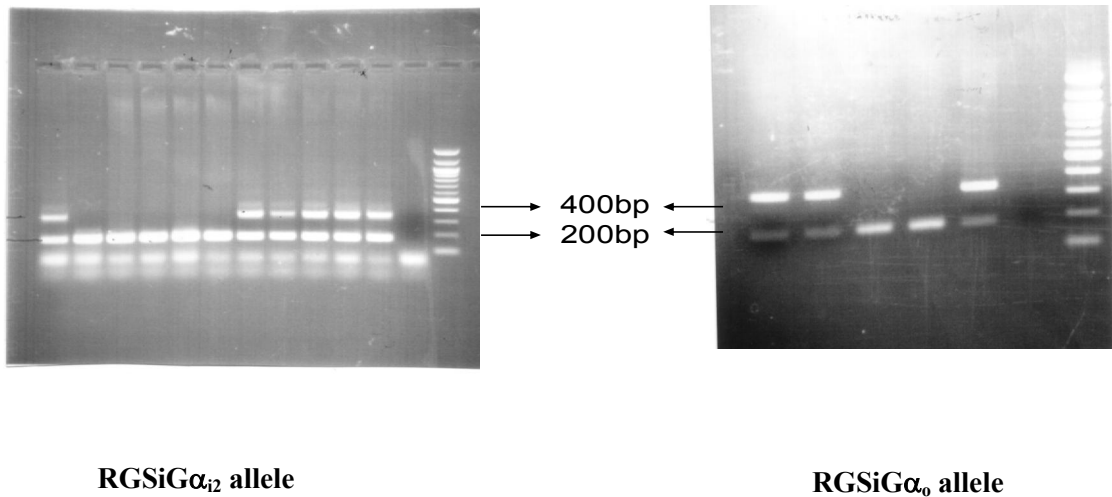


Figure 2.4 Gel of PCR of RGSiG α_{i2} and RGSiG α_o genotyping. RGSiG α_{i2} and RGSiG α_o both per shows heterozygote band of both 400bp and 200bp and 200bp alone for the wild type .

2.2.5 G α_s floxed and conduction system cre genotyping

G α_s lox-P (floxed allele) genotyping was performed using the following primers from Invitrogen 25nmole desalted: G α_s LoxF 5'- TTCGG TCTCG TCCCC TTAGT TG-3' and G α_s LoxR 5'-AACAA ATCGC ACACC CCAGT GAGG-3' using betaine (1.5M) in the PCR master mix to obtain a WT band corresponding to ~216bp and a G α_s floxed band corresponding to ~264bp respectively. Cre mediated excision was confirmed by G α_s cre F 5'-GAGAGCGAGAGGAAGACAGC-3' and G α_s cre R 5'-AGCCCTACTCTGTCGCAGTC-3' primers which gives a band of ~250bp upon cre mediated excision of exon 1 (Fig.2.5).

Identification of HCN4 cre expression was determined using the following primer sets: HCN4KiF 5'-CCCGCGCTGGAGTTTCAATA-3' and HCN4KiR 5'-CTTCGCCAGTT GATCATGTG-3'. The presence of the conduction system cre transgene was determined by the presence of a cre band (383bp) (Fig.2.5). PCR conditions are summarised below.

G α_s lox-P allele cre PCR

NEB 10x buffer	5.0 μ l
2.5mM dNTP	4.0 μ l
G α_s LoxF (10 μ M)	2.0 μ l
G α_s LoxR (10 μ M)	2.0 μ l
NEB taq polymerase	0.2 μ l
Deionised water	6.8 μ l
Genomic DNA	1.0 μ l

Conduction cre PCR


NEB 10x buffer	10.0 μ l
25mM dNTP	1.0 μ l
100 μ M cre F	1.0 μ l
100 μ M cre R	1.0 μ l
NEB taq polymerase	1.0 μ l
Deionised water	84.0 μ l
Use 35ul of above mix and genomic DNA	1.0 μ l

G α_s lox-P allele PCR programme

Heated lid 110°C for 15min

94°C for 5 min

94°C for 30 sec
63°C for 30 sec
72°C for 45 sec



40 cycles

72°C for 7 min


Samples stored at 8°C until gel run

Conduction cre allele PCR programme

Heated lid 110°C for 15min

94°C for 5 min

94°C for 30 sec
59°C for 1 min
72°C for 1 min



30 cycles

72°C for 10 min

Samples stored at 8°C until gel run

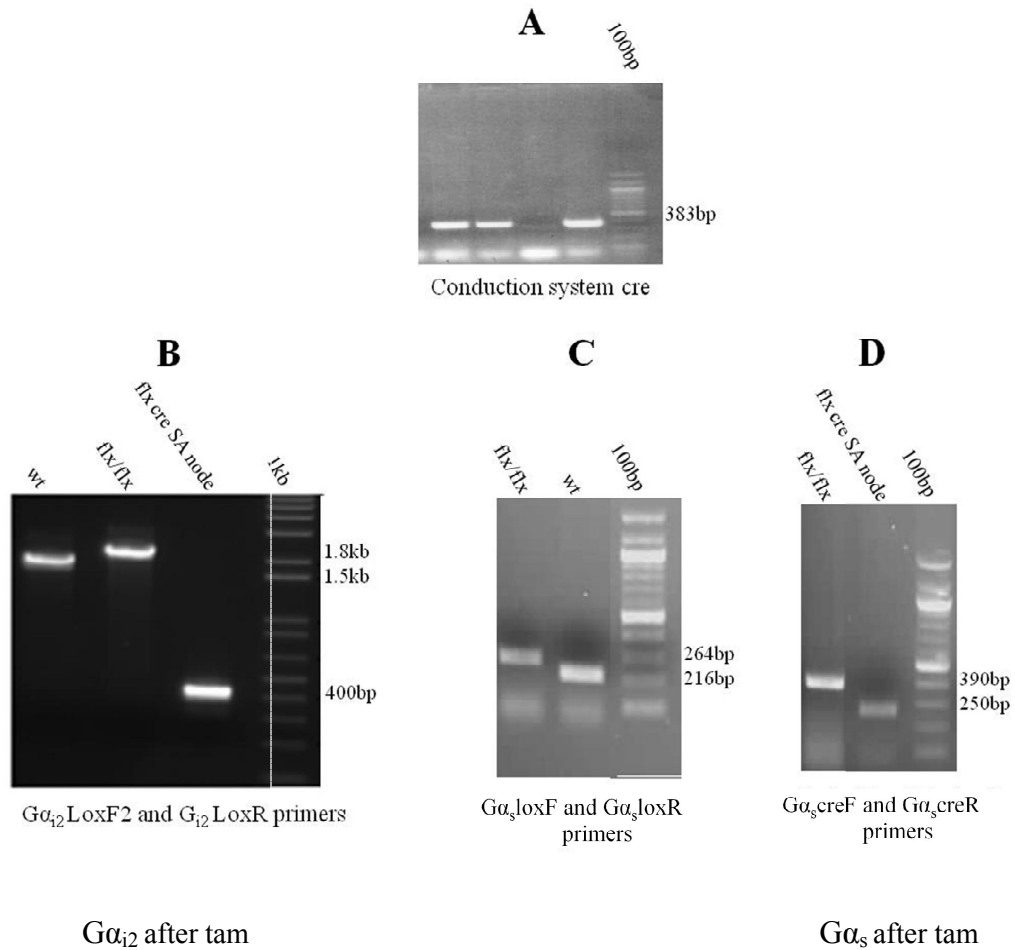


Figure 2.5 Gel PCR of $G\alpha_{i2}$ flx/flx, $G\alpha_s$ flx/flx and cre allele. A) shows conduction system cre per confirmed as a 300bp band. Lower panel shows cre mediated deletion in $G\alpha_{i2}$ floxed allele and $G\alpha_s$ floxed allele. B) G_{i2} floxed allele and WT allele where floxed allele shows a higher bp band in heart due to the presence of lox-P sites for $G\alpha_{i2}$ (1.8kb) to WT allele (1.5kb) and after cre mediated excision in SA node shows floxed cre allele of 400bp band for $G\alpha_{i2}$ floxed cre allele. C) $G\alpha_s$ floxed allele and WT allele, where floxed allele shows a higher bp band in heart due to the presence of lox-P sites for $G\alpha_s$ (264bp) to WT allele (216bp). D) After cre mediated excision (after tamoxifen) in SA node shows floxed cre allele of 250bp band in the SA of $G\alpha_s$ floxed cre allele and 390 bp in the heart of $G\alpha_s$ floxed cre allele.

2.3 Quantitative Real-time PCR on isolated ventricle and SA nodal tissue

The advent of PCR by Kary B. Mullis in the mid-1980s revolutionized molecular biology. It is used to amplify and simultaneously quantify the targeted DNA molecule. The amount of an expressed gene in a cell can be measured by the number of copies of an mRNA transcript of that gene present in a sample. In order to detect and quantify gene expression from small amounts of RNA, extracted RNA is first reverse transcribed to cDNA using reverse transcriptase. Then by using specific primers for the gene of interest and a fluorescent labelled probe (e.g. taqman probe) fluorescence of the fluorophore can be measured which will be proportional to the amount of cDNA present in the sample. The data generated can be analyzed by computer software to calculate relative gene expression (or mRNA copy number) Fig 2.6.

RNA was isolated from the ventricles, brain and tail of $G\alpha_{i2}$ flx/flx α MHC cre⁺, $G\alpha_o$ flx/flx α MHC cre⁺ and control mice and also from SA node and ventricle after tamoxifen treatment in both $G\alpha_s$ flx/flx HCN4 cre⁺, $G\alpha_{i2}$ flx/flx HCN4 cre⁺ and their control mice using the RNeasy kit (Qiagen). Briefly, hearts were removed from each group of mice (control and KO), washed with cold PBS and immediately placed in liquid nitrogen. They were ground in liquid nitrogen with a pestle and mortar and then extraction of RNA using RNeasy kit (cat no. 74104 Qiagen) was carried out. cDNA was synthesized using the High capacity cDNA reverse transcription Kit (4368814 Applied Biosystems). cDNA was quantified and 50ng of cDNA/20 μ l was used for the subsequent real time expression assay. All genes were assayed in triplicate and GAPDH was used as the house keeping gene. Real-time PCR was performed using Taqman gene expression Assays (Applied Biosystems) using either inventoried or made to order assays. The protocol followed was based on the information provided

by the supplier, which is available on their website (http://www3.appliedbiosystems.com/cms/groups/mcb_support/documents/cms_041280.pdf). By using Taqman gene expression assay (Assay ID: Mm03945887_s1) which spans exon 1, $G\alpha_s$ cDNA was quantified. $G\alpha_{i2}$ cDNA was then quantified using the Taqman gene expression assay kit using custom designed primers spanning exon 2 boundary TGG AGA GTC AGG GAA GAG CA and exon3 TAG ACC ACG GCA CGG TAC T (Applied Biosystems). $G\alpha_o$ cDNA was quantified using Taqman gene expression assay (Assay ID: Mm01249631_m1) which spans exon 5-6 of $G\alpha_o$. All genes were assayed in triplicates and relative gene expression was quantified using the comparative C_T method with GAPDH as the reference housekeeping gene.

High capacity cDNA PCR	High capacity cDNA PCR programme
Qiagen 10x RT buffer 2.0 μ l	Heated lid 110°C for 15min
25x dNTP mix (100mM) 0.8 μ l	37°C for 60 min
10x random primers 2.0 μ l	95°C for 5 min
Reverse transcriptase 1.0 μ l	Samples stored at 8°C until use for
RNase Inhibitor 1.0 μ l	Taq man gene expression assay.
Nuclease free water 3.2 μ l	
Use 10 μ l of above mix + 10 μ l of up to 0.2 μ g of RNA per tube.	

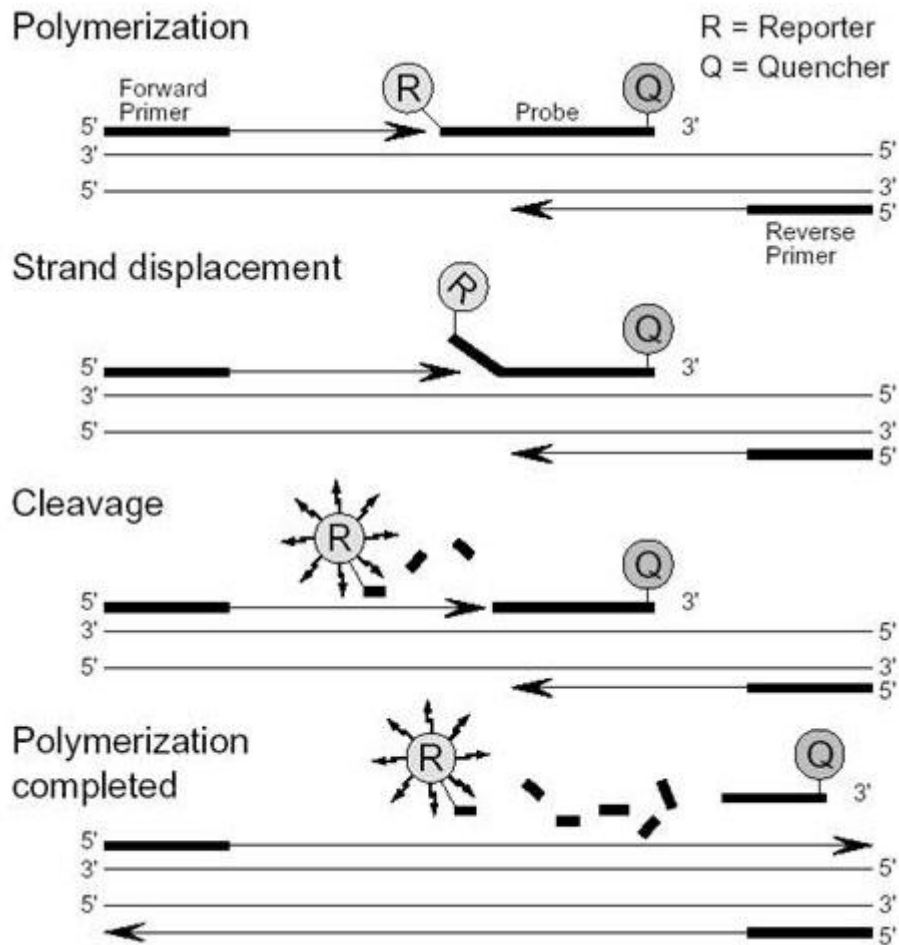


Figure 2.6 Real-time PCR using Taqman probe. The Taqman probe has a Quencher dye (Q) and a Reporter dye (R). The quenching dye disrupts the observable signal from the reporter dye when it is within a short distance. When the probe is annealed to the target and is intact there is no fluorescence. After binding of the Taqman® probe and primer to the target DNA, Taq polymerase creates a complementary strand. As the primer anneals and extends to the probe, it cleaves the probe, due to 5' nuclease activity of Taq and the reporter dye is released from the extending double-stranded DNA. Following the separation of the reporter dye and quencher dye, fluorescence can be detected. Figure adapted from life technologies - Taqman gene expression assays.

2.4 Murine electrocardiogram (ECG) telemetry & heart rate analysis

Telemetric ECG recording in mice is essential in understanding the mechanisms behind arrhythmias, conduction disorders and sudden cardiac death. Implantable ECG telemeters offer the advantages of simple surgical implantation and long-term recording of signals in ambulatory mice. Continuous surface ECG tracings were recorded from mice using surgically implantable telemetry devices (Data Science International, DSI). Using this technology, continuous ECG sampling for up to 4 months can be recorded from individual animals. Potential hazards of animal restraint and anaesthesia are removed and multiple electrophysiological parameters can be measured including basal HR, exercise induced HR (and HR recovery), the effects of pharmacological intervention on HR, circadian HR rhythms and heart rate variability patterns. ECG parameters such as PR or QT interval can also be readily measured in a physiological setting (see Fig. 2.7). Additionally long term recordings can be inspected for spontaneous arrhythmia.

An ECG recording simply reflects the electrical potential difference between two adjacent electrode pairs. Signal is sampled at a programmable frequency from the probe and the ECG signal transmitted to a receiver mat by radio wave and digitised into a conventional ECG tracing with the aid of computer processing. Commercially available software (DATAQUEST ART v3.0/Chart v7.0) can then be used to delineate individual parameters from the raw ECG tracing e.g. heart rate.

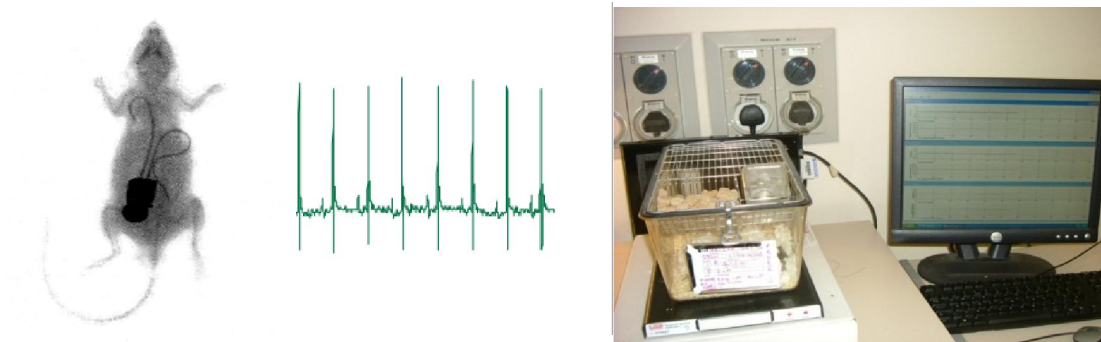


Figure 2.7 Schematic diagram of murine telemetry and ambulatory ECG. The telemetry device is implanted within the abdomen. ECG signal is transmitted by radio wave to a receiver. The signal is then digitised and displayed on a computer console. The trace in the middle illustrates a mouse surface ECG rhythm strip recorded in a conscious freely moving mouse.

2.5 Telemetry probe implantation

Mice were individually caged for 48 hours prior to device implantation. Implantation was performed with close attention to good surgical technique and in an aseptic environment throughout. Inhalation anaesthesia by means of isoflurane was used and murine anaesthesia was maintained with 1.7% isoflurane combined with oxygen. Mice were placed on a sterile drape rested on a heating mat set to regulate the mouse temperature at 37°C. Mice were then secured with masking tape in a supine position. The abdominal wall was swabbed with 70% ethanol solution as a disinfectant and then an induction bolus of buprenorphine (0.2mg/kg) and prophylactic antibiotics (5µl 1% Baytril) were administered by intraperitoneal injection. A midline laparotomy was performed, skin, muscle layer and peritoneum was carefully divided; the peritoneal cavity was then inspected to check sizing suitability for probe implantation. Specifically designed murine telemetry probes (model TAE10-F20, DSI) were then carefully placed within the abdominal cavity taking care not to disturb or compress

bowel loops and other intra-abdominal visceral organs. Attached to the main probe were two electrode leads coated in insulating rubber. These were colour coded: colourless (negative) and red (positive). Two stab incisions were made in the upper anterior abdominal wall, either side of the major incision, to allow for the passage of the electrodes into the subcutaneous tissue plane. The abdominal wall was then closed using interrupted silk stitches. The ends of each electrode were cut to approximate length and a small sheath of insulating rubber cut back from the electrode tips to exposing bare metal wire. Two further incisions were performed, one in the anterior right shoulder position, and one at the cardiac apex. The leads were then subcutaneously tunnelled from the abdomen to these respective positions; the bare electrode tips were stitched to the chest wall muscle to ensure good tissue contact in a Lead II ECG configuration. Each incision was then closed in layers. At the end of the procedure (approximately 20 to 30 minutes) 200-300 μ l of prewarmed 5% dextrose/saline was administered IP for post-operative hydration. Mice were then returned to housing cages placed on warming mats for surgical recovery. Additional analgesia was administered at 6hr and/or 24 hours post procedure if deemed necessary. Mouse recovery from the procedure was generally rapid (typically 1 to 2 days), however we elected to observe mice for at least 7-10 days prior to any ECG recording to ensure full surgical recovery prior to any physiological ECG recording. Each telemetry probe had a magnetic switch which could be turned on or off (to save battery life) with the aid of a magnetic wand at times of ECG recording. After switching the device on, mice cages were placed on receiving mats to allow for non-invasive ECG recording and the signal sampled at 2000Hz. Before recording, mice were given a thirty minute “run in” period. For serial heart rate measurements, 15s recordings were measured every 30 minutes over 2 days using a “scheduled sampling” protocol. From this data-

set it was possible to observe diurnal changes in HR between day and night and also calculate mean HR.

2.5.1 Heart rate variability assessment

Heart rate variability is a measure of the mean changes in the interval or distance between one beat of the heart and the next. Heart rhythm, even in a mouse shows subtle beat to beat variations between successive R-R intervals (See Fig. 2.8). The inter beat interval (IBI) is the time between one R-wave (or heart beat) and the next, in milliseconds. The IBI is highly variable within any given time period. Measurements of such R-R interval variability during sinus rhythm under basal conditions, constitutes heart rate variability (HRV) analysis. HRV is used principally as a non-invasive measurement of autonomic tone, measured as a modulation of sinus node function and can be used to specifically determine the parasympathetic contribution to HRV (Pumprla, Howorka, Groves, Chester, & Nolan 2002; Wickman, Nemeč, Gendler, & Clapham 1998). HRV recordings were performed between 12-2pm only (during “lights on” to simulate daylight). Mice are largely nocturnal in nature; they are mainly active at night and rest/sleep during the day. Autonomic tone is known to modulate circadian HR rhythm (Stauss 2003), mice have reversed circadian rhythms compared to man reflecting their nocturnal nature, therefore we recorded HRV specifically during “midday” in order to capture heart rate dynamics at a time when HR would be slowest (and parasympathetic tone presumably highest) reflecting a true “basal/rest” physiological state.

R-R interval was recorded from ECG tracings continuously over 20 minutes (divided by the software into ten 2 minute epochs) at 2000Hz sampling frequency. Data was

then imported in CHART v7.0 (ADInstruments), the current industry standard for analysis of physiological data and analysed using a HRV extension module. Raw tracings were manually inspected and any electrical signal interference/artefact manually edited. An R-wave detection algorithm was then applied to ensure all R-waves were accurately detected (Fig. 2.8 A). The data set of consecutive R-R intervals (typically over ~12000 sinus beats per mouse recording) was then mathematically analysed in both the linear time and frequency-domains (Fig. 2.8 B), as has been applied by others to murine HRV analysis (Ecker et al. 2006;Gehrmann et al. 2000;Uechi, Asai, Osaka, Smith, Sato, Wagner, Ishikawa, Hayakawa, Vatner, Shannon, Homcy, & Vatner 1998).

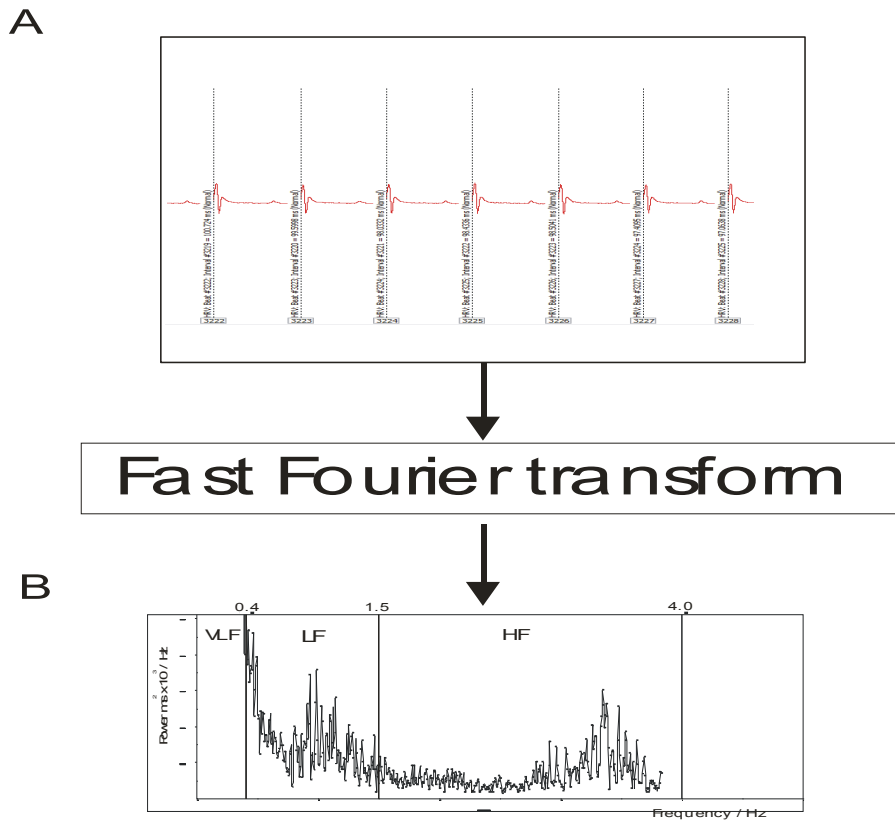


Figure 2.8 Representative ECG telemetry and power spectral density transformation. A raw ECG tracing recorded from a conscious freely moving mouse is shown (A). Using Chart data processing software, R wave signal is identified; successive R-R intervals are then calculated. The R-R interval data set can then be converted in the frequency-domain after Fourier transform to generate a power spectral density plot (PSD) demonstrating characteristic frequency distribution. Frequency bands are displayed on the x-axis. Characteristic frequency peaks can be seen in both the LF (0.4-1.5 Hz) band width and in the HF (1.5-4.0 Hz) range. The HF band is a selective marker of parasympathetic tone.

2.5.2 Time-domain analysis

The variations in heart rate may be evaluated by a number of methods. Perhaps the simplest to perform are the time-domain measures. In these methods, either the heart rate at any point in time or the intervals between successive normal complexes are determined. In a continuous ECG record, each QRS complex is detected, and the so-called normal-to-normal (NN) intervals (that is, all intervals between adjacent QRS complexes resulting from sinus node depolarizations) or the instantaneous heart rate is

determined. Simple time-domain variables that can be calculated include the mean NN interval, the mean heart rate, the difference between the longest and shortest NN interval, the difference between night and day heart rate, and so forth (Thireau et al. 2008). Time-domain measurements determine simple variance of R-R interval signal over the entire length of recording, they are relatively crude indices of variability but have been equated prospectively with clinical outcome in man (Stein, Borer, Okin, & Kligfield 1992). Classical indices include:

R-R interval/ R-R variability where R is a point corresponding to the peak of the QRS complex of the ECG wave; and R-R is the interval between successive R's, used to visualise R-R variation on a beat to beat level. It represents a successive R-R interval plot against successive beats number over the length of an ECG recording. Tachogram recordings give an overview of both short term and longer term signal oscillations. (Wickman, Nemeč, Gendler, & Clapham 1998)

Standard Deviation of the N-to-N interval: The N-to-N interval is the “normalized” beat to beat interval. The SDNN is the standard deviation of those intervals, a measure of their variability. The SDNN is expressed in milliseconds (ms) and it is an overall index of signal variation over the entire ECG tracing. (Uechi, Asai, Osaka, Smith, Sato, Wagner, Ishikawa, Hayakawa, Vatner, Shannon, Homcy, & Vatner 1998)

Mean R-R: Averaged heart rate over the ECG recording (Fox et al. 2007).

pNN50: This index measures what percentage of the IBI differ from neighbouring intervals by 50 milliseconds or more. The pNN50 is expressed in percentages and is interpreted as a measure of cardiac parasympathetic modulation (Ewing et al. 1984)

RMSSD: The square root of the mean of sum of square differences between adjacent normal R-R intervals. It is an index of beat to beat R-R interval variation used as a surrogate for rapid beat to beat changes in parasympathetic activity (Ecker, Lin, Powers, Kobilka, Dubin, & Bernstein 2006; Pumprla, Howorka, Groves, Chester, & Nolan 2002). This measure estimates high frequency variations in HR in short-term recordings that reflect parasympathetic regulation of the heart.

2.5.3 Frequency-domain analysis

It is difficult to obtain precise physiological data regarding changes in autonomic state solely from time-domain measurements. A more precise method involving frequency analysis has enabled investigators to delineate individual components of autonomic signal from R-R interval data using power spectral analysis. The most important concept in the frequency-domain analysis is the transformation. Transformation is used to convert a time-domain function to a frequency-domain function and vice versa. The most common transformation used in the frequency-domain is the Fourier transformation. Fourier transformation is used to convert a signal of any shape into a sum of infinite number of sinusoidal waves. Since analysing sinusoidal functions is easier than analysing general shaped functions, this method is very useful and widely used. While time-domain analysis shows how a signal changes over time, frequency-domain analysis shows how the signal's energy is distributed over a range of frequencies.

An example is the Fourier transform, which decomposes a function into the sum of a (potentially infinite) number of sine wave frequency components. The 'spectrum' of frequency components is the frequency-domain representation of the signal.

Power spectral analysis is reliant on fast Fourier transform (FFT). This mathematical transformation allows for the isolation of cyclical patterns within the signal (See Fig. 2.8 B). With reference to HRV, murine HRV parameters have recently been defined; three different frequency-domain measures of HRV were computed. Cut-off frequencies for power in the low-frequency range (LF) and high-frequency range (HF) were based on those utilized in human studies multiplied by a factor of 10 for HR adjustment (the approximate ratio between murine and human HR) and defined as 0.4–1.5 Hz and 1.5–4 Hz, respectively; total power was defined as 0.00–4 Hz. (Gehrmann, Hammer, Maguire, Wakimoto, Triedman, & Berul 2000). LF and HF were also measured in normalized units, which represent the relative value of each power component in proportion to the sum of the HF and LF components. A high frequency (HF) component occurs between 1.5 to 4.0 Hz in the mouse and is modulated purely by parasympathetic tone whereas a “lower frequency” signal (LF) occurring between 0.4 and 1.5Hz has dual sympathetic/parasympathetic modulation (Ecker, Lin, Powers, Kobilka, Dubin, & Bernstein 2006;Gehrmann, Hammer, Maguire, Wakimoto, Triedman, & Berul 2000;Wickman, Nemeč, Gendler, & Clapham 1998). Conversion of R-R intervals by FFT produces a power spectral density plot. Frequency ranges (x-axis) and total number of events occurring at particular individual frequency (y-axis) (i.e. frequency of frequencies) is presented graphically on PSD plots (See Fig.2.8 B). PSD tracings characteristically have LF and HF peaks within frequency ranges. Variability for individual frequency components

e.g. between 1.5-4.0 Hz for HF for example, is determined by the integral sum (Power) of the area under the curve between pre-specified frequency cut-offs. Frequency-domain indices are summarised below.

High Frequency range (HF) is associated with parasympathetic pathways and is synchronous with respiration. This frequency range is associated with the influence of blood pressure (baroreceptors) on heart rhythms, and meditative/slow breathing augments this range. The frequency range is 1.5-4.0Hz (Wickman, Nemeč, Gendler, & Clapham 1998).

Low Frequency range (LF) is associated with sympathetic activation, or more probably the withdrawal of parasympathetic braking, and also by the influences of visceral and thermal regulation. Rumination and worry augment this range and the frequency range is from 0.4 – 1.5Hz. Some suggest that LF appears to be mediated by both the vagus and cardiac sympathetic nerves (Gehrmann, Hammer, Maguire, Wakimoto, Tiedman, & Berul 2000).

Very low frequency range (VLF) is associated with the slower-acting biological influences. Significance is unclear in the mouse and its frequency is less than 0.4 Hz. (Stauss 2003).

Total Power (TP) is total variability over all defined frequency ranges similar to SD_{NN} in the time domain. The total power of a signal, integrated over all frequencies, is equal to the variance of the entire signal (Uechi, Asai, Osaka, Smith, Sato, Wagner, Ishikawa, Hayakawa, Vatner, Shannon, Homcy, & Vatner 1998).

Some investigators have used the ratio of the low-to-high frequency spectra as an index of parasympathetic-sympathetic balance; however, this remains controversial because of our lack of complete understanding of the low frequency component (which seems to be affected by centrally generated brainstem rhythms, baroreceptor feedback influences, as well as both sympathetic and vagal input).

2.6 Pharmacological studies

After initial evaluation of basal heart rate variability dynamics in conscious telemetered littermate controls, pharmacological interventions were employed using atropine a classical muscarinic M₂ receptor antagonist (#A0132 Sigma) propranolol, β -2AR antagonist (#P0884 Sigma) carbachol, an M₂ selective agonist (#C4382 Sigma), CCPA (2 chloro-N⁶-cyclo-pentyladenosine), a selective A₁-receptor agonist (#C7938 Sigma) and isoprenaline a β -AR agonist (#I5627 Sigma).

2.6.1 Intrinsic heart rate determination

Basal HR is modulated by autonomic tone, in man basal HR is predominantly modulated by vagal tone. To determine the relative importance of sympathetic and parasympathetic tone in the mouse we used telemetry in combination with dual autonomic blockade in conscious freely moving mice. HR was recorded over for 5 minutes then atropine (1mg/kg) (to block parasympathetic) and propranolol (1mg/kg) (to block sympathetic) were administered simultaneously by IP to induce combined autonomic blockade; serial HR measurements were determined over the next 10 minutes. Pharmacological action of these agents in the mouse occurs within 3 minutes after IP injection (De et al. 2004).

2.6.2 Pharmacological provocations

Chronotropic responses were examined using the following:

Carbachol (0.5mg/kg IP), a long acting muscarinic M₂ receptor agonist.

CCPA (0.1 mg/kg IP), a long acting specific A₁ receptor agonist.

Isoprenaline (3.0µg/kg IP), a β-AR agonist.

Heart rate after pharmacological challenge was determined over a 30-minute time course or was measured until it had reached a steady state. After initial baseline heart rate stabilisation, HR was recorded over for 5 minutes; the drugs above were administered by IP. HR measurements were determined over the next 30 minutes. Before proceeding to any other drug protocol, a period of at least 48 hours recovery was allowed between experiments.

2.7 Myocardial Infarction (MI) and murine left ventricular remodelling

The advent of cell type specific, inducible KO or transgenic strategies has made the mouse an invaluable tool to study the pathogenesis of heart failure and to identify novel therapeutic targets. There are different ways to induce MI or develop heart failure models in mice and these are summarized in the table below (Patten & Hall-Porter 2009).

Table 2.1 Commonly used heart failure models

Methods	Models	Description	Reference
Left Anterior descending Artery (LAD) occlusion	Induces MI and HF	Significant expertise and expense for mouse surgery but it has similar effects of human MI, leading to LV remodelling	(Michael, Entman, Hartley, Youker, Zhu, Hall, Hawkins, Berens, & Ballantyne 1995;Patten et al. 1998;Patten &

		hypertrophy and dilatation.	Hall-Porter 2009)
Transverse Aortic Constriction (TAC)/Aortic banding	Pressure overload induced hypertrophy and HF	Greater surgical expertise required but able to quantify the pressure gradient across aortic stricture that allow stratification of LV hypertrophy.	(Rockman, Ross, Harris, Knowlton, Steinhelper, Field, Ross, Jr., & Chien 1991;Rockman et al. 1994)
Muscle Lim protein KO	Induces dilated cardiomyopathy	No surgery required, causes disturbed interaction between cytoskeleton and mitochondria affecting energy sensing and transfer and defects in mitochondrial structure is associated with CV diseases and cardiomyopathy.	(Arber et al. 1997;Ross, Jr. 2002)
Cardiomyocyte specific overexpression of TNF α -	Induces dilated cardiomyopathy	No surgery is required, overexpression leads to LV hypertrophy, dilatation, profound systolic dysfunction associated with heart failure and premature death.	(Kubota, McTiernan, Frye, Slawson, Lemster, Koretsky, Demetris, & Feldman 1997)
Cryo injury	Induces MI	Cryoinfarction was produced by applying a cryoprobe of 2 or 3 mm in diameter to the anterior LV free wall followed by freezing for 10 s. technically simple, but may not always induce a trans mural	(Strungs et al. 2013;van den Bos et al. 2005)

		lesion and they recover without any fibrosis, aneurysm and remodelling	
Ethanol/doxorubicin/ Homocysteine	Induces heart failure	Ethanol and doxorubicin are cardiotoxins and elevated levels of homocysteine develops heart failure in humans and can be induced in mice by heterozygous deletion of cystathionine β synthase	(Berk, Block, Toselli, & Ullrick 1975; Delgado, III, Nawar, Zewail, Kar, Vaughn, Wu, Aleksic, Sivasubramanian, McKay, Mann, & Willerson 2004; Vacek et al. 2009)

Acute MI in humans results from coronary atherosclerosis and in a variety of animal models this condition can be mimicked by ligation of the left coronary artery (Tarnavski et al. 2004). Ligation of the left coronary artery (LAD) models heart failure following myocardial infarction by myocardial scar and subsequent congestive heart failure. This predicts a clear model of completed human myocardial infarction but has its own experimental drawbacks of high postoperative mortality, less reproducibility and technical challenges of a microsurgical procedure (Breckenridge 2010). Although highly representative of ischemic cell death as occurs in humans, the ligation model is inherently associated with infarcts of variable size, requiring large group numbers of mice in studies that evaluate modelling therapies (van den Bos, Mees, de Waard, de, & Duncker 2005). Permanent ligation of LAD still remains the most widely studied model of murine MI. We decided to take up the challenge of technical difficulties and use this as a model of heart failure to study left ventricular remodelling in $G\alpha_s$ flx/flx HCN4 cre⁺ and $G\alpha_{i2}$ flx/flx HCN4 cre⁺ mice.

2.8 Murine *in vivo* model of myocardial infarction

The MI model employed for this study comprised of occlusion of LAD coronary artery. The main surgical procedure is described by Fisher and Marber (Fisher and Marber 2002) and modifications were made as described in (Van Laake et al. 2007). General advice was taken from the Handbook of Laboratory Animal Management and Welfare by Sarah Wolfensohn and Lloyd and the veterinary officer at the surgical facility.

All surgical procedures were conducted in a controlled sterile surgical theatre and aseptic operating practices were adhered to throughout the procedure. Instruments were autoclaved prior to the operating session and a hot bead steriliser was used to sterilise instruments between animals. A heating mat covered with a sterile material drape was used for all surgeries. Animals were prepared for surgery by chlorohexidine wipe to clean the neck and chest region. Additional chlorohexidine washes were observed prior to skin opening and immediately following skin closure. ECG was recorded throughout the procedure where ECG electrodes were positioned on both forelimbs (positive and negative) and the right hind limb (reference lead) and monitored by Power lab coupled to chart 7.0. Temperature was monitored by a rectal thermoprobe and was maintained at $37^{\circ}\text{C} \pm 0.5$. Surgical depth of anaesthesia was assessed before initiating and throughout the procedure and was confirmed by loss of pedal reflex to toe-pinch stimulus. In addition breathing rate was observed as an important indication of anaesthetic depth; where slow shallow and deep gasping breath were suggestive of over dosing of anaesthesia. Artificial ventilation was provided throughout the main surgical procedure by means of a MiniVent mouse

ventilator (HSE-HA MiniVent Mouse Ventilator # 730027 Harvard Apparatus, March-Hugstetten, Germany) (Fig. 2.9)

2.8.1 Anaesthesia: Mice were anaesthetised with isoflurane vaporised in oxygen. Induction of anaesthesia was in a gas chamber supplied with 1.5L/minute and 5% isoflurane. Intermediate maintenance of anaesthesia via nose cone (modified 2ml BD syringe) was supplied with 1.5L/minute and 2% isoflurane. Long term anaesthesia, via the ventilator was supplied with 1.5L/minute and 2% isoflurane and a tidal volume of 300 μ l at 120cycles /minute. Rapid intubation was imperative in order to maintain surgical anaesthesia during this period of no direct isoflurane administration.

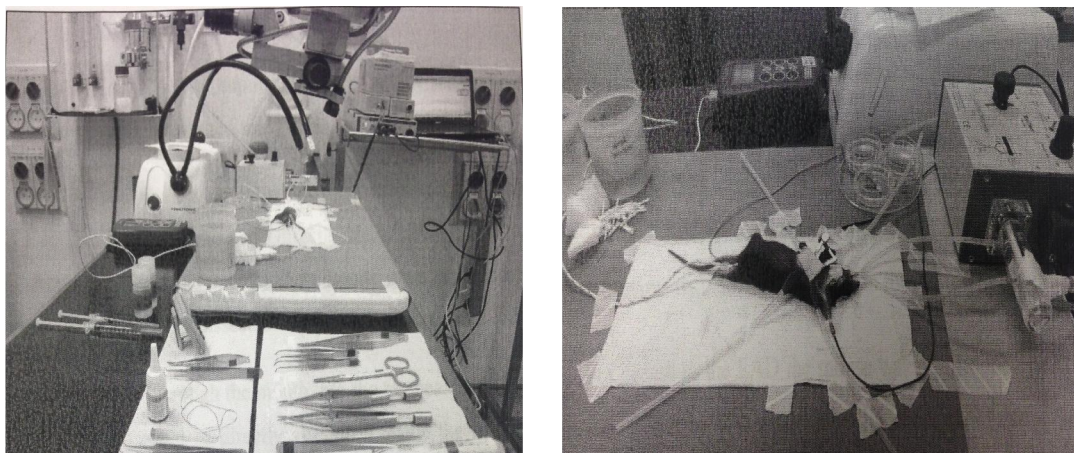


Figure 2.9 Surgical set up for *in vivo* MI model A) Animals were placed on a heated operating table connected to constant ECG recording Power lab and rectal temperature continually monitored. A high powered surgical microscope was used to aid all surgery. B) Mice were intubated and connected to a small animal Mini ventilator supplied with isoflurane saturated with oxygen and ventilator exhaust was connected to a scavenger system.

2.8.2 Intubation: Mice were placed in the supine position with neck extended using a suture hooked around the incisor and secured using adhesive tape. Analgesia was provided by buprenorphine (Vetergesic 0.1mg/kg intra muscular) at the start of the procedure to ensure effective analgesia at recovery. A small skin incision of no greater

than 1 cm was made to the neck directly above the visible midline of the underlying salivary glands. The skin and sub maxillary glands were gently teased apart and the underlying paratracheal blunt to expose the trachea. The ventilation cannula was passed through the mouth into the trachea. Successful intubation was confirmed once the cannula could be directly visualised inside trachea and further confirmed by observing regular chest movements upon ventilation. In the event of unsuccessful intubation, the ventilation cannula was removed and further attempts were made. Ideal intubation was completed within two attempts with no visible trauma to trachea or surrounding tissues.

2.8.3 Chest opening: For access to the LAD, the mouse was repositioned by crossing the left leg over the body (Fig. 2.10 A). A skin incision was made laterally across the chest at the approximate position of the 3rd and 4th intercostal space. The major and minor pectoral muscles were blunt dissected and reflected outward using hook stays; caution was taken to preserve the integrity of pectoral muscles for optimal chest closure. The fourth intercostal space was identified by evaluation of lung position- the fourth space being the one prior to the curvature of the base of the lung and confirmed by the presence of a large branching vessel along the surface of the rib. Dissection was performed by creating a small hole using sharp pointed scissors followed by insertion of a small animal retractor. Access to the LAD was facilitated by opening of the pericardium using blunt tweezers. The LAD is identifiable by its bright red colour and occasionally its pulsating appearance, if not in a visible position, it was approximated from experience. LAD was under run by 8.0 prolene suture (#W2775 ETHICON), ideally 2 mm below the tip of the left atrium (Fig. 2.10 B). The suture was double-knotted in order to occlude the LAD. Successful MI upon occlusion was confirmed

primarily by myocardial colour change from red to pink and ST segment elevation
Fig. 2.10 B.

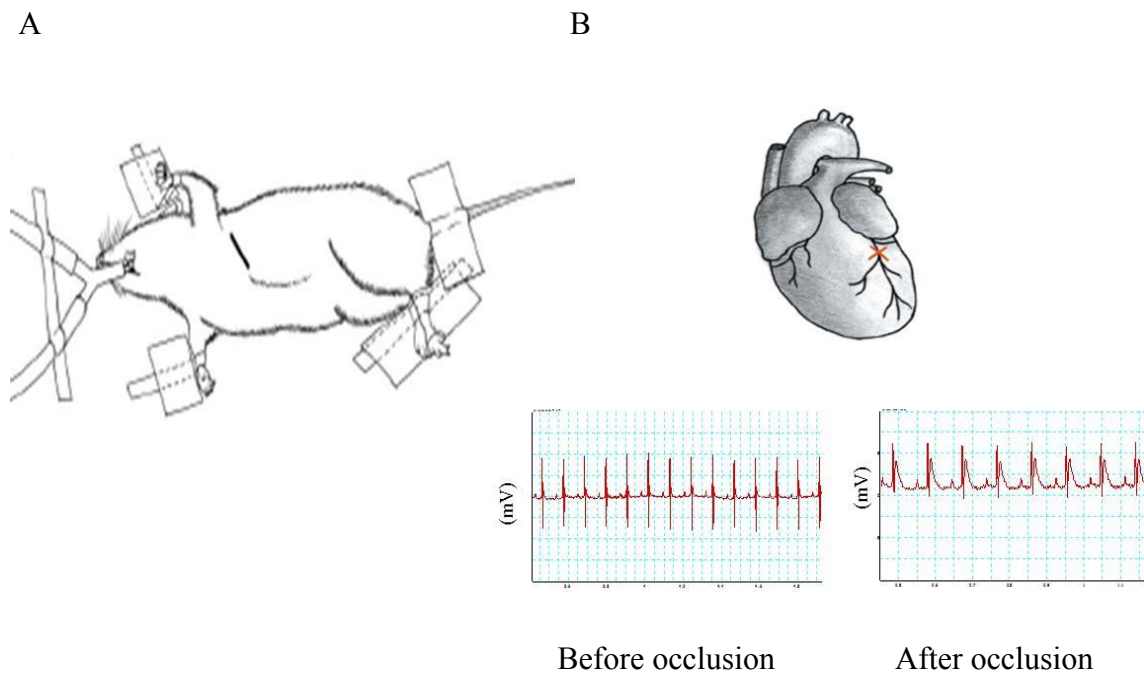


Figure 2.10 LAD occlusion - mouse positioning and ST elevation. A) Positioning of the mouse to expose the LAD: the left leg was crossed over the body to the right so that when opened below the armpit between the 3 and 4th intercostal space the LAD is exposed. B) LAD occlusion at 2mm below left atrium and lower panel shows normal ECG pattern before MI and ST segment elevation after MI visualized on Lab chart windows by means of ECG leads tied on the limbs.

The intercostal space was closed using two 5-0 mersilk sutures (#W595 ETHICON). Ventilation positive end pressure was applied by submersion of the ventilator outlet tube in 2cm of water. This served to re-inflate the lungs and thus helps to improve the respiratory function upon recovery. Effective intercostal space closure was confirmed by application of tissue adhesive Vet bond to the suture sites. The major and minor pectoral muscles were unfolded back to cover the underlying intercostal space and skin was closed by 5-0 mersilk sutures. Further doses of vetergesic (0.1mg/kg intramuscular) were administered if needed at 6 and 24 hrs following the surgery. Upon withdrawal of isoflurane and initiation of independent breathing extubation was

facilitated by gentle removal of ventilation cannula. Supplemental oxygen was provided by a nose cone for 5 minutes. Animals commonly regained consciousness within 3-5 minutes and mice were expected to be active within an hour. Animals were allowed to recover for two weeks and were subjected to echocardiographic measurements (described below).

2.9 Murine Echocardiography

Echocardiography is a useful non-invasive tool to visualise cardiovascular structures and evaluate cardiac function in mice. It is an extremely versatile method for cardiovascular research by allowing the evaluation of left ventricular (LV) systolic, diastolic, regional and vascular function in mouse cardiomyopathy models (Asai et al. 1999;Iwase, Bishop, Uechi, Vatner, Shannon, Kudej, Wight, Wagner, Ishikawa, Homcy, & Vatner 1996;Iwase, Uechi, Vatner, Asai, Shannon, Kudej, Wagner, Wight, Patrick, Ishikawa, Homcy, & Vatner 1997), myocardial ischemia models (Odashima et al. 2007) and chronic pressure overload induced by transverse aortic constriction (TAC) models (Depre et al. 2006;Gelpi et al. 2009). Classic methods of evaluating ventricular function by means of ventricular catheterization (Lorenz and Robbins 1997), nuclear imaging using positron emission tomography (PET) (Inubushi et al. 2004) and magnetic resonance imaging (Chin et al. 2007;Voelkl et al. 2011) require instrumentation and microsurgical techniques and are difficult to perform more than once in the same animal. Also ultrasound imaging provides a fast and inexpensive alternative to all the instrumentation described above when performing longitudinal follow-up studies of cardiac remodelling.

Echocardiography was performed using a Vevo 770 ultrasound system (Visualsonics, Toronto, Canada) equipped with a real-time micro-visualization scan probe head (RMV-707B) working at a frame rate of 100 frames per second. The transducer used

has a central frequency of 30MHz, focal length of 12.7mm and 55um of nominal spatial resolution. The Vevo 770 is equipped with ECG gated kilohertz visualisation software (EKV™) which synthesises high temporal resolution B-mode images by combining several ECG synchronised heart cycles. The EKV image reconstruction software produced B-mode sequences at up to 1000 frames per second (Benavides-Vallve et al. 2012).

2.9.1 Animal preparation

Mice were anesthetized with isoflurane, at a concentration of 4% (induction) and 1.5% (maintenance) in 100% oxygen. Each animal was placed on a heating table in a supine position with the extremities tied to the table through surgical tape (Transpore™). The hair from the chest was removed using a chemical hair remover (Veet hair removal gel cream). Warmed ultrasound gel (Aquagel lubricating Gel from Parker Labs, New Jersey) was applied to the thorax surface to optimize the visibility of the cardiac chambers. Temperature was monitored by rectal thermoprobe and was maintained at $37^{\circ}\text{C} \pm 0.5$ by adjusting the temperature on the heating table. Surgical depth of anaesthesia was assessed before initiating and throughout the procedure and was confirmed by loss of pedal reflex to toe-pinch stimulus. The heart rate (HR) of the animals was carefully monitored and the isoflurane levels during the echocardiographic study as this have an effect on the echo measurements. By placing the transducer along the long-axis of the LV, and directing it to the right side of the neck of the mouse, two-dimensional LV long-axis is obtained. Then the transducer is rotated clockwise by 90° perpendicular to IVS (interventricular septum), and the LV short-axis view is visualized (Fig. 2.11 A). 2D-guided LV M-mode at the papillary muscle level is recorded from either the short-axis view and/or the long-axis view view at the level of papillary muscles (Fig. 2.11 B and C).

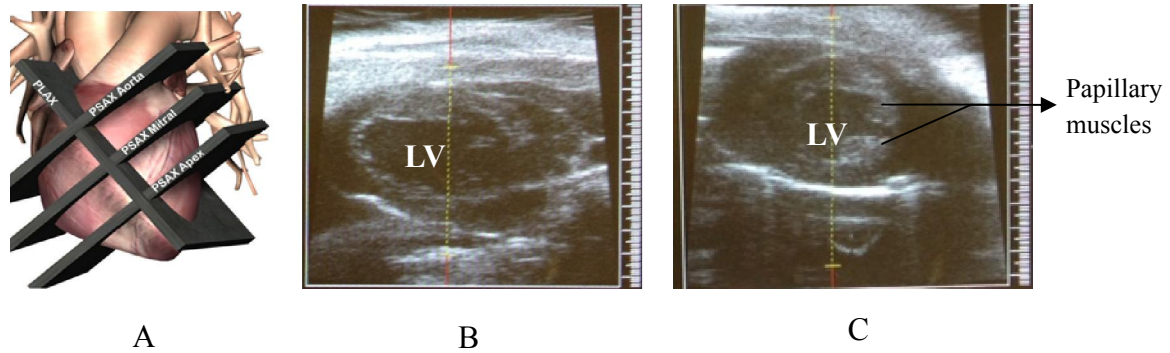


Figure 2.11 Diagrams for basic mouse echocardiographic views. A) Position and direction of the probe for LV long axis and LV short axis. B) LV long axis view (Parasternal Long axis view) and C) LV short axis view (parasternal short axis view).

2.9.2 Measurements

Measurements were done 3 times - before the start of the study, after tamoxifen injection and then after MI. Measurements were made using the leading edge to leading edge method according to the guidelines and standards of the American Society of Echocardiography (Sahn et al. 1978). LV function can be assessed both structurally and functionally. Structurally by means of measuring LV chamber dimensions and functionally by means of calculations based on these measurements. To accomplish this measurement, wall thickness and chamber dimension are determined from M-mode tracings Fig. 2.12. LV wall thickness is evaluated in the interventricular septum (IVS) and the posterior wall (LVPW). End-diastolic measurements (Interventricular septal thickness diastolic (IVSd), left ventricular posterior wall thickness diastolic (LVPWd) and left ventricular internal dimension diastolic (LVIDd) are obtained at the point of maximal LV diastolic dimension. LV end-systolic dimensions (IVSs, LVPWs, and LVIDs) are obtained at the time of most anterior systolic excursion of the LVPW associated with minimal chamber dimension. All LV dimensions are presented as the average of measurements using the leading-edge technique of 3 to 5 consecutive selected sinus beats.

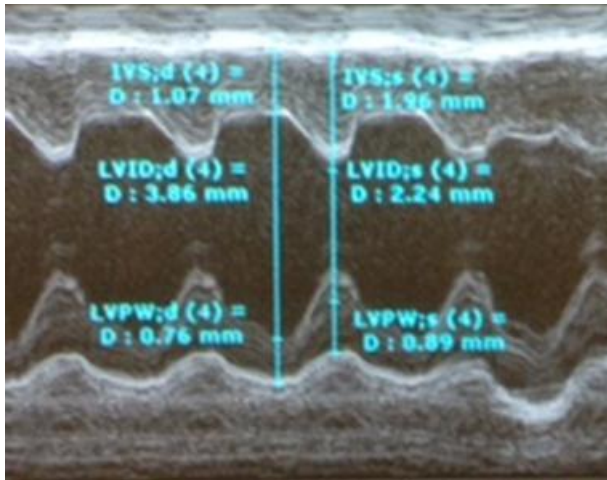


Figure 2.12 Wall dimension measurements on M-mode echocardiography. Echocardiographic measurements for determination of left ventricular function from M-mode measurements obtained with conscious transthoracic echocardiography in mice.

The most common parameters used to evaluate the systolic function of the LV are the fractional shortening (FS%), ejection fraction (EF%) and cardiac output (CO) (Rottman et al. 2007). In the absence of regional wall motion abnormalities, FS% and EF% are predictably related. In mice however, the extent of the typical cavity obliteration and the associated error introduced in the volumetric measurements is far greater than in humans. Consequently, the use of FS% is more appropriate (Rottman, Ni, & Brown 2007) The FS% and EF% are routinely calculated using the Teichholz method, (Teichholz et al. 1974) which assumes that the left ventricular cavity can be represented as a 3D ellipsoid of revolution. However, this might not be a reasonable assumption when the LV adopts the complex shapes caused by regional wall motion abnormalities that are common after MI. Therefore, an alternative approach to calculating EF% exists, based on the shape independent Simpson's rule (Gao et al. 2000; Ino et al. 1989; Kanno et al. 2002) where the LV endocardial border is traced in multiple slices both in systole and diastole, and the volumes are computed from these tracings. Using the above method, the LV function can also be measured as the

percentage of change in left ventricular cross-sectional area between diastole and systole (fractional area change, FAC%), which has been found to correlate well with EF% both in normal and abnormal subjects (Domanski et al. 1992). The standard method to estimate FAC% uses cross-sectional area short-axis views at different ventricular levels. FS% and EF% and FAC% are then calculated from M-mode-derived LV dimensions using the formula below (Gardin et al. 1995; Pollick et al. 1995; Syed et al. 2005; Tanaka et al. 1996).

$$EF\% = 100 \times [(LVIDd^3 - LVIDs^3) / LVIDd^3]$$

$$FS\% = 100 \times [(LVIDd - LVIDs) / LVIDd]$$

$$FAC\% = 100 \times (\text{Endo area}_d - \text{Endo area}_s) / \text{Endo area}_d$$

$$LV \text{ mass} = 1.05 [(IVSd + LVIDd + PWD)^3 - LVIDd^3]$$

2.10 Tissue processing and TTC staining

After MI studies the heart was excised, washed in cold PBS, frozen at -80 for 10 min, the atria were removed, and the heart was sectioned into five to six transverse slices from the apex to the base by placing in a mold in the shape of the heart. The slices were arranged on a tissue culture dish in the order from apex to base. The slices were then incubated with 2ml of 1% 2,3,5-triphenyltetrasodium chloride (TTC #T8877 Sigma) in PBS for 30 min at 37°C, fixed in 4% formalin for 24 h, washed with PBS and scanned. TTC stains viable myocardium brick red as it is reduced by NADH, whereas necrotic myocardium appears pale yellow (Basalay et al. 2012). The infarcted area was determined by computerized planimetry using Image J software, where the infarcted area and total area are assessed and the infarct size is expressed as a % of total area.

2.11 Statistical Analysis

Data are reported as mean \pm S.E.M. Statistical significance of multiple treatments was determined by 1-way or 2-way ANOVA followed by non-parametric Kruskal-Wallis and Dunn's post-hoc analysis. Non-parametric tests were used as the data was assumed not to follow a Gaussian distribution. Statistical significance between 2 groups was determined by 2-tailed Student's *t* tests, as appropriate. In all instances, $P < 0.05$ was considered significant. Statistical analysis was carried out using the commercially available software, Prism version 4.0 (Graph Pad software, San Diego, California; www.graphpad.com).

Chapter 3

RESULTS I

3.1 *In vivo* cardiac modulation in RGS-insensitive $G\alpha_o$ knock-in mice (RGSi $G\alpha_o$) and RGS-insensitive $G\alpha_{i2}$ knock-in mice (RGSi $G\alpha_{i2}$)

Activation of the GIRK channels by $\beta\gamma$ subunits released from $G\alpha_i$ contributes approximately 50% of the *in vivo* bradycardic response to vagal stimulation (Fu, Huang, Zhong, Mortensen, D'Alecy, & Neubig 2006). The strength and duration of G-protein signalling is attenuated by RGS proteins acting as GAPs for $G\alpha$ subunits but the relative contribution of different $G\alpha$ subunits to *in vivo* cardiac automaticity is poorly defined. RGS proteins are functionally redundant, which makes single KO of limited value or will underestimate the overall role RGS protein function *in vivo*. Another difficulty in unravelling the function of RGS proteins has been the complex interactions of the many subtypes of both G-proteins and RGS proteins. It was proposed recently that RGS proteins represent potential new therapeutic targets for cardiovascular diseases (Riddle, Schwartzman, Bond, & Insel 2005). However, it has been difficult to ascertain the full physiological role of endogenous RGS proteins *in vivo* in part because of their functional redundancy (Lan, Sarvazyan, Taussig, Mackenzie, DiBello, Dohlman, & Neubig 1998).

To determine the full contribution of RGS proteins as a group to biological responses mediated by a particular G-protein (e.g. G_o and G_i), we took advantage of a $G\alpha$ -subunit point mutation first found in the yeast *Saccharomyces cerevisiae* (DiBello et al. 1998) that prevents RGS binding to the $G\alpha$ subunit and GAP activity. These RGS-insensitive (RGSi) mutant $G\alpha$ subunits, which contain a $G^{184}S$ point mutation in their switch I region prevents binding of RGS proteins and subsequent $G\alpha$ deactivation. The analogous mutation (Gly¹⁸⁴ to Ser) in mammalian $G\alpha_o$ and $G\alpha_{i1}$ prevented the GAP activity of RGS4 and RGS7 and blocked RGS4 binding to aluminium fluoride-activated $G\alpha$ subunits (Lan, Sarvazyan, Taussig, Mackenzie, DiBello, Dohlman, &

Neubig 1998). These mutations do not affect other functions of the $G\alpha$ subunit, such as the intrinsic GTPase activity of the G-protein or its coupling to $\beta\gamma$ subunits, receptor and downstream effectors (Day et al. 2004;Fu, Zhong, Nanamori, Mortensen, Huang, Lan, & Neubig 2004). Thus, the only known effect of the G^{184S} mutation in $G\alpha_o$ and $G\alpha_{i2}$ is to prevent RGS action on $G\alpha$. Several publications using overexpression of these RGS-insensitive $G\alpha$ subunits revealed profound slowing of the channel response kinetics and/or increased potency of agonist responses in neurons (Chen and Lambert 2000;Clark et al. 2003;Jeong and Ikeda 2000). In this chapter, I have studied the heterozygotes of RGSi $G\alpha_{i2}$ and RGSi $G\alpha_o$ knock-in mice as the homozygotes were not viable. The effects on the *in-vivo* regulation have not been previously described and whether these mice are predisposed to spontaneous arrhythmia such as atrial fibrillation is unknown.

3.2 RGSi $G\alpha_o$ and RGSi $G\alpha_{i2}$ mice lost diurnal variation in heart rate

RGS-insensitive knock-in mice of $G\alpha_{i2}$ and $G\alpha_o$ (RGSi $G\alpha_{i2}$ and RGSi $G\alpha_o$) had a phenotype slightly different from control. These mice exhibited normal growth, but were hyperactive and exhibited day time tachycardia and were fertile. Homozygotes couldn't survive due to neonatal/embryonic lethality.

Using ambulatory telemetry studies we found that RGSi $G\alpha_o$ and RGSi $G\alpha_{i2}$ both exhibited high heart rate during both night and day (RGSi $G\alpha_o$ day 601 bpm \pm 28.8, * P <0.05, night 617 bpm \pm 30.7, n =8, RGSi $G\alpha_{i2}$ day 612 bpm \pm 33.9, * P <0.05, night 615 bpm \pm 15.8, n =8, WT controls day 430 bpm \pm 39.2, night 535 bpm \pm 46.8, n =8) showing that they have lost their normal diurnal variation in the heart rate as seen in Fig. 3.1. The night time heart rate was also found to be higher in both RGSi $G\alpha_o$ and RGSi $G\alpha_{i2}$ though not significantly different when compared with the littermate

control night time heart rate. The effects of autonomic tone on HR are complex. Ambient temperature and levels of physical activity modulate sympathovagal balance. Specifically, it is possible for mice to have high vagal tone under some conditions like exercise training and temperatures of thermoneutrality $\sim 30^{\circ}\text{C}$ (De, Wichi, Jesus, Moreira, Morris, Krieger, & Irigoyen 2004; Just et al. 2000; Swoap et al. 2008). These animals were found to be hyperactive (data not shown, visual observation) and a high heart rate in them may reflect a high sympathetic tone. Recent studies with homozygous $\text{RGSiG}\alpha_{i2}$ knock-in mice also showed increased heart rate during day time and increased contractility on echocardiography reflecting a high sympathetic tone (Huang, Fu, Charbeneau, Saunders, Taylor, Hankenson, Russell, D'Alecy, & Neubig 2006). Enhanced tachycardia in $\text{RGSiG}\alpha_{i2}$ mice was not expected, since G_i mediates GIRK activation, which slows heart rates. The increased heart rate is likely due to central nervous system effects.

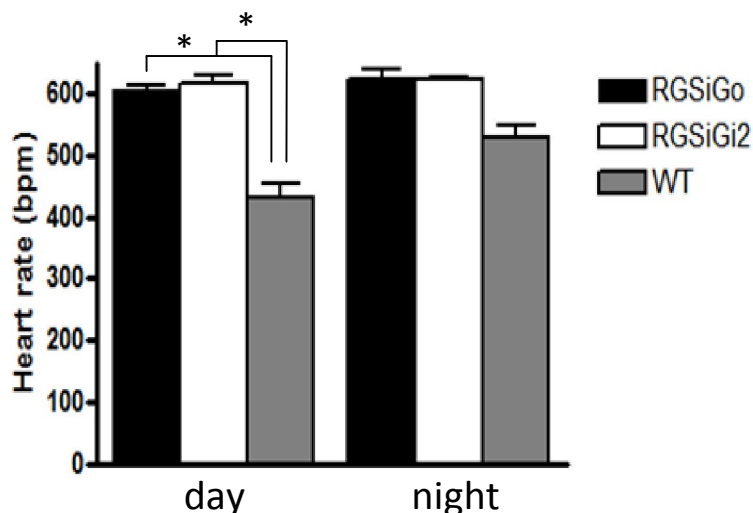


Figure 3.1 Loss of diurnal heart rate response in $\text{RGSiG}\alpha_0$ and $\text{RGSiG}\alpha_{i2}$ mice. $\text{RGSiG}\alpha_0$ and $\text{RGSiG}\alpha_{i2}$ lost their diurnal variation in heart rate compared with littermate wild type controls on the same genetic background (n=8, $*P < 0.05$). Diurnal variation between day and night was well preserved in wild type controls.

3.3 ECG analysis reveals shorter R-R intervals in RGSiG α_0 and RGSiG α_{i2} mice compared to control

ECG traces measured in RGSiG α_0 and RGSiG α_{i2} mice using chart 7.0 software shows that R-R interval was shorter as would be expected given the higher mean heart rate in RGSiG α_0 and RGSiG α_{i2} mice compared to their littermate controls (Fig.3.1). Measurements were taken over a 20 minute recording time at rest during the day. In both RGSiG α_0 and RGSiG α_{i2} knock-in mice, RGS is unable to bind to G α_i and G α_0 to bring it back to its GDP bound inactive form, as a result it is constitutively expressed so one would expect bradycardia from these mice, however I found that both set of knock-in mice lost their diurnal variation (above Fig.3.1) with an increase in heart rate, which is also reflected clearly in the R-R interval measurements (Fig.3.2). RGSiG α_0 had R-R interval of 104.4 ms \pm 7.2, n=8 *P <0.05 and RGSiG α_{i2} 101.8 ms \pm 7.4, n=8 *P<0.05 while control had R-R interval of 114.9 ms \pm 15.9, n=8 (Table 3.1). Other ECG parameters like the PR interval and QRS duration didn't show any significant difference between the 2 knock-in groups and control mice. I did not observe any episodes of spontaneous arrhythmia.

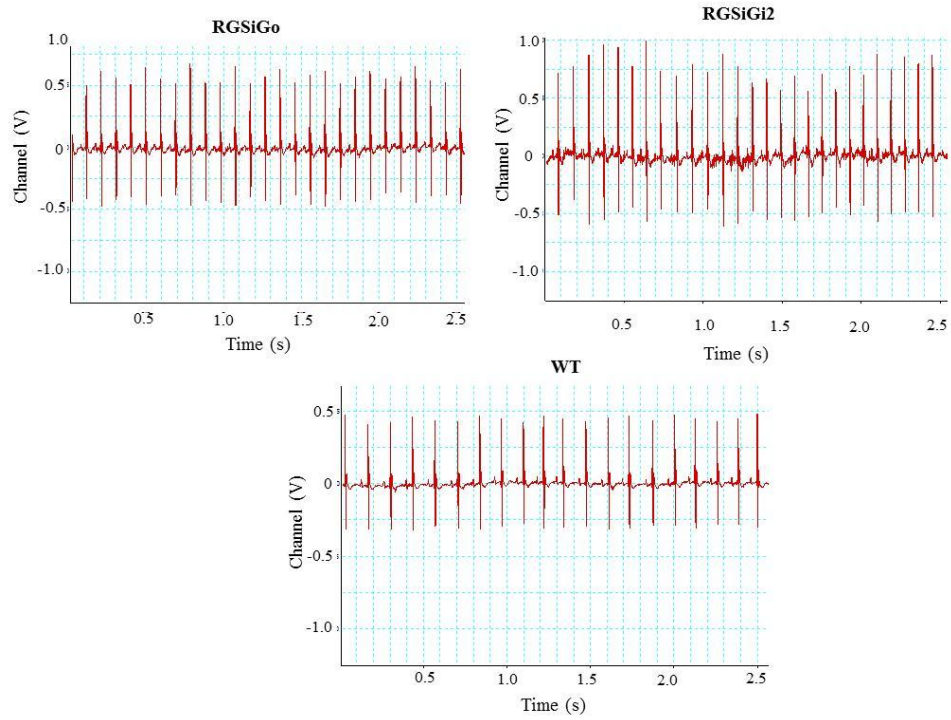


Figure 3.2 Representative ECG traces from RGSiG α_0 and RGSiG α_2 mice .RGSiG α_0 and RGSiG α_2 mice (upper panel) shows shorter R-R intervals compared to their control mice (lower panel).

		RGSiG ₀	RGSiG _{i2}	Control
		n=8	n=8	n=8
	RR (ms)	104.4±7.2*	101.8±7.4*	114.9±15.9
	PR (ms)	35.95±2.9	35.19±5.4	35.82±5.6
ECG	QRS (ms)	9.86±1.5	9.34±0.93	9.40±1.45
	QTc (ms)	62.3±9.7	54.2±8.3	54.75±8.16
	HR (bpm)	600±41.4*	598±62.2*	545.8±38.9
	SDNN	5.51±3.2	4.02±1.5	3.72±1.0
HRV	RMSSD	6.8±2.1	9.8±3.2	5.9±2.8
	LFnu	63.1±8.7*	50.3±11.2	55.3±9.7
	HFnu	31.89±3.9*	38.7±7.7	42.4±8.6

Table 3.1 ECG and HRV parameters in conscious ambulatory telemetered RGSiG₀ and RGSiG_{i2} mice. Table shows shorter R-R intervals in RGSiG₀ and RGSiG_{i2} mice compared to their controls. No difference in rest of the ECG parameters. Heart rate was found to be higher in both RGSiG₀ and RGSiG_{i2}. LFnu was higher and HFnu was lower in RGSiG₀ compared to controls. All observations are mean ± S.E.M and are compared against control, HR - heart rate, SDNN is standard deviation of normalized RR interval, LFnu is normalized LF frequency, HFnu is normalized HF frequency and *P<0.05).

3.4 HRV analysis reveals loss of HRV in RGSiG₀ but no change in RGSiG_{i2} mice compared to control

HRV analysis in the time and frequency-domain reveals differences in heart rate, LF and HF domain in RGSiG₀ and RGSiG_{i2} when compared with the controls. More specifically heart rate was found to be higher in both knock-in groups (RGSiG₀ 600 bpm ± 41.1, n=8 *P<0.05 and RGSiG_{i2} 598 bpm ± 62.2, n=8 *P<0.05) compared to controls (545 bpm ± 38.9, n=8). SDNN -standard deviation of mean NN intervals - that correlates very well with LF component of HRV was found to be similar in RGSiG₀, RGSiG_{i2} and control mice (Table 3.1). RMSSD (root mean square of successive NN intervals) is a measure of parasympathetic activity and represents vagal-mediated cardiac control that correlates well with the HF domain of the

frequency of HRV was found to be unaltered. LF frequency which is driven by both the sympathetic and the parasympathetic systems was found to be higher in RGSiG α_0 (63.1 nu \pm 8.7, n=8 *P<0.05) compared to RGSiG α_{i2} (50.3 nu \pm 11.2, n=8) and the control group (55.3 nu \pm 9.7, n=8). Interestingly in the same group RGSiG α_0 the HF component of the HRV signature was found to be lower (31.89 nu \pm 3.9, n=8 *P<0.05) compared to RGSiG α_{i2} (38.7 nu \pm 7.7, n=8) and control group (42.4 nu \pm 8.6, n=8) (Fig. 3.3 and Table 3.1). The selective loss of HF power of HRV was also observed with the global KO of G α_{i2} mice in our lab (Zuberi, Birnbaumer, & Tinker 2008) which show an impairment of the parasympathetic activity as G α_{i2} plays a major role in parasympathetic modulation of the heart rate. In my study, I couldn't see any difference in the HF component of HRV in RGSiG α_{i2} mice although an improved HF signal was expected.

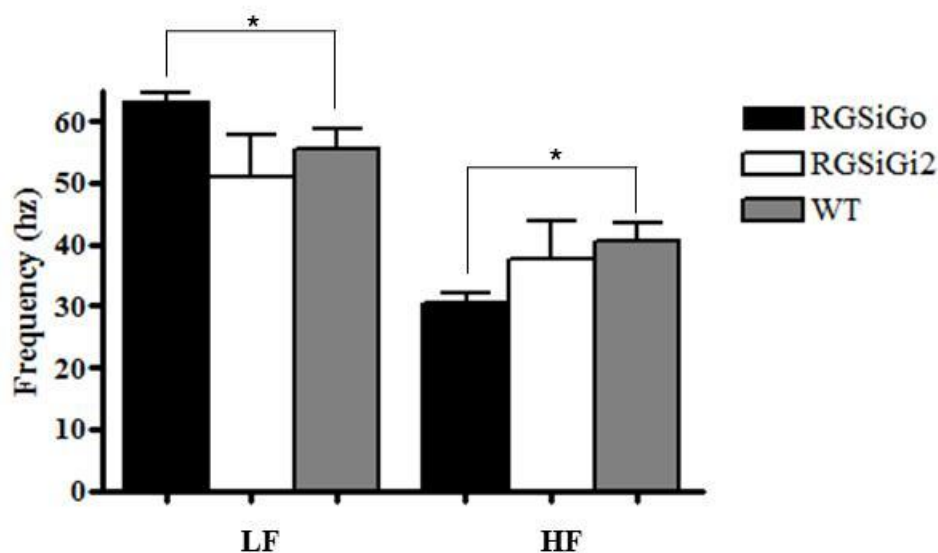


Figure 3.3 HRV signatures in RGSiG α_0 and RGSiG α_{i2} mice. Loss of HRV in RGSiG α_0 mice (n=8) with an increase in LF power (*P<0.05) and a loss of HF power (*P<0.05) compared with WT (n=8) littermate controls. While the LF and HF power was more or less the same in RGSiG α_{i2} (n=8).

Power spectral analysis of the LF and HF signature of HRV in RGSiG α_0 and RGSiG α_{i2} also showed a similar picture as shown in Fig. 3.4. Power spectral density plots shows spectral peaks in both the LF and HF range for the control group, for RGSiG α_0 there is an increase in LF and loss of HF and in RGSiG α_{i2} LF and HF were well preserved. RGSiG α_0 showed a HRV phenotype different from that of control. No arrhythmias were seen on the ECG traces of both RGSiG α_0 and RGSiG α_{i2} knock-in mice. G α_0 is the mainly expressed in the brain and central nervous system so the effects we observed with these knock-in mice suggest a central effect.

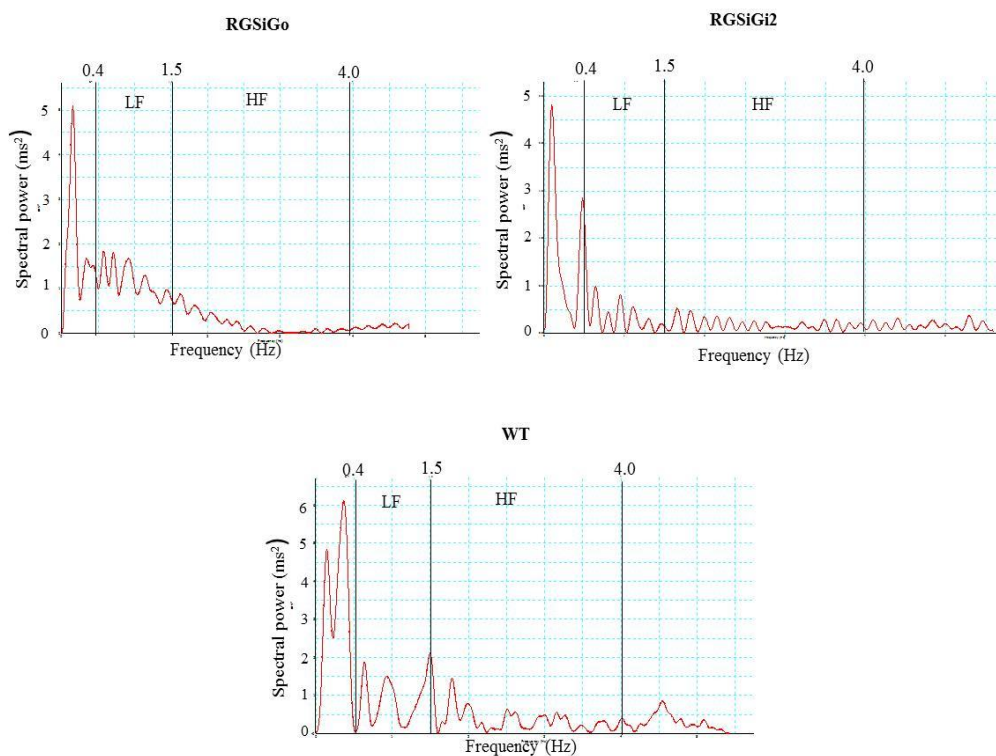


Figure 3.4 Representative PSD from RGSiG α_0 and RGSiG α_{i2} mice. PSDs showing a loss of HF and increase in LF in RGSiG α_0 (upper left panel) and preserved LF and HF power in RGSiG α_{i2} (upper right panel) while control shows good spectral peaks for LF and HF (lower panel).

3.5 Enhanced bradycardic response to carbachol (M₂ receptor agonist) with RGSiGα₀ and RGSiGα_{i2} mice

Carbachol, an M₂R agonist slows down the heart rate in wild type mice. My results showed an enhanced bradycardic response in both RGSiGα₀ (34 ± 3%, n=8 *P<0.05) and RGSiGα_{i2} (39 ± 2%, n=8 **P<0.01) compared to wild type (14 ± 2.5%, n=8), and the inhibition with carbachol was more with RGSiGα_{i2} (Fig. 3.5), probably due to the fact that Gα_{i2} is the predominant cardiac isoform. This reveals that the loss of RGS regulation on both Gα_{i2} and Gα₀ due to mutation, leads to an enhanced bradycardic action of carbachol. Both Gα_{i2} and Gα₀ were able to elicit M₂R mediated bradycardic response. No specific types of conduction block or arrhythmias were observed in these groups treated with carbachol. Similarly, studies with embryonic stem cell-derived cardiomyocytes of RGSiGα₀ and RGSiGα_{i2} showed enhanced muscarinic bradycardic responses when challenged with the M₂R agonist, carbachol (Fu, Huang, Zhong, Mortensen, D'Alecy, & Neubig 2006). Dramatic sensitivity to M₂ receptor activation suggests that Gα_{i2} appears to be a critical link between the M₂R and GIRK channels in mediating vagal responses.

3.6 A₁ receptor agonist (CCPA) showed increased inhibition with RGSiGα₀ mice but not with RGSiGα_{i2} mice

It has been reported previously that in animals and ES-cell derived cardiomyocytes, Gα_{i2} signalling due to loss of RGS regulation preferentially amplifies M₂R mediated responses, but not of A₁R (Fu, Huang, Zhong, Mortensen, D'Alecy, & Neubig 2006;Fu, Huang, Piao, Lopatin, & Neubig 2007) . *In vivo* telemetry studies with RGSiGα₀ and RGSiGα_{i2} further confirm these findings (Fig. 3.5) but A₁R mediated inhibitory response is higher in RGSiGα₀ (42 ± 4%, n=8 **P<0.01) compared to

RGSiG α_{i2} ($19 \pm 3\%$, $n=8$ * $P<0.05$). Interestingly RGSiG α_{i2} appears to play a lesser role in the adenosine receptor-mediated bradycardic response as the inhibitory response was even lower than wild type ($30 \pm 3\%$, $n=8$). Thus loss of RGS control on G α_o enhanced bradycardic response to A $_1$ R and confirms the specificity of G α_o for A $_1$ R.

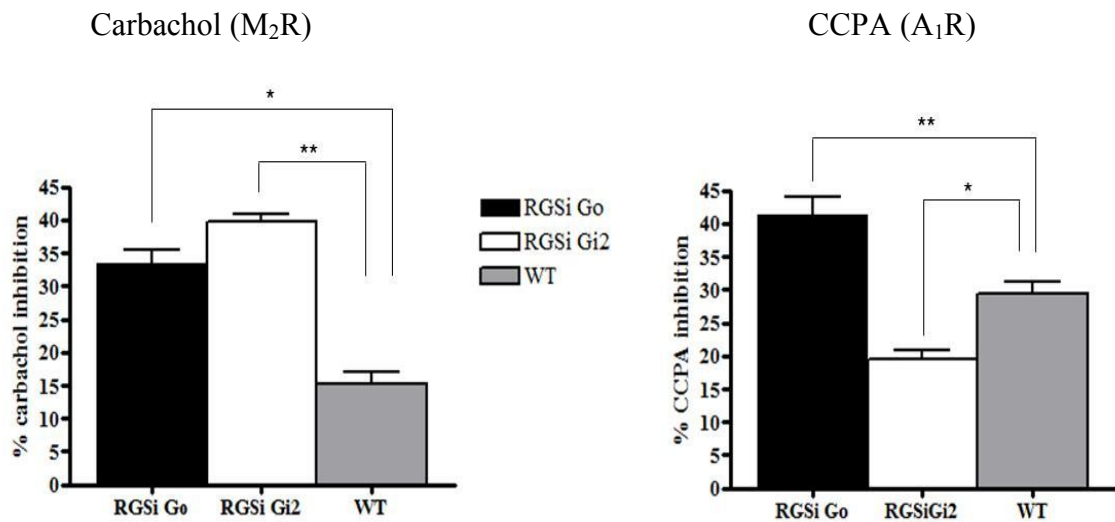


Figure 3.5 Inhibition of heart rate by M₂R and A₁R on RGSiG α_o and RGSiG α_{i2} mice. % inhibition on heart rate was found to be significantly higher in both RGSiG α_o ($n=8$) and RGSiG α_{i2} ($n=8$) with the M₂R agonist, carbachol compared to WT ($n=8$) (G α_o * $P<0.05$, G α_{i2} ** $P<0.01$). Effect of the A₁R agonist, CCPA was specific towards G α_o (** $P<0.01$) as seen by its inhibition on heart rate, rather inhibition on G α_{i2} was even less than that of WT (* $P<0.05$).

Discussion

3.7 RGSiG α_{i2} and RGSiG α_0 mice showed enhanced resting tachycardia and bradycardic responses with agonists

Interestingly, RGSiG α_{i2} and RGSiG α_0 were found to be tachycardic and lost their diurnal variation in heart rhythm and this suggest a role of the central nervous system in controlling the heart rate in these knock-ins and the results were counterintuitive. Studies by Huang et al. on RGSiG α_{i2} also found they were tachycardic along with growth retardation, reduced viability, smaller size and multiple neurologic defects pointing to the fact that cardiovascular phenotypes were an outcome of increased central sympathetic tone (Huang, Fu, Charbeneau, Saunders, Taylor, Hankenson, Russell, D'Alecy, & Neubig 2006). However, carbachol still has a negative chronotropic effect. G α_0 is the predominant isoform in the brain and expressed at higher levels than other inhibitory G-proteins in neuronal tissue (Wettschureck & Offermanns 2005) and G α_0 may in some way regulate central control of autonomic tone. But a small amount of G α_0 is also expressed in cardiac tissues and is found to play an important role in the regulation of automaticity and contractility of the heart by regulation of I $_{Ca, L}$ (Ye et al. 1999). On the other hand, G α_{i2} is also expressed in neuronal tissues but global deletion of G α_{i2} , did not have a gross neurological phenotype (Zuberi, Birnbaumer, & Tinker 2008). Owing to its significance in the central nervous system, it is possible that a defect in the central nervous system in G α_0 or G α_{i2} signalling, could potentially affect regulation of HRV. It is also worthy to postulate the influence of such central effects on the phenotype with inactivation of other inhibitory G-proteins, and these questions will only be definitively answered by tissue-specific gene-targeting approaches. In *in vivo* models there is a possibility of

developing various developmental adaptive measures to balance out the effects of the absence of one gene by another to rescue the pathways. Nevertheless, there were practical problems working with these mice, as breeding was difficult.

It has also been previously reported that in intact animals and in embryonic stem cell derived cardiomyocytes augmented $G\alpha_{i2}$ signalling due to the loss of RGS regulation preferentially amplifies M_2 receptor-mediated responses (Fu, Huang, Zhong, Mortensen, D'Alecy, & Neubig 2006). As observed in our studies an enhanced bradycardic response to carbachol in both $RGSiG\alpha_{i2}$ and $RGSiG\alpha_o$ may be due to enhanced GIRK channel activation though this wasn't formally tested. These data suggest a role of RGS in regulating muscarinic receptor-mediated $G\alpha_o$ and $G\alpha_{i2}$ bradycardic responses and the loss of RGS inhibition could enhance $G\alpha_o$ and $G\alpha_{i2}$ signalling in cardiac tissue and most probably in the SA node. This observation needs to be further confirmed by looking at various ion channels by patch clamping techniques. Moreover, cardiac overexpression of $G\alpha_s$ leads to tachycardia (Uechi, Asai, Osaka, Smith, Sato, Wagner, Ishikawa, Hayakawa, Vatner, Shannon, Homcy, & Vatner 1998), so one would expect that enhanced $G\alpha_i$ function *via* these knock-ins should have the opposite effect. Thus, these observations of the increased heart rate and the observed hyperactivity (not recorded, visual observations) are likely due to central nervous system effects rather than effects on cardiac function.

Studies on embryonic stem cell-derived cardiomyocytes demonstrated that enhanced bradycardia in $RGSiG\alpha_{i2}$ cardiomyocytes is primarily due to increased GIRK currents upon M_2R activation. The response to carbachol was also studied *ex-vivo* and led to increased AV conduction block (Fu, Huang, Zhong, Mortensen, D'Alecy, & Neubig 2006). We didn't observe any arrhythmias with $RGSiG\alpha_{i2}$ and $RGSiG\alpha_o$ mice. GIRK currents are involved in the parasympathetic control of heart rate and have been

implicated in the development of atrial fibrillation (AF). Studies have suggested abnormal activation of GIRK currents is associated with AF (Fu, Huang, Piao, Lopatin, & Neubig 2007). GIRK currents are constitutively active in the heart of chronic AF patients (Dobrev et al. 2005). Since GIRK currents are preferentially activated upon by M₂ receptor-mediated signalling (vagal stimulation), when the effects of RGS proteins on G α_{i2} are inhibited, it is possible that RGSiG α_{i2} mutant mice may have increased risk of AF as well. Hence further characterization of RGSiG α_{i2} and RGSiG α_0 mice may be justified to explore this question using *in vivo* electrophysiological studies such as cardiac pacing to see whether they are prone to atrial fibrillation and AV conduction block.

As the results from the initial screening on RGSiG α_{i2} and RGSiG α_0 knock-ins using telemetry (HRV and ECG) were unexpected and inconclusive, I screened another group of mice where G α_{i2} and G α_0 is knocked down specifically in the heart, and this is discussed in the next chapter.

Chapter 4

RESULTS II

4.1 Heart rate modulation in cardiac-specific deletion of $G\alpha_{i2}$ and $G\alpha_o$ with α MHC cre

Various attempts have been made to address the identity of the molecular players in vagal-mediated heart rate slowing. It is generally agreed that the M_2 muscarinic receptor is the major isoform responsible for vagally-mediated bradycardia in conduction tissues, and this is supported by studies on mice with global genetic deletion of the gene encoding for this protein (Fisher et al. 2004). However, the identity of the inhibitory $G\alpha$ isoform(s) involved in heart rate slowing *in vivo* remains unclear. It is known that $G\alpha_{i1}$, $G\alpha_{i2}$ and $G\alpha_{i3}$ isoforms are widely expressed and $G\alpha_{i2}$ is the predominant cardiac isoform (DeGeorge & Koch 2008; Gohla, Klement, Piekorz, Pexa, vom, Spicher, Dreval, Haussinger, Birnbaumer, & Nurnberg 2007). Using ES cell-derived cardiomyocytes with targeted inactivation of specific G-protein α subunits, it has been shown that expression of both α_{i2} and α_{i3} is required for muscarinic and adenosine receptor-mediated regulation of $I_{K_{ACh}}$ in intact cells (Sowell, Ye, Ricupero, Hansen, Quinn, Vassilev, & Mortensen 1997). Another study showed that $G\alpha_{i3}$ when expressed in heterologous expression systems (*Xenopus Oocytes*) seems to couple GIRK channel activation particularly efficaciously (Ivanina et al. 2004) and lastly, murine $G\alpha_o$ deletion has been reported to selectively impair parasympathetic responses (Duan, Christe, Milstone, & Mortensen 2007). With regards to cardiac pacemaking function, the identity of the inhibitory $G\alpha$ -subunit protein(s) involved in modulating parasympathetic control of intrinsic cardiac automaticity remains undetermined. Previous findings from our lab concluded that $G\alpha_{i2}$ had a major role in heart rate dynamics as there was a selective defect of parasympathetic heart rate modulation in mice with $G\alpha_{i2}$ deletion Table 4.1 (Zuberi, Birnbaumer, & Tinker 2008).

$G\alpha_{i2}$	$G\alpha_o$
Tachycardic	Tachycardic (both day and night) and loss of diurnal variation in heart rate.
Selective attenuation of the HF domain of HRV which corresponds to parasympathetic drive	Loss of the LF component of HRV
HRV signature is similar to mice treated with tertiapin Q and atropine	HRV signature is different from mice treated with tertiapin Q and atropine.
Negative chronotropic effect of carbachol is abolished	Carbachol had negative chronotropic effect
They had prolonged QT interval making them more susceptible to ventricular arrhythmia	Being expressed, high levels in neuronal tissue, HRV signature is similar to those seen in patients with brain stem death
An increase in L-type Ca channel activity and an increase in ventricular action potential duration shown by patch-clamping studies on isolated ventricular myocytes.	

Table 4.1 Comparison of the effects of global KOs of $G\alpha_{i2}$ and $G\alpha_o$ on heart rate dynamics. Work carried out in our lab showing the differences between global KOs of $G\alpha_{i2}$ and $G\alpha_o$ (Zuberi et al. 2008).

There were several disadvantages of working with mice with global genetic deletion of $G\alpha_{i2}$ (-/-) and $G\alpha_o$ (-/-);

1. The effect seen may be due to deletion in the central and peripheral nervous system as $G\alpha_{i2}$ and $G\alpha_o$ was globally deleted in all tissues.
2. With $G\alpha_{i2}$ (-/-) growth retardation was observed, very few litters were produced and occasional unexpected death was seen.

3. With $G\alpha_o$ (-/-) survival rate was poor, they showed more of a neurological phenotype, seizures were observed and they didn't survive beyond 2 months.

From the $G\alpha_o$ studies we hypothesised given the phenotype of global $G\alpha_o$ deletion (tachycardia, loss of diurnal heart rate variation and LF power attenuation) that $G\alpha_o$ may play an important role in central (brainstem) modulation of HRV and $G\alpha_{i2}$ may be of interest in the cardiac context. Global deletion may have important systemic effects which could add confusion to the interpretation of data. To overcome this problem targeted organ (cardiac) specific deletion, using cre lox-P technology which deletes $G\alpha_{i2}$ and $G\alpha_o$ specifically in the cardiac tissue, has been used in my experiments. Hence, I moved to using conditional genetic deletion of $G\alpha_{i2}$ and $G\alpha_o$ in cardiac tissue using α MHC cre recombinase.

4.2 Cardiac specific-deletion of $G\alpha_{i2}$ and $G\alpha_o$ with α MHC cre

Given the practical problems of working with global $G\alpha_{i2}$ (-/-) and $G\alpha_o$ (-/-) mice, a conditional KO mouse line was generated with cardiac-specific $G\alpha_{i2}$ and $G\alpha_o$ deletion, using an α MHC cre mouse crossed with $G\alpha_{i2}/G\alpha_o$ floxed mice. In order to determine if $G\alpha_{i2}$ and $G\alpha_o$ -mediated signalling directly influences HRV at the level of the heart (rather than centrally), the HRV signature was determined against an appropriate control group. It is important to note that these mice were of a mixed background strain (combined C57/black and Sv129 cross) which may influence interpretation.

Conditional $G\alpha_{i2}$ and $G\alpha_o$ -deleted mice ($G\alpha_o$ flx/flx cre⁺ and $G\alpha_{i2}$ flx/flx cre⁺) had a phenotype similar to control. These mice exhibited normal growth, normal behaviour and were fertile. Proof of cardiac specific-deletion at a molecular level (shown in Fig.

4.1), confirmed a substantial decrease in mRNA expression for $G\alpha_{i2}$ (16 fold) and $G\alpha_o$ (6 fold) using real-time PCR (RT-PCR) (Zuberi et al. 2010). At the genomic level deletion is shown and discussed in materials and methods (Fig. 2.3).

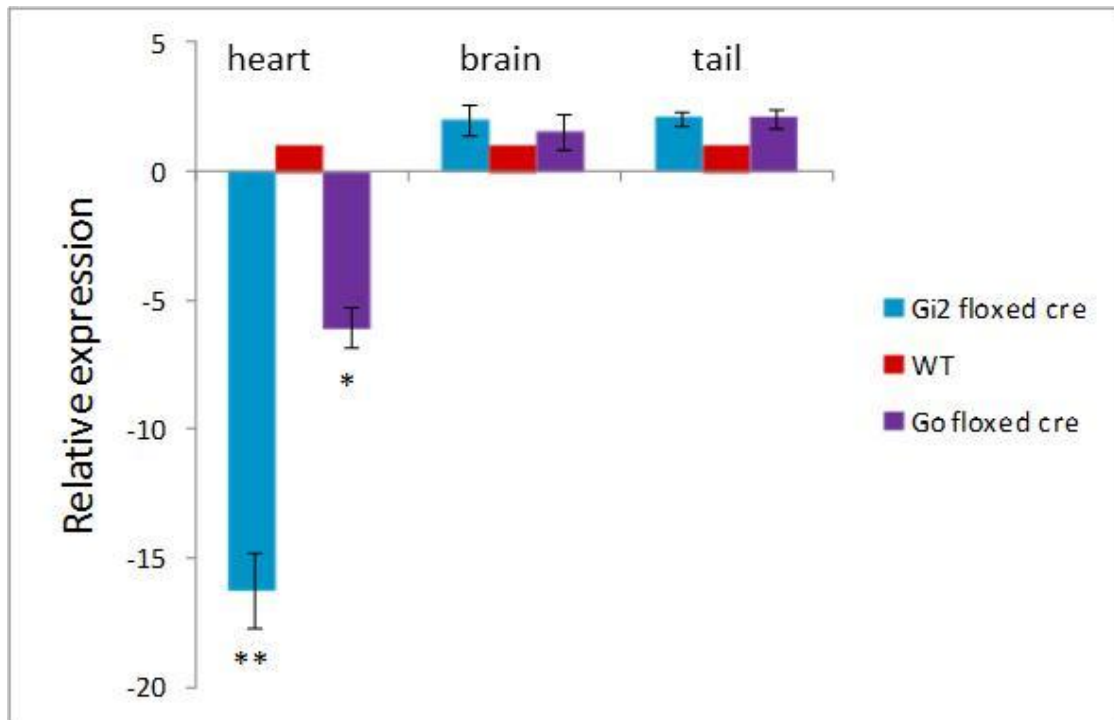


Figure 4.1 RT-PCR showing deletion of $G\alpha_{i2}$ and $G\alpha_o$ in the cardiac tissue. Relative expression of $G\alpha_{i2}$ and $G\alpha_o$ with respect to WT as a calibrator (=1). Taqman probe directed to deleted exons of 2-3 of $G\alpha_{i2}$ shows a significant reduction in expression (** $P < 0.01$) and probe directed to deleted 5-6 of $G\alpha_o$ also shows a significant reduction (* $P < 0.05$) in expression. GAPDH was used as the house keeping gene.

4.3 Preservation of diurnal variation in heart rate in $G\alpha_{i2}$ flx/flx cre⁺ and $G\alpha_o$

flx/flx cre⁺ mice

Using telemetry recordings in conscious mice no significant differences in mean heart rate were observed both at night and during the day with respect to the cardiac-specific inhibitory $G\alpha_{i2}$ and $G\alpha_o$ subunit isoform. Mice are largely active at night and sleep during the day and their increased nocturnal heart rate reflects this. There wasn't

a significant difference in the heart rate between $G\alpha_{i2}$ flx/flx cre⁺ and $G\alpha_o$ flx/flx cre⁺ compared to control during the night ($G\alpha_{i2}$ flx/flx cre⁺ 519 bpm \pm 50, n=6, $G\alpha_o$ flx/flx cre⁺ 485 bpm \pm 37.6, n=6, and control 530.5 bpm \pm 28.3, n=8, P>0.05) and day time ($G\alpha_{i2}$ flx/flx cre⁺ 455 bpm \pm 50, n=6, $G\alpha_o$ flx/flx cre⁺ 456 bpm \pm 37.6, n=6 and control 479 bpm \pm 28.3, n=8, P>0.05) heart rate was compared (Fig. 4.2). All of the groups maintained a diurnal variation in the heart rate with a higher night heart rate compared to day time, even though it was not statistically significant.

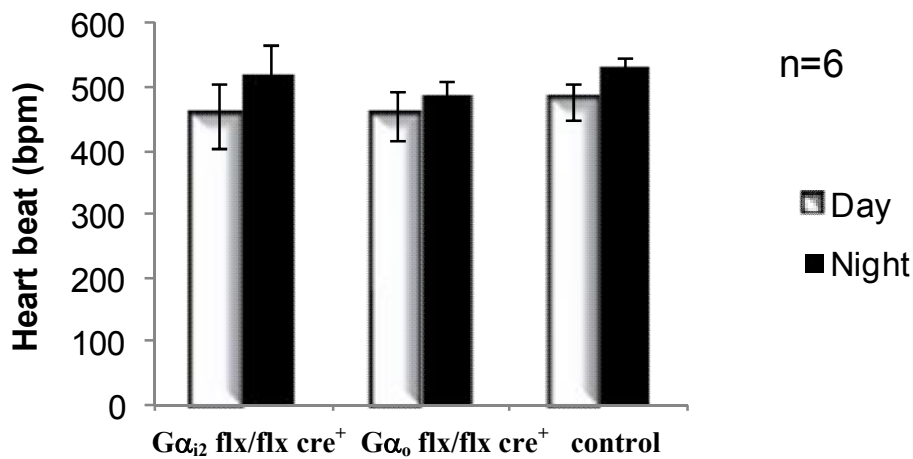


Figure 4.2 Preservation of diurnal variation in the heart rate in $G\alpha_{i2}$ flx/flx cre⁺, $G\alpha_o$ flx/flx cre⁺ and WT littermate controls. No difference was seen in diurnal variation between $G\alpha_{i2}$ flx/flx cre⁺ (n=6) $G\alpha_o$ flx/flx cre⁺ mice (n=6) compared with their littermate controls (n=8) (P>0.05).

4.4 HRV in mice with cardiac-specific $G\alpha_{i2}$ and $G\alpha_o$ deletion with α MHC cre is similar to control

Mice with cardiac specific $G\alpha_o$ deletion ($G\alpha_o$ flx/flx cre⁺) and $G\alpha_{i2}$ deletion ($G\alpha_{i2}$ flx/flx cre⁺) have a HRV phenotype which is very similar to control, in both the time and frequency-domains (See Table 4.2). Specifically in the frequency-domain normalized HF power (HFnu) appears to be preserved in $G\alpha_{i2}$ flx/flx cre⁺ mice (35.6

$\text{ms}^2 \pm 6.31$, $n=6$) and $G\alpha_o$ flx/flx cre⁺ mice ($43.7 \text{ ms}^2 \pm 10.3$, $n=6$) compared with littermate controls ($38.20 \text{ ms}^2 \pm 8.8$, $n=6$, ns). Normalized LF power (LFnu) was also seen to be similar in $G\alpha_{i2}$ flx/flx cre⁺ mice ($61.9\text{ms}^2 \pm 6.17$, $n=6$) and $G\alpha_o$ flx/flx cre⁺ mice ($50.1\text{ms}^2 \pm 13.7$, $n=6$) compared with control ($60.0\text{ms}^2 \pm 8.23$, $n=6$, ns).

Deletion of specific inhibitory $G\alpha_{i2}$ and $G\alpha_o$ subunits exhibited similar HRV characteristics that were not significantly different from wild type controls under basal conditions in the time-domain as well (Fig. 4.3 and Table 4.2). Tachogram tracings and measurements in the time-domain in $G\alpha_{i2}$ flx/flx cre⁺ and $G\alpha_o$ flx/flx cre⁺ mice show no R-R variability compared with controls (Fig. 4.3 and Table 4.2). $G\alpha_{i2}$ flx/flx cre⁺ and $G\alpha_o$ flx/flx cre⁺ mice showed no significant R-R variability under basal conditions compared with controls.

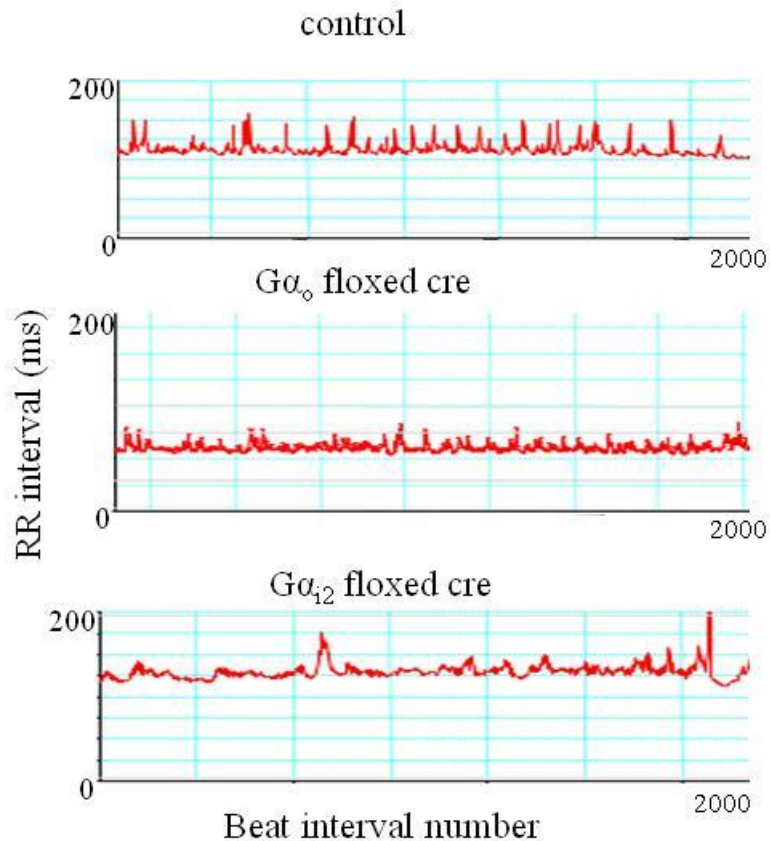


Figure 4.3 HRV in $G\alpha_{i2}$ flx/flx cre⁺ and $G\alpha_0$ flx/flx cre⁺ mice presented in the time-domain recorded from conscious freely moving mice. Representative tracing of tachograms from a control, $G\alpha_0$ flx/flx cre⁺ and $G\alpha_{i2}$ flx/flx cre⁺ mice over a 10 min recording time shows no significant R-R variability among the three groups.

Power spectral analysis of LF and HF of $G\alpha_{i2}$ flx/flx cre⁺ and $G\alpha_0$ flx/flx cre⁺ also reflects the data above (Fig. 4.4). Power spectral-density plots reveal spectral peaks within both the LF and HF range for all $G\alpha_{i2}$ flx/flx cre⁺, $G\alpha_0$ flx/flx cre⁺ mice and control mice and no significant difference was found between the groups. It is possible that outbreeding of these mice results in a more physiological genotype facilitating larger degrees of HRV than observed in the inbred Sv129 strain and emphasizes that even within mice strains, significant differences in HRV signature can occur.

On the ECG parameters measured in $G\alpha_{i2}$ flx/flx cre⁺ and $G\alpha_0$ flx/flx cre⁺ using Chart 7.0 software also showed no significant difference between $G\alpha_{i2}$ flx/flx cre⁺, $G\alpha_0$ flx/flx cre⁺ and their WT littermate controls (Table 4.2). Additionally mean heart rate determined over a 20 minute continuous recording showed no significant difference between all three groups.

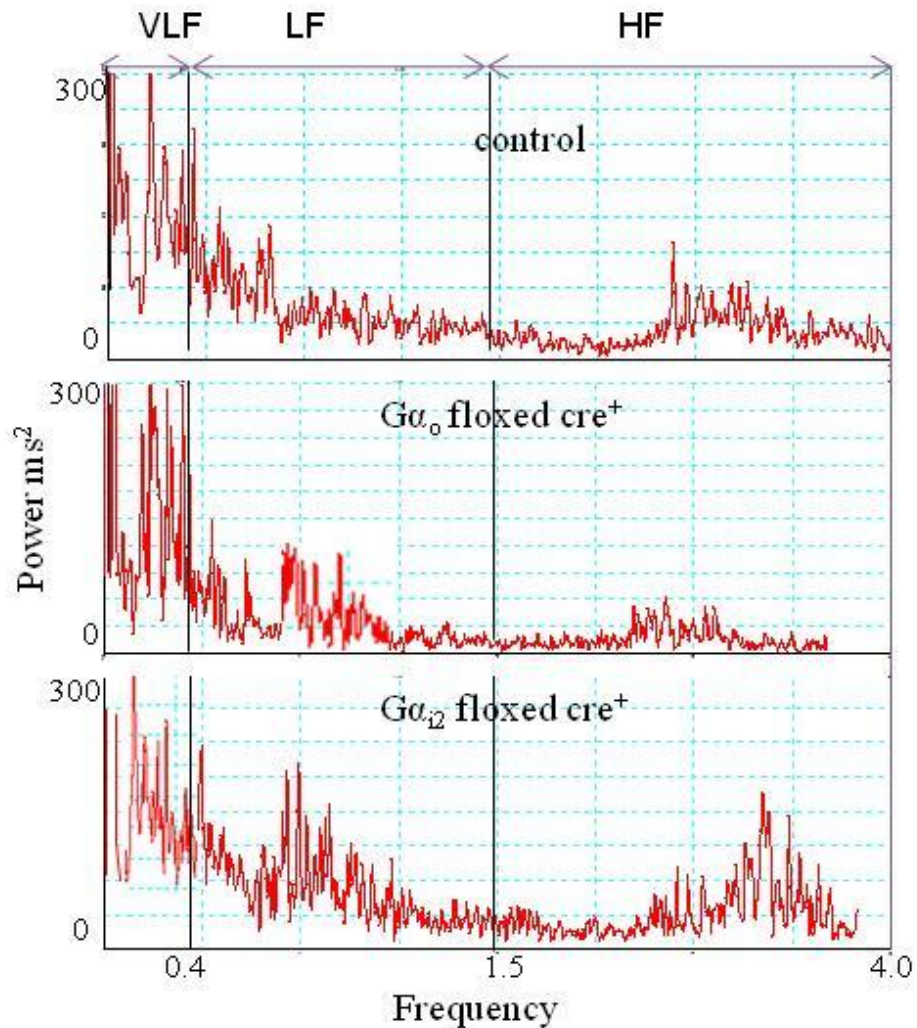


Figure 4.4 HRV in $G\alpha_{i2}$ flx/flx cre⁺ and $G\alpha_0$ flx/flx cre⁺ mice presented in the frequency-domain recorded from conscious freely moving mice. Representative power spectral plot traces of a control, $G\alpha_0$ flx/flx cre⁺ and $G\alpha_{i2}$ flx/flx cre⁺ mice over a 10 min recording time. Good spectral peaks were observed for both LF and HF in both $G\alpha_{i2}$ flx/flx cre⁺ and $G\alpha_0$ flx/flx cre⁺ mice which were similar to the peaks observed in control mice.

		Gα_{i2} flx/flx cre⁺ n=6	Gα_o flx/flx cre⁺ n=4	control n=8
ECG	PR(ms)	36.3±1.78	35.6±3.02	37.7±1.66
	QRS(ms)	10.2±0.68	10.6±1.62	9.1±0.35
	QT _c (ms)	65.5±10.2	63.5±10.7	61.4±9.1
	RR(ms)	116.3±17	124.8±18	120.3±14
HRV	HR(bpm)	546±68.9	551±62	508±65.4
	SDNN	10.4±1.98	12.7±4.06	10.9±3.12
	LFnu	61.9±6.17	50.1±13.7	60.0±8.23
	HFnu	35.6±6.31	43.7±10.3	38.2±8.8

Table 4.2 HRV and ECG parameters measured in the time and frequency-domains during conscious ambulatory telemetry of Gα_{i2} flx/flx cre⁺, Gα_o flx/flx cre⁺ and their WT littermate controls. All observations are ± S.E.M and are compared against control. HR (heart rate), SDNN (standard deviation of normalized RR interval), LFnu (normalized LF frequency), and HFnu (normalized HF frequency). nHF and nLF are normalised to exclude VLF and presented in normalised power units. No significant differences were found between Gα_{i2}flx/flx cre⁺ mice, Gα_oflx/flx cre⁺ mice and their WT litter mate controls.

Discussion

4.5 Mice with cardiac specific-deletion of $G\alpha_{i2}$ and $G\alpha_o$ with α MHC cre exhibited no specific phenotype differences from their littermate controls.

In contrast to the finding in our lab with global knock-outs (Zuberi, Birnbaumer, & Tinker 2008), cardiac-specific deletion of either $G\alpha_{i2}$ or $G\alpha_o$ didn't show any difference in the parameters such as, ECG, HRV and diurnal variation in heart rate. There could be many reasons for these findings.

- The phenotype observed in the global knock-outs may be due to an effect from deletion in peripheral nervous system and or central nervous system.
- The cre-mediated deletion of $G\alpha_{i2}$ and $G\alpha_o$ may not be perfect for the entire region of heart, specifically it may be poor in SA nodal cells.
- Other chronic compensation may be possible in these cardiac-specific knock-outs as a developmental modification and the observations could be adaptive.

Previous studies in our lab with global knock-outs of $G\alpha_o$ (-/-) showed LF power attenuation, significant increase in heart rate both during the night and day and loss of diurnal heart rate rhythm. The observed phenotype is similar to that seen in examples of brainstem dysfunction (Baillard et al. 2002) and has features consistent with a central role for $G\alpha_o$ in modulating HRV. Conditional $G\alpha_o$ -deleted mice ($G\alpha_o$ flx/flx cre⁺ve) had a phenotype similar to control. Specifically there were no features of a gross neurological phenotype as observed with global $G\alpha_o$ deletion (Zuberi, Birnbaumer, & Tinker 2008). These mice exhibited normal growth, normal behaviour and were fertile. Selective cardiac $G\alpha_o$ deletion exhibited normal diurnal heart rate fluctuation and preserved HRV phenotype. Proof of the cardiac-specific deletion at a

molecular level is shown in chapter 2 by genomic PCR as well as a substantial decrease in mRNA expression for $G\alpha_o$ using real-time pcr (Fig 4.1). One possible explanation is that, $G\alpha_o$ is by far the predominant inhibitory $G\alpha$ within brain tissue and so may in some way regulate central control of autonomic tone.

Similarly the cardiac-specific deletion of $G\alpha_{i2}$ ($G\alpha_{i2}$ flx/flx cre⁺) showed a phenotype that was not the same as observed with the global knock-out of $G\alpha_{i2}$ (-/-) in our lab, rather there was no difference in these group compared to wild type controls. With global knock-outs of $G\alpha_{i2}$ (-/-) we did observe increased heart rate, selective abolishment of HF domain of HRV and lack of negative chronotropic response to carbachol. $G\alpha_{i2}$ (-/-) mice also exhibited prolonged QT on telemetry ECG measurements and were prone to ventricular arrhythmia to account for the sudden death phenotype by *in vivo* electrophysiological studies. Patch clamp studies performed on ventricular myocytes of $G\alpha_{i2}$ (-/-) mice also showed prolongation of ventricular action potential duration in $G\alpha_{i2}$ (-/-) mice and enhanced L-type Ca²⁺ currents, which further confirms L type Ca²⁺ channel activity as the mechanism of QT interval prolongation (Zuberi, Nobles, Sebastian, Dyson, Lim, Breckenridge, Birnbaumer, & Tinker 2010). However with $G\alpha_{i2}$ flx/flx cre⁺ we didn't observe any such phenotype (such as prolonged QT on the ECG, spontaneous ventricular ectopic beats or sudden death) so further characterisation was not carried out.

I would like to mention here that these mice ($G\alpha_o$ flx/flx cre⁺ and $G\alpha_{i2}$ flx/flx cre⁺) have not been completely characterised at present in terms of expression at the protein level due to a lack of suitable and specific antibodies. Additionally, the efficacy of the cardiac cre in this setting needs to be formally tested. For example in our experiments partial/incomplete cre-mediated $G\alpha_{i2}$ and $G\alpha_o$ deletion in the SA node could explain

the observed phenotype, as G-protein and GIRK channels and their downstream effects are more prominent in the atrial and nodal tissues. Also in the literature, in studies where a cross of α MHC cre and a Lac Z reporter strain have reported incomplete deletion within the SA node (Herrmann et al. 2007). Therefore, the possible explanation for an absence of differences between the floxed cre and control mice could be attributed to incomplete deletion in the nodal cells. Also in addition, the mosaic nature of the transgene expression, (Guo et al. 2002) line-to-line variations in the level of expression, effects of the genomic site of integration and wide differences in the copy number of the transgene can all contribute to differences in phenotypic expression (Chien 2001).

Lack of difference in HRV and ECG parameters in cardiac-specific deletion of $G\alpha_{i2}$ and $G\alpha_o$ using α MHC cre mice suggests that, probably one of the reasons for not seeing the expected difference is that deletion may not be complete in cardiac pacemaker cells. It also throws light on the fact that a ventricular phenotype is not enough to see the effect of any cardiovascular change or rather it seems to be some mechanism outside the ventricles. Also, $G\alpha_o$ seems to be more prominent in brain tissues than in the heart, as results indicate more of its role in the central nervous system. As a result of this, I decided to use $G\alpha_s$ knock-out mice, which should exhibit effects opposing to those of $G\alpha_{i2}$ in the remainder of my studies and a colleague Richard Ang pursued further study of $G\alpha_o$ mice and its tissue-specific expression in brain. Also, I moved on to try another cre mice (conduction system cre HCN4 -KiT) which deletes $G\alpha_{i2}$ and $G\alpha_s$ in the conduction system upon administration of tamoxifen. These mice (with specific deletion of $G\alpha_{i2}$ and $G\alpha_s$ in the conduction system tissues) were used to assess the effect of deletion of $G\alpha_{i2}$ and $G\alpha_s$ on HRV and the data is presented and discussed in the next chapter 5.

Chapter 5

RESULTS III

5.1 Heart rate modulation in conduction system-specific deletion of $G\alpha_{i2}$ and $G\alpha_s$ with a conduction system cre (HCN4 cre⁺)

The HCN4 cre⁺ mice line is the new strain added in this chapter. The HCN4 gene encodes for the hyperpolarization-activated cyclic nucleotide-gated potassium and sodium channels, mutations in which have been linked to sick sinus syndrome 2, also known as atrial fibrillation with bradyarrhythmia or familial sinus bradycardia (Laish-Farkash et al. 2010; Schulze-Bahr et al. 2003). Hyperpolarization-activated cyclic nucleotide-gated (HCN) channels, mediate the I_f current in the heart (and I_h in neurons) (Herrmann, Stieber, Stockl, Hofmann, & Ludwig 2007; Ludwig et al. 1998) and they are thought to be key players in generating and regulating pacemaker activity. Sympathetic activation by β -AR in sinoatrial node cells accelerates heart rate by increasing cAMP levels and these channels are modulated by direct binding of cAMP (DiFrancesco & Tortora 1991) suggesting that the cAMP-mediated enhancement of HCN channel activity is largely responsible for this increase in heart rate (DiFrancesco 1993). Four genes encoding HCN channels have been identified (HCN1–4). HCN4 is the most highly expressed HCN isoform in the sinoatrial node (Moosmang et al. 2001) where different isoforms of G-proteins exert their heart modulatory functions.

Here, we have investigated the role of $G\alpha_{i2}$ and $G\alpha_s$ for cardiac pace-making by combining a temporally controlled gene-knock-out approach with analyses of heart rate and rhythm in intact animals by ambulatory telemetry recordings. My colleague Richard Ang helped me to maintain the number of $G\alpha_{i2}$ flx/flx HCN4 cre⁺ mice when I was on maternity leave. $G\alpha_s$ was chosen to ascertain if it has the opposing effects to $G\alpha_{i2}$.

5.2 Study plan for tamoxifen-induced cre deletion in the conduction system

A study plan was drawn initially to study the effects of HCN4 cre-mediated deletion in the conduction system of $G\alpha_{i2}$ flx/flx HCN4 cre⁺ and $G\alpha_s$ flx/flx HCN4 cre⁺ mice (Fig. 5.1).

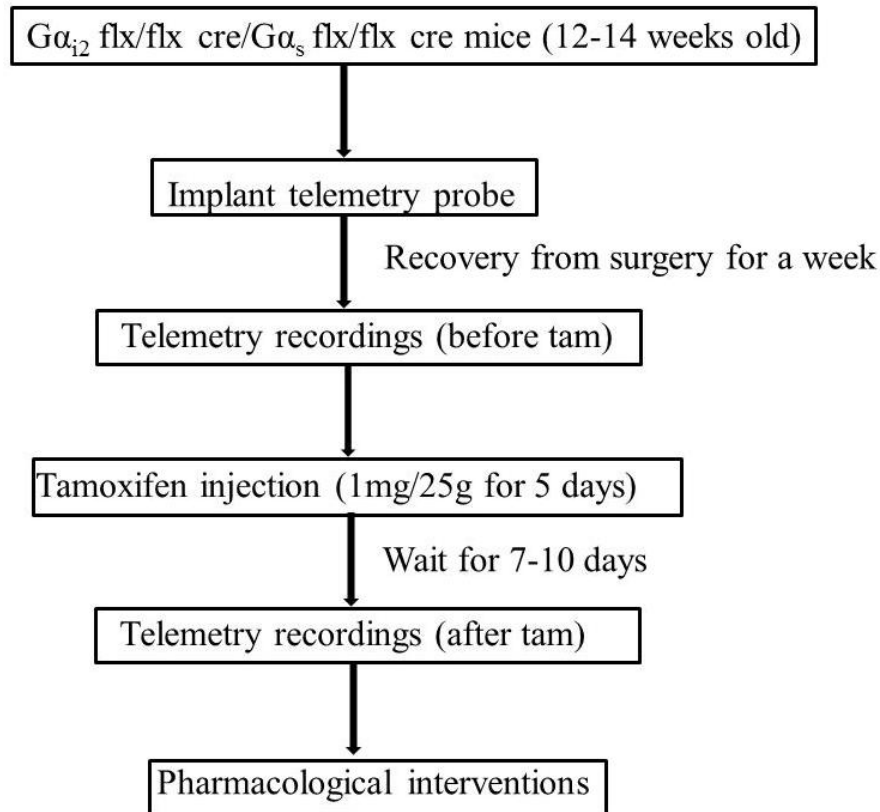


Figure 5.1 Study plan for tamoxifen-induced cre deletion in the conduction system. Telemetry probes were implanted in 12-14 weeks of $G\alpha_{i2}$ flx/flx HCN4 cre⁺ and $G\alpha_s$ flx/flx HCN4 cre⁺ mice and allowed them to recover from surgery for a week. Telemetry recordings were carried out followed by tamoxifen injection for 5 consecutive days. After 7-10 days, telemetry recordings were performed again. Later, pharmacological agents were administered to see their effects on these mice.

5.3 Real time PCR shows deletion of $G\alpha_{i2}$ and $G\alpha_s$ in SA nodal tissues

We performed quantitative real-time RT-PCR on RNA extracted from the SA node and ventricle using Taqman probes targeted at the floxed exons in $G\alpha_{i2}$ (exons 2-3)

and $G\alpha_s$ (exon 1) and this showed the deletion of $G\alpha_{i2}$ and $G\alpha_s$ in nodal tissues. We normalized measurements in the $G\alpha_s$ flx/flx HCN4 cre⁺ and $G\alpha_{i2}$ flx/flx HCN4 cre⁺ mice to expression in control mice (both after the administration of tamoxifen) in ventricle and SA node. There was a significant reduction in relative $G\alpha_s$ and $G\alpha_{i2}$ RNA expression in the SA node but not ventricle ($G\alpha_s$ flx/flx HCN4 cre⁺ SA node=0.18, (95%CI 0.17-0.18, **P<0.01), ventricle=1.01, (95%CI 0.99-1.03), and $G\alpha_{i2}$ flx/flx HCN4 cre⁺ SA node=0.11 (95%CI 0.09-0.24, **P<0.01), ventricle=1.04 (95%CI 0.80-1.36); n=2 and 3 mice respectively in triplicate for all groups) (Fig. 5.2). We also confirmed the deletion at the genomic level from genomic DNA isolated from cardiac ventricle and SA node and performed PCR which confirmed cre-mediated deletion of exon1 of *Gnas* and exons 2-4 in *Gnai2* in the SA node but not in the ventricle or tail (Materials and Methods Fig. 2.5).

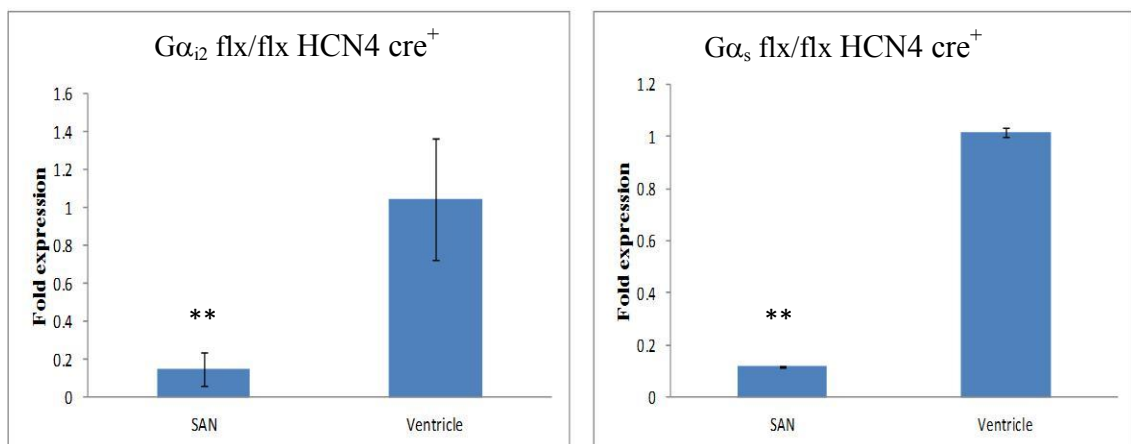


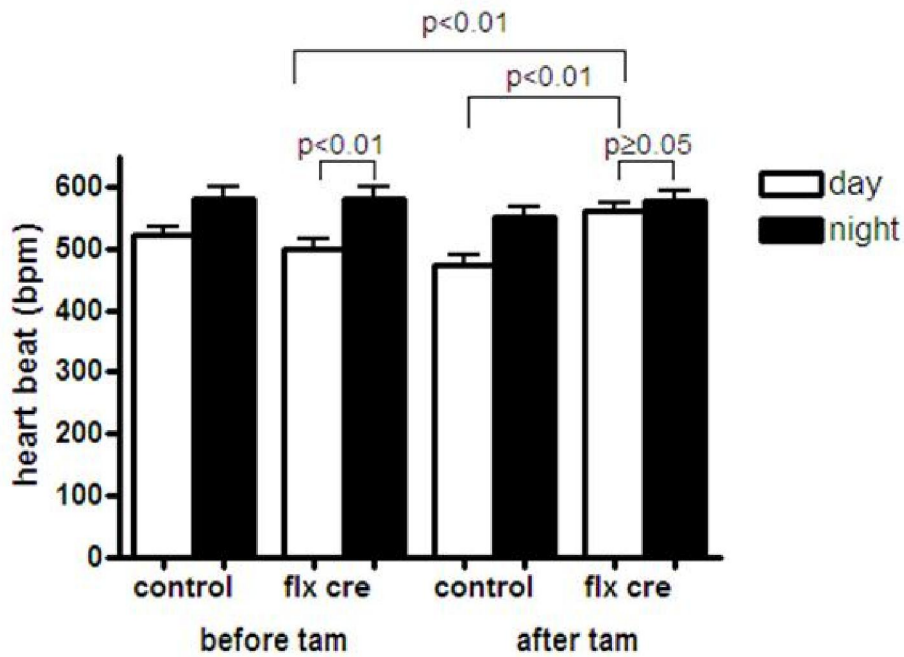
Figure 5.2 Real-time PCR showing cre-mediated deletion in SA node tissues of $G\alpha_{i2}$ and $G\alpha_s$ mice. Both $G\alpha_{i2}$ flx/flx HCN4 cre⁺ and $G\alpha_s$ flx/flx HCN4 cre⁺ mice showed low of expression of $G\alpha_{i2}$ and $G\alpha_s$ respectively after tamoxifen injection in the SA node compared to ventricles. All genes were assayed in triplicates and relative gene expression was quantified using the comparative C_T method with GAPDH as the reference housekeeping gene (n=2 for SA node and n=3 for ventricles, **P<0.01).

5.4 Diurnal variation in heart rate was lost in mice with conduction system-specific deletion of $G\alpha_{i2}$ and $G\alpha_s$

After injection of tamoxifen for 5 consecutive days to achieve cre-mediated deletion in conduction system tissues, telemetry studies were done in conscious mice. These showed significant differences in mean heart rate observed both at night and during the day in control mice with respect to $G\alpha_{i2}$ and $G\alpha_s$. Mice are largely active at night and sleep during the day and the increased nocturnal heart rate reflects this. In Fig. 5.3, I have compared heart rate before and after tamoxifen in both control and flx/flx HCN4 cre⁺ mice $G\alpha_{i2}$ and $G\alpha_s$. Both $G\alpha_{i2}$ flx/flx HCN4 cre⁺ and $G\alpha_s$ flx/flx HCN4 cre⁺ lost diurnal variation with similar night and day time heart rates. Significant diurnal variation in heart rate was observed in control after tamoxifen treatment (489 bpm \pm 25 day; 545 bpm \pm 20 night, n=9, **P<0.01), but not in $G\alpha_{i2}$ flx/flx HCN4 cre⁺ (552 bpm \pm 23.8 day; 578 bpm \pm 42 night, n=12), although $G\alpha_{i2}$ flx/flx HCN4 cre⁺ maintained diurnal variation in heart rate before tamoxifen treatment (502 bpm \pm 28 day; 541 bpm \pm 25 night, n=12 **P<0.01). Also there was an increase in the heart rate after tamoxifen in $G\alpha_{i2}$ flx/flx HCN4 cre⁺ during the day (552 bpm \pm 23.8 day) compared to before tamoxifen (502 bpm \pm 28 day; n=12 **P<0.01). The same pattern of increase in the heart rate was seen after tamoxifen treatment during the day in $G\alpha_{i2}$ flx/flx HCN4 cre⁺ (552 bpm \pm 23.8 day n=12 *P<0.01) mice compared to control (489 bpm \pm 25 day; n=9) (Fig. 5.3 A). Thus, mice with conduction-specific deletion of $G\alpha_{i2}$ by tamoxifen-inducible conduction system cre ($G\alpha_{i2}$ flx/flx HCN4 cre⁺) were tachycardic during night and day.

Similarly before tamoxifen, $G\alpha_s$ flx/flx HCN4 cre⁺ and control mice exhibited significant diurnal variation in heart rate (**P<0.01). However after tamoxifen significant diurnal variation in the heart rate was observed only in control mice (560 bpm \pm 15 day; 630 bpm \pm 16 night n=8 *P<0.05), but not in $G\alpha_s$ flx/flx HCN4 cre⁺ (452 bpm \pm 25 day; 470 bpm \pm 16 night n=8) (Fig. 5.3 B). Also there was a decrease in the heart rate after tamoxifen in $G\alpha_s$ flx/flx HCN4 cre⁺ during the day (452 bpm \pm 25 day) compared to before tamoxifen (592 bpm \pm 37 day; n=8, *P<0.05). Significant reduction in the night time heart rate was also observed in this $G\alpha_s$ flx/flx HCN4 cre⁺ group before (687 bpm \pm 40 night) and after tamoxifen (470 bpm \pm 16 night n=8, ***P<0.001). It is clear from Fig. 5.3B that mice with conduction-specific deletion of $G\alpha_s$ ($G\alpha_s$ flx/flx HCN4 cre⁺) were bradycardic during the night and the day.

A $G\alpha_{i2}$



B $G\alpha_s$

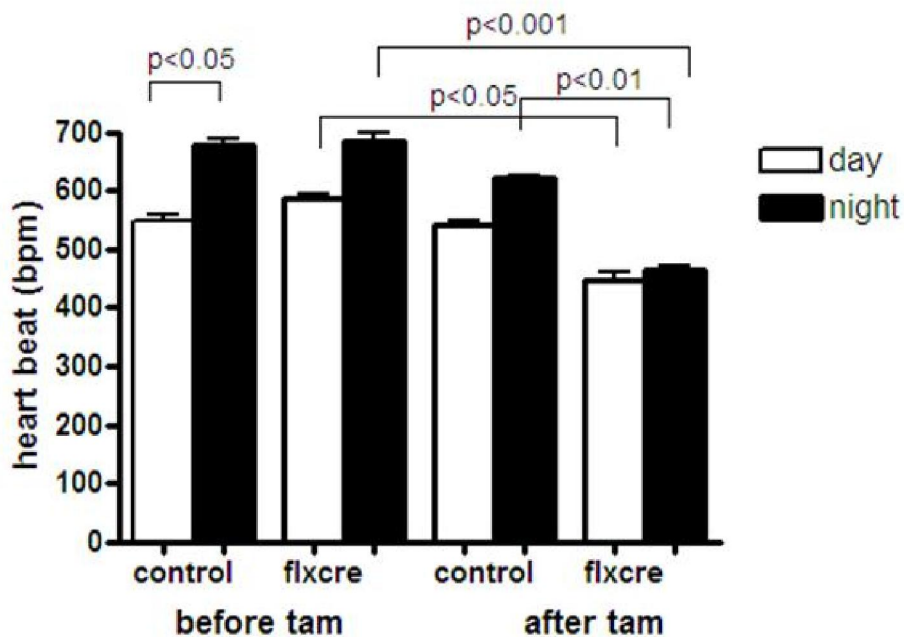
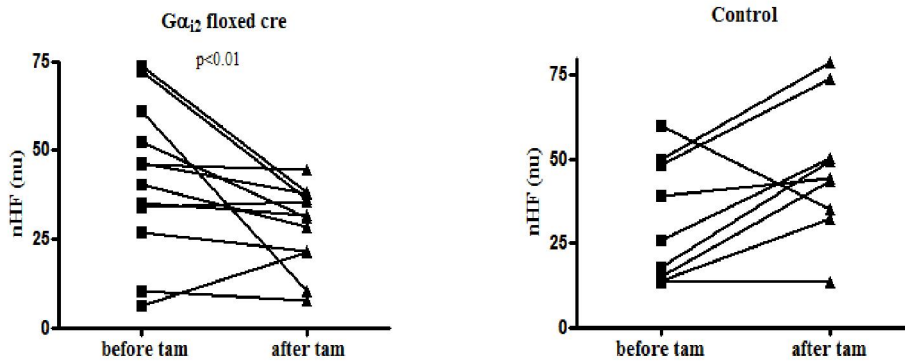


Fig 5.3 Mean day and night heart rate in mice with selective $G\alpha_{i2}$ and $G\alpha_s$ deletion in the conduction system. Panel A. Mean heart rate measured in $G\alpha_{i2}$ flx/flx HCN4 cre⁺ mice (n=12) and its litter mate controls (n=9) during day and night. Panel B summarises mean heart rate in $G\alpha_s$ flx/flx HCN4 cre⁺ (n=8) during day and night with respect to control (n=8). Both $G\alpha_{i2}$ flx/flx HCN4 cre⁺ and $G\alpha_s$ flx/flx HCN4 cre⁺ mice lost their diurnal variations in heart rate compared to their respective control groups after tamoxifen treatment and was found to be tachycardic and bradycardic respectively.

5.5 HRV analysis reveals selective loss of the HF component in conduction system-specific $G\alpha_{i2}$ knock-out mice.

After getting positive results with respect to heart rate in these mice, I went on to compare heart rate variability in these conditional KOs of $G\alpha_{i2}$ and $G\alpha_s$ in both the time and frequency-domain. Compared to conditional KOs using α MHC cre mice, where there was no difference in LF and HF components of HRV, the conditional KO of $G\alpha_{i2}$ flx/flx HCN4 cre⁺ using tamoxifen inducible cre mice showed loss of the HF component of the HRV signature, ($G\alpha_{i2}$ flx/flx HCN4 cre⁺ before tam $42.05 \text{ ms}^2 \pm 5.9$; and after tam $30.21 \text{ ms}^2 \pm 2.2$; n=12 **P<0.01) while in controls the HF component was preserved after tam (control before tam $37.73 \text{ ms}^2 \pm 5.25$; and after tam $45.95 \text{ ms}^2 \pm 4.5$ n=9) (Fig. 5.4 A). There was no change in any other parameters of HRV time-domain as reflected in the Table 5.1. Also selective deletion of $G\alpha_{i2}$ in the nodal cells preserved the LF component in $G\alpha_{i2}$ flx/flx HCN4 cre⁺ (before tam $47.5 \text{ ms}^2 \pm 5.08$ and after tam $44.7 \text{ ms}^2 \pm 5.97$, n=12) which was similar to control (before tam $36.6 \text{ ms}^2 \pm 6.14$; after tam $35.4 \text{ ms}^2 \pm 3.31$ n=9) (Fig. 5.4 B). It is to be noted that there were a few outliers in both groups of control and $G\alpha_{i2}$ flx/flx HCN4 cre⁺ because of which there is a huge variation in SE. The controls used here is a pool of $G\alpha_{i2}$ wt/wt cre⁺ and $G\alpha_{i2}$ wt/wt cre⁻. Selective attenuation of HF power was also observed with the global KOs of $G\alpha_{i2}$ (Zuberi, Birnbaumer, & Tinker 2008) which shows an impairment of parasympathetic activity. $G\alpha_{i2}$ plays a major role in the parasympathetic modulation of the heart rate, so it is not surprising the HF component which represents the vagal (parasympathetic) tone of the HRV signature was lost in the absence of $G\alpha_{i2}$.

A



B

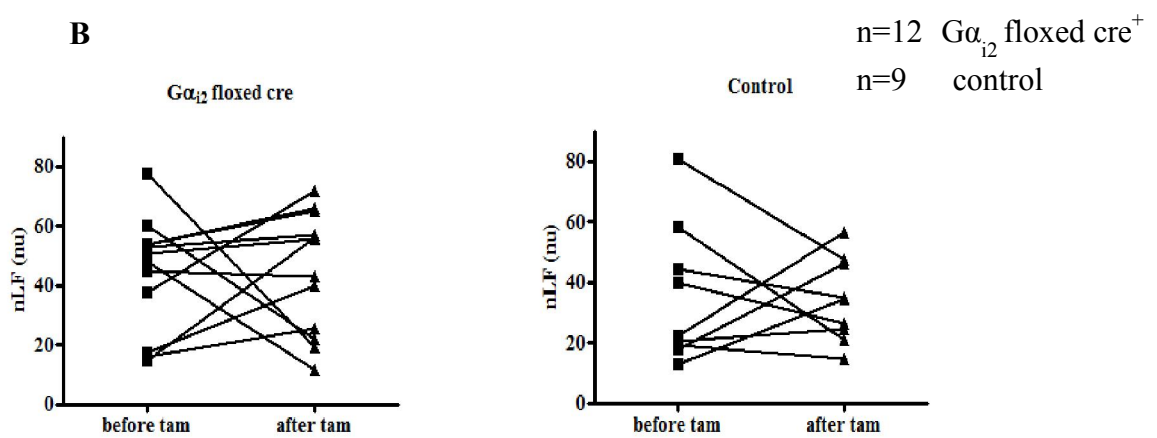


Figure 5.4 HF and LF power in Gα_{i2} flx/flx HCN4 cre⁺ mice before and after tamoxifen A. Loss of the HF component of HRV in Gα_{i2} flx/flx HCN4 cre⁺ mice after tamoxifen compared to before tamoxifen and controls. B. Preservation of LF component of HRV in Gα_{i2} flx/flx HCN4 cre⁺ before and after tamoxifen similar to that of litter mate controls (n=12 Gα_{i2} flx/flx HCN4 cre⁺ mice, n=9 controls).

5.6 HRV analysis reveals selective loss of the LF component in conduction system-specific Gα_s knock-out mice.

Similar to mice with selective deletion of Gα_{i2} deletion (Gα_{i2} flx/flx HCN4 cre⁺), mice with conduction system-specific Gα_s deletion (Gα_s flx/flx HCN4 cre⁺) have a HRV phenotype which is different from controls (pool of Gα_s wt/wt cre⁺ and Gα_s wt/wt cre⁻) in both the time and the frequency-domains. The conditional Gα_s KO (Gα_s flx/flx

HCN4 cre⁺) mice showed a loss of the LF component of the HRV signature, ($G\alpha_s$ flx/flx HCN4 cre⁺ before tam: $55.16 \text{ ms}^2 \pm 5.97$; and after tam $37.08 \text{ ms}^2 \pm 3.83$; n=8, *P<0.05) while there wasn't much change in the LF component before and after tam in controls (before tam $40.01 \text{ ms}^2 \pm 3.43$; and after tam $45.27 \text{ ms}^2 \pm 3.17$, n=8) (Fig. 5.5 A). There was no change in any other parameters of the HRV time-domain as shown in the Table 5.1. In contrast to $G\alpha_{i2}$, selective deletion of $G\alpha_s$ in the nodal cells preserved the HF component of the signature in $G\alpha_s$ flx/flx HCN4 cre⁺ (before tam, $42.7 \text{ ms}^2 \pm 7.52$ and after tam $41.72 \text{ ms}^2 \pm 4.60$ n=8) which was similar to control (before tam $48.63 \text{ ms}^2 \pm 3.75$; after tam $45.61 \text{ ms}^2 \pm 4.44$ n=8) (Fig. 5.5 B). Here, like $G\alpha_{i2}$ flx/flx HCN4 cre⁺ there are a few outliers in $G\alpha_s$ flx/flx HCN4 cre⁺ because of which there is a variation in SE. It is noteworthy that mixed strained animals appear to have greater HRV (~ 4-5 fold larger) than pure inbred strains emphasising the importance of a mixed strain littermate comparison group.

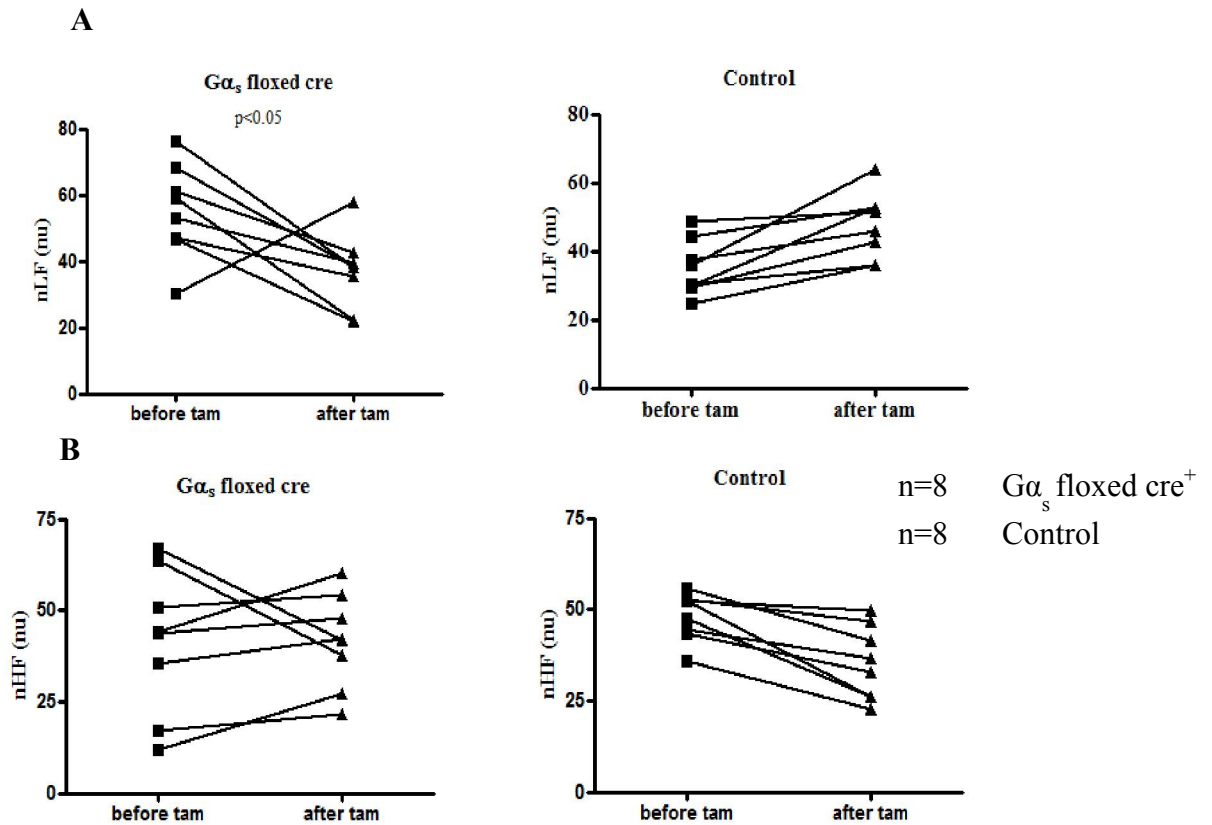


Figure 5.5 HF and LF power in $G\alpha_s$ flx/flx HCN4 cre⁺ mice before and after tamoxifen
 A. Loss of LF component of HRV in $G\alpha_s$ flx/flx HCN4 cre⁺ mice after tamoxifen compared to before tamoxifen and controls B. Preservation of the HF component of HRV in $G\alpha_s$ flx/flx HCN4 cre⁺ mice before and after tamoxifen similar to that of litter mate controls (n=8 $G\alpha_s$ flx/flx HCN4 cre⁺ mice, n=8 controls).

In both $G\alpha_s$ flx/flx HCN4 cre⁺ and $G\alpha_{i2}$ flx/flx HCN4 cre⁺ mice, HRV was altered after tamoxifen treatment. This was detectable in an individual mouse in power spectral density analysis (Fig. 5.6). Specifically there was a selective loss of normalised low frequency (LF) power in $G\alpha_s$ flx/flx HCN4 cre⁺ mice seen as loss of spectral peaks in the low frequency range (0.4-1.5Hz) (Fig. 5.6 A- before tam and B- after tam), while in contrast in $G\alpha_{i2}$ flx/flx HCN4 cre⁺ mice there was a selective loss in normalised high frequency (HF) power perceived as loss of spectral peaks in high frequency range (1.5-4.0) (Fig. 5.6 C- before tam and D- after tam and Table 5.1).

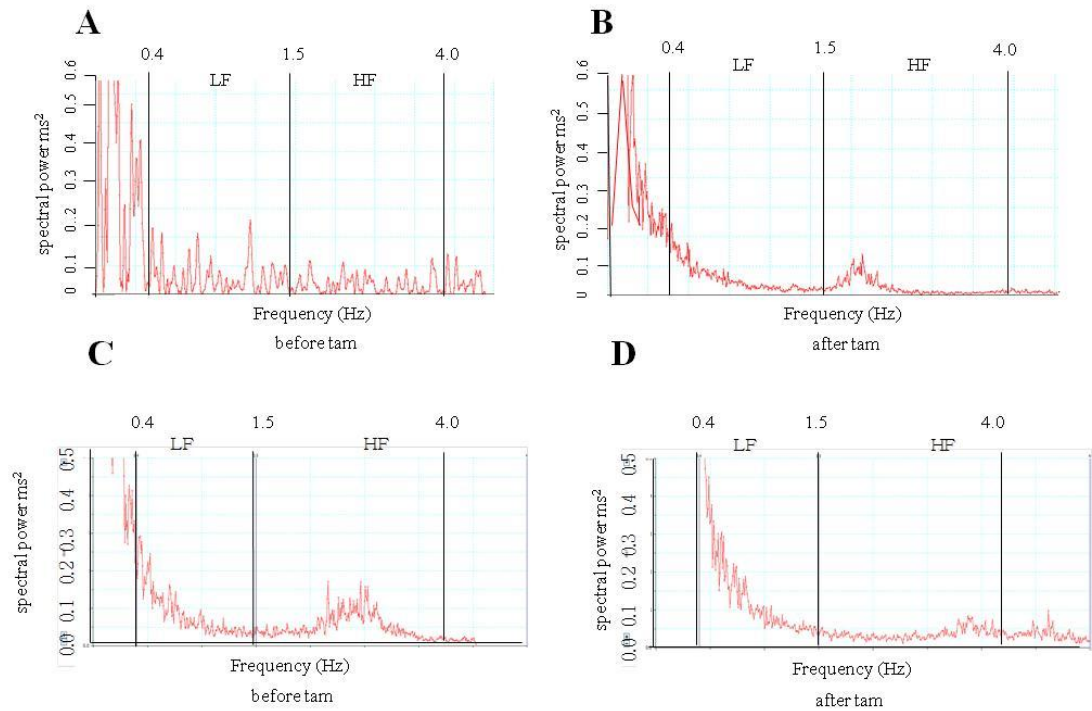


Figure 5.6 HRV from power spectral density (PSD) plots in $G\alpha_s$ flx/flx HCN4 cre⁺ and $G\alpha_{i2}$ flx/flx HCN4 cre⁺ mice. Representative power spectrum density traces for A) $G\alpha_s$ flx/flx HCN4 cre⁺ mice before tam, B) $G\alpha_s$ flx/flx HCN4 cre⁺ mice after tam where there is loss of LF power, C) $G\alpha_{i2}$ flx/flx HCN4 cre⁺ mice before tam and D) $G\alpha_{i2}$ flx/flx HCN4 cre⁺ mice after tam where there is loss of HF power after its administration.

Measurements in the time-domain in $G\alpha_{i2}$ flx/flx HCN4 cre⁺ and $G\alpha_s$ flx/flx HCN4 cre⁺ mice showed no significant variation in SDNN and RMSSD compared with controls (Table 5.1). However, more revealingly in the frequency-domain, there was loss of HF power after tam in $G\alpha_{i2}$ flx/flx HCN4 cre⁺ ($30.21 \text{ nu} \pm 2.2$, $n=12$ * $P<0.05$) compared with controls ($45.95 \text{ nu} \pm 4.55$, $n=9$) and loss of LF with $G\alpha_s$ flx/flx HCN4 cre⁺ mice ($37.08 \text{ nu} \pm 3.82$, $n=8$ * $P<0.05$) compared with controls ($45.27 \text{ nu} \pm 3.17$, $n=8$) (Table 5.1). In the frequency-domain, TP and VLF power were unchanged.

Animal ID	SD nn(ms)	RMSSD(ms)	TP(ms ²)	VLF(ms ²)	LF(ms ²)	HF(ms ²)	nLF(nu)	nHF(nu)
Gα _s flx cre before tam	2.92±0.65	2.08±2.51	131±5.58	60.23±9.2	39.53±7.6	30.21±7.9	55.16±5.9	42.7±7.52
Gα _s flx cre after tam	5.05±1.00	7.14±6.11	160±82	85.12±9.9	36.4±8.9	37.35±6.7	37.08±3.82*	41.72±4.60
Gα _s control before tam	14.75±3.50	15.20±3.63	297±84	185.35±15.2	42.23±8.1	57.26±12.7	40.01±3.43	48.63±3.75
Gα _s control after tam	12.51±5.27	7.58±0.62	200±5.72	101.98±5.9	48.6±7.8	45.23±7.2	45.27±3.17	45.61±4.44
Gα ₁₂ flx cre before tam	23.8±7.57	11.7±2.66	215±81.4	97.7±8.2	56.1±9.2	49.5±5.8	47.5±5.08	42.05±5.9
Gα ₁₂ flx cre after tam	31.4±6.64	13.6±5.49	1302±432	1201±110	44.6±7.8	31.2±6.7	44.7±5.97	30.21±2.2*
Gα ₁₂ control before tam	11.80±4.50	8.24±0.81	134±15.8	65.6±12.7	25.01±5.2	21.76±5.9	36.6±6.14	37.7±5.25
Gα ₁₂ control after tam	5.778±5.92	7.12±0.97	248±5.5	171.2±10.2	27.1±3.4	36.2±7.2	35.4±3.31	45.95±4.55

Table 5.1 Summarised HRV parameters for mice with conditional Gα₁₂ deletion and Gα_s deletion compared with littermate controls in time and frequency-domains. All observations are ± S.E.M and are compared against control, P<0.05 = *. RMSSD (root mean square of successive differences), SD NN (Standard deviation of “normal” sinus rhythm R-R/n-n intervals, TP (Total Power), VLF power (very low frequency <0.4Hz), LF power (low frequency 0.4-1.5Hz), HF power high frequency 1.5-4.0 Hz), nHF and nLF are normalised to exclude VLF and presented in normalised power units (n=12 for Gα₁₂ flx/flx HCN4 cre⁺ mice, n=8 for its controls and n=8 for Gα_s flx/flx HCN4 cre⁺ mice and its controls).

5.7 No change in ECG parameters measured by ambulatory telemetry in mice with conduction system-specific deletion of $G\alpha_{i2}$ and $G\alpha_s$

Sudden death syndromes and ventricular arrhythmia often result from abnormal ventricular repolarisation. We observed sudden death in several mice with global deletion of $G\alpha_{i2}$ (-/-) mice (Thesis Zia Zuberi). This prompted us to closely examine the surface ECG characteristics in these mice. We examined ECG parameters and there were no significant difference in PR interval, QRS duration or any evidence of spontaneous arrhythmia such as heart block (Table 5.2). However unexpectedly we observed a significantly shorter QTc in the $G\alpha_s$ flx/flx HCN4 cre⁺ mice (after tam 40.08 ms \pm 2.07; before tam 62.28 ms \pm 2.08, n=8 *P<0.05) compared to littermate controls (before tam 67.75 ms \pm 0.55 n=8; after tam 67.05 ms \pm 4.46 n=8) despite relative bradycardia, which would be expected to prolong QT interval, but this was not investigated further in this study. R-R interval was found to be longer in $G\alpha_s$ flx/flx HCN4 cre⁺ mice after tam (148.8 ms \pm 4.05 n=8) compared to before tam (96.9 ms \pm 2.46, n=8 *P<0.05) and littermate controls, (before tam 95.57 ms \pm 0.064; after tam 101.1 ms \pm 0.95, n=8) which is in line with the bradycardia observed in these mice. Similarly in $G\alpha_{i2}$ flx/flx HCN4 cre⁺ mice, R-R interval was found to be shorter after tam (98.94 ms \pm 7.8, n=12) compared to before tam (113.0 ms \pm 8.4, n=12 *P<0.05) and littermate controls (before tam 119.9 ms \pm 10.1; after tam 123.7 ms \pm 1.7, n=9). The shorter R-R interval observed in these $G\alpha_{i2}$ flx/flx HCN4 cre⁺ mice is in agreement with the tachycardic phenotype observed in them.

Animal ID	PR(ms)	QRS(ms)	QT _c (ms)	R-R(ms)
Gα _s flx cre before tam	32.50±1.50	9.84±1.1	62.28±2.08	96.9±2.46
Gα _s flx cre after tam	32.60±1.22	9.92±0.87	40.08±2.07*	148.8±4.05*
Gα _s control before tam	34.96±0.82	11.35±0.66	67.75±0.55	95.57±0.064
Gα _s control after tam	38.81±0.44	9.93±0.27	67.05±4.46	101.1±0.95
Gα _{i2} flx cre before tam	33.12±0.49	10.41±0.63	69.84±4.98	113.1±8.4
Gα _{i2} flx cre after tam	34.06±0.88	9.96±0.37	69.21±3.43	98.94±7.8*
Gα _{i2} control before tam	35.07±0.31	9.52±0.452	61.63±3.78	119.9±10.1
Gα _{i2} control after tam	36.33±1.04	10.12±0.35	62.36±3.76	123.7±1.7

Table 5.2 Mean ECG parameters in conscious ambulatory mice with conditional Gα_{i2} deletion and Gα_s deletion compared with littermate controls. All observations are ± S.E.M., P<0.05 = *. A mouse QT correction formula (QT_c) was used to allow for comparison of QT relative to heart rate (QT/ ((R-R/100) ^0.5). (n=12 for Gα_{i2} flx/flx HCN4 cre⁺ mice, n=9 for control, n=8 for Gα_s flx/flx HCN4 cre⁺ mice and n=8 for controls).

Analysis ECG traces of Gα_{i2} flx/flx HCN4 cre⁺ before tamoxifen and after tamoxifen show significantly shorter R-R intervals, after tamoxifen (Fig. 5.7). On the other hand in Gα_s flx/flx HCN4 cre⁺ mice showed longer R-R intervals after tamoxifen. Both the observations aligns very well with the heart rate measurements in these groups as Gα_{i2} flx/flx HCN4 cre⁺ mice were found to be tachycardic (shorter R-R intervals in ECG traces) and Gα_s flx/flx HCN4 cre⁺ mice were found to be bradycardic (longer R-R intervals in ECG traces), compared with their littermate controls.

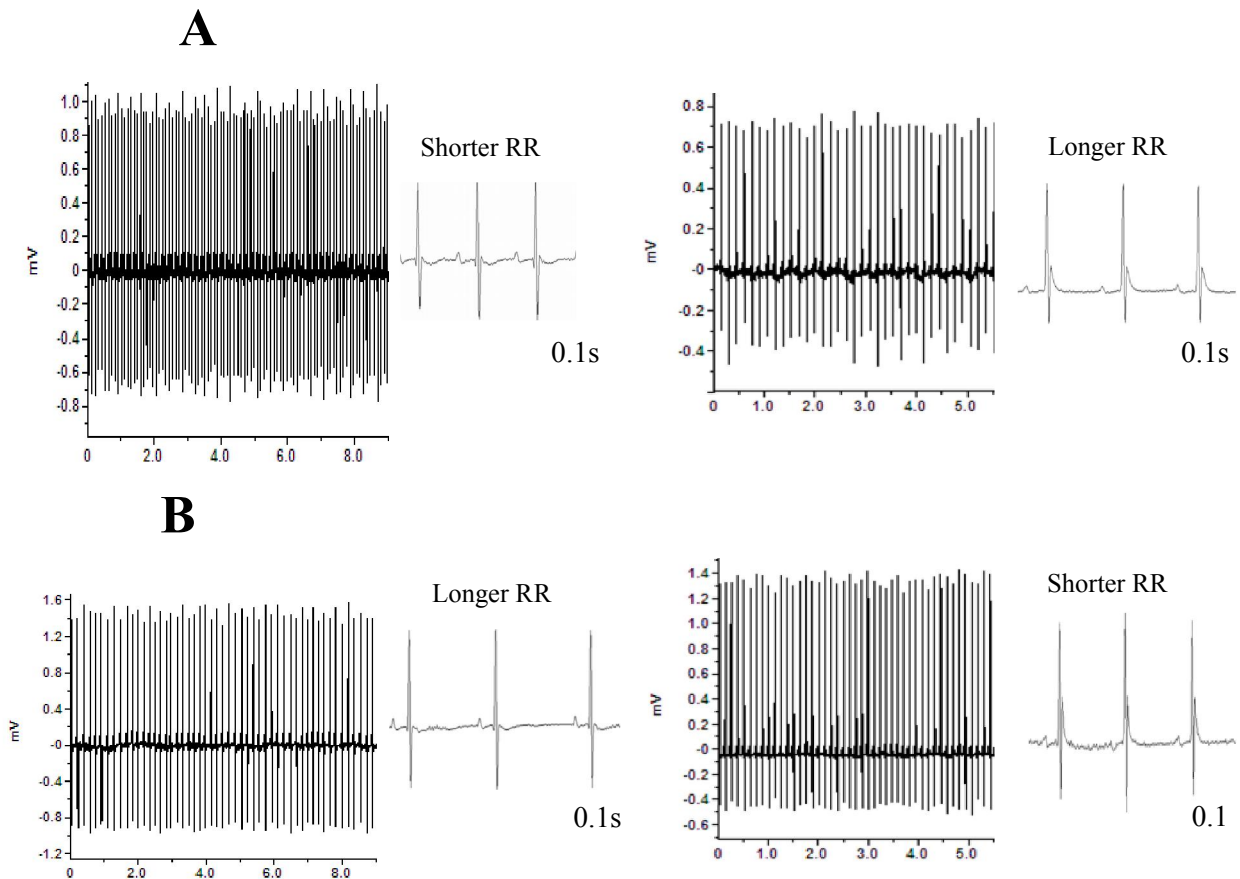


Figure 5.7 Representative ECG traces from $G\alpha_s$ flx/flx HCN4 cre⁺ and $G\alpha_{i2}$ flx/flx HCN4 cre⁺ mice Panel A) $G\alpha_s$ flx/flx HCN4 cre⁺ mice ECG traces before and after tam shows longer R-R intervals after tam. Similarly, panel B shows $G\alpha_{i2}$ flx/flx HCN4 cre⁺ mice traces before and after tam with shorter R-R intervals after tam.

5.8 Intrinsic heart rate determination

In a separate group of experiments, heart rate was determined using telemetry combined with dual pharmacological autonomic blockade (atropine and propranolol). For complete autonomic blockade, atropine and propranolol were administered together in $G\alpha_{i2}$ flx/flx HCN4 cre⁺ mice and $G\alpha_s$ flx/flx HCN4 cre⁺ mice before and after treatment with tamoxifen and compared to control littermate mice. Fig. 5.8A and Table 5.3 show that that there was no significant change in intrinsic heart rate in both $G\alpha_s$ flx/flx HCN4 cre⁺ and $G\alpha_{i2}$ flx/flx HCN4 cre⁺, though all maintained a higher

heart rate after the administration of atropine and propranolol, showing a vagal predominance in these mice. We also examined the effects of the combined atropine and propranolol treatment on HRV before and after tamoxifen administration in $G\alpha_s$ flx/flx HCN4 cre⁺ and $G\alpha_{i2}$ flx/flx HCN4 cre⁺ mice. The administration of the two drugs led to a decrease in HRV across all the frequency spectra (Table 5.3). There was no difference between the two genotypes in this behaviour before (not shown) or after tamoxifen administration (Fig. 5.8 and Table 5.3). In Fig. 5.8B, representative power spectra shows abrogation of HF and LF power in both $G\alpha_s$ flx/flx HCN4 cre⁺ and $G\alpha_{i2}$ flx/flx HCN4 cre⁺ mice after atropine and propranolol administration.

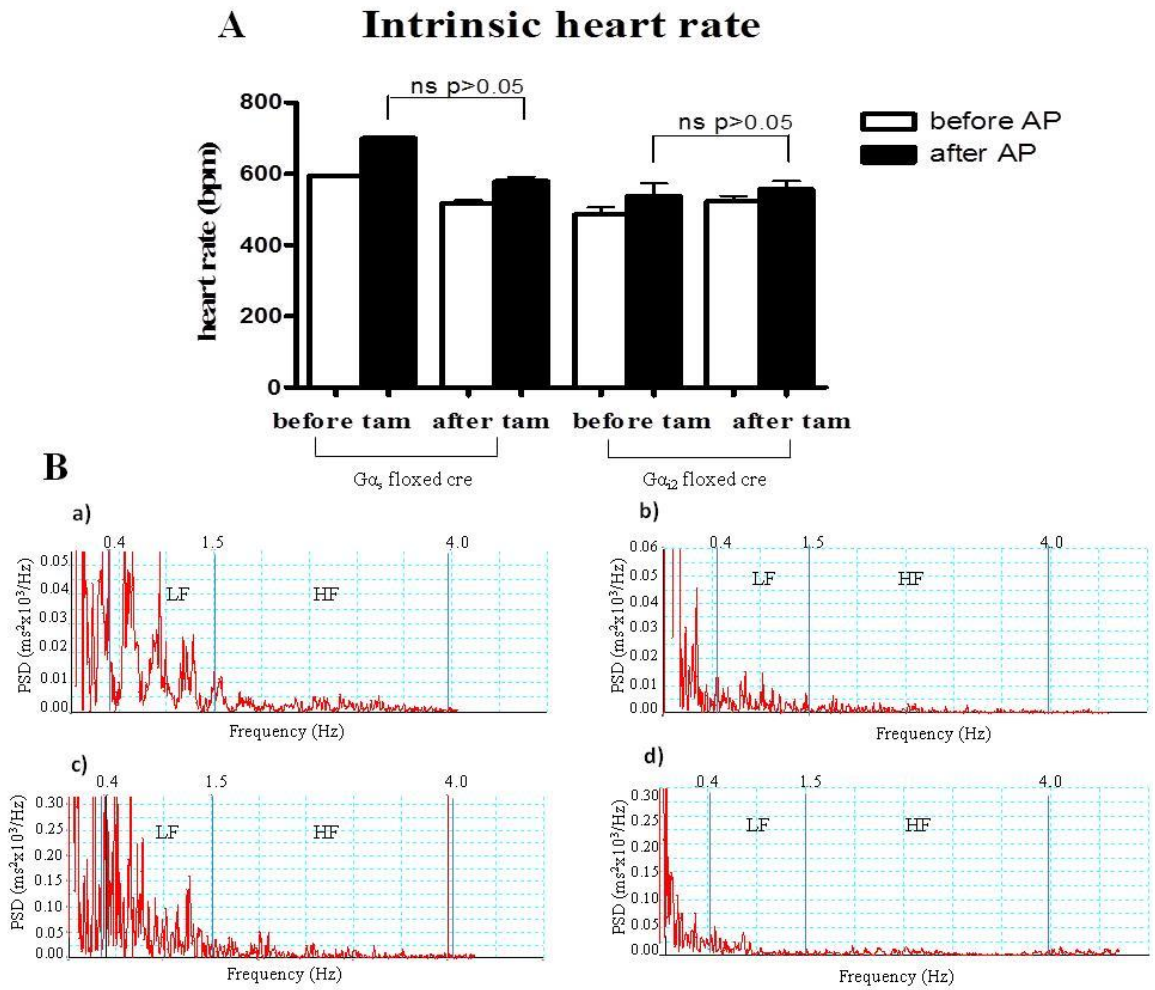


Figure 5.8 Autonomic blockade in $G\alpha_{12}$ flx/flx HCN4 cre⁺ and $G\alpha_s$ flx/flx HCN4 cre⁺ mice. A) The intrinsic heart rate after autonomic blockade with atropine and propranolol in $G\alpha_s$ flx/flx HCN4 cre⁺ and $G\alpha_{12}$ flx/flx HCN4 cre⁺ mice (n=6 in both groups). The data are mean \pm S.E.M. B) Representative PSD traces for $G\alpha_s$ flx/flx HCN4 cre⁺ mice (upper panel a- $G\alpha_s$ flx/flx HCN4 cre⁺ before AP, b- after AP) and for $G\alpha_{12}$ flx/flx HCN4 cre⁺ mice (lower panel c- $G\alpha_{12}$ flx/flx HCN4 cre⁺ before AP, d- after AP shows loss of spectral power in both $G\alpha_s$ flx/flx HCN4 cre⁺ and $G\alpha_{12}$ flx/flx HCN4 cre⁺ mice.

Animal ID	Mean NN(ms)	HR(bpm)	SDNN (ms)	RMSSD	TP(ms ²)	VLF(ms ²)	LF(ms ²)	LFnu	HF(ms ²)	HFnu	LF/HF
Gα _{i2} before AP	107.8±7.1	535±29	8.5±2.9	4.87±0.78	130±23.1	86.2±9.5	32.9±9.7	75.1±9.3	10.2±3.2	23.3±4.7	3.2±0.84
Gα _{i2} after AP	100.3±9.6	597±21	7.4±1.9	3.89±0.28	56.4±10.7 **	37.6±5.68 *	12.2±5.4 **	65.4±10	5.2±1.2 *	27.6±6.9	2.2±0.35
Gα _s before AP	108.2±7.2	555±29	8.8±3.8	5.78±0.34	104±8.9	81.0±10.2	12.8±4.8	55.65±8.2	10.2±24	44.3±8.3	1.25±0.32
Gα _s after AP	98.63±10	606±29	4.9±0.64	3.33±0.87	23.7±9.8 **	14.07±6.6 *	5.4±1.4 *	56.3±9.7	3.1±0.24 *	32.5±5.8	1.7±0.34

Table 5.3 HRV parameters after atropine and propranolol (autonomic blockade) in Gα_{i2} flx/flx HCN4 cre⁺ and Gα_s flx/flx HCN4 cre⁺ mice. There was decrease in LF, HF and total power for both Gα_s flx/flx HCN4 cre and Gα_{i2} flx/flx HCN4 cre mice after tamoxifen, leading to a decrease in HRV. AP- atropine and propranolol, ** indicates P<0.01, * indicates P<0.05. (n=6 in both Gα_s flx/flx HCN4 cre⁺ and Gα_{i2} flx/flx HCN4 cre⁺ mice)

5.9 Pharmacological modulation of heart rate

Previous studies in our lab with global $G\alpha_{i2}$ (-/-) mice has shown a selective defect in HF power in $G\alpha_{i2}$ (-/-) mice and selective attenuation of cardio-inhibitory response to carbachol (0.5mg/kg) (Zuberi, Birnbaumer, & Tinker 2008). In light of the above observation we went on to examine the M_2 $G\alpha_{i2}$ and β_1 - $G\alpha_s$ pathway using an *in vivo* pharmacology approach to look for differential chronotropic response to agonist challenge.

We measured the chronotropic response after the administration of isoprenaline and carbachol in $G\alpha_s$ flx/flx HCN4 cre⁺ and $G\alpha_{i2}$ flx/flx HCN4 cre⁺ mice, respectively, after treatment with tamoxifen and compared this to control littermate mice (Fig. 5.9). The positive chronotropic response to isoprenaline was abrogated but not abolished in $G\alpha_s$ flx/flx HCN4 cre⁺ mice and there was only a small nonsignificant reduction in the negative chronotropic response to carbachol in $G\alpha_{i2}$ flx/flx HCN4 cre⁺ mice. There was no evidence of conduction block or arrhythmias occurring after drug administration.

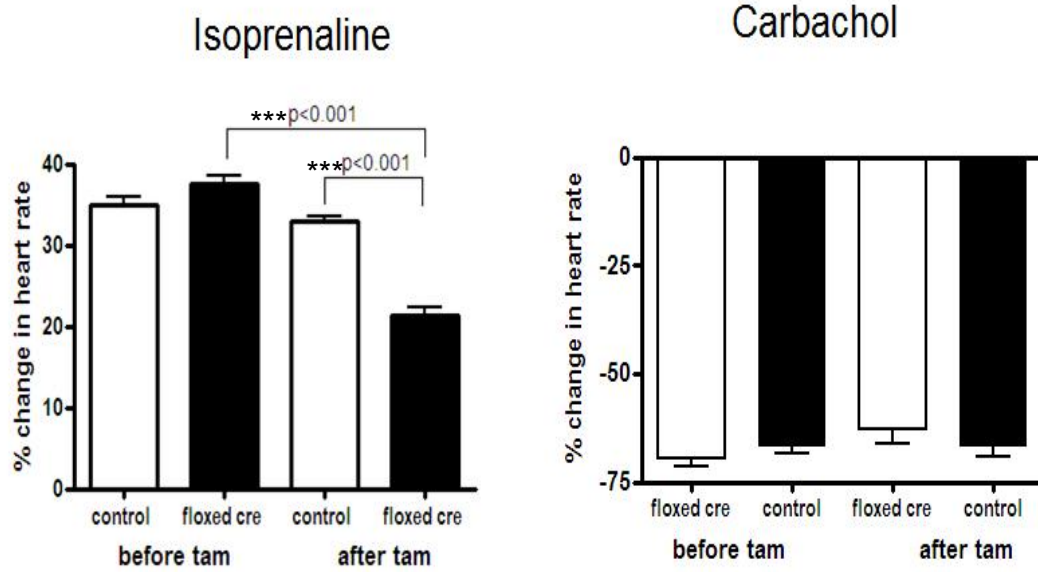


Figure 5.9 Response of heart rate to pharmacological agents. The percentage change in heart rate in $G\alpha_s$ flx/flx HCN4 cre⁺ (n=8) and control (n=8) mice after isoprenaline administration (left panel) and for $G\alpha_{i2}$ flx/flx HCN4 cre⁺ (n=11) and control (n=9) mice (right panel) after carbachol administration (right panel). The data are shown as mean \pm S.E.M. ***=P <0.001.

Discussion

5.10 Mice with conduction system-specific knock-out of $G\alpha_{i2}$ and $G\alpha_s$ with tamoxifen-induced cre showed patterns in HRV and ECG different from controls.

The results from this chapter show that selective deletion of $G\alpha_s$ and $G\alpha_{i2}$ in the conduction system of the mouse impairs physiological heart rate regulation. Mice are more active at night and more sedentary during the day and this is reflected in their diurnal variation in heart rate. The higher mean rate at night reflects their increased movement and higher sympathetic drive. Mice with the selective deletion of $G\alpha_s$ in the conduction system showed loss of normal diurnal variation and were found to be no longer tachycardic at night and thus relatively bradycardic compared to control. On the other hand, mice with selective deletion $G\alpha_{i2}$ in the conduction system also lost normal diurnal variation and were relatively more tachycardic during the day consistent with a drop in parasympathetic modulation of the SA node. I also looked into the intrinsic heart rate using pharmacological blockade of the autonomic nervous system with atropine and propranolol and found that the intrinsic heart rate was not significantly different between the two groups of mice. This result shows that *in-vivo* the fundamental inherent pacemaker is not determined by $G\alpha_s$ and $G\alpha_{i2}$ and pathways downstream of the G-protein.

A physiological variation in heart rate is shown in a number of frequency-domains. Compared to frequency-domains in human, a high frequency (HF) component (0.15 to 0.4 Hz), a low frequency (LF) component (0.04 to 0.15 Hz) and a very low frequency component (<0.04 Hz) are distinguished in the mouse. The frequencies defining each band are ten-fold higher than in man (Thireau, Zhang, Poisson, & Babuty 2008). The

high frequency component is generally thought to reflect vagal input whilst the low frequency component reflects both sympathetic and vagal input. My data support a scenario where physiological $G\alpha_{i2}$ -mediated signalling in the SA node reflects the HF component and $G\alpha_s$ signalling reflects the LF component and these two are distinct with little crosstalk. In other words this would correspond to delineation between parasympathetic and sympathetic accounting largely for most of HF and LF power respectively. It is worth noting that we use a standard normalisation procedure and once this is done the correlation between LF and sympathetic activity is clearer (Anon 1996). HRV is a widely used non-invasive technique to assess autonomic tone particularly in human studies and has prognostic significance in patients after myocardial infarction, with hypertension and in many other diseases (1996;Thayer et al. 2010).

I would like to compare here HRV data between mice with conditional genetic deletion of $G\alpha_s$ and $G\alpha_{i2}$ in the SA node, before and after drug administration and in mice with global genetic deletion of $G\alpha_{i2}$. The global genetic deletion of $G\alpha_s$ in mice is embryonically lethal and thus the animal was unavailable to study for any heart phenotype (Weinstein, Xie, Zhang, & Chen 2007). In mice with global genetic deletion of $G\alpha_{i2}$, the administration of atropine, tertiapin and propranolol and atropine (together) suppressed HRV in the time domain and in the frequency-domain and generally had effects across all three frequency spectra (Zuberi, Birnbaumer, & Tinker 2008). In contrast, the effect of conditional deletion in the SA node was more subtle and was revealed when variation in VLF was removed by the normalisation of HF and LF. It can be seen that VLF accounts for the majority of the power in the HRV signal. There are some technical issues that need to be considered. Non-stationarities

in the HRV signal can be a confounding factor, e.g. monitoring HRV throughout the day as human subjects go about their daily activities may overestimate the sympathetic contribution (Berntson et al. 1997; Magagnin et al. 2011). We seek to minimise this effect by using the recommended approaches i.e. monitoring the mice at rest during the day (12pm-2pm) for a short recording period. Furthermore, it is important the mice are allowed to recover from surgery (generally 7-10 days) and resume normal activity after probe implantation before measurements are made. These factors are the same between our current and previous studies and thus the differences are likely real. Factors outside the SA node such as effects in the central and peripheral nervous system which have an important influence on HRV could be a factor in the observed differences. For example, $G\alpha_{i2}$ is expressed in the nervous system and drugs such as propranolol with a high lipophilicity cross the blood brain barrier. In this regard the HCN4-KiT mouse does not lead to deletion of genes in the brain after the administration of tamoxifen (Hoesl, Stieber, Herrmann, Feil, Tybl, Hofmann, Feil, & Ludwig 2008).

It is important to clearly define *in vivo* the molecular isoforms responsible for physiological heart rate regulation. The *Gnas* gene locus is complex with imprinting, though not in cardiac tissues, and roles of a long and extra-long isoforms of *Gnas* in signalling are not clear (Weinstein, Xie, Zhang, & Chen 2007). The data here clearly implicate canonical $G\alpha_s$ though the mice do not distinguish long and short forms of $G\alpha_s$. Our results are consistent with recent studies in pigs using adenoviral transfer of small interfering RNA to $G\alpha_s$ where they found a suppression in heart rate (Lugenbiel et al. 2012). Furthermore, there has been debate about the inhibitory G-protein isoform underlying physiological heart rate modulation (Ang, Opel, & Tinker

2012;Zuberi, Birnbaumer, & Tinker 2008). The fundamental issue is that a wide variety of different approaches and experimental systems have been used ranging from expression in heterologous system, knock-outs in differentiated embryonic stem cells and genetically modified mice. Our data here support an important role for $G\alpha_{i2}$ but do not exclude a contribution from other isoforms.

After selective deletion of $G\alpha_{i2}$ in the conduction system the heart rate slowing response to carbachol is relatively well preserved whilst with $G\alpha_s$ the response to isoprenaline was significantly attenuated but not abolished. This contrasts with the situation in the global knock-out of $G\alpha_{i2}$ where it was significantly attenuated. The studies with isoprenaline and carbachol are a pronounced pharmacological challenge, e.g. with carbachol the heart rate falls to levels much below that normally seen physiologically even in normal situations such as sleep. It is known that the sino-atrial node is actually quite an extensive and heterogeneous structure and that the primary pacemaking site moves from one region to another as the sympathovagal balance changes (Monfredi et al. 2010;Shibata et al. 2001). Thus it is possible that the pacemaking site shifts to a small region that is not solely dependent on the deleted G-protein or a site in which the HCN4 promoter driven cre-mediated deletion is not so complete (Sebastian et al. 2013).

There is great interest in the role that heart rate *per se* has in the outcome of heart failure after the use of ivabradine in the SHIFT trial (Bohm et al. 2010). These mouse lines may be useful resources in addressing this interesting question as they have changes in heart rate generated independently of pharmacological manipulation. I follow up this question in the next chapter.

Chapter 6

RESULTS IV

6.1 Ventricular remodelling in $G\alpha_s$ flx/flx HCN4 cre⁺ and $G\alpha_{i2}$ flx/flx HCN4 cre⁺ mice after myocardial infarction

My next step was to further explore the role of the $G\alpha_{i2}$ and $G\alpha_s$ genes in a murine model of myocardial infarction and heart failure. $G\alpha_{i2}$ flx/flx HCN4 cre⁺ mice were found to be tachycardic and $G\alpha_s$ flx/flx HCN4 cre⁺ mice were bradycardic. The aim was to see whether the bradycardic phenotype in the absence of Gs is protective in $G\alpha_s$ flx/flx HCN4 cre⁺ or tachycardia in the absence of G_{i2} is detrimental to the $G\alpha_{i2}$ flx/flx HCN4 cre⁺ when challenged with MI. Here, we have explored the role of heart rate, $G\alpha_{i2}$ and $G\alpha_s$ in the SA node in ventricular remodelling after myocardial infarction by combining the same temporally controlled gene-knock-out approach described earlier in Materials and Methods (for $G\alpha_{i2}$ and $G\alpha_s$ using tamoxifen-inducible knock-outs) by assessing their ventricular function using serial echocardiography.

6.2 Survival rates in $G\alpha_{i2}$ flx/flx HCN4 cre⁺ and $G\alpha_s$ flx/flx HCN4 cre⁺ mice after MI

Mice were first subjected to echocardiography to analyse their baseline measurements of ventricular function and the outline of the study is described in Fig. 6.1. The survival rates are also shown in the Fig. 6.1. Control mice had a survival rate of 66-68% while $G\alpha_{i2}$ flx/flx HCN4 cre⁺ mice and $G\alpha_s$ flx/flx HCN4 cre⁺ mice had survival rates of 38% had 45%, respectively. These differences are not statistically significant ($P>0.05$ Fishers exact test). I would like to mention here that these deaths occurred soon after the procedure (2-3 days) and an initial post mortem examination in 6 mice found cardiac rupture to be the likely reason for death after MI. This is well described in this model (Gao, Dart, Dewar, Jennings, & Du 2000).

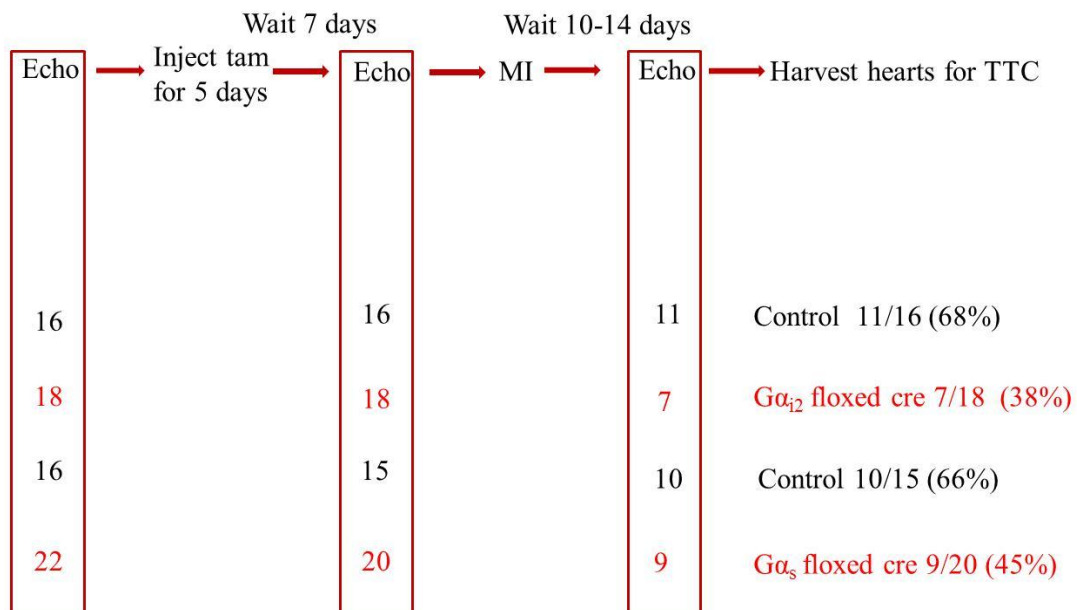


Figure 6.1 Study plan for the myocardial infarction protocol. Mice in different groups were subjected to echocardiography followed by tamoxifen injection for 5 days, after which echocardiographic measurements were again carried out and mice were then subjected to MI, allowed to recover for 14 days then echo'd again. Finally, tissues were harvested for TTC staining.

6.3 M- mode Echocardiography shows impaired LV function

After MI, the left ventricular wall definitions (IVS, LVID and LVPW in both systole and diastole) are less well defined as seen in Fig. 6.2. There are several factors for this. The orientation of the heart changes after MI and while imaging the heart, there is interference from the rib cage which affects the quality of the image scan. Other reasons include, an infarcted anterior wall being invisible due to wall thinning, no wall motion or postoperative adhesion (Gao, Dart, Dewar, Jennings, & Du 2000). Left ventricle contraction is decreased and LV dimensions are increased after MI.

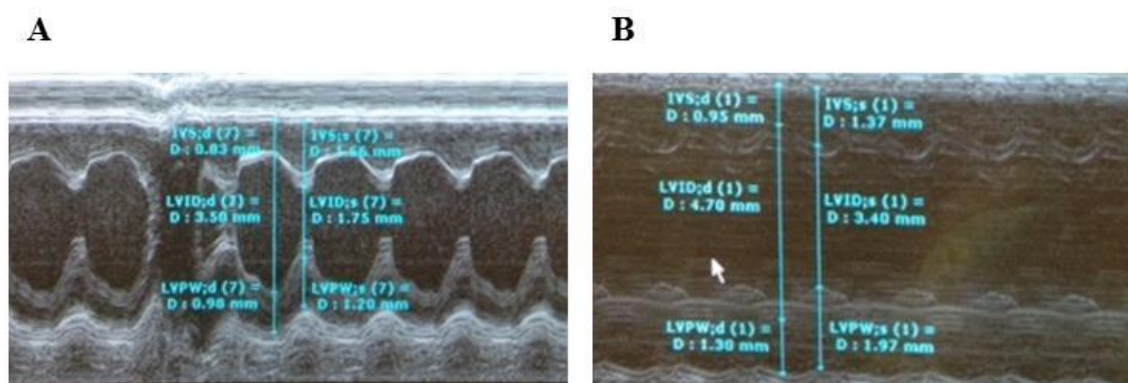
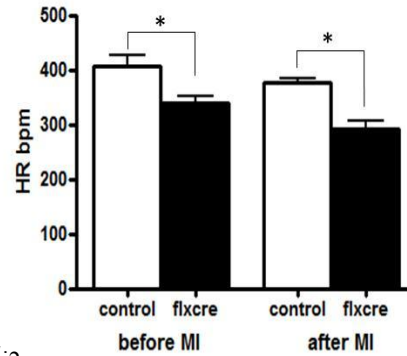
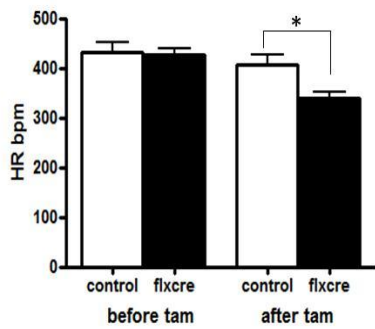


Figure 6.2 Representative M-mode image of a control mouse before and after MI. A) Before MI well defined wall dimension of left ventricle are displayed. **B)** After MI clear wall definition is lost showing the signs of infarction.

6.4 $G\alpha_s$ flx/flx HCN4 cre⁺ mice were found to be bradycardic and $G\alpha_{i2}$ flx/flx HCN4 cre⁺ mice were found to be tachycardic under anaesthesia.

Mice in all groups (before and after tamoxifen) were subjected to echocardiographic analysis. We found that under isoflurane-induced anaesthesia heart rates were higher in $G\alpha_{i2}$ flx/flx HCN4 cre⁺ mice (486 bpm \pm 22.9, n=7 *P<0.05) compared to controls (393 bpm \pm 15.8, n=11) and were lower in $G\alpha_s$ flx/flx HCN4 cre⁺ mice (357 bpm \pm 18.8, n=9 *P<0.05) compared to controls (411 bpm \pm 12.7, n=10) after administration of tamoxifen. Since mice are anaesthetised heart rate is typically lower among all groups (Fig. 6.3). After MI, the pattern of tachycardia remains unchanged in $G\alpha_{i2}$ flx/flx HCN4 cre⁺ mice (407 bpm \pm 13.8, n=7 *P<0.05) compared to controls (351 bpm \pm 15.9, n=11) and $G\alpha_s$ flx/flx cre⁺ mice (311 bpm \pm 17.9, n=9 *P<0.05) compared to controls (389 bpm \pm 10.89, n=10) remained bradycardic. Thus, it seems that under anaesthesia as well when conscious, heart rates in $G\alpha_{i2}$ flx/flx HCN4 cre⁺ and $G\alpha_s$ flx/flx HCN4 cre⁺ mice are found to be tachycardic and bradycardic, respectively after tamoxifen.

$G\alpha_s$



$G\alpha_{i2}$

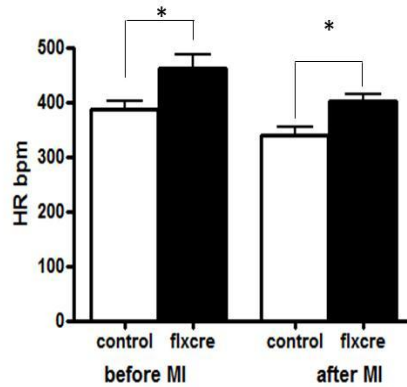
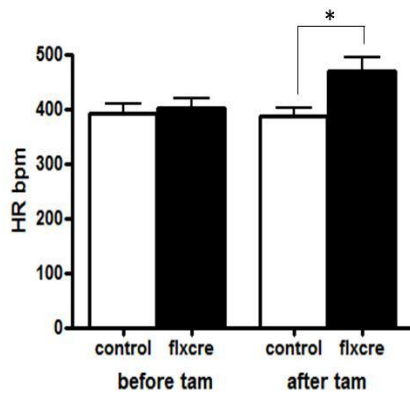


Figure 6.3 Heart rate in $G\alpha_s$ flx/flx HCN4 cre⁺ and $G\alpha_{i2}$ flx/flx HCN4 cre⁺ mice before and after tam and before and after MI under anaesthetic conditions. $G\alpha_s$ flx/flx HCN4 cre⁺ mice (n=9) were found to be bradycardic after tam (upper left panel) and remained bradycardic after MI (upper right panel) compared to control (n=10) (*P<0.05). On the other hand $G\alpha_{i2}$ flx/flx HCN4 cre⁺ mice (n=7) were found to be tachycardic after tam (lower left panel) and remained the same after MI compared to control mice (n=11) (lower

6.5 Fractional shortening was not changed in $G\alpha_s$ flx/flx HCN4 cre⁺ mice while it was reduced in $G\alpha_{i2}$ flx/flx HCN4 cre⁺ mice post MI

Fractional shortening (FS) was calculated from the dimensions of the left ventricle obtained by M-mode echocardiography as explained in Materials and Methods and is a common parameter to evaluate systolic function of the left ventricle. Before tamoxifen, FS% was found to be similar in both control, $G\alpha_s$ flx/flx HCN4 cre⁺ mice (n=9) and $G\alpha_{i2}$ flx/flx HCN4 cre⁺ mice (n=7). However after tamoxifen, in $G\alpha_s$ flx/flx HCN4 cre⁺ mice there was an increase in FS% (before tam 36.05 ± 1.34 after tam 45.00 ± 1.18 , n=9 **P<0.01) compared to controls (before tam 35.95 ± 2.79 , after tam 36.37 ± 2.52), n=10) (Fig. 6.4A). After MI there was reduction in FS% observed in the control group (before MI 36.37 ± 2.52 , after MI 28.8 ± 1.32 , n=10 *P<0.05), FS% wasn't much lower compared to before MI in $G\alpha_s$ flx/flx HCN4 cre⁺ mice (before MI 45.00 ± 1.18 , after MI 41.65 ± 1.90 n=9) Fig. 6.4A. This suggests that that absence of $G\alpha_s$ in conduction system tissues is protecting the heart when challenged with MI. On the other hand in $G\alpha_{i2}$ flx/flx HCN4 cre⁺ mice after tamoxifen there was no change in FS% compared to their littermate controls (control 39.42 ± 2.52 , n=11 and with $G\alpha_{i2}$ flx/flx HCN4 cre⁺ 37.80 ± 1.95 , n=7) Fig. 6.4B. However, after MI there was a significant reduction in FS% in both the control (before MI 39.42 ± 2.52 after MI 27.89 ± 2.26 , n=11 **P<0.01) and $G\alpha_{i2}$ flx/flx HCN4 cre⁺ mice (before MI 37.80 ± 1.95 , after MI 29.66 ± 1.57 , n=7 *P<0.05). Absence of $G\alpha_{i2}$ in the conduction system was not found to be worse for outcome, even though there was reduction in FS but compared to controls there wasn't a significant difference.

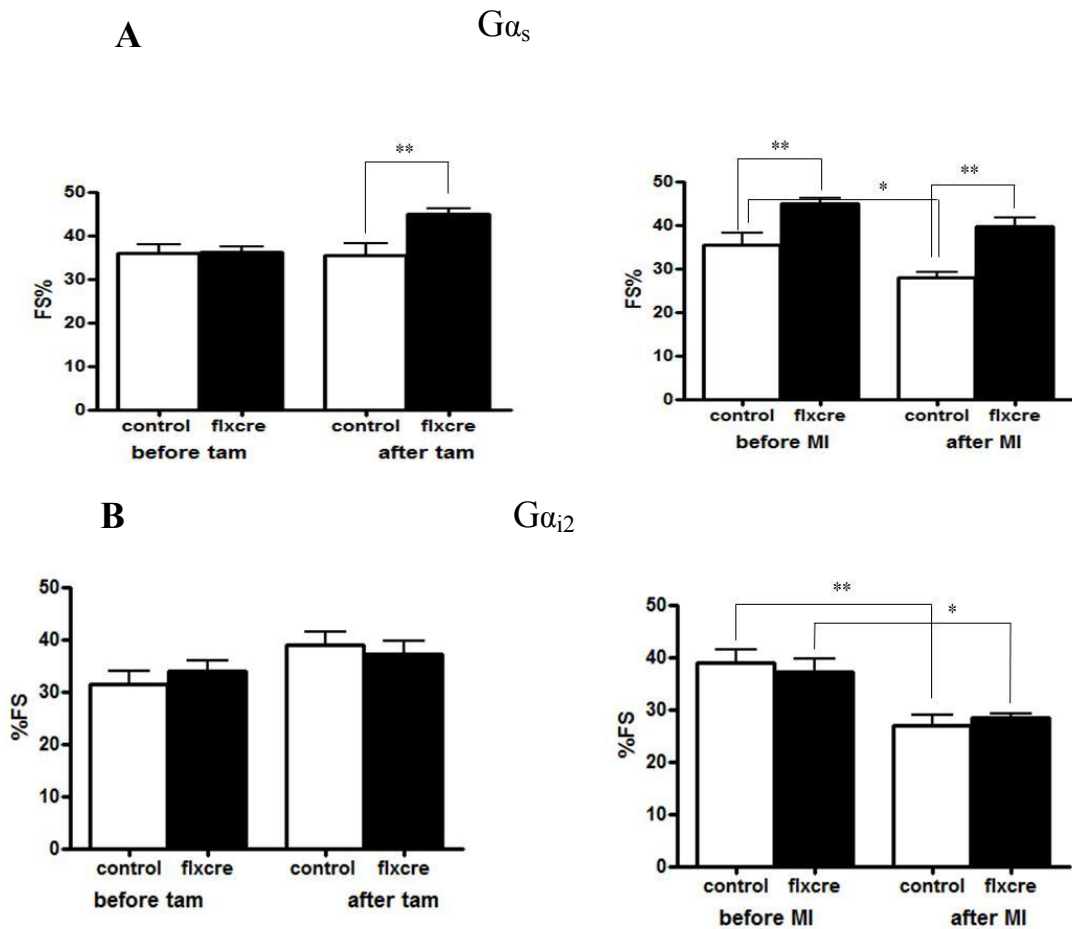


Figure 6.4 FS% in $G\alpha_s$ flx/flx HCN4 cre⁺ and $G\alpha_{i2}$ flx/flx HCN4 cre⁺ mice before and after tam and before and after MI A) FS is increased in $G\alpha_s$ flx/flx HCN4 cre⁺ mice (n=9) after tam (left panel) and after MI (right panel) compared to control (n=10). B) There was no change in FS after tam (left panel) in $G\alpha_{i2}$ flx/flx HCN4 cre⁺ mice (n=7) but there was a significant reduction of FS in both $G\alpha_{i2}$ flx/flx HCN4 cre⁺ mice and control mice (n=11) after MI (right panel) (**P<0.01,*P<0.05).

6.6 There is no change in ejection fraction in $G\alpha_s$ flx/flx HCN4 cre⁺ mice, while it is decreased in $G\alpha_{i2}$ flx/flx HCN4 cre⁺ mice post MI

Ejection fraction (EF), another parameter of ventricular function was also found to be enhanced in $G\alpha_s$ flx/flx HCN4 cre⁺ mice, after tamoxifen and after MI it remained more or less the same, while it was found to be decreased in $G\alpha_{i2}$ flx/flx HCN4 cre⁺ mice. Ventricular function is impaired after MI which is reflected in EF% of littermate controls in both the groups. After tamoxifen, in $G\alpha_s$ flx/flx HCN4 cre⁺ mice there was an increase in EF% (75.05 ± 3.96 , n=9 *P<0.05) compared to controls (63.71 ± 6.79 , n=10) Fig. 6.5A. After MI, there was a reduction in EF% observed in control group (before MI 63.71 ± 6.79 , after MI 49.40 ± 1.32 , n=10 **P<0.01) compared to $G\alpha_s$ flx/flx HCN4 cre⁺ mice (before MI 75.05 ± 3.96 , after MI 71.46 ± 2.17 , n=9). EF% was found to be significantly lower in controls after MI compared to $G\alpha_s$ flx/flx HCN4 cre⁺ mice (control 49.40 ± 1.32 , n=10 and $G\alpha_s$ flx/flx HCN4 cre⁺ mice 71.46 ± 2.17 , n=9 **P<0.01). In $G\alpha_{i2}$ flx/flx HCN4 cre⁺ mice there was no difference in EF% before and after tamoxifen in both controls and $G\alpha_{i2}$ flx/flx HCN4 cre⁺ mice (Fig. 6.5B). But after MI, EF% was decreased in both control (before MI 61.58 ± 3.77 , after MI 52.36 ± 2.93 , n=11*P<0.05) and $G\alpha_{i2}$ flx/flx HCN4 cre⁺ mice (before MI 62.59 ± 3.08 , after MI 44.58 ± 3.93 , n=7 **P<0.01) and the degree of reduction was found to be more in $G\alpha_{i2}$ flx/flx HCN4 cre⁺ mice than in their controls.

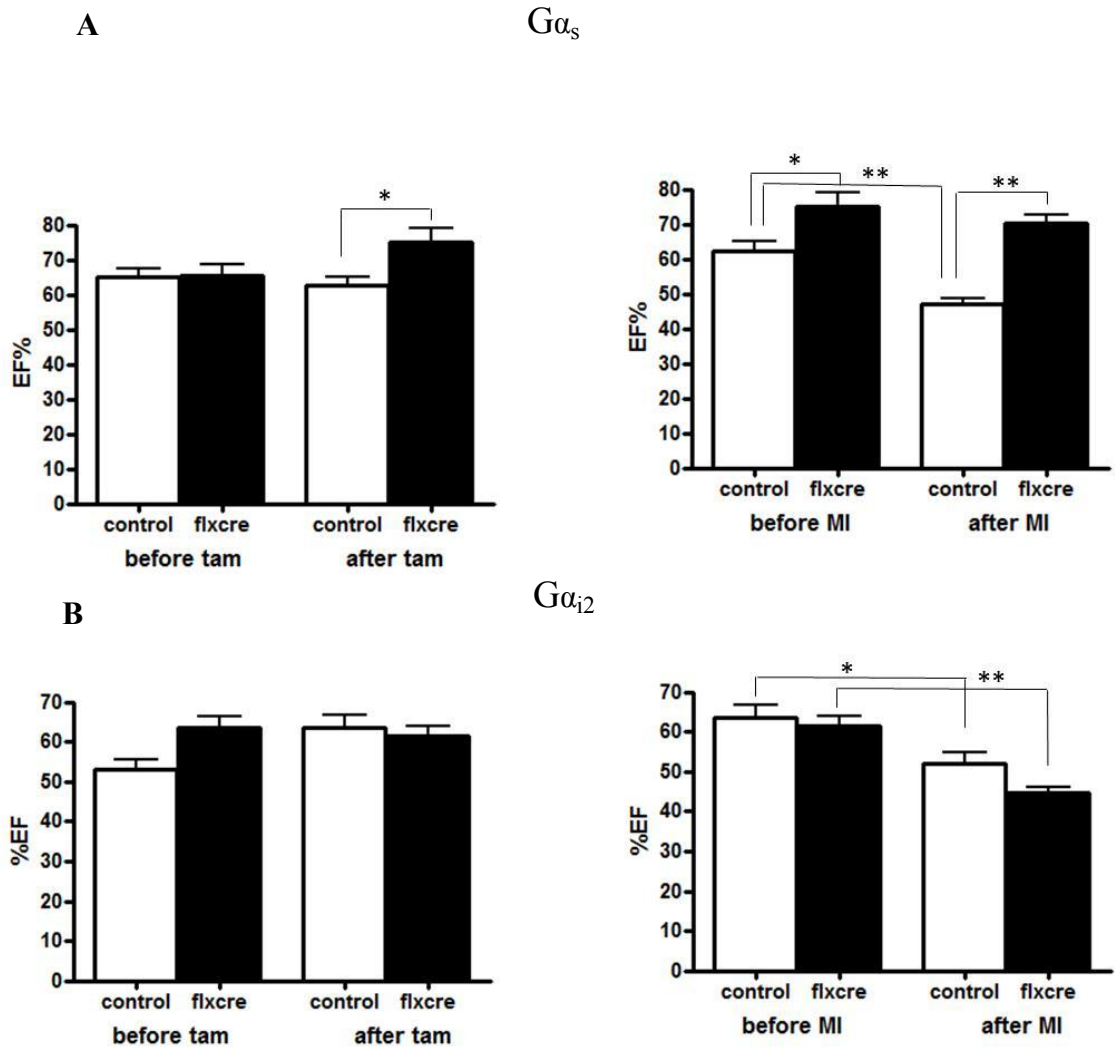
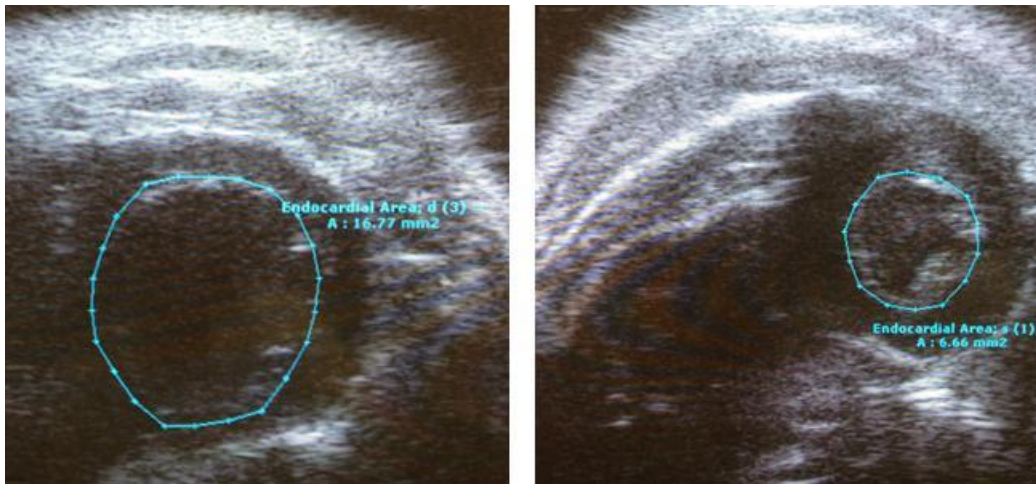


Figure 6.5 EF% in $G\alpha_s$ flx/flx HCN4 cre⁺ and $G\alpha_{i2}$ flx/flx HCN4 cre⁺ mice before and after tam and before and after MI. A) EF% is increased in $G\alpha_s$ flx/flx HCN4 cre⁺ mice (n=9) after tam (left panel) and after MI (right panel) compared to control (n=10). B) There was no change in EF% after tam (left panel) in $G\alpha_{i2}$ flx/flx HCN4 cre⁺ mice (n=7) but there was a significant reduction of EF% in both $G\alpha_{i2}$ flx/flx HCN4 cre⁺ mice and control mice (n=11) after MI (right panel), (*P<0.05, **P<0.01).

6.7 FAC% was found to be enhanced in $G\alpha_s$ flx/flx HCN4 cre⁺ mice, while there was no change in $G\alpha_{i2}$ flx/flx HCN4 cre⁺ mice

Left ventricular function can also be measured as a percentage of change in left ventricular cross-sectional area between diastole and systole, which is called fractional area change (FAC %) shown in Fig. 6.6 (upper panel). FAC% measured on the LV short axis 14 days post MI showed a decrease in FAC% in the littermate control groups of both $G\alpha_s$ flx/flx HCN4 cre⁺ mice and $G\alpha_{i2}$ flx/flx HCN4 cre⁺ mice (Fig. 6.6B). In the $G\alpha_s$ flx/flx HCN4 cre⁺ group post MI, there was a trend towards an enhancement in FAC% although this was not significant statistically (Fig. 6.6B). However, in controls in the same group, there was an obvious decrease in FAC% after MI (29.28 ± 3.12) compared to before MI (37.43 ± 2.89 , $n=9$ * $P<0.05$). A comparison of the FAC% between $G\alpha_s$ flx/flx HCN4 cre⁺ mice and their littermate controls post MI was statistically significant (controls after MI, 29.28 ± 3.12 , $n=9$, $G\alpha_s$ flx/flx HCN4 cre⁺ after MI, 43.14 ± 3.94 , $n=10$ ** $P<0.01$). There could be a possibility that the absence of $G\alpha_s$ may be having a protective role in heart failure. On the other hand, $G\alpha_{i2}$ flx/flx HCN4 cre⁺ control group did show a significant reduction in FAC% post MI (before MI 40.32 ± 2.68 , after MI 33.89 ± 2.97 , $n=11$ * $P<0.05$), while $G\alpha_{i2}$ flx/flx HCN4 cre⁺ mice, even though there was reduction in FAC% after MI it didn't reach statistical significance (before MI 41.82 ± 2.97 , after MI 37.12 ± 3.27 , $n=7$).

A



B

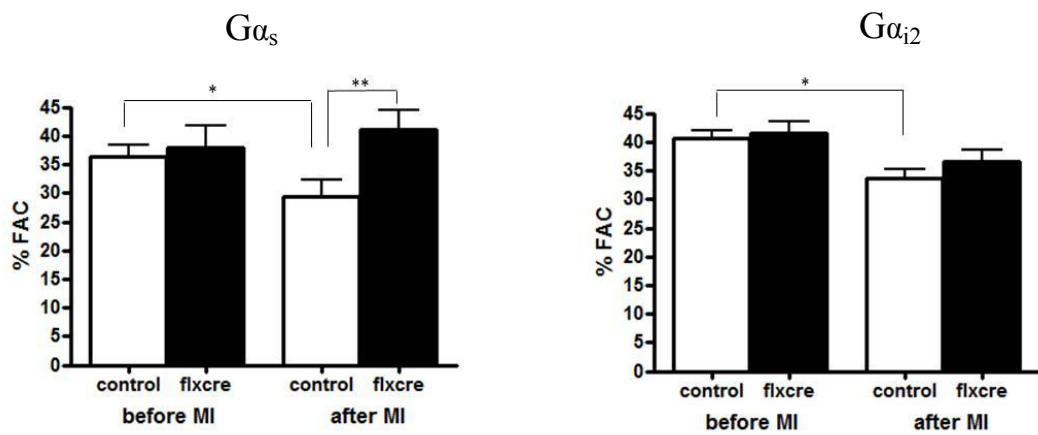


Figure 6.6 Measurement of FAC% by tracing the endocardial border and FAC% in $G\alpha_s$ flx/flx HCN4 cre⁺ and $G\alpha_{i2}$ flx/flx HCN4 cre⁺ mice before and after MI. A) Upper panel shows traces of the endocardial border during systole (left) and diastole (right) on B-mode echocardiography. B) FAC % is decreased in control mice (n=10*) while there was not much change in $G\alpha_s$ flx/flx HCN4 cre⁺ mice (n=9) after MI. B) FAC % was found to be decreased in both control (n=11*) and $G\alpha_{i2}$ flx/flx HCN4 cre⁺ mice (n=7) though it was significant only in the control group (*P<0.05, **P<0.01).

6.8 Structural analysis of the left ventricular chamber shows changes in $G\alpha_s$ flx/flx HCN4 cre⁺ mice but not in $G\alpha_{i2}$ flx/flx HCN4 cre⁺ mice

Left ventricular remodelling can also be assessed from the measurements of chamber dimensions of the left ventricle on M-mode echocardiography. Chamber dilatation is one of the common features of LV remodelling after MI, and this is caused by the redistribution of increased regional wall stress to preserve the cardiac function (Sutton and Sharpe 2000). This is assessed by means of left ventricular dimensions during systole and diastole. In our study with $G\alpha_s$ flx/flx HCN4 cre⁺ mice, only the control group showed a significant increase in posterior wall thickness after MI (before MI 1.25mm \pm 0.091, after MI 1.47mm \pm 0.01, n=10 *P<0.05), while in $G\alpha_s$ flx/flx HCN4 cre⁺ mice there was a trend towards a decrease in posterior wall thickness after MI (before MI 1.36mm \pm 0.09, after MI 1.12mm \pm 0.08, n=9) (Fig. 6.7A). But when compared with controls, $G\alpha_s$ flx/flx HCN4 cre⁺ mice after MI there was a significant difference between both groups in terms of posterior wall thickness (control post MI 1.47mm \pm 0.01, n=10, $G\alpha_s$ flx/flx HCN4 cre⁺ post MI 1.12mm \pm 1.01, n=9 **P<0.01) Decreased posterior wall thickness in $G\alpha_s$ flx/flx HCN4 cre⁺ mice after MI (compared to control) may indicate that left ventricular hypertrophy does not occur in the absence of $G\alpha_s$. While in the case of $G\alpha_{i2}$ flx/flx HCN4 cre⁺ mice there was an increase in posterior wall dimensions after MI in both the control and $G\alpha_{i2}$ flx/flx HCN4 cre⁺ mice compared to before MI (control before MI 1.135mm \pm 0.04, control after MI 1.39mm \pm 0.02, n=11 *P<0.05, $G\alpha_{i2}$ flx/flx HCN4 cre⁺ before MI 0.93mm \pm 0.03; after MI 1.22mm \pm 0.06, n=7 *P<0.05) (Fig. 6.7B).

Measurement of left ventricular internal dimension during diastole (LVIDd) also revealed ventricular chamber dilation. As seen in Fig. 6.7C (lower panel) in $G\alpha_s$

flx/flx HCN4 cre⁺ mice, the increase in LVIDd was not significant after MI (4.37mm ± 0.148) compared to before MI (3.88mm ± 0.16, n=9), while in the littermate control mice showed a significant increase in chamber dimension after MI (4.63mm ± 0.11) when compared to before MI 3.78mm ± 0.13, n=10 **P<0.01). But there was no difference between control (4.63mm ± 0.11, n=10) and Gα_s flx/flx HCN4 cre⁺ mice (4.37mm ± 0.148, n=9) after MI. While with Gα_{i2} flx/flx HCN4 cre⁺ mice there was an increase in dimensions in both control (before MI 3.71mm ± 0.08, after MI 4.54mm ± 0.09, n=11 **P<0.01) and Gα_{i2} flx/flx HCN4 cre⁺ mice (before MI 4.00mm ± 0.11, after MI 4.68mm ± 0.22, n=7 **P<0.01) after MI compared to before MI (Fig. 6.7D).

These data suggest that LV remodelling is occurring in Gα_{i2}flx/flxHCN4 cre⁺ mice after MI and Gα_s flx/flx HCN4 cre⁺ mice are protected against remodelling. Further research is needed to further characterize these observations in Gα_s flx/flx HCN4 cre⁺ mice.

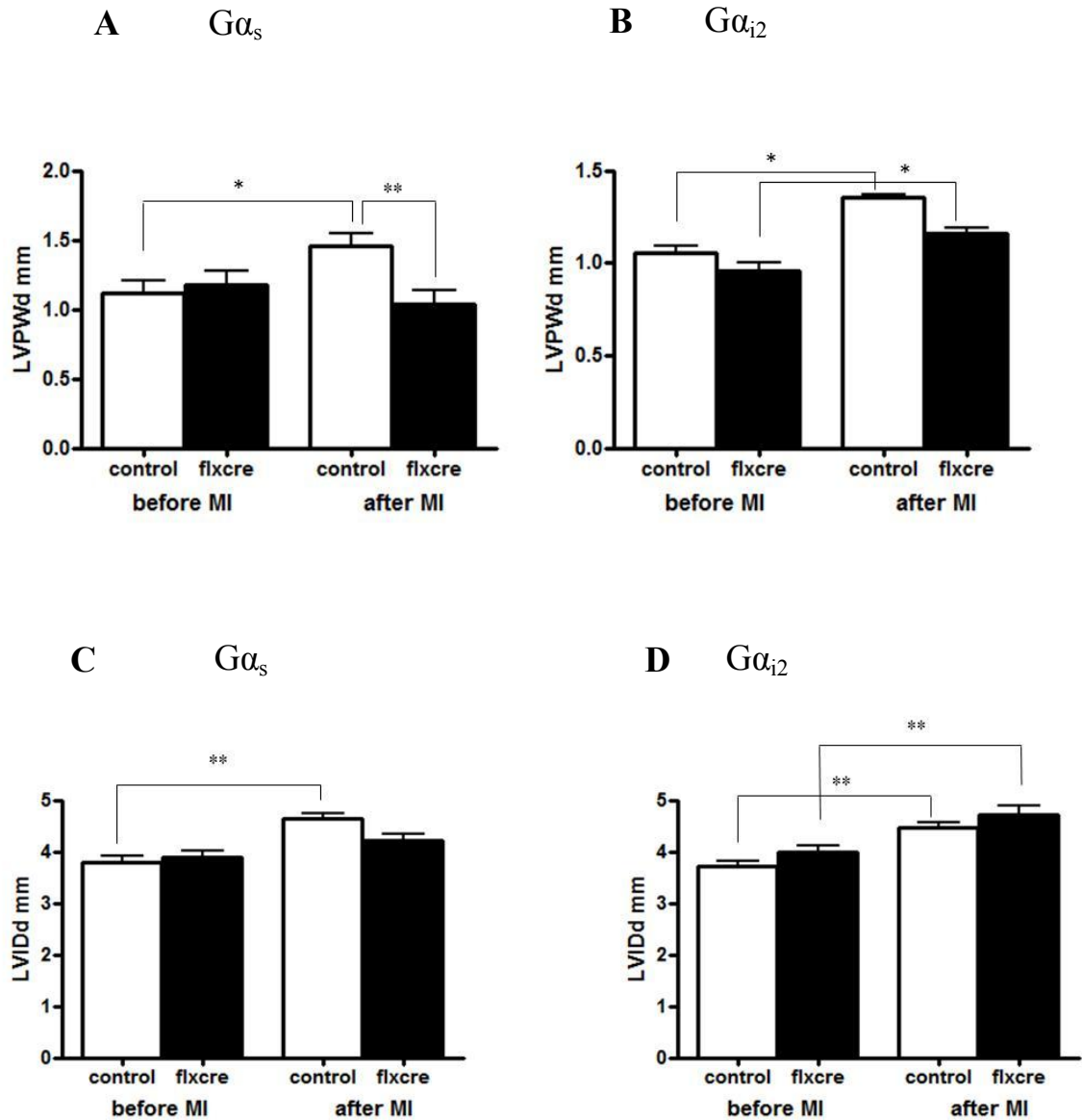


Figure 6.7 LVPWd and LVIDd measurements in $G\alpha_s$ flx/flx HCN4 cre⁺ and $G\alpha_{i2}$ flx/flx HCN4 cre⁺ mice before and after MI. A) LVPWd before and after MI in $G\alpha_s$ flx/flx HCN4 cre⁺ mice shows an increase in values for control (n=10*) but not in $G\alpha_s$ flx/flx HCN4 cre⁺ mice (n=9*) after MI while B) in $G\alpha_{i2}$ flx/flx HCN4 cre⁺ mice (n=7) shows increase in LVPWd similar to control mice (n=11) after MI C) LVIDd before and after MI in $G\alpha_s$ flx/flx HCN4 cre mice shows an increase in values for control (n=10*) but not in $G\alpha_s$ flx/flx HCN4 cre⁺ mice (n=9*) after MI while D) in $G\alpha_{i2}$ flx/flx HCN4 cre⁺ mice (n=7) shows increase in LVIDd similar to that seen in control mice (n=11) after MI (*P<0.05, **P<0.01).

6.9 Hypertrophy was observed in $G\alpha_{i2}$ flx/flx HCN4 cre⁺ mice but not in $G\alpha_s$ flx/flx HCN4 cre⁺ mice post MI

Hypertrophy of heart is a common feature after MI and it is a measurement of LV remodelling post MI. So we measured heart:body weight ratio after the studies. As expected from the results above we found an increase in heart weight: body weight ratio in $G\alpha_{i2}$ mice after MI (6.87 ± 0.462 , n=7) and it was not different from the control group (6.67 ± 0.258 , n=11) (Fig. 6.8 upper panel). While with $G\alpha_s$ after MI there was no increase in heart weight:body weight ratio, while control mice showed an increase in ratio after MI ($G\alpha_s$ flx/flx HCN4 cre⁺ mice 5.13 ± 0.587 , n=9 *P<0.05, control 6.08 ± 0.287 , n=10) (Fig. 6.8). LV mass calculated from echocardiography also showed an increase in $G\alpha_{i2}$ floxed cre⁺ group (before MI 164.5 ± 6.58 ; after MI 205 ± 6.17 , n=7 *P<0.05) and the control group (before MI 144.5 ± 4.69 , after MI 210 ± 4.2 , n=11*P<0.05), even though there was no difference between both control and $G\alpha_{i2}$ flx/flx HCN4 cre⁺ mice after MI (bottom right Fig. 6.8). In $G\alpha_s$ flx/flx HCN4 cre⁺ mice, only the control group showed an increase in LV mass after MI (before MI 148.4 ± 3.58 , after MI 225 ± 3.89 , n=10 *P<0.05) while in floxed cre⁺ mice there was no change (before MI 178 ± 4.04 , after MI 170 ± 5.48 , n=9) but when $G\alpha_s$ flx/flx HCN4 cre⁺ mice were compared with controls after MI there was significant increase of LV mass in control group (control after MI 225 ± 3.89 , n=10; $G\alpha_s$ flx/flx HCN4 cre⁺ mice after MI 170 ± 5.48 , n=9 * P<0.05) (bottom left Fig. 6.8). Hypertrophy was observed as a part of ventricular remodelling in $G\alpha_{i2}$ floxed cre⁺ mice but not in $G\alpha_s$ flx/flx HCN4 cre⁺ mice.

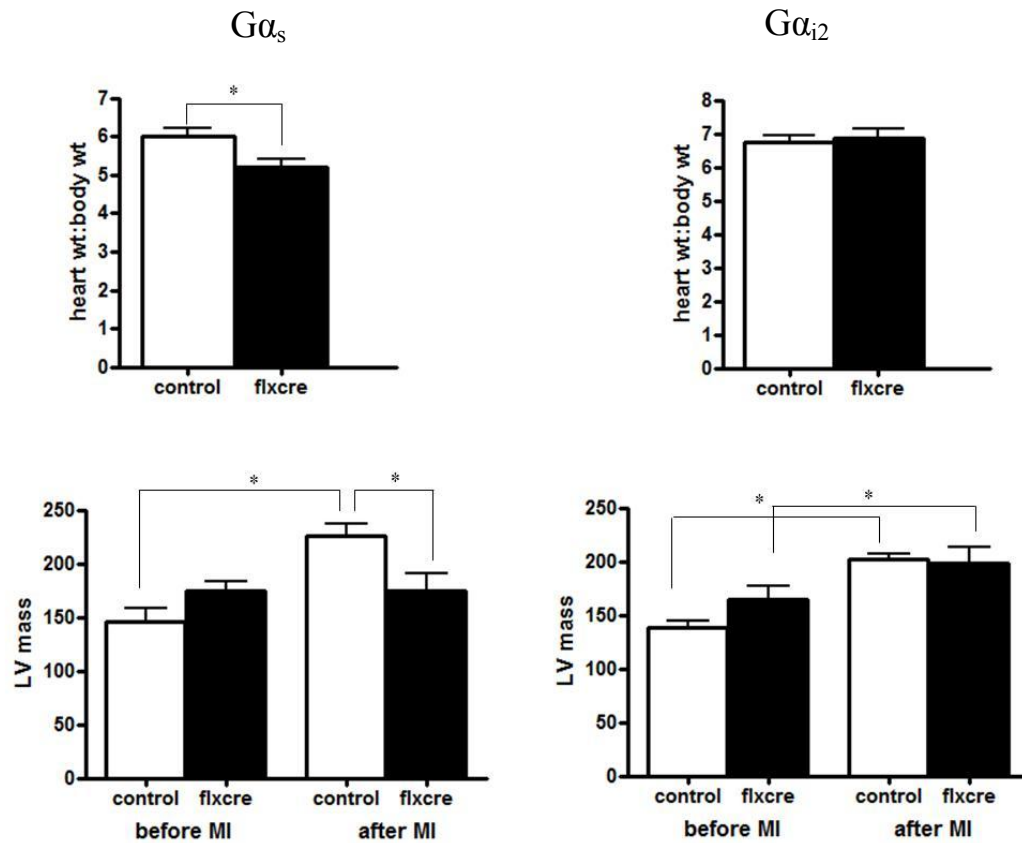


Figure 6.8 Heart weight:body weight and LV mass in $G\alpha_s$ flx/flx HCN4 cre⁺ and $G\alpha_{i2}$ flx/flx HCN4 cre⁺ mice before and after MI. upper panel shows heart weight:body weight in both $G\alpha_s$ floxed cre⁺ mice (left) and $G\alpha_{i2}$ floxed cre⁺ mice (right). Bottom panel left shows LV mass by echocardiography reveals an increase in LV mass was observed only with the control group not with $G\alpha_s$ floxed cre⁺ mice (* $P < 0.05$) while in $G\alpha_{i2}$ floxed cre⁺ mice and its controls show an increase in LV mass.

6.10 Triphenyltetrasodium chloride (TTC) staining reveals infarct size was found to be similar in all groups

TTC staining at the end of the studies and its subsequent analysis of area using image J software reveals infarct size was found the same among controls (14.4 ± 1.90 ; $n=21$ (pooled together), $G\alpha_s$ flx/flx HCN4 cre⁺ mice 14.5 ± 0.87 , $n=9$ and $G\alpha_{i2}$ flx/flx HCN4 cre⁺ mice (17.49 ± 1.61 , $n=7$) Fig. 6.9C. This infarction size was less compared to other studies where they have reported ~30% infarction of left ventricle.(Michael et al.

1999). This could be reason for less adverse results with $G\alpha_{i2}$ flx/flx HCN4 cre⁺ mice, even though with this infarct size we could see some effect in $G\alpha_s$ flx/flx HCN4 cre⁺ mice. Fig. 6.9A shows the measurement of area of infarct using Image J and comparison between an infarcted heart, 6.9B non-infarcted heart and 6.9D shows scar in one of the hearts isolated after MI before TTC staining. Another important point that needs to be mentioned here is that the strain differences in mice are an important factor in determining the outcome of infarct. Here $G\alpha_{i2}$ flx/flx cre⁺ mice and $G\alpha_s$ flx/flx cre⁺ mice were on Sv129 back ground and HCN4 cre⁺ was on c57 back ground. Studies have shown that infarct rupture, a feature of MI is of high incidence in Sv129 background strain and this is associated with high systolic blood pressure in them after infarct compared to other strains. Also in these mice, the incidence is higher in males compared to females. The survival rate post MI was found to be low in Sv129 strain compared to C57 background (Gao et al. 2005; van den Borne et al. 2009). The mixed background nature of mice used here could be a factor in explaining some differences with other studies.

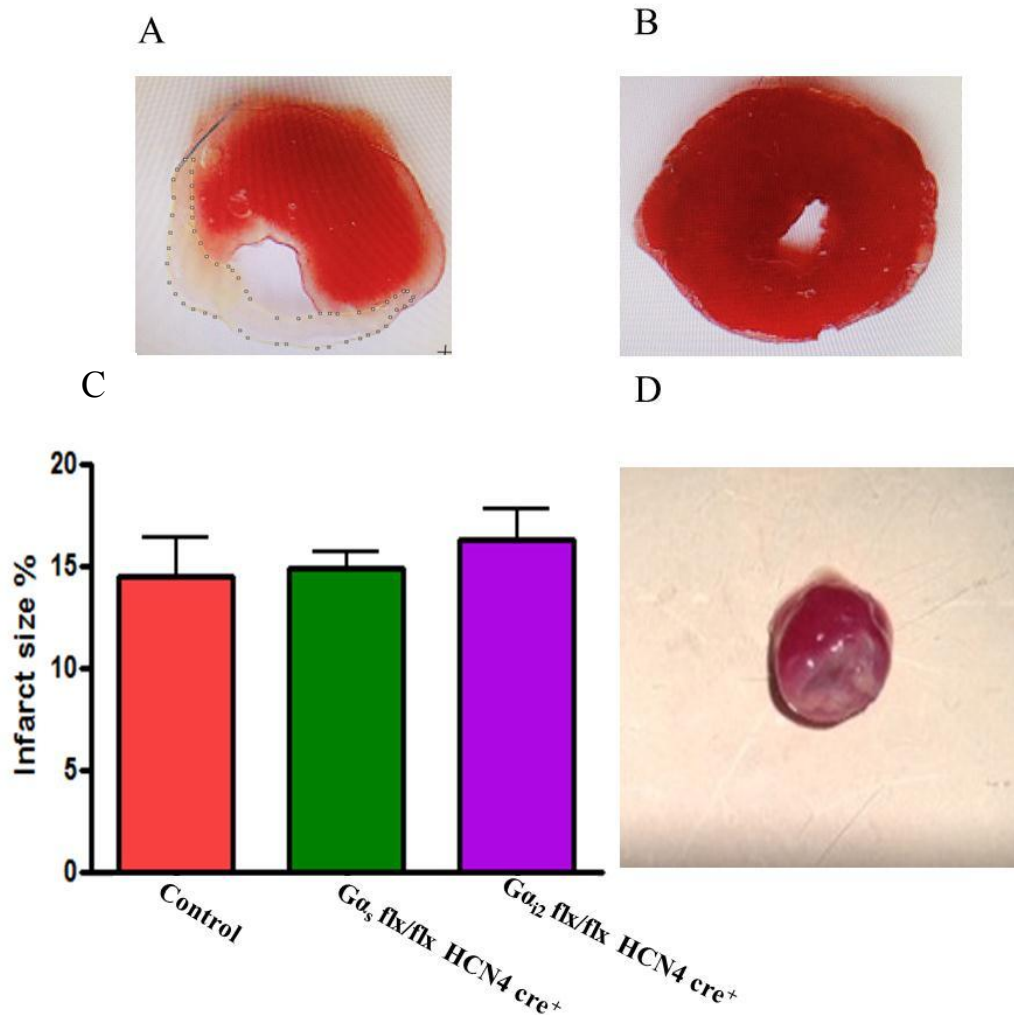


Figure 6.9 TTC staining and % infarct size after MI. Upper panel A) infarcted zone after MI, B) non infarcted tissue after MI, C) % infarct size calculated using Image J software and D) infarcted heart showing scar tissue after the MI.

Subject losses are a main feature to any surgical model. It is a big challenge to keep these losses to a minimum for scientific, humane and economic reasons. In the literature, LAD ligation is recommended 2 mm below the left atria, to achieve roughly 40-50% of infarction (Tarnavski, McMullen, Schinke, Nie, Kong, & Izumo 2004) but in my hands when I tried to reproduce that the survival rate was poor. So I modified the position of ligation to 3 mm from the left atria, with that I was able to achieve a reasonable survival rate. I examined the process of LV remodelling after MI and our findings do throw some light on cardiac structural and functional adaptation following

MI in the cardiac conduction system-specific knock-outs of $G\alpha_s$ and $G\alpha_{i2}$. LV remodelling followed by MI is a progressive process involving chamber dilatation of LV, infarcted wall thinning and compensatory thickening of non-infarcted wall (Sharpe 1992). These are the processes to redistribute the regional wall stress to restore stroke volume and to preserve cardiac function. In patients, serial echocardiographic studies following MI showed that LV dilatation can be observed as early as 3 days and can last up to 30 days and the dilatation involved both infarcted and non-infarcted regions (Eaton et al. 1979). In the initial days after MI, regional dilatation and infarction expansion contribute to ventricular enlargement. Cardiac rupture was one of the features observed in mice that died few days after MI. Cardiac rupture could be a result of infarction expansion in an extreme form in which the expanded infarct zone is not able to maintain the integrity of ventricular wall before the deposition of collagen and scar formation (Schuster and Bulkley 1979). LV remodelling after MI in mice is a time dependent process and early remodelling results in high risk of rupture of the myocardium and those that survived the rupture had the remodelling going on with chamber dilatation and the thickness of the anterior wall reduced by 50% (Gao, Dart, Dewar, Jennings, & Du 2000).

Echocardiography is an inexpensive, easily applicable and readily interpreted tool in evaluating ventricular function in mice, using techniques and indices familiar from human echocardiography (Rottman, Ni, & Brown 2007). One limitation in the study is the use of anaesthesia for echocardiography. Generally, anaesthesia produces cardiac and respiratory depression as well as fluctuations in body temperature via either a direct or indirect action on the central nervous system and heart. And in animals with cardiac pathology such as MI in mice, alteration of the autonomic nervous system by

anaesthetics may further jeopardize cardiovascular function complicating interpretation of haemodynamic data and potentially underestimating LV function (Yang et al. 1999). By maintaining the isoflurane levels (1-1.5%) and keeping the heating pad at 42°C, we could carefully maintain the heart rate at a more or less uniform rate for all groups.

Discussion

6.11 LV dysfunction and remodelling was not observed with $G\alpha_s$ HCN4 cre⁺ mice after MI

I measured EF, FS and FAC in the $G\alpha_s$ HCN4 cre⁺ mice and found all of them to be preserved compared to control after MI. In addition, FS% and EF% and were found to be increased in $G\alpha_s$ flx/flx HCN4 cre⁺ mice after tamoxifen prior to infarction. Thus, there may a rate-dependent change in LV function occurring in them as a result of deletion of $G\alpha_s$ in nodal cells. This may reflect a negative Bowditch staircase, where there is increased contractility of cardiac muscle with a decrease in heart rate, which is known to occur in the mouse. Lack of $G\alpha_s$ possibly prevents the β AR signalling and its subsequent activation of AC leading to low amount of cAMP, and this could be protective in a heart failure scenario.

After MI the survival was lower in this group (45%) compared to its controls (68%) though not statistically significant. Mortality was largely due to cardiac rupture in the first 2-3 days as observed in post mortem of animals that had died. Cardiac rupture is one of the known reasons for early mortality from MI (Gao, Dart, Dewar, Jennings, & Du 2000). There was no trend towards larger infarcts in the control group as observed by staining in all animals after the study. Furthermore chamber dimensions were preserved and there was no evidence of hypertrophy in response to MI. Thus, despite a similar sized infarct these mice have preserved LV function and there was no evidence of pathological remodelling. There was no change in LV dilation as indicated by no change in LVIDd and LVPWd measurements after MI in $G\alpha_s$ flx/flx HCN4 cre⁺ mice after 14 days post MI. The bradycardia in these mice may protect the heart against the subsequent ischemic insult. The precise mechanisms by which absence of $G\alpha_s$ in the

SA node and the consequent bradycardia mitigates against adverse LV remodelling remain to be explored.

Telemetry studies in $G\alpha_s$ flx/flx HCN4 cre⁺ mice showed that mice with conduction system-specific deletion of $G\alpha_s$ ambulatory heart rates lower than its control littermates. After MI, we also found that $G\alpha_s$ flx/flx HCN4 cre⁺ mice were bradycardic but there were no signs of ventricular arrhythmias was observed after MI. These data suggest that conduction system deletion of $G\alpha_s$ does not increase susceptibility to ventricular arrhythmias.

6.12 LV remodelling was not remarkable in $G\alpha_{i2}$ HCN4 cre⁺ mice after MI

In the context of myocardial ischemia and the progression towards heart failure the role of Gi signaling is not clearly understood. One salient characteristic of the failing heart is up-regulation of $G\alpha_{i2}$ at the protein and transcript levels (Feldman et al. 1988). Till now, however, the picture is not clear about the beneficial or maladaptive nature of this up-regulation (Baker et al. 2001). Activation of many Gi-coupled receptors (adenosine, sphingosine-1-phosphatete, opioid etc.) can reduce ischemia-reperfusion injury. Studies also show absence of $G\alpha_{i2}$ specifically in myocytes, results in increased susceptibility to I/R injury and increased apoptotic cell death in mice with cardiomyocyte-specific loss of expression of $G\alpha_{i2}$ (Degeorge, Jr., Gao, Boucher, Vinge, Martini, Raake, Chuprun, Harris, Kim, Soltys, Eckhart, & Koch 2008). In our lab we observed sudden death in mice with global deletion of $G\alpha_{i2}$ for reasons unknown. These observations all point to a protective role of $G\alpha_{i2}$ in heart failure. Mice lacking the $G\alpha_{i2}$ specifically in conduction system tissues have allowed us to directly address the role of $G\alpha_{i2}$ signaling in the SA node in response to stress in the form of myocardial infarction.

FS%, EF% and FAC% were reduced after MI in $G\alpha_{i2}$ flx/flx HCN4 cre⁺ mice but these didn't reach statistical significance compared with the controls. There was a significant difference in chamber dilatation in the LV marked by an increase in LVIDd and LVPWd measurements in $G\alpha_{i2}$ flx/flx HCN4 cre⁺ mice after 14 days post MI, although not significant when compared with control. This suggests LV remodelling is happening to an extent which is comparable to control. It also suggests that moderate tachycardia is not substantially detrimental or that we may need larger numbers of mice to detect it. Studies using an RGS-insensitive mouse model ($G\alpha_{i2}$ G^{184S}) where there is enhanced $G\alpha_{i2}$ signaling showed detrimental effects, after isoprenaline-induced injury marked by increased fibrosis, and increased cardiac fibroblast activity ERK and cell proliferation (Kaur et al. 2012). Increased levels of $G\alpha_{i2}$ in these models didn't show any protective effects as expected. But another study demonstrates a significant increase in mRNA levels of $G\alpha_{i2}$ in human end-stage heart failure caused by idiopathic dilated cardiomyopathy and ischemic cardiomyopathy without changes in $G\alpha_{i3}$ and $G\alpha_s$ mRNA levels (Eschenhagen, Mende, Nose, Schmitz, Scholz, Haverich, Hirt, Doring, Kalmar, & Hoppner 1992). The ambiguous significance of $G\alpha_{i2}$ signalling in myocardial injury muddles efforts to regulate its function as a therapeutic strategy. Studies on protective roles of $G\alpha_{i2}$ signalling used cardiac myocytes or *in vivo* genetic manipulations specific to cardiac myocytes and didn't take into account other cell types like fibroblasts which are also key cells in cardiac remodelling.

$G\alpha_{i2}$ flx/flx HCN4 cre⁺ mice showed an increase in heart weight : body weight and an increase in LV mass, which shows hypertrophy and was observed to same extent in both control and $G\alpha_{i2}$ flx/flx HCN4 cre⁺ mice due to some adaptive changes.

LVhypertrophy is a compensatory mechanism to reduce wall stress and to maintain normal cardiac function for a period of time.

Ambulatory telemetry studies in $G\alpha_{i2}$ flx/flx HCN4 cre⁺ mice showed that mice with conduction system-specific deletion of $G\alpha_{i2}$ had heart rates higher than to its control littermates. After MI also, we found that, $G\alpha_{i2}$ flx/flx HCN4 cre⁺ mice were tachycardic but no signs of ventricular arrhythmias were witnessed on the ECG traces during echocardiography. From these observations it is difficult to dissect out the role of SA node deletion $G\alpha_{i2}$ in heart failure. Previous studies in our lab on global $G\alpha_{i2}$ knock-out shows no evidence of functional impairment in contractile function or other abnormalities as assessed using echocardiography in $G\alpha_{i2}$ (-/-) mice compared to control wild-type mice (Zuberi, Nobles, Sebastian, Dyson, Lim, Breckenridge, Birnbaumer, & Tinker 2010).

6.13 Role of calcium in cardiac hypertrophy

In response to stress, increased work load or from pathological conditions such as MI and hypertension, the heart undergoes a growth process known as hypertrophy which eventually gives rise to pathological ventricular remodelling and dilatation. A major cause of cardiac hypertrophy in the context of LV remodelling after MI is possibly due to Ca^{2+} signalling (discussed below).

Binding of catecholamines, endothelin-I, angiotensin-II (released in response to neurohormonal and compensatory mechanism in heart failure) to GPCRs coupled to $G\alpha_{q/11}$ leads to activation and mobilization of Ca^{2+} through the inositol 1,4,5-triphosphate (Ins(1,4,5)P3) pathway Fig (6.10). Ca^{2+} can also be released from excitation-contraction coupling in myocytes, enhanced myocardial stress and also

from PKA-mediated release of Ca^{2+} as the heart tries to improve its function by enhanced β -AR signalling. Increased release of calcium in the myocyte can recruit other players like calcium calmodulin (CaM), calcium calmodulin-dependent protein kinase II (CaMKII), calcineurin (CaN) and nuclear factor of activated T cells (NFAT). $\text{G}\alpha_{q/11}$ signalling activates phospholipase C (PLC), which catalyses the synthesis of Ins(1,4,5)P3 and diacyl glycerol (DAG). Ins(1,4,5)P3 induces intracellular Ca^{2+} release which then activates CaMKinase or calcineurin, which mediate cardiomyocyte growth. Calcineurin is a calcium-dependent protein phosphatase that dephosphorylates NFAT transcription factors. NFAT forms complexes with the cofactors GATA-4 or myocyte enhancer factor-2 (MEF-2) to transactivate the transcription of hypertrophic target genes (Heineke and Molkenin 2006;Maillet et al. 2013).

Also involved are histone deacetylases (HDACs), which are regulated by phosphorylation and shuttle between the cytoplasm and nucleus. When phosphorylated, by CaMKII δ and PKD, these enzymes are bound and are sequestered in the cytoplasm; dephosphorylation results in translocation to the nucleus where in association with MEF-2 transcription factors they deacetylate histone proteins and inhibit transcription factors. This way they regulate cardiac specific gene expression and class II HDACs repress cardiac growth via MEF-2. In the heart, phosphorylation of these HDACs appears to be particularly mediated by CaM kinases in response to an increase in intracellular/nuclear Ca^{2+} , further leading to activation of MEF-2 (Clerk, Cullingford, Fuller, Giraldo, Markou, Pikkarainen, & Sugden 2007).

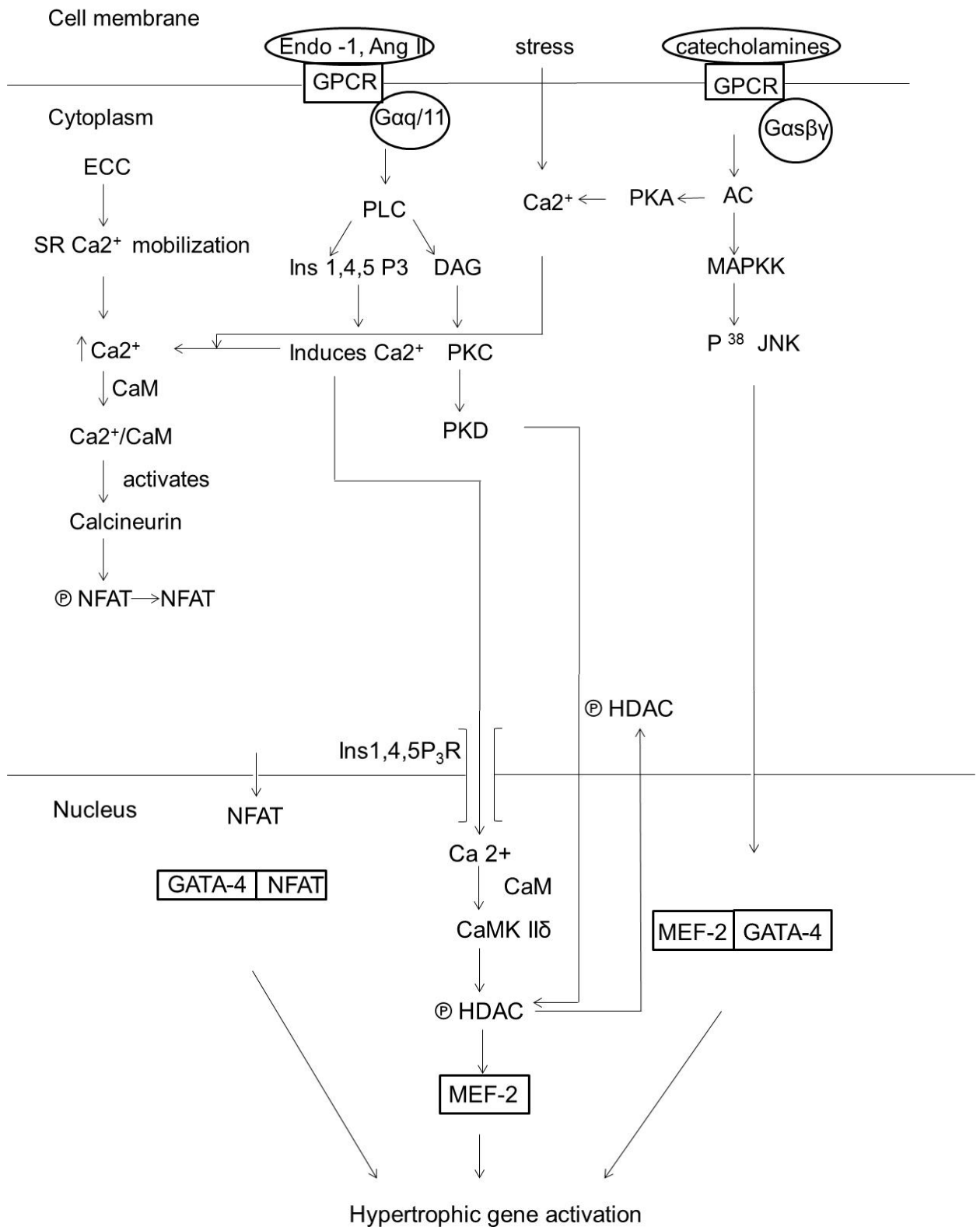


Figure 6.10 Role of Ca²⁺ in the hypertrophy signalling pathway. Ca²⁺ is released from excitation-contraction coupling, Gαq/11 and Gαs signalling activates CaM, CaMKIIδ and calcineurin and in the nucleus it activates several transcription factors which in turn switch on hypertrophic gene activation leading to cardiomyocyte growth. ECC- excitation contraction coupling, PLC-Phospholipase C, MAPKK-Mitogen activated protein kinase, Endo-1-Endothelin - 1, Ang II- angiotensin -II, JNK-c-Jun N-terminal kinase, Ⓢ-phosphorylation, HDAC- histone deacetylase.

Other mediators of pathological cardiac hypertrophy are the p38 and c-Jun N-terminal kinase (JNK) branches of the MAPK cascade, which phosphorylate and activate the GATA-4 transcription factor. Prolonged p38 or JNK activation in the heart leads to cardiomyopathy and heart failure. Catecholamines can also activate AC to induce activation of PKA, which then phosphorylates an array of intracellular targets, leading to increased calcium release and enhanced contractility; the end result of this appears to be cardiomyopathic, as it results in increased myocyte apoptosis and necrosis (Maillet, van Berlo, & Molkentin 2013).

In $G\alpha_{i2}$ flx/flx HCN4 cre⁺ mice due to their higher heart rate, they might be more prone to hypertrophy which in turn leads to apoptosis and heart failure as there is more Ca²⁺ available in these mice as a result of their phenotype. On the other hand $G\alpha_s$ flx/flx HCN4 cre⁺ mice are protected due to their bradycardic nature and less Ca²⁺ is available in their ventricular myocytes, so they are less likely to develop hypertrophy and further downstream effects. To investigate further this hypothesis, targeting a few genes in the hypertrophic signalling pathway like CaMKII δ , and calcineurin may perhaps help us in understanding the role of Ca²⁺ in determining the observed phenotype in these mice.

The positive adaptive response seen with the MI model in $G\alpha_s$ flx/flx HCN4 cre⁺ mice tempts us to investigate further these results in a different experimental model like hypertrophy-induced heart failure by Transverse Aortic Constriction (TAC) to further confirm these findings.

Summary

Mice with cardiac specific deletion of $G\alpha_{i2}$ and $G\alpha_o$ using α MHC cre didn't show any difference in HRV and ECG. This could be due to incomplete cre-mediated deletion of $G\alpha_{i2}$ and $G\alpha_o$ specifically to the SA nodal cells. Another possible explanation is other chronic compensation may be possible in these cardiac specific knock-outs as a developmental modification and the observations could be adaptive.

Interestingly, studies with $RGSiG\alpha_{i2}$ and $RGSiG\alpha_o$ suggested possible role of the central nervous system in controlling the heart rate, as they were found to be tachycardic, hyperactive and they lost their diurnal variation in heart rhythm. However despite this there was an enhanced bradycardic response to carbachol in both $RGSiG\alpha_{i2}$ and $RGSiG\alpha_o$.

The selective deletion of $G\alpha_s$ in the conduction system results in loss of normal diurnal variation with the mice no longer tachycardic at night and thus relatively bradycardic compared to control. In contrast, mice with selective deletion of $G\alpha_{i2}$ in the conduction system also lost normal diurnal variation but this occurs because they are relatively more tachycardic during the day consistent with a decline in parasympathetic modulation of the SA node. After selective deletion of $G\alpha_s$ in conduction system the response to isoprenaline was significantly attenuated but not abolished whilst with $G\alpha_{i2}$ deletion the heart rate slowing response to carbachol is relatively well preserved. Specifically, there was a selective loss of normalised low frequency (LF) power in $G\alpha_s$ flx/flx HCN4 cre⁺ mice seen as loss of spectral peaks in the low frequency range,(0.4-1.5Hz) while in contrast in $G\alpha_{i2}$ flx/flx HCN4 cre⁺ mice there was a selective loss in normalised high frequency (HF) power perceived as loss of spectral peaks in high frequency range (1.5-4.0). Thus, deletion of $G\alpha_s$ and $G\alpha_{i2}$ in

the conduction system of the adult mouse impairs physiological heart rate regulation in the intact awake animal.

Data from M-mode echocardiography suggests that SAN-specific knock-out of $G\alpha_s$ attenuates LV dilation and preserves LV contractile function after MI. FS% and EF% were found to be increased in $G\alpha_s$ flx/flx HCN4 cre⁺ mice after tamoxifen which shows a possible increase in contractility is occurring in them as a result of deletion of $G\alpha_s$ in nodal cells which may be protective in nature. So in these mice after MI absence of $G\alpha_s$ in the conduction system tissues is helping them to overcome the effects of LV remodelling. On the other hand, FS% and FAC% showed a decrease after MI in $G\alpha_{i2}$ flx/flx HCN4 cre⁺ mice but didn't reach a significance when compared with the controls. There was significant difference in chamber dilatation in LV marked by increase in the measurement of LVIDd and LVPWd measurements after MI in $G\alpha_{i2}$ flx/flx HCN4 cre⁺ mice after 14 days post MI, although not significant when compared with control.

Future directions

Cardiac specific deletion of $G\alpha_s$ and $G\alpha_{i2}$ in the conduction system ($G\alpha_s$ flx/flx HCN4 cre⁺ and $G\alpha_{i2}$ flx/flx HCN4 cre⁺) showed some interesting phenotypes of being tachycardic and bradycardic respectively and a loss of HF power of HRV with $G\alpha_{i2}$ HCN4 cre⁺ mice and a loss of LF power of HRV with $G\alpha_{i2}$ HCN4 cre⁺ mice. It would be interesting to know how these changes in heart rate and the conduction system, remodel the ventricle and affect the expression and function of protective signalling pathways.

Studies with RGS sensitive knock-ins of $G\alpha_{i2}$ and $G\alpha_o$ showed a potential role of the central nervous system in controlling the heart rate, as they were found to be tachycardic and they lost their diurnal variation in heart rhythm. Also we observed in our studies an enhanced bradycardic response to carbachol in both RGSi $G\alpha_{i2}$ and RGSi $G\alpha_o$ which could be due to enhanced GIRK channel activation and suggests it has a role in cardiac automaticity. This observation needs to be further confirmed by looking at various ion channels like e.g. GIRK by patch clamping techniques (single cell electrophysiology). As an effector for parasympathetic control of heart rate GIRK currents have been implicated in the development of atrial fibrillation (AF) and several lines of evidence have suggested that abnormal activation of GIRK currents is associated with AF (Dobrev, Friedrich, Voigt, Jost, Wettwer, Christ, Knaut, & Ravens 2005). Since GIRK currents are preferentially activated upon M₂R activation when actions of RGS proteins on $G\alpha_{i2}$ are impaired, it is conceivable that RGSi $G\alpha_{i2}$ mutant mice may have an increased risk of AF as well. By using *in vivo* electrophysiological studies (cardiac pacing) further characterization of RGSi $G\alpha_{i2}$ and RGSi $G\alpha_o$ needs to be done to see whether they are prone to atrial fibrillation and AV conduction block.

Studies with MI models of $G\alpha_{i2}$ and $G\alpha_s$ with tamoxifen inducible conduction cre, found to be promising with respect to $G\alpha_s$ HCN4 cre⁺ mice. It would be supportive and favourable to determine the degree of apoptosis and hypertrophy in $G\alpha_{i2}$ flx/flx HCN4 cre⁺ and $G\alpha_s$ flx/flx HCN4 cre⁺ mice. Also, further characterization of these mice by histology, gene expression studies and biochemical assays needs to be done. Calcium handling properties of the cells may have altered with prolonged bradycardia ($G\alpha_s$ flx/flx HCN4 cre⁺) and tachycardia ($G\alpha_{i2}$ flx/flx HCN4 cre⁺) in these mice after the MI or even before that (after tamoxifen treatment), so assessment of the activation status of calcium dependent calmodulin kinase II (CaMKII) is another potential candidate to explore. Since we found that the absence of $G\alpha_s$ in the conduction system tissues is protective in the context of MI, it would be of great relevance if I could prove the same in another model of heart failure and hypertrophy such as transverse aortic banding.

BIBLIOGRAPHY

References

1996. Heart rate variability. Standards of measurement, physiological interpretation, and clinical use. Task Force of the European Society of Cardiology and the North American Society of Pacing and Electrophysiology. *Eur.Heart J.*, 17, (3) 354-381 available from: PM:8737210
- Adamson, P.B., Smith, A.L., Abraham, W.T., Kleckner, K.J., Stadler, R.W., Shih, A., & Rhodes, M.M. 2004. Continuous autonomic assessment in patients with symptomatic heart failure: prognostic value of heart rate variability measured by an implanted cardiac resynchronization device. *Circulation*, 110, (16) 2389-2394 available from: PM:15313946
- Agah, R., Frenkel, P.A., French, B.A., Michael, L.H., Overbeek, P.A., & Schneider, M.D. 1997. Gene recombination in postmitotic cells. Targeted expression of Cre recombinase provokes cardiac-restricted, site-specific rearrangement in adult ventricular muscle in vivo. *J.Clin.Invest*, 100, (1) 169-179 available from: PM:9202069
- Anderson, G.R., Posokhova, E., & Martemyanov, K.A. 2009. The R7 RGS protein family: multi-subunit regulators of neuronal G protein signaling. *Cell Biochem.Biophys.*, 54, (1-3) 33-46 available from: PM:19521673
- Ang, R., Opel, A., & Tinker, A. 2012. The Role of Inhibitory G Proteins and Regulators of G Protein Signaling in the in vivo Control of Heart Rate and Predisposition to Cardiac Arrhythmias. *Front Physiol*, 3, 96 available from: PM:22783193
- Arber, S., Hunter, J.J., Ross, J., Jr., Hongo, M., Sansig, G., Borg, J., Perriard, J.C., Chien, K.R., & Caroni, P. 1997. MLP-deficient mice exhibit a disruption of cardiac cytoarchitectural organization, dilated cardiomyopathy, and heart failure. *Cell*, 88, (3) 393-403 available from: PM:9039266
- Asai, K., Yang, G.P., Geng, Y.J., Takagi, G., Bishop, S., Ishikawa, Y., Shannon, R.P., Wagner, T.E., Vatner, D.E., Homcy, C.J., & Vatner, S.F. 1999. Beta-adrenergic receptor blockade arrests myocyte damage and preserves cardiac function in the transgenic G(salpa) mouse. *J.Clin.Invest*, 104, (5) 551-558 available from: PM:10487769
- Baillard, C., Vivien, B., Mansier, P., Mangin, L., Jasson, S., Riou, B., & Swynghedauw, B. 2002. Brain death assessment using instant spectral analysis of heart rate variability. *Crit Care Med.*, 30, (2) 306-310 available from: PM:11889299
- Baker, A.J., Redfern, C.H., Harwood, M.D., Simpson, P.C., & Conklin, B.R. 2001. Abnormal contraction caused by expression of G(i)-coupled receptor in transgenic model of dilated cardiomyopathy. *Am.J.Physiol Heart Circ.Physiol*, 280, (4) H1653-H1659 available from: PM:11247776
- Basalay, M., Barsukevich, V., Mastitskaya, S., Mrochek, A., Pernow, J., Sjoquist, P.O., Ackland, G.L., Gourine, A.V., & Gourine, A. 2012. Remote ischaemic pre- and

delayed postconditioning - similar degree of cardioprotection but distinct mechanisms. *Exp.Physiol*, 97, (8) 908-917 available from: PM:22427438

Benavides-Vallve, C., Corbacho, D., Iglesias-Garcia, O., Pelacho, B., Albiasu, E., Castano, S., Munoz-Barrutia, A., Prosper, F., & Ortiz-de-Solorzano, C. 2012. New strategies for echocardiographic evaluation of left ventricular function in a mouse model of long-term myocardial infarction. *PLoS.One.*, 7, (7) e41691 available from: PM:22848568

Berk, S.L., Block, P.J., Toselli, P.A., & Ullrick, W.C. 1975. The effects of chronic alcohol ingestion in mice on contractile properties of cardiac and skeletal muscle: a comparison with normal and dehydrated-malnourished controls. *Experientia*, 31, (11) 1302-1303 available from: PM:1239385

Berlot, C.H. & Bourne, H.R. 1992. Identification of effector-activating residues of Gs alpha. *Cell*, 68, (5) 911-922 available from: PM:1547491

Berntson, G.G., Bigger, J.T., Jr., Eckberg, D.L., Grossman, P., Kaufmann, P.G., Malik, M., Nagaraja, H.N., Porges, S.W., Saul, J.P., Stone, P.H., & van der Molen, M.W. 1997. Heart rate variability: origins, methods, and interpretive caveats. *Psychophysiology*, 34, (6) 623-648 available from: PM:9401419

Berridge, M.J. 2006. Cell signalling biology. available from: <http://www.biochemj.org/csb>

Berul, C.I., Aronovitz, M.J., Wang, P.J., & Mendelsohn, M.E. 1996. In vivo cardiac electrophysiology studies in the mouse. *Circulation*, 94, (10) 2641-2648 available from: PM:8921812

Berul, C.I., Christe, M.E., Aronovitz, M.J., Seidman, C.E., Seidman, J.G., & Mendelsohn, M.E. 1997. Electrophysiological abnormalities and arrhythmias in alpha MHC mutant familial hypertrophic cardiomyopathy mice. *J.Clin.Invest*, 99, (4) 570-576 available from: PM:9045856

Bigger, J.T., Fleiss, J.L., Rolnitzky, L.M., & Steinman, R.C. 1993. The ability of several short-term measures of RR variability to predict mortality after myocardial infarction. *Circulation*, 88, (3) 927-934 available from: PM:8353919

Birnbaumer, L. Signal transduction by G-proteins-Basic principles, molecular diversity, and structural basis of their actions. 2, 557-569. 2004. Handbook of cell signalling.

Ref Type: Generic

Birnbaumer, L. 2007. Expansion of signal transduction by G proteins. The second 15 years or so: from 3 to 16 alpha subunits plus betagamma dimers. *Biochim.Biophys.Acta*, 1768, (4) 772-793 available from: PM:17258171

Bogdanov, K.Y., Vinogradova, T.M., & Lakatta, E.G. 2001. Sinoatrial nodal cell ryanodine receptor and Na(+)-Ca(2+) exchanger: molecular partners in pacemaker regulation. *Circ.Res.*, 88, (12) 1254-1258 available from: PM:11420301

- Bohm, M., Gierschik, P., Knorr, A., Schmidt, U., Weismann, K., & Erdmann, E. 1993. Cardiac adenylyl cyclase, beta-adrenergic receptors, and G proteins in salt-sensitive hypertension. *Hypertension*, 22, (5) 715-727 available from: PM:8225531
- Bohm, M., Kirchmayr, R., & Erdmann, E. 1995. Myocardial Gi alpha-protein levels in patients with hypertensive cardiac hypertrophy, ischemic heart disease and cardiogenic shock. *Cardiovasc.Res.*, 30, (4) 611-618 available from: PM:8575009
- Bohm, M., Swedberg, K., Komajda, M., Borer, J.S., Ford, I., Dubost-Brama, A., Lerebours, G., & Tavazzi, L. 2010. Heart rate as a risk factor in chronic heart failure (SHIFT): the association between heart rate and outcomes in a randomised placebo-controlled trial. *Lancet*, 376, (9744) 886-894 available from: PM:20801495
- Bokoch, G.M., Katada, T., Northup, J.K., Ui, M., & Gilman, A.G. 1984. Purification and properties of the inhibitory guanine nucleotide-binding regulatory component of adenylate cyclase. *J.Biol.Chem.*, 259, (6) 3560-3567 available from: PM:6323429
- Bosche, L.I., Wellner-Kienitz, M.C., Bender, K., & Pott, L. 2003. G protein-independent inhibition of GIRK current by adenosine in rat atrial myocytes overexpressing A1 receptors after adenovirus-mediated gene transfer. *J.Physiol*, 550, (Pt 3) 707-717 available from: PM:12815176
- Braunwald, E. 1997. Essential atlas of heart diseases.
- Braunwald, E., Zipes, D.P., & Libby, P. 2001. *Heart disease a textbook of cardiovascular medicine*, 6th ed ed. Philadelphia, Saunders.
- Bray, P., Carter, A., Simons, C., Guo, V., Puckett, C., Kamholz, J., Spiegel, A., & Nirenberg, M. 1986. Human cDNA clones for four species of G alpha s signal transduction protein. *Proc.Natl.Acad.Sci.U.S.A.*, 83, (23) 8893-8897 available from: PM:3024154
- Breckenridge, R. 2010. Heart failure and mouse models. *Dis.Model.Mech.*, 3, (3-4) 138-143 available from: PM:20212081
- Brodde, O.E., Vogelsang, M., Broede, A., Michel-Reher, M., Beisenbusch-Schafer, E., Hakim, K., & Zerkowski, H.R. 1998. Diminished responsiveness of Gs-coupled receptors in severely failing human hearts: no difference in dilated versus ischemic cardiomyopathy. *J.Cardiovasc.Pharmacol.*, 31, (4) 585-594 available from: PM:9554809
- Brown, L.A. & Harding, S.E. 1992. The effect of pertussis toxin on beta-adrenoceptor responses in isolated cardiac myocytes from noradrenaline-treated guinea-pigs and patients with cardiac failure. *Br.J.Pharmacol.*, 106, (1) 115-122 available from: PM:1324064
- Cannavo, A., Liccardo, D., & Koch, W.J. 2013. Targeting cardiac beta-adrenergic signaling via GRK2 inhibition for heart failure therapy. *Front Physiol*, 4, 264 available from: PM:24133451

- Chaggar, P.S., Malkin, C.J., Shaw, S.M., Williams, S.G., & Channer, K.S. 2009. Neuroendocrine effects on the heart and targets for therapeutic manipulation in heart failure. *Cardiovasc.Ther.*, 27, (3) 187-193 available from: PM:19689618
- Chen, H. & Lambert, N.A. 2000. Endogenous regulators of G protein signaling proteins regulate presynaptic inhibition at rat hippocampal synapses. *Proc.Natl.Acad.Sci.U.S.A.*, 97, (23) 12810-12815 available from: PM:11050179
- Chen, L.A., Vatner, D.E., Vatner, S.F., Hittinger, L., & Homcy, C.J. 1991. Decreased Gs alpha mRNA levels accompany the fall in Gs and adenylyl cyclase activities in compensated left ventricular hypertrophy. In heart failure, only the impairment in adenylyl cyclase activation progresses. *J.Clin.Invest*, 87, (1) 293-298 available from: PM:1824633
- Chen, M., Gavrilova, O., Zhao, W.Q., Nguyen, A., Lorenzo, J., Shen, L., Nackers, L., Pack, S., Jou, W., & Weinstein, L.S. 2005. Increased glucose tolerance and reduced adiposity in the absence of fasting hypoglycemia in mice with liver-specific Gs alpha deficiency. *J.Clin.Invest*, 115, (11) 3217-3227 available from: PM:16239968
- Chien, K.R. 2001. To Cre or not to Cre: the next generation of mouse models of human cardiac diseases. *Circ.Res.*, 88, (6) 546-549 available from: PM:11282885
- Chin, B.B., Metzler, S.D., Lemaire, A., Curcio, A., Vemulapalli, S., Greer, K.L., Petry, N.A., Turkington, T.G., Coleman, R.E., Rockman, H., & Jaszczak, R.J. 2007. Left ventricular functional assessment in mice: feasibility of high spatial and temporal resolution ECG-gated blood pool SPECT. *Radiology*, 245, (2) 440-448 available from: PM:17940303
- Cho, H.C. & Marban, E. 2010. Biological therapies for cardiac arrhythmias: can genes and cells replace drugs and devices? *Circ.Res.*, 106, (4) 674-685 available from: PM:20203316
- Cifelli, C., Rose, R.A., Zhang, H., Voightlaender-Bolz, J., Bolz, S.S., Backx, P.H., & Heximer, S.P. 2008. RGS4 regulates parasympathetic signaling and heart rate control in the sinoatrial node. *Circ.Res.*, 103, (5) 527-535 available from: PM:18658048
- Clapham, D.E. & Neer, E.J. 1997. G protein beta gamma subunits. *Annu.Rev.Pharmacol.Toxicol.*, 37, 167-203 available from: PM:9131251
- Clark, M.J., Harrison, C., Zhong, H., Neubig, R.R., & Traynor, J.R. 2003. Endogenous RGS protein action modulates mu-opioid signaling through Galphao. Effects on adenylyl cyclase, extracellular signal-regulated kinases, and intracellular calcium pathways. *J.Biol.Chem.*, 278, (11) 9418-9425 available from: PM:12524446
- Clerk, A., Cullingford, T.E., Fuller, S.J., Giraldo, A., Markou, T., Pikkarainen, S., & Sugden, P.H. 2007. Signaling pathways mediating cardiac myocyte gene expression in physiological and stress responses. *J.Cell Physiol*, 212, (2) 311-322 available from: PM:17450511
- Codina, J., Yatani, A., Grenet, D., Brown, A.M., & Birnbaumer, L. 1987. The alpha subunit of the GTP binding protein Gk opens atrial potassium channels. *Science*, 236, (4800) 442-445 available from: PM:2436299

- Coffino, P., Bourne, H.R., & Tomkins, G.M. 1975. Somatic genetic analysis of cyclic AMP action: selection of unresponsive mutants. *J.Cell Physiol*, 85, (3) 603-610 available from: PM:167036
- Coplen, S.E., Antman, E.M., Berlin, J.A., Hewitt, P., & Chalmers, T.C. 1990. Efficacy and safety of quinidine therapy for maintenance of sinus rhythm after cardioversion. A meta-analysis of randomized control trials. *Circulation*, 82, (4) 1106-1116 available from: PM:2144796
- Curry, C.W., Nelson, G.S., Wyman, B.T., Declerck, J., Talbot, M., Berger, R.D., McVeigh, E.R., & Kass, D.A. 2000. Mechanical dyssynchrony in dilated cardiomyopathy with intraventricular conduction delay as depicted by 3D tagged magnetic resonance imaging. *Circulation*, 101, (1) E2 available from: PM:10618315
- D'Angelo, D.D., Sakata, Y., Lorenz, J.N., Boivin, G.P., Walsh, R.A., Liggett, S.B., & Dorn, G.W. 1997. Transgenic Galphaq overexpression induces cardiac contractile failure in mice. *Proc.Natl.Acad.Sci.U.S.A*, 94, (15) 8121-8126 available from: PM:9223325
- Danik, S.B., Rosner, G., Lader, J., Gutstein, D.E., Fishman, G.I., & Morley, G.E. 2008. Electrical remodeling contributes to complex tachyarrhythmias in connexin43-deficient mouse hearts. *FASEB J*, 22, (4) 1204-1212 available from: PM:17984180
- Davies, S.J. & Hughes, H.E. 1993. Imprinting in Albright's hereditary osteodystrophy. *J.Med.Genet.*, 30, (2) 101-103 available from: PM:8383205
- Davis, R.C., Hobbs, F.D., & Lip, G.Y. 2000. ABC of heart failure. History and epidemiology. *BMJ*, 320, (7226) 39-42 available from: PM:10617530
- Day, P.W., Wedegaertner, P.B., & Benovic, J.L. 2004. Analysis of G-protein-coupled receptor kinase RGS homology domains. *Methods Enzymol.*, 390, 295-310 available from: PM:15488185
- De, A.K., Wichi, R.B., Jesus, W.R., Moreira, E.D., Morris, M., Krieger, E.M., & Irigoyen, M.C. 2004. Exercise training changes autonomic cardiovascular balance in mice. *J.Appl.Physiol (1985.)*, 96, (6) 2174-2178 available from: PM:14729725
- De, V.L., Mousli, M., Wurmser, A., & Farquhar, M.G. 1995. GAIP, a protein that specifically interacts with the trimeric G protein G alpha i3, is a member of a protein family with a highly conserved core domain. *Proc.Natl.Acad.Sci.U.S.A*, 92, (25) 11916-11920 available from: PM:8524874
- DeGeorge, B.R., Jr., Gao, E., Boucher, M., Vinge, L.E., Martini, J.S., Raake, P.W., Chuprun, J.K., Harris, D.M., Kim, G.W., Soltys, S., Eckhart, A.D., & Koch, W.J. 2008. Targeted inhibition of cardiomyocyte Gi signaling enhances susceptibility to apoptotic cell death in response to ischemic stress. *Circulation*, 117, (11) 1378-1387 available from: PM:18316484
- DeGeorge, B.R. & Koch, W.J. 2008. Gi/o signaling and its potential role in cardioprotection. *Expert.Rev.Cardiovasc.Ther.*, 6, (6) 785-787 available from: PM:18570615

- Delgado, R.M., III, Nawar, M.A., Zewail, A.M., Kar, B., Vaughn, W.K., Wu, K.K., Aleksic, N., Sivasubramanian, N., McKay, K., Mann, D.L., & Willerson, J.T. 2004. Cyclooxygenase-2 inhibitor treatment improves left ventricular function and mortality in a murine model of doxorubicin-induced heart failure. *Circulation*, 109, (11) 1428-1433 available from: PM:15023870
- Depre, C., Wang, Q., Yan, L., Hedhli, N., Peter, P., Chen, L., Hong, C., Hittinger, L., Ghaleh, B., Sadoshima, J., Vatner, D.E., Vatner, S.F., & Madura, K. 2006. Activation of the cardiac proteasome during pressure overload promotes ventricular hypertrophy. *Circulation*, 114, (17) 1821-1828 available from: PM:17043166
- DiBello, P.R., Garrison, T.R., Apanovitch, D.M., Hoffman, G., Shuey, D.J., Mason, K., Cockett, M.I., & Dohlman, H.G. 1998. Selective uncoupling of RGS action by a single point mutation in the G protein alpha-subunit. *J.Biol.Chem.*, 273, (10) 5780-5784 available from: PM:9488712
- DiFrancesco, D. 1985. The cardiac hyperpolarizing-activated current, *if*. Origins and developments. *Prog.Biophys.Mol.Biol.*, 46, (3) 163-183 available from: PM:2418458
- DiFrancesco, D. 1993. Pacemaker mechanisms in cardiac tissue. *Annu.Rev.Physiol*, 55, 455-472 available from: PM:7682045
- DiFrancesco, D. 2006. Funny channels in the control of cardiac rhythm and mode of action of selective blockers. *Pharmacol.Res.*, 53, (5) 399-406 available from: PM:16638640
- DiFrancesco, D. & Tortora, P. 1991. Direct activation of cardiac pacemaker channels by intracellular cyclic AMP. *Nature*, 351, (6322) 145-147 available from: PM:1709448
- Dobrev, D., Friedrich, A., Voigt, N., Jost, N., Wettwer, E., Christ, T., Knaut, M., & Ravens, U. 2005. The G protein-gated potassium current I(K,ACh) is constitutively active in patients with chronic atrial fibrillation. *Circulation*, 112, (24) 3697-3706 available from: PM:16330682
- Dobrzynski, H., Boyett, M.R., & Anderson, R.H. 2007. New insights into pacemaker activity: promoting understanding of sick sinus syndrome. *Circulation*, 115, (14) 1921-1932 available from: PM:17420362
- Doevendans, P.A., Daemen, M.J., de Muinck, E.D., & Smits, J.F. 1998. Cardiovascular phenotyping in mice. *Cardiovasc.Res.*, 39, (1) 34-49 available from: PM:9764188
- Dohlman, H.G. & Thorner, J. 1997. RGS proteins and signaling by heterotrimeric G proteins. *J.Biol.Chem.*, 272, (7) 3871-3874 available from: PM:9064301
- Domanski, M.J., Cunnion, R.E., & Roberts, W.C. 1992. Analysis of fractional area change at various levels in the normal left ventricle. *Am.J.Cardiol.*, 70, (15) 1367-1368 available from: PM:1442593
- Doupnik, C.A., Davidson, N., Lester, H.A., & Kofuji, P. 1997. RGS proteins reconstitute the rapid gating kinetics of gbetagamma-activated inwardly rectifying K+

channels. *Proc.Natl.Acad.Sci.U.S.A*, 94, (19) 10461-10466 available from: PM:9294233

Douppnik, C.A., Xu, T., & Shinaman, J.M. 2001. Profile of RGS expression in single rat atrial myocytes. *Biochim.Biophys.Acta*, 1522, (2) 97-107 available from: PM:11750060

Duan, S.Z., Christe, M., Milstone, D.S., & Mortensen, R.M. 2007. Go but not Gi2 or Gi3 is required for muscarinic regulation of heart rate and heart rate variability in mice. *Biochem.Biophys.Res.Commun.*, 357, (1) 139-143 available from: PM:17418106

Eaton, L.W., Weiss, J.L., Bulkley, B.H., Garrison, J.B., & Weisfeldt, M.L. 1979. Regional cardiac dilatation after acute myocardial infarction: recognition by two-dimensional echocardiography. *N.Engl.J.Med.*, 300, (2) 57-62 available from: PM:758578

Echt, D.S., Liebson, P.R., Mitchell, L.B., Peters, R.W., Obias-Manno, D., Barker, A.H., Arensberg, D., Baker, A., Friedman, L., Greene, H.L., & . 1991. Mortality and morbidity in patients receiving encainide, flecainide, or placebo. The Cardiac Arrhythmia Suppression Trial. *N.Engl.J.Med.*, 324, (12) 781-788 available from: PM:1900101

Ecker, P.M., Lin, C.C., Powers, J., Kobilka, B.K., Dubin, A.M., & Bernstein, D. 2006. Effect of targeted deletions of beta1- and beta2-adrenergic-receptor subtypes on heart rate variability. *Am.J.Physiol Heart Circ.Physiol*, 290, (1) H192-H199 available from: PM:16113068

Engelhardt, S., Hein, L., Wiesmann, F., & Lohse, M.J. 1999. Progressive hypertrophy and heart failure in beta1-adrenergic receptor transgenic mice. *Proc.Natl.Acad.Sci.U.S.A*, 96, (12) 7059-7064 available from: PM:10359838

Eschenhagen, T., Friedrichsen, M., Gsell, S., Hollmann, A., Mittmann, C., Schmitz, W., Scholz, H., Weil, J., & Weinstein, L.S. 1996a. Regulation of the human Gi alpha-2 gene promoter activity in embryonic chicken cardiomyocytes. *Basic Res.Cardiol.*, 91 Suppl 2, 41-46 available from: PM:8957543

Eschenhagen, T., Mende, U., Diederich, M., Hertle, B., Memmesheimer, C., Pohl, A., Schmitz, W., Scholz, H., Steinfath, M., Bohm, M., Michel, M.C., Brodde, O.E., & Raap, A. 1996b. Chronic treatment with carbachol sensitizes the myocardium to cAMP-induced arrhythmia. *Circulation*, 93, (4) 763-771 available from: PM:8641006

Eschenhagen, T., Mende, U., Nose, M., Schmitz, W., Scholz, H., Haverich, A., Hirt, S., Doring, V., Kalmar, P., Hoppner, W., & . 1992. Increased messenger RNA level of the inhibitory G protein alpha subunit Gi alpha-2 in human end-stage heart failure. *Circ.Res.*, 70, (4) 688-696 available from: PM:1551195

Esposito, G., Prasad, S.V., Rapacciuolo, A., Mao, L., Koch, W.J., & Rockman, H.A. 2001. Cardiac overexpression of a G(q) inhibitor blocks induction of extracellular signal-regulated kinase and c-Jun NH(2)-terminal kinase activity in in vivo pressure overload. *Circulation*, 103, (10) 1453-1458 available from: PM:11245652

- Ewing, D.J., Neilson, J.M., & Travis, P. 1984. New method for assessing cardiac parasympathetic activity using 24 hour electrocardiograms. *Br.Heart J.*, 52, (4) 396-402 available from: PM:6383446
- Feldman, A.M., Cates, A.E., Bristow, M.R., & Van, D.C. 1989. Altered expression of alpha-subunits of G proteins in failing human hearts. *J.Mol.Cell Cardiol.*, 21, (4) 359-365 available from: PM:2501499
- Feldman, A.M., Cates, A.E., Veazey, W.B., Hershberger, R.E., Bristow, M.R., Baughman, K.L., Baumgartner, W.A., & Van, D.C. 1988. Increase of the 40,000-mol wt pertussis toxin substrate (G protein) in the failing human heart. *J.Clin.Invest*, 82, (1) 189-197 available from: PM:2839545
- Feldman, A.M., Ray, P.E., & Bristow, M.R. 1991. Expression of alpha-subunits of G proteins in failing human heart: a reappraisal utilizing quantitative polymerase chain reaction. *J.Mol.Cell Cardiol.*, 23, (12) 1355-1358 available from: PM:1811054
- Feuerstein, G.Z. & Rozanski, D. 2000. G proteins and heart failure: is Galphaq a novel target for heart failure? *Circ.Res.*, 87, (12) 1085-1086 available from: PM:11110763
- Fisher, J.T., Vincent, S.G., Gomeza, J., Yamada, M., & Wess, J. 2004. Loss of vagally mediated bradycardia and bronchoconstriction in mice lacking M2 or M3 muscarinic acetylcholine receptors. *FASEB J.*, 18, (6) 711-713 available from: PM:14977875
- Fisher, S.G. & Marber, M.S. 2002. An in vivo model of ischaemia-reperfusion injury and ischaemic preconditioning in the mouse heart. *J.Pharmacol.Toxicol.Methods*, 48, (3) 161-169 available from: PM:14986865
- Foerster, K., Groner, F., Matthes, J., Koch, W.J., Birnbaumer, L., & Herzig, S. 2003. Cardioprotection specific for the G protein Gi2 in chronic adrenergic signaling through beta 2-adrenoceptors. *Proc.Natl.Acad.Sci.U.S.A*, 100, (24) 14475-14480 available from: PM:14612574
- Fox, K., Borer, J.S., Camm, A.J., Danchin, N., Ferrari, R., Lopez Sendon, J.L., Steg, P.G., Tardif, J.C., Tavazzi, L., & Tendera, M. 2007. Resting heart rate in cardiovascular disease. *J.Am.Coll.Cardiol.*, 50, (9) 823-830 available from: PM:17719466
- Fox, K., Ford, I., Steg, P.G., Tendera, M., Robertson, M., & Ferrari, R. 2008. Heart rate as a prognostic risk factor in patients with coronary artery disease and left-ventricular systolic dysfunction (BEAUTIFUL): a subgroup analysis of a randomised controlled trial. *Lancet*, 372, (9641) 817-821 available from: PM:18757091
- Fredriksson, R., Lagerstrom, M.C., Lundin, L.G., & Schioth, H.B. 2003. The G-protein-coupled receptors in the human genome form five main families. Phylogenetic analysis, paralogon groups, and fingerprints. *Mol.Pharmacol.*, 63, (6) 1256-1272 available from: PM:12761335
- Frenneaux, M.P. 2004. Autonomic changes in patients with heart failure and in post-myocardial infarction patients. *Heart*, 90, (11) 1248-1255 available from: PM:15486114

- Fu, Y., Huang, X., Piao, L., Lopatin, A.N., & Neubig, R.R. 2007. Endogenous RGS proteins modulate SA and AV nodal functions in isolated heart: implications for sick sinus syndrome and AV block. *Am.J.Physiol Heart Circ.Physiol*, 292, (5) H2532-H2539 available from: PM:17277016
- Fu, Y., Huang, X., Zhong, H., Mortensen, R.M., D'Alecy, L.G., & Neubig, R.R. 2006. Endogenous RGS proteins and Galpha subtypes differentially control muscarinic and adenosine-mediated chronotropic effects. *Circ.Res.*, 98, (5) 659-666 available from: PM:16456099
- Fu, Y., Zhong, H., Nanamori, M., Mortensen, R.M., Huang, X., Lan, K., & Neubig, R.R. 2004. RGS-insensitive G-protein mutations to study the role of endogenous RGS proteins. *Methods Enzymol.*, 389, 229-243 available from: PM:15313569
- Fujita, S., Inanobe, A., Chachin, M., Aizawa, Y., & Kurachi, Y. 2000. A regulator of G protein signalling (RGS) protein confers agonist-dependent relaxation gating to a G protein-gated K⁺ channel. *J.Physiol*, 526 Pt 2, 341-347 available from: PM:10896722
- Gao, X.M., Dart, A.M., Dewar, E., Jennings, G., & Du, X.J. 2000. Serial echocardiographic assessment of left ventricular dimensions and function after myocardial infarction in mice. *Cardiovasc.Res.*, 45, (2) 330-338 available from: PM:10728353
- Gao, X.M., Xu, Q., Kiriazis, H., Dart, A.M., & Du, X.J. 2005. Mouse model of post-infarct ventricular rupture: time course, strain- and gender-dependency, tensile strength, and histopathology. *Cardiovasc.Res.*, 65, (2) 469-477 available from: PM:15639486
- Gardin, J.M., Siri, F.M., Kitsis, R.N., Edwards, J.G., & Leinwand, L.A. 1995. Echocardiographic assessment of left ventricular mass and systolic function in mice. *Circ.Res.*, 76, (5) 907-914 available from: PM:7729009
- Gaudin, C., Ishikawa, Y., Wight, D.C., Mahdavi, V., Nadal-Ginard, B., Wagner, T.E., Vatner, D.E., & Homcy, C.J. 1995. Overexpression of Gs alpha protein in the hearts of transgenic mice. *J.Clin.Invest*, 95, (4) 1676-1683 available from: PM:7706476
- Gehrmann, J. & Berul, C.I. 2000. Cardiac electrophysiology in genetically engineered mice. *J.Cardiovasc.Electrophysiol.*, 11, (3) 354-368 available from: PM:10749360
- Gehrmann, J., Hammer, P.E., Maguire, C.T., Wakimoto, H., Triedman, J.K., & Berul, C.I. 2000. Phenotypic screening for heart rate variability in the mouse. *Am.J.Physiol Heart Circ.Physiol*, 279, (2) H733-H740 available from: PM:10924073
- Gelpi, R.J., Gao, S., Zhai, P., Yan, L., Hong, C., Danridge, L.M., Ge, H., Maejima, Y., Donato, M., Yokota, M., Molkentin, J.D., Vatner, D.E., Vatner, S.F., & Sadoshima, J. 2009. Genetic inhibition of calcineurin induces diastolic dysfunction in mice with chronic pressure overload. *Am.J.Physiol Heart Circ.Physiol*, 297, (5) H1814-H1819 available from: PM:19717730
- Geng, Y.J., Ishikawa, Y., Vatner, D.E., Wagner, T.E., Bishop, S.P., Vatner, S.F., & Homcy, C.J. 1999. Apoptosis of cardiac myocytes in Galpha transgenic mice. *Circ.Res.*, 84, (1) 34-42 available from: PM:9915772

- Geurts, M., Maloteaux, J.M., & Hermans, E. 2003. Altered expression of regulators of G-protein signaling (RGS) mRNAs in the striatum of rats undergoing dopamine depletion. *Biochem.Pharmacol.*, 66, (7) 1163-1170 available from: PM:14505795
- Gill, D.M. & Meren, R. 1978. ADP-ribosylation of membrane proteins catalyzed by cholera toxin: basis of the activation of adenylate cyclase. *Proc.Natl.Acad.Sci.U.S.A.*, 75, (7) 3050-3054 available from: PM:210449
- Gilman, A.G. 1987. G proteins: transducers of receptor-generated signals. *Annu.Rev.Biochem.*, 56, 615-649 available from: PM:3113327
- Gilman, A.G. 1995. Nobel Lecture. G proteins and regulation of adenylyl cyclase. *Biosci.Rep.*, 15, (2) 65-97 available from: PM:7579036
- Ginsburg, K.S. & Bers, D.M. 2004. Modulation of excitation-contraction coupling by isoproterenol in cardiomyocytes with controlled SR Ca²⁺ load and Ca²⁺ current trigger. *J.Physiol*, 556, (Pt 2) 463-480 available from: PM:14724205
- Gohla, A., Klement, K., Piekorz, R.P., Pexa, K., vom, D.S., Spicher, K., Dreval, V., Haussinger, D., Birnbaumer, L., & Nurnberg, B. 2007. An obligatory requirement for the heterotrimeric G protein Gi3 in the antiautophagic action of insulin in the liver. *Proc.Natl.Acad.Sci.U.S.A.*, 104, (8) 3003-3008 available from: PM:17296938
- Gottshall, K.R., Hunter, J.J., Tanaka, N., Dalton, N., Becker, K.D., Ross, J., Jr., & Chien, K.R. 1997. Ras-dependent pathways induce obstructive hypertrophy in echo-selected transgenic mice. *Proc.Natl.Acad.Sci.U.S.A.*, 94, (9) 4710-4715 available from: PM:9114056
- Grimm, M., Gsell, S., Mittmann, C., Nose, M., Scholz, H., Weil, J., & Eschenhagen, T. 1998. Inactivation of (G α) proteins increases arrhythmogenic effects of beta-adrenergic stimulation in the heart. *J.Mol.Cell Cardiol.*, 30, (10) 1917-1928 available from: PM:9799646
- Grueter, C.E., Colbran, R.J., & Anderson, M.E. 2007. CaMKII, an emerging molecular driver for calcium homeostasis, arrhythmias, and cardiac dysfunction. *J.Mol.Med.*, 85, (1) 5-14 available from: PM:17119905
- Grupp, I.L., Subramaniam, A., Hewett, T.E., Robbins, J., & Grupp, G. 1993. Comparison of normal, hypodynamic, and hyperdynamic mouse hearts using isolated work-performing heart preparations. *Am.J.Physiol*, 265, (4 Pt 2) H1401-H1410 available from: PM:7694487
- Guo, C., Yang, W., & Lobe, C.G. 2002. A Cre recombinase transgene with mosaic, widespread tamoxifen-inducible action. *Genesis.*, 32, (1) 8-18 available from: PM:11835669
- Hagendorff, A., Schumacher, B., Kirchhoff, S., Luderitz, B., & Willecke, K. 1999. Conduction disturbances and increased atrial vulnerability in Connexin40-deficient mice analyzed by transesophageal stimulation. *Circulation*, 99, (11) 1508-1515 available from: PM:10086977

- Hayward, B.E., Barlier, A., Korbonits, M., Grossman, A.B., Jacquet, P., Enjalbert, A., & Bonthron, D.T. 2001. Imprinting of the G(s)alpha gene *GNAS1* in the pathogenesis of acromegaly. *J.Clin.Invest*, 107, (6) R31-R36 available from: PM:11254676
- Hayward, B.E., Moran, V., Strain, L., & Bonthron, D.T. 1998. Bidirectional imprinting of a single gene: *GNAS1* encodes maternally, paternally, and biallelically derived proteins. *Proc.Natl.Acad.Sci.U.S.A*, 95, (26) 15475-15480 available from: PM:9860993
- Hein, L., Stevens, M.E., Barsh, G.S., Pratt, R.E., Kobilka, B.K., & Dzau, V.J. 1997. Overexpression of angiotensin AT1 receptor transgene in the mouse myocardium produces a lethal phenotype associated with myocyte hyperplasia and heart block. *Proc.Natl.Acad.Sci.U.S.A*, 94, (12) 6391-6396 available from: PM:9177228
- Heineke, J. & Molkenin, J.D. 2006. Regulation of cardiac hypertrophy by intracellular signalling pathways. *Nat.Rev.Mol.Cell Biol.*, 7, (8) 589-600 available from: PM:16936699
- Herrmann, S., Stieber, J., Stockl, G., Hofmann, F., & Ludwig, A. 2007. HCN4 provides a 'depolarization reserve' and is not required for heart rate acceleration in mice. *EMBO J.*, 26, (21) 4423-4432 available from: PM:17914461
- Hershberger, R.E., Feldman, A.M., & Bristow, M.R. 1991. A1-adenosine receptor inhibition of adenylate cyclase in failing and nonfailing human ventricular myocardium. *Circulation*, 83, (4) 1343-1351 available from: PM:1901530
- Heximer, S.P., Knutsen, R.H., Sun, X., Kaltenbronn, K.M., Rhee, M.H., Peng, N., Oliveira-dos-Santos, A., Penninger, J.M., Muslin, A.J., Steinberg, T.H., Wyss, J.M., Mecham, R.P., & Blumer, K.J. 2003. Hypertension and prolonged vasoconstrictor signaling in RGS2-deficient mice. *J.Clin.Invest*, 111, (8) 1259 available from: PM:12697745
- Ho, K.K., Pinsky, J.L., Kannel, W.B., & Levy, D. 1993. The epidemiology of heart failure: the Framingham Study. *J.Am.Coll.Cardiol.*, 22, (4 Suppl A) 6A-13A available from: PM:8376698
- Hoesl, E., Stieber, J., Herrmann, S., Feil, S., Tybl, E., Hofmann, F., Feil, R., & Ludwig, A. 2008. Tamoxifen-inducible gene deletion in the cardiac conduction system. *J.Mol.Cell Cardiol.*, 45, (1) 62-69 available from: PM:18538341
- Hollinger, S. & Hepler, J.R. 2002. Cellular regulation of RGS proteins: modulators and integrators of G protein signaling. *Pharmacol.Rev.*, 54, (3) 527-559 available from: PM:12223533
- Huang, C.L., Lei, L., Matthews, G.D., Zhang, Y., & Lei, M. 2012. Pathophysiological Mechanisms of Sino-Atrial Dysfunction and Ventricular Conduction Disease Associated with *SCN5A* Deficiency: Insights from Mouse Models. *Front Physiol*, 3, 234 available from: PM:22783200
- Huang, X., Fu, Y., Charbeneau, R.A., Saunders, T.L., Taylor, D.K., Hankenson, K.D., Russell, M.W., D'Alecy, L.G., & Neubig, R.R. 2006. Pleiotropic phenotype of a

genomic knock-in of an RGS-insensitive G184S Gnai2 allele. *Mol.Cell Biol.*, 26, (18) 6870-6879 available from: PM:16943428

Huser, J., Blatter, L.A., & Lipsius, S.L. 2000. Intracellular Ca²⁺ release contributes to automaticity in cat atrial pacemaker cells. *J.Physiol*, 524 Pt 2, 415-422 available from: PM:10766922

Inanobe, A., Fujita, S., Makino, Y., Matsushita, K., Ishii, M., Chachin, M., & Kurachi, Y. 2001. Interaction between the RGS domain of RGS4 with G protein alpha subunits mediates the voltage-dependent relaxation of the G protein-gated potassium channel. *J.Physiol*, 535, (Pt 1) 133-143 available from: PM:11507164

Ino, T., Benson, L.N., Mikalian, H., Freedom, R.M., & Rowe, R.D. 1989. Determination of left ventricular volumes by Simpson's rule in infants and children with congenital heart disease. *Br.Heart J.*, 61, (2) 182-185 available from: PM:2923757

Inubushi, M., Jordan, M.C., Roos, K.P., Ross, R.S., Chatziioannou, A.F., Stout, D.B., Dahlbom, M., & Schelbert, H.R. 2004. Nitrogen-13 ammonia cardiac positron emission tomography in mice: effects of clonidine-induced changes in cardiac work on myocardial perfusion. *Eur.J.Nucl.Med.Mol.Imaging*, 31, (1) 110-116 available from: PM:14551749

Ischia, R., Lovisetti-Scamihorn, P., Hogue-Angeletti, R., Wolkersdorfer, M., Winkler, H., & Fischer-Colbrie, R. 1997. Molecular cloning and characterization of NESP55, a novel chromogranin-like precursor of a peptide with 5-HT_{1B} receptor antagonist activity. *J.Biol.Chem.*, 272, (17) 11657-11662 available from: PM:9111083

Ishii, M., Inanobe, A., Fujita, S., Makino, Y., Hosoya, Y., & Kurachi, Y. 2001. Ca²⁺ elevation evoked by membrane depolarization regulates G protein cycle via RGS proteins in the heart. *Circ.Res.*, 89, (11) 1045-1050 available from: PM:11717162

Ishikawa, Y., Bianchi, C., Nadal-Ginard, B., & Homcy, C.J. 1990. Alternative promoter and 5' exon generate a novel Gs alpha mRNA. *J.Biol.Chem.*, 265, (15) 8458-8462 available from: PM:2111318

Ivanina, T., Varon, D., Peleg, S., Rishal, I., Porozov, Y., Dessauer, C.W., Keren-Raifman, T., & Dascal, N. 2004. Galphai1 and Galphai3 differentially interact with, and regulate, the G protein-activated K⁺ channel. *J.Biol.Chem.*, 279, (17) 17260-17268 available from: PM:14963032

Iwase, M., Bishop, S.P., Uechi, M., Vatner, D.E., Shannon, R.P., Kudej, R.K., Wight, D.C., Wagner, T.E., Ishikawa, Y., Homcy, C.J., & Vatner, S.F. 1996. Adverse effects of chronic endogenous sympathetic drive induced by cardiac GS alpha overexpression. *Circ.Res.*, 78, (4) 517-524 available from: PM:8635208

Iwase, M., Uechi, M., Vatner, D.E., Asai, K., Shannon, R.P., Kudej, R.K., Wagner, T.E., Wight, D.C., Patrick, T.A., Ishikawa, Y., Homcy, C.J., & Vatner, S.F. 1997. Cardiomyopathy induced by cardiac Gs alpha overexpression. *Am.J.Physiol*, 272, (1 Pt 2) H585-H589 available from: PM:9038982

- Jackson, G., Gibbs, C.R., Davies, M.K., & Lip, G.Y. 2000. ABC of heart failure. Pathophysiology. *BMJ*, 320, (7228) 167-170 available from: PM:10634740
- James, J.F., Hewett, T.E., & Robbins, J. 1998. Cardiac physiology in transgenic mice. *Circ.Res.*, 82, (4) 407-415 available from: PM:9506700
- Jeong, S.W. & Ikeda, S.R. 2000. Endogenous regulator of G-protein signaling proteins modify N-type calcium channel modulation in rat sympathetic neurons. *J.Neurosci.*, 20, (12) 4489-4496 available from: PM:10844018
- Jiang, M., Gold, M.S., Boulay, G., Spicher, K., Peyton, M., Brabet, P., Srinivasan, Y., Rudolph, U., Ellison, G., & Birnbaumer, L. 1998. Multiple neurological abnormalities in mice deficient in the G protein Go. *Proc.Natl.Acad.Sci.U.S.A*, 95, (6) 3269-3274 available from: PM:9501252
- Jones, D.T., Masters, S.B., Bourne, H.R., & Reed, R.R. 1990. Biochemical characterization of three stimulatory GTP-binding proteins. The large and small forms of Gs and the olfactory-specific G-protein, Golf. *J.Biol.Chem.*, 265, (5) 2671-2676 available from: PM:2105931
- Joung, B., Ogawa, M., Lin, S.F., & Chen, P.S. 2009. The calcium and voltage clocks in sinoatrial node automaticity. *Korean Circ.J.*, 39, (6) 217-222 available from: PM:19949626
- Just, A., Faulhaber, J., & Ehmke, H. 2000. Autonomic cardiovascular control in conscious mice. *Am.J.Physiol Regul.Integr.Comp Physiol*, 279, (6) R2214-R2221 available from: PM:11080088
- Kaese, S. & Verheule, S. 2012. Cardiac electrophysiology in mice: a matter of size. *Front Physiol*, 3, 345 available from: PM:22973235
- Kannankeril, P.J., Mitchell, B.M., Goonasekera, S.A., Chelu, M.G., Zhang, W., Sood, S., Kearney, D.L., Danila, C.I., De, B.M., Wehrens, X.H., Pautler, R.G., Roden, D.M., Taffet, G.E., Dirksen, R.T., Anderson, M.E., & Hamilton, S.L. 2006. Mice with the R176Q cardiac ryanodine receptor mutation exhibit catecholamine-induced ventricular tachycardia and cardiomyopathy. *Proc.Natl.Acad.Sci.U.S.A*, 103, (32) 12179-12184 available from: PM:16873551
- Kanno, S., Lerner, D.L., Schuessler, R.B., Betsuyaku, T., Yamada, K.A., Saffitz, J.E., & Kovacs, A. 2002. Echocardiographic evaluation of ventricular remodeling in a mouse model of myocardial infarction. *J.Am.Soc.Echocardiogr.*, 15, (6) 601-609 available from: PM:12050601
- Kardestuncer, T., Wu, H., Lim, A.L., & Neer, E.J. 1998. Cardiac myocytes express mRNA for ten RGS proteins: changes in RGS mRNA expression in ventricular myocytes and cultured atria. *FEBS Lett.*, 438, (3) 285-288 available from: PM:9827562
- Katada, T. & Ui, M. 1982. Direct modification of the membrane adenylate cyclase system by islet-activating protein due to ADP-ribosylation of a membrane protein. *Proc.Natl.Acad.Sci.U.S.A*, 79, (10) 3129-3133 available from: PM:6954463

- Kaur, K., Parra, S., Chen, R., Charbeneau, R.A., Wade, S.M., Jay, P.Y., & Neubig, R.R. 2012. Galphai2 signaling: friend or foe in cardiac injury and heart failure? *Naunyn Schmiedebergs Arch.Pharmacol.*, 385, (5) 443-453 available from: PM:22411356
- Kawamoto, H., Ohyanagi, M., Nakamura, K., Yamamoto, J., & Iwasaki, T. 1994. Increased levels of inhibitory G protein in myocardium with heart failure. *Jpn.Circ.J.*, 58, (12) 913-924 available from: PM:7699738
- Kehlenbach, R.H., Matthey, J., & Huttner, W.B. 1994. XL alpha s is a new type of G protein. *Nature*, 372, (6508) 804-809 available from: PM:7997272
- Kemp, C.D. & Conte, J.V. 2012. The pathophysiology of heart failure. *Cardiovasc.Pathol.*, 21, (5) 365-371 available from: PM:22227365
- Killeen, M.J., Thomas, G., Sabir, I.N., Grace, A.A., & Huang, C.L. 2008. Mouse models of human arrhythmia syndromes. *Acta Physiol (Oxf)*, 192, (4) 455-469 available from: PM:18045245
- Kim, S.J., Yatani, A., Vatner, D.E., Yamamoto, S., Ishikawa, Y., Wagner, T.E., Shannon, R.P., Kim, Y.K., Takagi, G., Asai, K., Homcy, C.J., & Vatner, S.F. 1999. Differential regulation of inotropy and lusitropy in overexpressed G α myocytes through cAMP and Ca $^{2+}$ channel pathways. *J.Clin.Invest*, 103, (7) 1089-1097 available from: PM:10194482
- Kirchhof, P., Fabritz, L., Fortmuller, L., Matherne, G.P., Lankford, A., Baba, H.A., Schmitz, W., Breithardt, G., Neumann, J., & Boknik, P. 2003. Altered sinus nodal and atrioventricular nodal function in freely moving mice overexpressing the A1 adenosine receptor. *Am.J.Physiol Heart Circ.Physiol*, 285, (1) H145-H153 available from: PM:12637351
- Kleuss, C., Raw, A.S., Lee, E., Sprang, S.R., & Gilman, A.G. 1994. Mechanism of GTP hydrolysis by G-protein alpha subunits. *Proc.Natl.Acad.Sci.U.S.A*, 91, (21) 9828-9831 available from: PM:7937899
- Kobilka, B.K. 2007. G protein coupled receptor structure and activation. *Biochim.Biophys.Acta*, 1768, (4) 794-807 available from: PM:17188232
- Korte, T., Fuchs, M., Guener, Z., Bonin, J., de, S.M., Niehaus, M., Tebbenjohanns, J., & Drexler, H. 2002. In-vivo electrophysiological study in mice with chronic anterior myocardial infarction. *J.Interv.Card Electrophysiol.*, 6, (2) 121-132 available from: PM:11992022
- Kovoor, P., Wickman, K., Maguire, C.T., Pu, W., Gehrman, J., Berul, C.I., & Clapham, D.E. 2001. Evaluation of the role of I(KACh) in atrial fibrillation using a mouse knockout model. *J.Am.Coll.Cardiol.*, 37, (8) 2136-2143 available from: PM:11419900
- Kozasa, T., Itoh, H., Tsukamoto, T., & Kaziro, Y. 1988. Isolation and characterization of the human Gs alpha gene. *Proc.Natl.Acad.Sci.U.S.A*, 85, (7) 2081-2085 available from: PM:3127824

- Kubota, T., McTiernan, C.F., Frye, C.S., Slawson, S.E., Lemster, B.H., Koretsky, A.P., Demetris, A.J., & Feldman, A.M. 1997. Dilated cardiomyopathy in transgenic mice with cardiac-specific overexpression of tumor necrosis factor-alpha. *Circ.Res.*, 81, (4) 627-635 available from: PM:9314845
- Laish-Farkash, A., Glikson, M., Brass, D., Marek-Yagel, D., Pras, E., Dascal, N., Antzelevitch, C., Nof, E., Reznik, H., Eldar, M., & Luria, D. 2010. A novel mutation in the HCN4 gene causes symptomatic sinus bradycardia in Moroccan Jews. *J.Cardiovasc.Electrophysiol.*, 21, (12) 1365-1372 available from: PM:20662977
- Lan, K.L., Sarvazyan, N.A., Taussig, R., Mackenzie, R.G., DiBello, P.R., Dohlman, H.G., & Neubig, R.R. 1998. A point mutation in Galphao and Galphai1 blocks interaction with regulator of G protein signaling proteins. *J.Biol.Chem.*, 273, (21) 12794-12797 available from: PM:9582306
- Leaney, J.L. & Tinker, A. 2000. The role of members of the pertussis toxin-sensitive family of G proteins in coupling receptors to the activation of the G protein-gated inwardly rectifying potassium channel. *Proc.Natl.Acad.Sci.U.S.A.*, 97, (10) 5651-5656 available from: PM:10779550
- Lewis, T. 1933. Diseases of the heart described for the practitioners and students.
- Li, T., Vu, T.H., Zeng, Z.L., Nguyen, B.T., Hayward, B.E., Bonthron, D.T., Hu, J.F., & Hoffman, A.R. 2000. Tissue-specific expression of antisense and sense transcripts at the imprinted Gnas locus. *Genomics*, 69, (3) 295-304 available from: PM:11056047
- Liu, J., Litman, D., Rosenberg, M.J., Yu, S., Biesecker, L.G., & Weinstein, L.S. 2000. A GNAS1 imprinting defect in pseudohypoparathyroidism type IB. *J.Clin.Invest*, 106, (9) 1167-1174 available from: PM:11067869
- Lloyd-Jones, D.M., Larson, M.G., Beiser, A., & Levy, D. 1999. Lifetime risk of developing coronary heart disease. *Lancet*, 353, (9147) 89-92 available from: PM:10023892
- Logothetis, D.E., Kurachi, Y., Galper, J., Neer, E.J., & Clapham, D.E. 1987. The beta gamma subunits of GTP-binding proteins activate the muscarinic K⁺ channel in heart. *Nature*, 325, (6102) 321-326 available from: PM:2433589
- Lohmeier, T.E. 2012. Angiotensin II infusion model of hypertension: is there an important sympathetic component? *Hypertension*, 59, (3) 539-541 available from: PM:22275539
- Lorenz, J.N. & Robbins, J. 1997. Measurement of intraventricular pressure and cardiac performance in the intact closed-chest anesthetized mouse. *Am.J.Physiol.*, 272, (3 Pt 2) H1137-H1146 available from: PM:9087586
- Ludwig, A., Zong, X., Jeglitsch, M., Hofmann, F., & Biel, M. 1998. A family of hyperpolarization-activated mammalian cation channels. *Nature*, 393, (6685) 587-591 available from: PM:9634236

- Lugenbiel, P., Bauer, A., Kelemen, K., Schweizer, P.A., Becker, R., Katus, H.A., & Thomas, D. 2012. Biological Heart Rate Reduction Through Genetic Suppression of Galpha(s) Protein in the Sinoatrial Node. *J.Am.Heart Assoc.*, 1, (2) available from: PM:23130123
- Magagnin, V., Bassani, T., Bari, V., Turiel, M., Maestri, R., Pinna, G.D., & Porta, A. 2011. Non-stationarities significantly distort short-term spectral, symbolic and entropy heart rate variability indices. *Physiol Meas.*, 32, (11) 1775-1786 available from: PM:22027399
- Maillet, M., van Berlo, J.H., & Molkenin, J.D. 2013. Molecular basis of physiological heart growth: fundamental concepts and new players. *Nat.Rev.Mol.Cell Biol.*, 14, (1) 38-48 available from: PM:23258295
- Maltsev, V.A. & Lakatta, E.G. 2008. Dynamic interactions of an intracellular Ca²⁺ clock and membrane ion channel clock underlie robust initiation and regulation of cardiac pacemaker function. *Cardiovasc.Res.*, 77, (2) 274-284 available from: PM:18006441
- McCudden, C.R., Hains, M.D., Kimple, R.J., Siderovski, D.P., & Willard, F.S. 2005. G-protein signaling: back to the future. *Cell Mol.Life Sci.*, 62, (5) 551-577 available from: PM:15747061
- Michael, L.H., Ballantyne, C.M., Zachariah, J.P., Gould, K.E., Pocius, J.S., Taffet, G.E., Hartley, C.J., Pham, T.T., Daniel, S.L., Funk, E., & Entman, M.L. 1999. Myocardial infarction and remodeling in mice: effect of reperfusion. *Am.J.Physiol*, 277, (2 Pt 2) H660-H668 available from: PM:10444492
- Michael, L.H., Entman, M.L., Hartley, C.J., Youker, K.A., Zhu, J., Hall, S.R., Hawkins, H.K., Berens, K., & Ballantyne, C.M. 1995. Myocardial ischemia and reperfusion: a murine model. *Am.J.Physiol*, 269, (6 Pt 2) H2147-H2154 available from: PM:8594926
- Milano, C.A., Allen, L.F., Rockman, H.A., Dolber, P.C., McMinn, T.R., Chien, K.R., Johnson, T.D., Bond, R.A., & Lefkowitz, R.J. 1994a. Enhanced myocardial function in transgenic mice overexpressing the beta 2-adrenergic receptor. *Science*, 264, (5158) 582-586 available from: PM:8160017
- Milano, C.A., Dolber, P.C., Rockman, H.A., Bond, R.A., Venable, M.E., Allen, L.F., & Lefkowitz, R.J. 1994b. Myocardial expression of a constitutively active alpha 1B-adrenergic receptor in transgenic mice induces cardiac hypertrophy. *Proc.Natl.Acad.Sci.U.S.A*, 91, (21) 10109-10113 available from: PM:7937846
- Milligan, G. & Kostenis, E. 2006. Heterotrimeric G-proteins: a short history. *Br.J.Pharmacol.*, 147 Suppl 1, S46-S55 available from: PM:16402120
- Mittmann, C., Chung, C.H., Hoppner, G., Michalek, C., Nose, M., Schuler, C., Schuh, A., Eschenhagen, T., Weil, J., Pieske, B., Hirt, S., & Wieland, T. 2002. Expression of ten RGS proteins in human myocardium: functional characterization of an upregulation of RGS4 in heart failure. *Cardiovasc.Res.*, 55, (4) 778-786 available from: PM:12176127

- Monfredi, O., Dobrzynski, H., Mondal, T., Boyett, M.R., & Morris, G.M. 2010. The anatomy and physiology of the sinoatrial node--a contemporary review. *Pacing Clin.Electrophysiol.*, 33, (11) 1392-1406 available from: PM:20946278
- Moosmang, S., Stieber, J., Zong, X., Biel, M., Hofmann, F., & Ludwig, A. 2001. Cellular expression and functional characterization of four hyperpolarization-activated pacemaker channels in cardiac and neuronal tissues. *Eur.J.Biochem.*, 268, (6) 1646-1652 available from: PM:11248683
- Nagata, K., Ye, C., Jain, M., Milstone, D.S., Liao, R., & Mortensen, R.M. 2000. Galpha(i2) but not Galpha(i3) is required for muscarinic inhibition of contractility and calcium currents in adult cardiomyocytes. *Circ.Res.*, 87, (10) 903-909 available from: PM:11073886
- Nerbonne, J.M., Nichols, C.G., Schwarz, T.L., & Escande, D. 2001. Genetic manipulation of cardiac K(+) channel function in mice: what have we learned, and where do we go from here? *Circ.Res.*, 89, (11) 944-956 available from: PM:11717150
- Neumann, J., Schmitz, W., Scholz, H., von, M.L., Doring, V., & Kalmar, P. 1988. Increase in myocardial Gi-proteins in heart failure. *Lancet*, 2, (8617) 936-937 available from: PM:2902384
- Noble, D. 1960. Cardiac action and pacemaker potentials based on the Hodgkin-Huxley equations. *Nature*, 188, 495-497 available from: PM:13729365
- Northup, J.K., Sternweis, P.C., Smigel, M.D., Schleifer, L.S., Ross, E.M., & Gilman, A.G. 1980. Purification of the regulatory component of adenylate cyclase. *Proc.Natl.Acad.Sci.U.S.A.*, 77, (11) 6516-6520 available from: PM:6935665
- Nuyens, D., Stengl, M., Dugarmaa, S., Rossenbacker, T., Compennolle, V., Rudy, Y., Smits, J.F., Flameng, W., Clancy, C.E., Moons, L., Vos, M.A., Dewerchin, M., Benndorf, K., Collen, D., Carmeliet, E., & Carmeliet, P. 2001. Abrupt rate accelerations or premature beats cause life-threatening arrhythmias in mice with long-QT3 syndrome. *Nat.Med.*, 7, (9) 1021-1027 available from: PM:11533705
- Ochi, R., Momose, Y., Oyama, K., & Giles, W.R. 2006. Sphingosine-1-phosphate effects on guinea pig atrial myocytes: Alterations in action potentials and K⁺ currents. *Cardiovasc.Res.*, 70, (1) 88-96 available from: PM:16545787
- Odashima, M., Usui, S., Takagi, H., Hong, C., Liu, J., Yokota, M., & Sadoshima, J. 2007. Inhibition of endogenous Mst1 prevents apoptosis and cardiac dysfunction without affecting cardiac hypertrophy after myocardial infarction. *Circ.Res.*, 100, (9) 1344-1352 available from: PM:17395874
- Oldham, W.M. & Hamm, H.E. 2008. Heterotrimeric G protein activation by G-protein-coupled receptors. *Nat.Rev.Mol.Cell Biol.*, 9, (1) 60-71 available from: PM:18043707
- Ono, K., Masumiya, H., Sakamoto, A., Christe, G., Shijuku, T., Tanaka, H., Shigenobu, K., & Ozaki, Y. 2001. Electrophysiological analysis of the negative chronotropic effect of endothelin-1 in rabbit sinoatrial node cells. *J.Physiol*, 537, (Pt 2) 467-488 available from: PM:11731579

- Ono, K., Tsujimoto, G., Sakamoto, A., Eto, K., Masaki, T., Ozaki, Y., & Satake, M. 1994. Endothelin-A receptor mediates cardiac inhibition by regulating calcium and potassium currents. *Nature*, 370, (6487) 301-304 available from: PM:8035879
- Overington, J.P., Al-Lazikani, B., & Hopkins, A.L. 2006. How many drug targets are there? *Nat.Rev.Drug Discov.*, 5, (12) 993-996 available from: PM:17139284
- Owen, V.J., Burton, P.B., Mullen, A.J., Birks, E.J., Barton, P., & Yacoub, M.H. 2001. Expression of RGS3, RGS4 and Gi alpha 2 in acutely failing donor hearts and end-stage heart failure. *Eur.Heart J.*, 22, (12) 1015-1020 available from: PM:11428836
- Park, H.J., Georgescu, S.P., Du, C., Madias, C., Aronovitz, M.J., Welzig, C.M., Wang, B., Begley, U., Zhang, Y., Blaustein, R.O., Patten, R.D., Karas, R.H., Van Tol, H.H., Osborne, T.F., Shimano, H., Liao, R., Link, M.S., & Galper, J.B. 2008. Parasympathetic response in chick myocytes and mouse heart is controlled by SREBP. *J.Clin.Invest.*, 118, (1) 259-271 available from: PM:18060044
- Patten, R.D., Aronovitz, M.J., Deras-Mejia, L., Pandian, N.G., Hanak, G.G., Smith, J.J., Mendelsohn, M.E., & Konstam, M.A. 1998. Ventricular remodeling in a mouse model of myocardial infarction. *Am.J.Physiol.*, 274, (5 Pt 2) H1812-H1820 available from: PM:9612394
- Patten, R.D. & Hall-Porter, M.R. 2009. Small animal models of heart failure: development of novel therapies, past and present. *Circ.Heart Fail.*, 2, (2) 138-144 available from: PM:19808329
- Peters, J., Wroe, S.F., Wells, C.A., Miller, H.J., Bodle, D., Beechey, C.V., Williamson, C.M., & Kelsey, G. 1999. A cluster of oppositely imprinted transcripts at the Gnas locus in the distal imprinting region of mouse chromosome 2. *Proc.Natl.Acad.Sci.U.S.A.*, 96, (7) 3830-3835 available from: PM:10097123
- Pizza, M., Bartoloni, A., Prugnola, A., Silvestri, S., & Rappuoli, R. 1988. Subunit S1 of pertussis toxin: mapping of the regions essential for ADP-ribosyltransferase activity. *Proc.Natl.Acad.Sci.U.S.A.*, 85, (20) 7521-7525 available from: PM:2902632
- Pollick, C., Hale, S.L., & Kloner, R.A. 1995. Echocardiographic and cardiac Doppler assessment of mice. *J.Am.Soc.Echocardiogr.*, 8, (5 Pt 1) 602-610 available from: PM:9417202
- Pruvot, E., Thonet, G., Vesin, J.M., van-Melle, G., Seidl, K., Schmidinger, H., Brachmann, J., Jung, W., Hoffmann, E., Tavernier, R., Block, M., Podczeck, A., & Fromer, M. 2000. Heart rate dynamics at the onset of ventricular tachyarrhythmias as retrieved from implantable cardioverter-defibrillators in patients with coronary artery disease. *Circulation*, 101, (20) 2398-2404 available from: PM:10821817
- Pumpkala, J., Howorka, K., Groves, D., Chester, M., & Nolan, J. 2002. Functional assessment of heart rate variability: physiological basis and practical applications. *Int.J.Cardiol.*, 84, (1) 1-14 available from: PM:12104056
- Rea, M.E. & Dunlap, M.E. 2008. Renal hemodynamics in heart failure: implications for treatment. *Curr.Opin.Nephrol.Hypertens.*, 17, (1) 87-92 available from: PM:18090676

- Reik, W. & Walter, J. 2001. Genomic imprinting: parental influence on the genome. *Nat.Rev.Genet.*, 2, (1) 21-32 available from: PM:11253064
- Reiss, K., Cheng, W., Ferber, A., Kajstura, J., Li, P., Li, B., Olivetti, G., Homcy, C.J., Baserga, R., & Anversa, P. 1996. Overexpression of insulin-like growth factor-1 in the heart is coupled with myocyte proliferation in transgenic mice. *Proc.Natl.Acad.Sci.U.S.A*, 93, (16) 8630-8635 available from: PM:8710922
- Remme, C.A. 2013. Transgenic models of cardiac arrhythmias and sudden death. *Front Physiol*, 4, 60 available from: PM:23544029
- Reuveny, E., Slesinger, P.A., Inglese, J., Morales, J.M., Iniguez-Lluhi, J.A., Lefkowitz, R.J., Bourne, H.R., Jan, Y.N., & Jan, L.Y. 1994. Activation of the cloned muscarinic potassium channel by G protein beta gamma subunits. *Nature*, 370, (6485) 143-146 available from: PM:8022483
- Riddle, E.L., Schwartzman, R.A., Bond, M., & Insel, P.A. 2005. Multi-tasking RGS proteins in the heart: the next therapeutic target? *Circ.Res.*, 96, (4) 401-411 available from: PM:15746448
- Robinson, R.B. & Siegelbaum, S.A. 2003. Hyperpolarization-activated cation currents: from molecules to physiological function. *Annu.Rev.Physiol*, 65, 453-480 available from: PM:12471170
- Robishaw, J.D. & Foster, K.A. 1989. Role of G proteins in the regulation of the cardiovascular system. *Annu.Rev.Physiol*, 51, 229-244 available from: PM:2565700
- Robishaw, J.D. & Hansen, C.A. 1994. Structure and function of G proteins mediating signal transduction pathways in the heart. *Alcohol Clin.Exp.Res.*, 18, (1) 115-120 available from: PM:8198206
- Rockman, H.A., Hamilton, R.A., Jones, L.R., Milano, C.A., Mao, L., & Lefkowitz, R.J. 1996. Enhanced myocardial relaxation in vivo in transgenic mice overexpressing the beta2-adrenergic receptor is associated with reduced phospholamban protein. *J.Clin.Invest*, 97, (7) 1618-1623 available from: PM:8601626
- Rockman, H.A., Koch, W.J., & Lefkowitz, R.J. 1997. Cardiac function in genetically engineered mice with altered adrenergic receptor signaling. *Am.J.Physiol*, 272, (4 Pt 2) H1553-H1559 available from: PM:9139936
- Rockman, H.A., Koch, W.J., & Lefkowitz, R.J. 2002. Seven-transmembrane-spanning receptors and heart function. *Nature*, 415, (6868) 206-212 available from: PM:11805844
- Rockman, H.A., Ross, R.S., Harris, A.N., Knowlton, K.U., Steinhilper, M.E., Field, L.J., Ross, J., Jr., & Chien, K.R. 1991. Segregation of atrial-specific and inducible expression of an atrial natriuretic factor transgene in an in vivo murine model of cardiac hypertrophy. *Proc.Natl.Acad.Sci.U.S.A*, 88, (18) 8277-8281 available from: PM:1832775
- Rockman, H.A., Wachhorst, S.P., Mao, L., & Ross, J., Jr. 1994. ANG II receptor blockade prevents ventricular hypertrophy and ANF gene expression with pressure

overload in mice. *Am.J.Physiol*, 266, (6 Pt 2) H2468-H2475 available from: PM:8024008

Rodbell, M. 1980. The role of hormone receptors and GTP-regulatory proteins in membrane transduction. *Nature*, 284, (5751) 17-22 available from: PM:6101906

Rodbell, M. 1995. Signal transduction: evolution of an idea. *Environ.Health Perspect.*, 103, (4) 338-345 available from: PM:7607133

Roger, V.L., Go, A.S., Lloyd-Jones, D.M., Adams, R.J., Berry, J.D., Brown, T.M., Camethon, M.R., Dai, S., de Simone, G., Ford, E.S., Fox, C.S., Fullerton, H.J., Gillespie, C., Greenlund, K.J., Hailpem, S.M., Heit, J.A., Ho, P.M., Howard, V.J., Kissela, B.M., Kittner, S.J., Lackland, D.T., Lichtman, J.H., Lisabeth, L.D., Makuc, D.M., Marcus, G.M., Marelli, A., Matchar, D.B., McDermott, M.M., Meigs, J.B., Moy, C.S., Mozaffarian, D., Mussolino, M.E., Nichol, G., Paynter, N.P., Rosamond, W.D., Sorlie, P.D., Stafford, R.S., Turan, T.N., Turner, M.B., Wong, N.D., & Wylie-Rosett, J. 2011. Heart Disease and Stroke Statistics-2011 Update A Report From the American Heart Association. *Circulation*, 123, (4) E18-E209 available from: ISI:000286727900001

Rogers, J.H., Tamirisa, P., Kovacs, A., Weinheimer, C., Courtois, M., Blumer, K.J., Kelly, D.P., & Muslin, A.J. 1999. RGS4 causes increased mortality and reduced cardiac hypertrophy in response to pressure overload. *J.Clin.Invest*, 104, (5) 567-576 available from: PM:10487771

Ross, E.M. & Wilkie, T.M. 2000. GTPase-activating proteins for heterotrimeric G proteins: regulators of G protein signaling (RGS) and RGS-like proteins. *Annu.Rev.Biochem.*, 69, 795-827 available from: PM:10966476

Ross, J., Jr. 2002. Dilated cardiomyopathy: concepts derived from gene deficient and transgenic animal models. *Circ.J.*, 66, (3) 219-224 available from: PM:11922267

Roth, D.A., Urasawa, K., Helmer, G.A., & Hammond, H.K. 1993. Downregulation of cardiac guanosine 5'-triphosphate-binding proteins in right atrium and left ventricle in pacing-induced congestive heart failure. *J.Clin.Invest*, 91, (3) 939-949 available from: PM:8383705

Rottman, J.N., Ni, G., & Brown, M. 2007. Echocardiographic evaluation of ventricular function in mice. *Echocardiography.*, 24, (1) 83-89 available from: PM:17214630

Roy, A.A., Lemberg, K.E., & Chidiac, P. 2003. Recruitment of RGS2 and RGS4 to the plasma membrane by G proteins and receptors reflects functional interactions. *Mol.Pharmacol.*, 64, (3) 587-593 available from: PM:12920194

Rudolph, U., Spicher, K., & Birnbaumer, L. 1996. Adenylyl cyclase inhibition and altered G protein subunit expression and ADP-ribosylation patterns in tissues and cells from Gi2 alpha-/-mice. *Proc.Natl.Acad.Sci.U.S.A*, 93, (8) 3209-3214 available from: PM:8622915

- Sadja, R., Alagem, N., & Reuveny, E. 2003. Gating of GIRK channels: details of an intricate, membrane-delimited signaling complex. *Neuron*, 39, (1) 9-12 available from: PM:12848928
- Sahn, D.J., DeMaria, A., Kisslo, J., & Weyman, A. 1978. Recommendations regarding quantitation in M-mode echocardiography: results of a survey of echocardiographic measurements. *Circulation*, 58, (6) 1072-1083 available from: PM:709763
- Salama, G. & London, B. 2007. Mouse models of long QT syndrome. *J.Physiol*, 578, (Pt 1) 43-53 available from: PM:17038432
- Schulze-Bahr, E., Neu, A., Friederich, P., Kaupp, U.B., Breithardt, G., Pongs, O., & Isbrandt, D. 2003. Pacemaker channel dysfunction in a patient with sinus node disease. *J.Clin.Invest*, 111, (10) 1537-1545 available from: PM:12750403
- Schuster, E.H. & Bulkley, B.H. 1979. Expansion of transmural myocardial infarction: a pathophysiologic factor in cardiac rupture. *Circulation*, 60, (7) 1532-1538 available from: PM:498481
- Sebastian, S., Ang, R., Abramowitz, J., Weinstein, L.S., Chen, M., Ludwig, A., Birnbaumer, L., & Tinker, A. 2013. The in vivo regulation of heart rate in the murine sinoatrial node by stimulatory and inhibitory heterotrimeric G proteins. *Am.J.Physiol Regul.Integr.Comp Physiol*, 305, (4) R435-R442 available from: PM:23697798
- Sethi, R., Bector, N., Takeda, N., Nagano, M., Jasmin, G., & Dhalla, N.S. 1994. Alterations in G-proteins in congestive heart failure in cardiomyopathic (UM-X7.1) hamsters. *Mol.Cell Biochem.*, 140, (2) 163-170 available from: PM:7898487
- Sethi, R., Elimban, V., Chapman, D., Dixon, I.M., & Dhalla, N.S. 1998. Differential alterations in left and right ventricular G-proteins in congestive heart failure due to myocardial infarction. *J.Mol.Cell Cardiol.*, 30, (11) 2153-2163 available from: PM:9925353
- Sharpe, N. 1992. Ventricular remodeling following myocardial infarction. *Am.J.Cardiol.*, 70, (10) 20C-26C available from: PM:1414891
- Shibata, N., Inada, S., Mitsui, K., Honjo, H., Yamamoto, M., Niwa, R., Boyett, M.R., & Kodama, I. 2001. Pacemaker shift in the rabbit sinoatrial node in response to vagal nerve stimulation. *Exp.Physiol*, 86, (2) 177-184 available from: PM:11429632
- Siderovski, D.P., Hessel, A., Chung, S., Mak, T.W., & Tyers, M. 1996. A new family of regulators of G-protein-coupled receptors? *Curr.Biol.*, 6, (2) 211-212 available from: PM:8673468
- Snabaitis, A.K., Muntendorf, A., Wieland, T., & Avkiran, M. 2005. Regulation of the extracellular signal-regulated kinase pathway in adult myocardium: differential roles of G(q/11), Gi and G(12/13) proteins in signalling by alpha1-adrenergic, endothelin-1 and thrombin-sensitive protease-activated receptors. *Cell Signal.*, 17, (5) 655-664 available from: PM:15683740
- Sowell, M.O., Ye, C., Ricupero, D.A., Hansen, S., Quinn, S.J., Vassilev, P.M., & Mortensen, R.M. 1997. Targeted inactivation of alpha12 or alpha13 disrupts activation

of the cardiac muscarinic K⁺ channel, IK_{ACh}, in intact cells. *Proc.Natl.Acad.Sci.U.S.A*, 94, (15) 7921-7926 available from: PM:9223288

Splawski, I., Timothy, K.W., Sharpe, L.M., Decher, N., Kumar, P., Bloise, R., Napolitano, C., Schwartz, P.J., Joseph, R.M., Condouris, K., Tager-Flusberg, H., Priori, S.G., Sanguinetti, M.C., & Keating, M.T. 2004. Ca(V)_{1.2} calcium channel dysfunction causes a multisystem disorder including arrhythmia and autism. *Cell*, 119, (1) 19-31 available from: PM:15454078

Stanley, W.C., Recchia, F.A., & Lopaschuk, G.D. 2005. Myocardial substrate metabolism in the normal and failing heart. *Physiol Rev.*, 85, (3) 1093-1129 available from: PM:15987803

Stauss, H.M. 2003. Heart rate variability. *Am.J.Physiol Regul.Integr.Comp Physiol*, 285, (5) R927-R931 available from: PM:14557228

Stein, K.M., Borer, J.S., Okin, P.M., & Kligfield, P. 1992. Prognostic value of heart rate variability measures in patients with chronic, nonischemic mitral regurgitation. *J.Electrocardiol.*, 25 Suppl, 220 available from: PM:1297700

Strungs, E.G., Ongstad, E.L., O'Quinn, M.P., Palatinus, J.A., Jourdan, L.J., & Gourdie, R.G. 2013. Cryoinjury models of the adult and neonatal mouse heart for studies of scarring and regeneration. *Methods Mol.Biol.*, 1037, 343-353 available from: PM:24029946

Sutton, M.G. & Sharpe, N. 2000. Left ventricular remodeling after myocardial infarction: pathophysiology and therapy. *Circulation*, 101, (25) 2981-2988 available from: PM:10869273

Swedberg, K., Komajda, M., Bohm, M., Borer, J.S., Ford, I., Dubost-Brama, A., Lerebours, G., & Tavazzi, L. 2010. Ivabradine and outcomes in chronic heart failure (SHIFT): a randomised placebo-controlled study. *Lancet*, 376, (9744) 875-885 available from: PM:20801500

Swoap, S.J., Li, C., Wess, J., Parsons, A.D., Williams, T.D., & Overton, J.M. 2008. Vagal tone dominates autonomic control of mouse heart rate at thermoneutrality. *Am.J.Physiol Heart Circ.Physiol*, 294, (4) H1581-H1588 available from: PM:18245567

Syed, F., Diwan, A., & Hahn, H.S. 2005. Murine echocardiography: a practical approach for phenotyping genetically manipulated and surgically modeled mice. *J.Am.Soc.Echocardiogr.*, 18, (9) 982-990 available from: PM:16153531

Takahashi, T., Tang, T., Lai, N.C., Roth, D.M., Rebolledo, B., Saito, M., Lew, W.Y., Clopton, P., & Hammond, H.K. 2006. Increased cardiac adenylyl cyclase expression is associated with increased survival after myocardial infarction. *Circulation*, 114, (5) 388-396 available from: PM:16864723

Tamirisa, P., Blumer, K.J., & Muslin, A.J. 1999. RGS4 inhibits G-protein signaling in cardiomyocytes. *Circulation*, 99, (3) 441-447 available from: PM:9918533

- Tanaka, N., Dalton, N., Mao, L., Rockman, H.A., Peterson, K.L., Gottshall, K.R., Hunter, J.J., Chien, K.R., & Ross, J., Jr. 1996. Transthoracic echocardiography in models of cardiac disease in the mouse. *Circulation*, 94, (5) 1109-1117 available from: PM:8790053
- Tang, K.M., Wang, G.R., Lu, P., Karas, R.H., Aronovitz, M., Heximer, S.P., Kaltenbronn, K.M., Blumer, K.J., Siderovski, D.P., Zhu, Y., & Mendelsohn, M.E. 2003. Regulator of G-protein signaling-2 mediates vascular smooth muscle relaxation and blood pressure. *Nat.Med.*, 9, (12) 1506-1512 available from: PM:14608379
- Tarnavski, O., McMullen, J.R., Schinke, M., Nie, Q., Kong, S., & Izumo, S. 2004. Mouse cardiac surgery: comprehensive techniques for the generation of mouse models of human diseases and their application for genomic studies. *Physiol Genomics*, 16, (3) 349-360 available from: PM:14679301
- Teichholz, L.E., Cohen, M.V., Sonnenblick, E.H., & Gorlin, R. 1974. Study of left ventricular geometry and function by B-scan ultrasonography in patients with and without asynergy. *N.Engl.J.Med.*, 291, (23) 1220-1226 available from: PM:4473184
- Thayer, J.F., Yamamoto, S.S., & Brosschot, J.F. 2010. The relationship of autonomic imbalance, heart rate variability and cardiovascular disease risk factors. *Int.J.Cardiol.*, 141, (2) 122-131 available from: PM:19910061
- Thireau, J., Zhang, B.L., Poisson, D., & Babuty, D. 2008. Heart rate variability in mice: a theoretical and practical guide. *Exp.Physiol*, 93, (1) 83-94 available from: PM:17911354
- Tinker, A. 2006. The selective interactions and functions of regulators of G-protein signalling. *Semin.Cell Dev.Biol.*, 17, (3) 377-382 available from: PM:16675274
- Uechi, M., Asai, K., Osaka, M., Smith, A., Sato, N., Wagner, T.E., Ishikawa, Y., Hayakawa, H., Vatner, D.E., Shannon, R.P., Homcy, C.J., & Vatner, S.F. 1998. Depressed heart rate variability and arterial baroreflex in conscious transgenic mice with overexpression of cardiac G α . *Circ.Res.*, 82, (4) 416-423 available from: PM:9506701
- Vacek, T.P., Sen, U., Tyagi, N., Vacek, J.C., Kumar, M., Hughes, W.M., Passmore, J.C., & Tyagi, S.C. 2009. Differential expression of Gs in a murine model of homocysteinemic heart failure. *Vasc.Health Risk Manag.*, 5, (1) 79-84 available from: PM:19436674
- Vaidya, D., Morley, G.E., Samie, F.H., & Jalife, J. 1999. Reentry and fibrillation in the mouse heart. A challenge to the critical mass hypothesis. *Circ.Res.*, 85, (2) 174-181 available from: PM:10417399
- Valenzuela, D., Han, X., Mende, U., Fankhauser, C., Mashimo, H., Huang, P., Pfeffer, J., Neer, E.J., & Fishman, M.C. 1997. G α (o) is necessary for muscarinic regulation of Ca²⁺ channels in mouse heart. *Proc.Natl.Acad.Sci.U.S.A*, 94, (5) 1727-1732 available from: PM:9050846
- van den Borne, S.W., van de Schans, V.A., Strzelecka, A.E., Vervoort-Peters, H.T., Lijnen, P.M., Cleutjens, J.P., Smits, J.F., Daemen, M.J., Janssen, B.J., & Blankesteijn,

- W.M. 2009. Mouse strain determines the outcome of wound healing after myocardial infarction. *Cardiovasc.Res.*, 84, (2) 273-282 available from: PM:19542177
- van den Bos, E.J., Mees, B.M., de Waard, M.C., de, C.R., & Duncker, D.J. 2005. A novel model of cryoinjury-induced myocardial infarction in the mouse: a comparison with coronary artery ligation. *Am.J.Physiol Heart Circ.Physiol*, 289, (3) H1291-H1300 available from: PM:15863462
- Van Laake, L.W., Passier, R., Monshouwer-Kloots, J., Nederhoff, M.G., Ward-van, O.D., Field, L.J., van Echteld, C.J., Doevendans, P.A., & Mummery, C.L. 2007. Monitoring of cell therapy and assessment of cardiac function using magnetic resonance imaging in a mouse model of myocardial infarction. *Nat.Protoc.*, 2, (10) 2551-2567 available from: PM:17947998
- Vinogradova, T.M., Bogdanov, K.Y., & Lakatta, E.G. 2002. Novel perspectives on the beating rate of the heart. *Circ.Res.*, 91, (4) e3 available from: PM:12193471
- Vivaudou, M., Chan, K. W., Sui, J. L., Jan, L. Y., Reuveny, E., & Logothetis, D. E. Probing the G-protein regulation of GIRK1 and GIRK4, the two subunits of the K-ACh channel, using functional homomeric mutants. *J.Biol.Chem.* 272[50], 31553-31560. 1997.
Ref Type: Journal (Full)
- Voelkl, J.G., Haubner, B.J., Kremser, C., Mayr, A., Klug, G., Loizides, A., Muller, S., Pachinger, O., Schocke, M., & Metzler, B. 2011. Cardiac imaging using clinical 1.5 t MRI scanners in a murine ischemia/reperfusion model. *J.Biomed.Biotechnol.*, 2011, 185683 available from: PM:21151667
- Wakimoto, H., Maguire, C.T., Kovoov, P., Hammer, P.E., Gehrmann, J., Triedman, J.K., & Berul, C.I. 2001. Induction of atrial tachycardia and fibrillation in the mouse heart. *Cardiovasc.Res.*, 50, (3) 463-473 available from: PM:11376622
- Wehrens, X.H., Lehnart, S.E., Reiken, S., Vest, J.A., Wronska, A., & Marks, A.R. 2006. Ryanodine receptor/calcium release channel PKA phosphorylation: a critical mediator of heart failure progression. *Proc.Natl.Acad.Sci.U.S.A*, 103, (3) 511-518 available from: PM:16407108
- Weinstein, L.S. 2001. The stimulatory G protein alpha-subunit gene: mutations and imprinting lead to complex phenotypes. *J.Clin.Endocrinol.Metab*, 86, (10) 4622-4626 available from: PM:11600514
- Weinstein, L.S., Liu, J., Sakamoto, A., Xie, T., & Chen, M. 2004. Minireview: GNAS: normal and abnormal functions. *Endocrinology*, 145, (12) 5459-5464 available from: PM:15331575
- Weinstein, L.S., Xie, T., Zhang, Q.H., & Chen, M. 2007. Studies of the regulation and function of the Gs alpha gene Gnas using gene targeting technology. *Pharmacol.Ther.*, 115, (2) 271-291 available from: PM:17588669
- Weinstein, L.S., Yu, S., Warner, D.R., & Liu, J. 2001. Endocrine manifestations of stimulatory G protein alpha-subunit mutations and the role of genomic imprinting. *Endocr.Rev.*, 22, (5) 675-705 available from: PM:11588148

- Wettschureck, N. & Offermanns, S. 2005. Mammalian G proteins and their cell type specific functions. *Physiol Rev.*, 85, (4) 1159-1204 available from: PM:16183910
- Whiteway, M., Hougan, L., Dignard, D., Thomas, D.Y., Bell, L., Saari, G.C., Grant, F.J., O'Hara, P., & MacKay, V.L. 1989. The STE4 and STE18 genes of yeast encode potential beta and gamma subunits of the mating factor receptor-coupled G protein. *Cell*, 56, (3) 467-477 available from: PM:2536595
- Wickman, K., Nemec, J., Gendler, S.J., & Clapham, D.E. 1998. Abnormal heart rate regulation in GIRK4 knockout mice. *Neuron*, 20, (1) 103-114
- Wickman, K.D. & Clapham, D.E. 1995. G-protein regulation of ion channels. *Curr.Opin.Neurobiol.*, 5, (3) 278-285 available from: PM:7580149
- Wickman, K.D., Iniguez-Lluhl, J.A., Davenport, P.A., Taussig, R., Krapivinsky, G.B., Linder, M.E., Gilman, A.G., & Clapham, D.E. 1994. Recombinant G-protein beta gamma-subunits activate the muscarinic-gated atrial potassium channel. *Nature*, 368, (6468) 255-257 available from: PM:8145826
- Wieland, T. & Mittmann, C. 2003. Regulators of G-protein signalling: multifunctional proteins with impact on signalling in the cardiovascular system. *Pharmacol.Ther.*, 97, (2) 95-115 available from: PM:12559385
- Wong, Y.H., Federman, A., Pace, A.M., Zachary, I., Evans, T., Pouyssegur, J., & Bourne, H.R. 1991. Mutant alpha subunits of Gi2 inhibit cyclic AMP accumulation. *Nature*, 351, (6321) 63-65 available from: PM:1851251
- Woo, A.Y. & Xiao, R.P. 2012. beta-Adrenergic receptor subtype signaling in heart: from bench to bedside. *Acta Pharmacol.Sin.*, 33, (3) 335-341 available from: PM:22286918
- Xiao, R.P., Ji, X., & Lakatta, E.G. 1995. Functional coupling of the beta 2-adrenoceptor to a pertussis toxin-sensitive G protein in cardiac myocytes. *Mol.Pharmacol.*, 47, (2) 322-329 available from: PM:7870040
- Xiao, R.P., Zhang, S.J., Chakir, K., Avdonin, P., Zhu, W., Bond, R.A., Balke, C.W., Lakatta, E.G., & Cheng, H. 2003. Enhanced G(i) signaling selectively negates beta2-adrenergic receptor (AR)--but not beta1-AR-mediated positive inotropic effect in myocytes from failing rat hearts. *Circulation*, 108, (13) 1633-1639 available from: PM:12975249
- Yamada, M., Inanobe, A., & Kurachi, Y. 1998. G protein regulation of potassium ion channels. *Pharmacol.Rev.*, 50, (4) 723-760 available from: PM:9860808
- Yang, X.P., Liu, Y.H., Rhaleb, N.E., Kurihara, N., Kim, H.E., & Carretero, O.A. 1999. Echocardiographic assessment of cardiac function in conscious and anesthetized mice. *Am.J.Physiol*, 277, (5 Pt 2) H1967-H1974 available from: PM:10564153
- Yatani, A., Mattera, R., Codina, J., Graf, R., Okabe, K., Padrell, E., Iyengar, R., Brown, A.M., & Birnbaumer, L. 1988. The G protein-gated atrial K⁺ channel is stimulated by three distinct Gi alpha-subunits. *Nature*, 336, (6200) 680-682 available from: PM:3143915

- Ye, C., Sowell, M.O., Vassilev, P.M., Milstone, D.S., & Mortensen, R.M. 1999. Galpha(i2), Galpha(i3) and Galpha(o) are all required for normal muscarinic inhibition of the cardiac calcium channels in nodal/atrial-like cultured cardiocytes. *J.Mol.Cell Cardiol.*, 31, (9) 1771-1781 available from: PM:10471359
- Yu, S., Yu, D., Lee, E., Eckhaus, M., Lee, R., Corria, Z., Accili, D., Westphal, H., & Weinstein, L.S. 1998. Variable and tissue-specific hormone resistance in heterotrimeric Gs protein alpha-subunit (Galpha) knockout mice is due to tissue-specific imprinting of the galpha gene. *Proc.Natl.Acad.Sci.U.S.A.*, 95, (15) 8715-8720 available from: PM:9671744
- Yutzey, K.E. & Robbins, J. 2007. Principles of genetic murine models for cardiac disease. *Circulation*, 115, (6) 792-799 available from: PM:17296868
- Zhang, H. & Vassalle, M. 2001. Role of I(K) and I(f) in the pacemaker mechanisms of sino-atrial node myocytes. *Can.J.Physiol Pharmacol.*, 79, (12) 963-976 available from: PM:11824940
- Zhang, R., Khoo, M.S., Wu, Y., Yang, Y., Grueter, C.E., Ni, G., Price, E.E., Jr., Thiel, W., Guatimosim, S., Song, L.S., Madu, E.C., Shah, A.N., Vishnivetskaya, T.A., Atkinson, J.B., Gurevich, V.V., Salama, G., Lederer, W.J., Colbran, R.J., & Anderson, M.E. 2005. Calmodulin kinase II inhibition protects against structural heart disease. *Nat.Med.*, 11, (4) 409-417 available from: PM:15793582
- Zhang, Y.H., Hinde, A.K., & Hancox, J.C. 2001. Anti-adrenergic effect of adenosine on Na(+)-Ca(2+) exchange current recorded from guinea-pig ventricular myocytes. *Cell Calcium*, 29, (5) 347-358 available from: PM:11292391
- Zheng, B., Ma, Y.C., Ostrom, R.S., Lavoie, C., Gill, G.N., Insel, P.A., Huang, X.Y., & Farquhar, M.G. 2001. RGS-PX1, a GAP for GalphaS and sorting nexin in vesicular trafficking. *Science*, 294, (5548) 1939-1942 available from: PM:11729322
- Zheng, M., Zhu, W., Han, Q., & Xiao, R.P. 2005. Emerging concepts and therapeutic implications of beta-adrenergic receptor subtype signaling. *Pharmacol.Ther.*, 108, (3) 257-268 available from: PM:15979723
- Zolotareva, A.G. & Kogan, M.E. 1978. Production of experimental occlusive myocardial infarction in mice. *Cor Vasa*, 20, (4) 308-314 available from: PM:729388
- Zuberi, Z., Birnbaumer, L., & Tinker, A. 2008. The role of inhibitory heterotrimeric G-proteins in the control of in-vivo heart rate dynamics. *Am.J.Physiol Regul.Integr.Comp Physiol*, 295, (6) R1822-R1830 available from: PM:18832081
- Zuberi, Z., Nobles, M., Sebastian, S., Dyson, A., Lim, S.Y., Breckenridge, R., Birnbaumer, L., & Tinker, A. 2010. Absence of the inhibitory G-protein Galphai2 predisposes to ventricular cardiac arrhythmia. *Circ.Arrhythm.Electrophysiol.*, 3, (4) 391-400 available from: PM:20495013